

**SUPERCRITICAL WATER OXIDATION AS A TECHNOLOGY FOR  
THE TREATMENT OF MODEL AND INDUSTRIAL WASTEWATERS:  
REACTION KINETICS AND REACTOR CONFIGURATIONS**

by

**IAIN NICHOLAS KINGS**

A thesis submitted to the University of Birmingham  
for the degree of  
**DOCTOR OF PHILOSOPHY**

Supercritical Fluids Technology Group  
School of Chemical Engineering  
College of Engineering and Physical Sciences  
University of Birmingham  
December 2012

**UNIVERSITY OF  
BIRMINGHAM**

**University of Birmingham Research Archive**

**e-theses repository**

This unpublished thesis/dissertation is copyright of the author and/or third parties. The intellectual property rights of the author or third parties in respect of this work are as defined by The Copyright Designs and Patents Act 1988 or as modified by any successor legislation.

Any use made of information contained in this thesis/dissertation must be in accordance with that legislation and must be properly acknowledged. Further distribution or reproduction in any format is prohibited without the permission of the copyright holder.

## ABSTRACT

The work presented herein was carried out with the aim of investigating the advantages of a multi-stage supercritical water oxidation (SCWO) reactor over a single-stage configuration in treating dimethylformamide (DMF), chosen as a model compound to represent a nitrogenous wastewater. Additionally, a single-stage configuration rig was used to destroy a complex industrial wastewater in order to investigate the applicability of SCWO to a multi-component hazardous industrial wastewater.

A flexible laboratory-scale tubular plug-flow reactor rig was designed, constructed, tested, and operated to investigate the various effects of physical and chemical process parameters on the yields of carbon- and nitrogen-containing species. The parameters that were investigated with the reactor temperature, the initial concentration of DMF, the stoichiometric ratio of oxidant to DMF and the reactor residence time, in addition to the location of the secondary oxidant injector and the proportion of the total deliverable oxidant that would be injected through such a secondary point. The results of the oxidation experiments showed that the temperature of the reaction was the critical variable in determining the rate of reaction, with temperatures in excess of 500°C invariably resulting in near-complete removal of TOC at even very short residence times (approx. 6 s). This was also true of the complex industrial wastewater, although longer residence times of up to 17 s at the temperature of 500°C were necessary to facilitate a similar TOC removal, probably due to the much larger aromatic and aliphatic components of which the waste samples were comprised. The oxidation of DMF adhered to Arrhenius-type

kinetics, and kinetic parameters were evaluated and found to be  $140 \text{ kJ mol}^{-1}$ ,  $1 \times 10^{12} \text{ litre}^{0.36} \text{ mol}^{0.36} \text{ s}^{-1}$  for the activation energy and pre-exponential factor respectively, and to be first order with respect to DMF and 0.36 order with respect to the oxidant.

It was found that there were certain configurations of oxidant injection that resulted in increased TOC removal when compared to a single-stage configuration, particularly when the secondary injector was placed halfway along the reactor length and the secondary port injected 50 – 67% of the total deliverable oxidant, although ammonia yield was also higher than for the single-stage configuration at these points. When the secondary port was fixed close to the primary port, i.e. at 25% of the reactor length, there was much less difference between the multi-stage and single-stage performance. There were several configurations where the single-stage design outperformed the multi-stage, likely related to the specific availability of oxidant at any one time.

It was shown that temperatures in excess of 500°C were suitable to treat the complex wastes and that complete conversion of TOC to products could likely be expected within 55 s. It was seen that TOC value alone may not be a suitable input when attempting to determine treatability in SCWO and that component assay must also be considered. It was found that SCWO was a suitable technology for the destruction of the complex organic wastewater, although engineering problems such as corrosion and agglomeration, and subsequent pipe blockages were encountered, requiring that adaptations be made to the apparatus if similar experiments are to be carried out in future.

## **ACKNOWLEDGEMENTS**

I wish to express my gratitude to the following people and organisations for their support and assistance during the time spent on this work:

My supervisors, Dr. Bushra Al-Duri and Dr. Phil Robbins for their advice, discussions on the work, and their invaluable support.

Prof. Yoshito Oshima and the students and staff of the Department of Environmental Systems, University of Tokyo, Kashiwa for their kindness and hospitality during time spent there in Autumn 2011.

Robert Sharpe and Bill Harris at the workshop of the School of Chemical Engineering, for invaluable advice and assistance in the construction of the experimental apparatus.

All of the staff and postgraduate research students in the School of Chemical Engineering who have helped to make my time at Birmingham so enjoyable.

My family for their influence, love, and assistance in bringing me to this point.

Finally, a special word of thanks to Hannah for her unrelenting love and support throughout this work's highs and lows. I am eternally grateful.

## **TABLE OF CONTENTS**

### **PART I - INTRODUCTION**

<b>CHAPTER 1 – INTRODUCTION.....</b>	<b>1</b>
1.1    Background and Aims .....	1
1.2    Structure of the Thesis .....	3

### **PART II - LITERATURE SURVEY**

<b>CHAPTER 2 – LITERATURE REVIEW .....</b>	<b>5</b>
2.1    Industrial Wastewater and Waste Treatment .....	5
2.1.1    Current Treatment Methods.....	7
2.1.1.1    Physical Methods .....	7
2.1.1.2    Biological Methods .....	8
2.1.1.3    Chemical Methods .....	8
2.1.1.4    Employed Waste Treatment Methods .....	10
2.1.1.5    Other Considerations .....	13
2.2    Introduction to Supercritical Fluids .....	13
2.2.1    Supercritical Water Oxidation (SCWO).....	17
2.2.2    Use of SCWO as a Wastewater Treatment Option.....	18
2.2.3    Treatment of Other Wastes .....	19
2.3    Current Research into SCWO Reactions .....	19
2.4    Treatment Efficacy, Kinetics, Mechanisms and Pathways .....	21

2.4.1	Nitrogenated Compounds .....	24
2.4.2	Non-nitrogenated Compounds .....	29
2.4.3	Heteroatom-containing Compounds .....	39
2.4.4	Co-oxidation Reactions.....	45
2.4.5	Treatment of Specific Wastes .....	48
2.5	Treatment of More Complex Wastes.....	49
2.6	Treatment Problems and Reactor Design .....	53
2.6.1	Salt Plugging.....	54
2.6.2	Corrosion .....	58
2.7	Current State of Industrial SCWO Technology .....	62
2.7.1	Energy Efficiency .....	64

## **PART III - EXPERIMENTAL WORK**

### **CHAPTER 3 – EXPERIMENTAL APPARATUS AND PROTOCOLS, AND ANALYTICAL TECHNIQUES .....** 71

3.1	Components and construction of experimental rig .....	71
3.1.1	Oven .....	73
3.1.2	Reagent Storage.....	75
3.1.3	Pumps .....	76
3.1.4	Preheating Coils .....	76
3.1.5	Reactor .....	77

3.1.5.1	Temperature Measurement and Profiles .....	77
3.1.5.2	Multi-stage Configuration .....	79
3.1.6	Cooler .....	80
3.1.7	Pressure Sensing and Control .....	81
3.1.8	Gas-Liquid Separator, Sampling and Gas Flow Measuring .....	83
3.2	Experimental Protocol .....	85
3.2.1	Generic Experimental Protocol .....	85
3.2.2	Experiment and Sampling .....	85
3.3	Analysis Techniques .....	87
3.3.1	Total Organic Carbon (TOC).....	88
3.3.1.1	Total Carbon (TC) .....	88
3.3.1.2	Inorganic Carbon (IC).....	89
3.3.1.3	Total Organic Carbon (TOC) Determination.....	90
3.3.2	Gas Chromatography – Thermal Conductivity Detector (GC-TCD) .....	90
3.3.3	Nitrogen Species Analysis .....	91
3.3.3.1	Ammonium Nitrogen .....	92
3.3.3.2	Nitrate Ion.....	92
3.3.3.3	Nitrite Ion.....	93
3.3.3.4	Total Nitrogen.....	93
3.3.4	Gas Chromatography – Flame Ionisation Detector (GC-FID) .....	94
3.3.5	Gas Chromatography – Mass Spectroscopy (GC-MS) .....	95

3.4 Calculation of Parameters .....	96
3.4.1 Thermophysical Properties .....	96
3.4.2 Volumetric Flowrate Changes.....	97
3.4.3 Reynolds Number.....	97
3.4.4 Péclet Number.....	98
3.4.5 Residence Time.....	98
3.4.6 Oxidant Delivered and Stoichiometric Ratio .....	99
3.4.7 Concentration at Reaction Conditions .....	99
3.4.8 Product Yields.....	100
3.5 Risk Assessments .....	100

## PART IV - RESULTS AND DISCUSSION

<b>CHAPTER 4 - SINGLE-STAGE SUPERCRITICAL WATER OXIDATION OF DIMETHYLFORMAMIDE.....</b>	<b>101</b>
4.1 The Oxidation of Dimethylformamide .....	101
4.2 Experimental Setup .....	103
4.3 Effect of System Parameters.....	104
4.3.1 Experimental Programme.....	104
4.3.2 Effect of Reactor Pressure.....	106
4.3.3 Effect of Residence Time.....	106
4.3.4 Effect of Temperature .....	108

4.3.5	Effect of DMF Concentration .....	113
4.3.6	Effect of Oxidant Ratio.....	124
4.4	Global Kinetics of DMF Oxidation .....	128
4.4.1	Derivation of Kinetics Models.....	129
4.4.1.1	Pseudo-first Order System.....	131
4.4.1.2	Non-unity Organic Reaction Order.....	131
4.4.1.3	Non-zero Oxidant Reaction Order.....	132
4.4.1.4	Matlab Regression Model.....	133
4.4.2	Pseudo-first Order Approximation.....	134
4.4.3	Global Power Law Models .....	138
4.4.4	Proposed Reaction Mechanisms .....	141
4.4.4.1	Trimethylamine.....	144
4.4.4.2	Dimethylamine .....	145
4.4.4.3	Methylamine.....	146
4.4.4.4	Ammonia Yields .....	148
4.5	Summary .....	149
<b>CHAPTER 5 – MULTI-STAGE SUPERCRITICAL WATER OXIDATION OF DIMETHYLFORMAMIDE.....</b>		<b>151</b>
5.1	Experimental Setup .....	151
5.2	Initial Multi-stage Experimental Runs .....	153
5.2.1	Implications of the Multi-stage Configuration .....	154

5.2.2	Effect of Residence Time.....	156
5.2.3	Effect of Varying Injector Position and Injection Proportion .....	159
5.2.4	Summary .....	169
5.3	Focused Multi-stage Experimental Runs.....	170
5.3.1	Effect of System Pressure .....	171
5.3.2	Effect of Temperature .....	171
5.3.3	Effect of Organic Concentration.....	177
5.3.4	Effect of Oxidant Ratio.....	181
5.3.5	Effect of Residence Time.....	186
5.4	Kinetics Analysis .....	189
5.4.1	Application of Single-stage Model to Series PFRs.....	189
5.4.2	Optimisation of Kinetic Model .....	195
5.4.3	Operation of Multi-stage Reactor.....	196
5.5	Summary .....	198
<b>CHAPTER 6 – SCWO OF REAL INDUSTRIAL WASTE AND INDUSTRIAL-SCALE TREATMENT EVALUATION .....</b>	<b>201</b>	
6.1	Specifications of the Waste Samples .....	201
6.2	Treatment Protocol.....	206
6.3	Experimental Runs .....	207
6.3.1	Initial Experiment and Reactor Adjustment.....	207
6.3.2	SCWO of Waste Samples .....	209

6.3.3	Assay Analysis of Feed Samples.....	210
6.3.4	Effect of Residence Time.....	219
6.3.5	Effect of Feed TOC Concentration and Type .....	227
6.4	Global Kinetics .....	231
6.4.1	Approximation to Pseudo-first Order System.....	233
6.4.2	Non-unity TOC Order Model .....	238
6.4.3	Non-zero Oxygen Reaction Order .....	241
6.4.4	Time to Complete TOC Removal.....	242
6.5	Assay Analysis after the SCWO Treatment.....	244
6.5.1	Samples E134 and E135 .....	246
6.5.2	Sample E72 .....	246
6.5.3	Sample E95 .....	247
6.5.4	Sample NE .....	248
6.5.5	Sample T105 .....	248
6.6	Engineering Issues.....	251
6.6.1	Solids Plugging .....	251
6.6.2	Corrosion .....	256
6.7	Summary.....	257

## **PART V - CONCLUSIONS**

### **CHAPTER 7 – CONCLUSIONS AND RECOMMENDATIONS FOR FURTHER WORK.....260**

7.1 Conclusions.....	260
7.1.1 Rig Apparatus .....	260
7.1.2 Study of the Single-stage Oxidation of DMF .....	261
7.1.3 Study of the Multi-stage Oxidation of DMF .....	261
7.1.4 Destruction of Real Waste .....	262
7.2 Recommendations for Further Work .....	263
7.2.1 Adiabatic Operation of a Multi-stage SCWO Rig .....	263
7.2.2 Co-oxidation of DMF and an Auxiliary Fuel .....	264
7.2.3 Destruction of More Complex Wastes .....	265
7.2.4 Simulation of DMF Reaction Kinetics.....	265

## **PART VI - APPENDICES**

<b>APPENDICES .....</b>	<b>266</b>
Appendix 1 Reaction Mechanism for C <sub>1</sub> Compounds .....	266
Appendix 2 Risk Assessments.....	270
Appendix 2.1 Hazard and Risk Assessment for DMF .....	270
Appendix 2.2 Hazard and Risk Assessment for Industrial Samples.....	272
Appendix 3 Mass Spectra Analysis of Complex Waste Feed Samples.....	274

Appendix 3.1 Sample T105.....	274
Appendix 3.2 Sample E72 .....	278
Appendix 3.3 Sample E95 .....	280
Appendix 3.4 Samples E134 and E135 .....	281
Appendix 3.5 Sample NE.....	282
Appendix 3.6 Assay Overviews.....	284
Appendix 4 Matlab Regression Regime for Kinetic Parameters.....	287
Appendix 4.1 Calling and Calculation Script .....	287
Appendix 4.2 Integral Function .....	289
Appendix 4.3 Minimisation Function .....	289
Appendix 5 Matlab Model for Parameter Evaluation .....	290
<b>LIST OF REFERENCES .....</b>	<b>291</b>
<b>LIST OF PUBLICATIONS.....</b>	<b>310</b>

## LIST OF FIGURES

Figure 2.1 – Phase diagram of water .....	14
Figure 2.2 – Density of water as a function of temperature and pressure .....	15
Figure 2.3 – Density, ionic product and dielectric constant of water.....	16
Figure 2.4 – Dynamics of MeOH, CHCO, CO and CO <sub>2</sub> in the SCWO of methanol ...	31
Figure 2.5 – Temperature profile during SCWO of acetic acid .....	34
Figure 2.6 – Variation of selected phenol oxidation with time.....	36
Figure 2.7 – TOC removal during SCWO of TDG .....	41
Figure 2.8 – Dechlorination reaction pathways.....	44
Figure 2.9 – Location of potential engineering issues associated with SCWO .....	54
Figure 2.10 – Diagram of Transpiring Wall Reactor .....	57
Figure 2.11 – Liner schematic of Transpiring Wall Reactor.....	57
Figure 2.12 – Mass gain of stainless steel .....	59
Figure 2.13 – XRD patterns from 316 SS exposed to SCW .....	60
Figure 2.14 – AquaCritox® Reactor .....	66
Figure 2.15 – TWR operating in a hydrothermal flame regime .....	69
Figure 3.1 – General flowchart of SCWO rig. ....	72
Figure 3.2 – View of the reactor inside the oven. ....	74
Figure 3.3 – Plan view of the oven .....	74
Figure 3.4 – Pumps used to deliver reactants .....	76
Figure 3.5 – Temperature logs at 400°C for the multi-stage configuration. ....	79
Figure 3.6 – Diagram of effluent stream cooler. ....	80
Figure 3.7 – Cooler module. ....	81
Figure 3.8 – Gas-liquid separator. ....	84

Figure 3.9 – Merck Spectroquant® Nova 60A Spectrophotometer.....	91
Figure 4.1 – Reactor schematic indicating the single-stage oxidation rig.....	103
Figure 4.2 – DMF, TOC and TC removal vs residence time.....	108
Figure 4.3 – Removal of DMF, TOC and TC vs temperature .....	110
Figure 4.4 – Carbon fraction yields as a function of temperature .....	111
Figure 4.5 – Nitrogen fraction yields as a function of temperature .....	112
Figure 4.6 – Removal of DMF, TOC and TC against feed concentration .....	115
Figure 4.7 – Removal of DMF, TOC and TC against feed concentration .....	116
Figure 4.8 – Removal of DMF, TOC and TC as a function of feed concentration....	117
Figure 4.9 – DMF removal as a function of concentration.....	118
Figure 4.10 – Carbon fraction yields as a function of concentration.....	118
Figure 4.11 – Nitrogen fraction yields as a function of concentration .....	119
Figure 4.12 – Carbon fraction yields as a function of concentration.....	120
Figure 4.13 – Nitrogen fraction yields with concentration .....	121
Figure 4.14 – Carbon fraction yields as a function of concentration .....	122
Figure 4.15 – Nitrogen fraction yields with concentration .....	122
Figure 4.16 – Removal of DMF, TOC and TC against SR.....	125
Figure 4.17 – DMF removal vs SR and concentration/SR relationship.....	126
Figure 4.18 – Carbon fraction yields as a function of SR .....	127
Figure 4.19 – Nitrogen fraction yields against SR .....	128
Figure 4.20 – Natural logarithms of $(1-X_{DMF})$ and $(1-X_{TOC})$ vs residence time .....	135
Figure 4.21 – Arrhenius plots for DMF and TOC .....	135
Figure 4.22 – Parity plot of DMF conversion for pseudo-first order model. ....	137
Figure 4.23 – Normalised DMF removal as a function of residence time .....	139

Figure 4.24 – Gradient of Figure 4.23 as a function of $\ln([O_2]_0)$ .....	139
Figure 4.25 – Parity plot of DMF conversion .....	141
Figure 4.26 – Formation of TMA via radical substitution of DMF.....	144
Figure 4.27 – Formation of DMA from radical substitution of DMF and TMA. ....	145
Figure 4.28 – DMF SCWO reaction mechanism. ....	147
Figure 5.1 – Reactor schematic indicating the multi-stage oxidation rig.....	152
Figure 5.2 – DMF removal for multi-stage SCWO – varying secondary injection ....	157
Figure 5.3 – TOC removal for multi-stage SCWO – varying secondary injection ....	158
Figure 5.4 – Removals for multi-stage SCWO with varying secondary injection .....	160
Figure 5.5 – DMF and TOC removals as a function of primary oxidant proportion..	162
Figure 5.6 – DMF and TOC removals as a function of primary oxidant proportion..	162
Figure 5.7 – Removals for multi-stage SCWO with varying secondary injection .....	163
Figure 5.8 – DMF traces for all cases at 33% and 66% primary oxidant .....	165
Figure 5.9 – TOC traces for all cases at 33% and 66% primary oxidant .....	165
Figure 5.10 – Nitrogen fraction yields as a function of primary oxidant proportion ..	167
Figure 5.11 – Removals of DMF, TOC and TC vs temperature.....	173
Figure 5.12 – Carbon fraction yields as a function of temperature .....	175
Figure 5.13 – Nitrogen fraction yields as a function of temperature .....	177
Figure 5.14 – Removal of DMF, TOC and TC vs concentration .....	178
Figure 5.15 – Comparison of DMF and TOC removals vs concentration .....	179
Figure 5.16 - Carbon fraction yields as a function of concentration.....	180
Figure 5.17 – Nitrogen fraction yields as a function of concentration .....	180
Figure 5.18 – DMF, TOC and TC removals as a function of SR.....	182
Figure 5.19 – DMF removal as compared to concentration/SR relationship. ....	183

Figure 5.20 – Carbon fraction yields as a function of SR .....	184
Figure 5.21 – Nitrogen fraction yields as a function of SR.....	184
Figure 5.22 – TOC removal as a function of residence time .....	187
Figure 5.23 – Parity plot of calculated and experimental conversions .....	191
Figure 5.24 – Parity plots for oxidant location and proportion experiments .....	191
Figure 5.25 – Parity plot for data in Figure 5.24 .....	193
Figure 5.26 – Parity plots for 75% oxidant delivered through the primary port .....	194
Figure 5.27 – Temperature profile in adiabatic multi-stage SCWO of MeOH .....	197
Figure 6.1 – GC retention profile of sample E95. ....	211
Figure 6.2 – Mass spectrum of component in sample E95.....	211
Figure 6.3 – TOC removal as a function of residence time .....	220
Figure 6.4 – Undiluted sample of E95 .....	222
Figure 6.5 – Comparison between diluted feed and oxidised E95 sample .....	222
Figure 6.6 – Carbon fraction yields of samples E134 and E135.....	224
Figure 6.7 – Nitrogen fraction yields for the oxidation of sample T105 .....	226
Figure 6.8 – TOC removal vs concentration and residence time.....	228
Figure 6.9 – 2D projection of TOC removal vs concentration (various times). ....	228
Figure 6.10 – TOC removal as a function of concentration .....	230
Figure 6.11 – TOC Removal vs residence time for ‘simple’ and ‘complex’ wastes..	230
Figure 6.12 – Parity plot of pseudo-first order model and experimental data .....	234
Figure 6.13 – Normalised decay versus residence time.....	235
Figure 6.14 – Parity plot of pseudo-first order model and samples .....	237
Figure 6.15 – Parity plots of ‘simple’ and ‘complex’ component TOC removals .....	238
Figure 6.16 – Parity plot for $a = 1.08$ and $k = 0.47 \text{ litre}^{0.08} \text{ mol}^{-0.08} \text{ s}^{-1}$ .....	240

Figure 6.17 – Parity plots of ‘simple’ and ‘complex’ component TOC removals .....	240
Figure 6.18 – Particulate matter present in samples. ....	251
Figure 6.19 – Suspended particulate matter causing opacity of sample T105. ....	252
Figure 6.20 – Particulate matter ejected from the organic sample preheater. ....	254

## LIST OF TABLES

Table 2.1 - Categories of filtration .....	8
Table 2.2 – UK generation of incinerable wastes ca.1994 .....	12
Table 2.3 – Municipal waste generation in 1999 .....	12
Table 2.4 – Critical parameters of selected organic compounds.....	14
Table 2.5 – Physicochemical properties of water at various states .....	17
Table 2.6 – Summary of kinetic parameters of selected nitro-organic compounds. ..	29
Table 2.7 – Conditions for the SCWO of MeOH .....	31
Table 2.8 – Summary of kinetic parameters of selected organic compounds. ....	39
Table 2.9 – Summary of kinetic parameters of selected heteroatom-containing organic compounds.....	45
Table 2.10 – Composition of cutting oils.....	51
Table 2.11 – SCWO facilities ca. 2006.....	63
Table 2.12 – Additional operational SCWO facilities as of 2012.....	64
Table 3.1 – GC-TCD conditions and program parameters .....	90
Table 3.2 – GC-FID conditions and program parameters.....	95
Table 4.1 – Properties of DMF .....	101
Table 4.2 – Experimental conditions for single-stage oxidation of DMF .....	106
Table 4.3 – Reaction orders of selected organic compounds.....	130
Table 5.1 – Multi-stage SCWO experimental conditions for varying oxidant injection configurations and ratios. ....	154
Table 5.2 – Multi-stage oxidation experimental conditions .....	171
Table 5.3 – Model parameters used to generate Figure 5.24.....	190
Table 6.1 – Feed concentrations of organic reactant after dilution.....	202

Table 6.2 – General reaction conditions for the treatment of waste samples .....	206
Table 6.3 – Initial experimental conditions .....	208
Table 6.4 – Experiment A1/A2 results.....	208
Table 6.5 – Amended experimental conditions.....	209
Table 6.6 – Identified components in sample T105.....	213
Table 6.7 – Identified components in sample E72.....	214
Table 6.8 – Identified components in sample E95.....	215
Table 6.9 – Identified component in samples E134 and E135.....	215
Table 6.10 – Identified compounds in sample NE. ....	216
Table 6.11 – TOC removal for each sample treatment.....	220
Table 6.12 – Carbon fraction yields for SCWO of industrial waste samples.....	223
Table 6.13 – Pseudo-first order reaction rate constants for each experiment. ....	233
Table 6.14 – Residual values for series in Figure 6.13.....	236
Table 6.15 – Best-fit first order rate constants for each sample. ....	236
Table 6.16 – TOC reaction order fitted to $a \neq 1$ model.....	239
Table 6.17 – Rate constants and predicted times to 99.99% TOC removal. ....	242
Table 6.18 – Number of discrete components eluted from each sample.....	245
Table 6.19 – Removal of E134 and E135 components .....	246
Table 6.20 – Removal of E72 components .....	247
Table 6.21 – Removal of E95 components .....	248
Table 6.22 – Removal of NE components .....	248
Table 6.23 – Removal of T105 components.....	249
Table 7.1 – Kinetic parameters of single-stage SCWO of DMF.....	261
Table 7.2 – Kinetic parameters for SCWO of wastewater samples.....	263

Table A.1 – List of elementary reactions of C <sub>1</sub> , H and oxidant compounds .....	266
Table A.2 – Reaction mechanism, continued. ....	267
Table A.3 – Reaction mechanism, continued. ....	268
Table A.4 – Reaction mechanism, continued. ....	269
Table A.5 – T105 Assay .....	284
Table A.6 – E72 Assay .....	284
Table A.7 – E95 Assay .....	285
Table A.8 – E134 Assay .....	285
Table A.9 – E135 Assay .....	285
Table A.10 – NE Assay .....	286

## **LIST OF ABBREVIATIONS AND SYMBOLS**

### **Abbreviations**

BOD	Biological Oxygen Demand
BPR	Back Pressure Regulator
COD	Chemical Oxygen Demand
DMF	Dimethylformamide
DMA	Dimethylamine
FID	Flame Ionisation Detector
GC	Gas Chromatograph
IC	Inorganic Carbon
MA	Methylamine
MS	Mass Spectroscopy
NO <sub>x</sub>	Nitrous Oxides
PFR	Plug flow reactor
SCWO	Supercritical Water Oxidation
SO <sub>x</sub>	Sulphur Oxides
SR	Stoichiometric Ratio
SS	Stainless Steel
TC	Total Carbon
TCD	Thermal Conductivity Detector
TMA	Trimethylamine
TN	Total Nitrogen
TOC	Total Organic Carbon
TWR	Transpiring Wall Reactor
WAO	Wet Air Oxidation

## Alphabetical Symbols

[A, B, C,...]	Concentration of reactant A, B, C..., etc.
A	Arrhenius-type rate expression pre-exponential factor
D	Pipe diameter
$D_m$	Mass diffusivity
$E_A$	Arrhenius-type rate expression activation energy
$F_1, F_2$	Volumetric flowrate at point 1, point 2
L	Reactor length
P	Pressure
$P_c$	Critical pressure
$Pe_e$	Péclet Number for energy transport
$Pe_m$	Péclet Number for mass transport
R	Universal gas constant
Re	Reynolds Number
T	Temperature
$T_c$	Critical temperature
$V_r$	Reactor volume
$X_{DMF}$	Conversion of DMF
$X_{TOC}$	Conversion of TOC
a	Order of reaction with respect to target reactant
b	Order of reaction with respect to oxidant
c	Order of reaction with respect to water
k	Reaction rate constant
r	Rate of reaction
$\bar{u}$	Mean fluid velocity

## Greek Symbols

$\Delta P$	Pressure drop
$\epsilon$	Pipe roughness factor
$\mu$	Dynamic viscosity
$V_{sc,0}$	Volumetric flowrate at reaction conditions
$\rho$	Fluid density
$\tau$	Reactor residence time
$\phi$	Pipe friction factor

## CHAPTER 1 – INTRODUCTION

### 1.1 Background and Aims

This work investigates the use of water in a very specific region of its phase diagram as a medium in which organic wastes can be oxidised. This process, known as Supercritical Water Oxidation (SCWO), has numerous physical and chemical advantages over other waste treatment methods (e.g. incineration) whilst simultaneously having a number of disadvantages (corrosion, precipitation blockages) that must be overcome or mitigated for if SCWO's prevalence as a technology is to increase.

Nitrogenated organics are common in the manufacture of pharmaceuticals (e.g. anti-epileptic drugs such as lamotrigine,  $C_9H_7Cl_2N_2$  and hypnotic drugs such as diazepam,  $C_{16}H_{13}ClN_2O$  (BNF, 2012)) and are thus also found in the waste streams from such manufacture. Their presence in pharmaceutical preparations means that they are also present in medical wastes, which are almost invariably destroyed by incineration. Thus, in the assessment of SCWO as a waste treatment technology, the destruction of nitrogenated organic compounds via SCWO is of investigative importance.

Dimethylformamide (DMF:  $C_3H_7NO$ ) was chosen as the primary compound to be investigated. This was partly due to its relatively simple nature as an aliphatic amide, and partly due to the fact that it can be found as a component in industrial waste streams.

The ability of SCWO to destroy organic compounds quickly (order of  $10^2$  seconds residence time) is established, but the rate at which the compound can be destroyed directly affects how efficient the process can be described to be. It was hypothesised that the different distribution of oxidising species and the additional mixing regimes that would be caused by employing a secondary oxidant injection point could increase the rate of destruction of DMF and TOC.

Consequently, the primary aims of this research were to investigate the destruction of a nitrogenated organic compound (DMF) in an aqueous feed in a multi-stage reactor, and to compare the reaction kinetics that occurred within each configuration under a variety of process conditions with those that were obtained with a single-stage oxidation. The use of multiple injections of oxidant has been simulated but there are very few instances in the literature where such a tubular reactor has been constructed, tested, and operated.

In order to investigate the treatability of DMF under such conditions, it was also necessary to design and build the reactor system. Such a design is presented in chapter 3.

A logical extension of an investigation of the optimum conditions for maximising destruction and restraining the production of undesirable oxidative intermediates would be to use the constructed rig in a single-stage configuration to destroy a sample of genuine industrial, pharmaceutical or medical waste. In order for SCWO to progress as a treatment technology, the treatability of complex wastes must be assessed, and there are precious few instances of such investigations in the

literature. Certainly, in comparison to investigations of model compounds, the incidences of testing of complex systems are in a very small minority.

A desire to treat medical waste turned out to be unfeasible due to safety considerations arising from their potentially pathogenic nature, which are inherent when treating samples that may be contaminated with bodily fluids, e.g. blood, and due also to the general difficulty in acquiring small samples. It was not possible to treat solid samples (e.g. syringes) using the rig as there was no means of dissolving the solid waste prior to reaction. Consequently, an industrial waste was acquired. An investigation into the treatability of a complex industrial waste would add to the sparse body of data that is available which pertains to the SCWO of such wastes.

Laboratory-scale investigations such as those that were to be undertaken are critical to informing the investigations that need to be undertaken at larger scales in order to refine SCWO as a viable treatment technology. Optimum reaction conditions, reactor configurations, and energy integration regimes can all be investigated at laboratory- and pilot-scales and the overall aim of this work is to contribute data conducive to increasing the viability of SCWO technology as a waste treatment protocol.

## 1.2 Structure of the Thesis

Chapter 2 initially presents an introduction to current waste and wastewater treatment technologies, and an explanation of the nature of SCW and why it is suitable as an oxidation reaction medium. This is followed by a comprehensive overview of the state of SCWO research and technology: the types of compounds and wastes that have had their treatabilities assessed at a variety of scales, the

engineering issues (pertaining to both design and operation) that have been encountered with the solutions to these issues that have been proposed, and the current state of SCWO technology in the area of waste and wastewater treatment.

The design of the SCWO apparatus, experimental procedures and analytical techniques employed in order to acquire the data presented in this work are presented in chapter 3.

Chapter 4 presents the SCWO of DMF in a single-stage reactor operated at a range of conditions such that the kinetic parameters could be determined. This section of the work also serves as a base case to which the study in chapter 5 can be compared.

Chapter 5 presents the SCWO of DMF in a multi-stage reactor configuration and assesses the differences in treatability that arise as a function of the differing oxidant injection profiles, whilst also comparing these data to the single-stage reaction presented in chapter 4.

An analysis of the SCWO of a range of complex waste samples is presented in chapter 6. The treatability of each specific sample is assessed and a more generalised view of the destruction of the total organic carbon (TOC) derived. There were a number of operational issues that arose during the SCWO of these complex samples and these are also commented upon.

Finally, chapter 7 encompasses the main findings and conclusions of the body of the experimental work and makes recommendations for further work that it was felt would be a beneficial addition to body of research pertaining to SCWO already in existence, and would serve as a logical extension to the work presented herein.

## CHAPTER 2 – LITERATURE REVIEW

This chapter will provide both an in-depth review of the research that has been conducted into SCWO and an overview of the current state of SCWO waste treatment technology.

### 2.1 Industrial Wastewater and Waste Treatment

All industrial operations produce some wastewaters that must be returned to the environment (Perry and Green, 1997). These can be classified as:

- Domestic wastewaters – produced from plant workers and non-engineering operations. These are usually treated by normal municipal sewerage systems in order to prevent the spread of pathogenic micro-organisms.
- Process wastewaters – include aqueous wastes from product manufacture, product washing, leaks, and spills. Clearly, how hazardous process wastewaters are will depend on the nature of the process, but they can range from the relatively benign (e.g. the food processing industries in which water is a major component in food hydrocolloids and where wastewater may contain emulsification agents (Dickinson, 2009; Philips *et al.*, 1997) resulting in oil/water systems) to very toxic (e.g. water waste as a by-product during the demilitarisation of conventional and chemical munitions (Veriansyah and Kim, 2007) which is generally treated by incineration), that can also be recalcitrant and very difficult to treat. This class can also include cleaning- and

sterilisation-in place processes which are inherent parts of food and pharmaceutical manufacture processes in particular (Perry and Green, 2007).

- Cooling wastewaters – the result of a variety of cooling processes that can be grouped into single-pass processes in which the cooling water is used once and then returned to the environment and multiple-recycling processes in which the water is used to cool multiple times with various types of cooling towers being used to return heat to the environment.

Wastewaters being discharged to groundwater, rivers, streams or other navigable bodies or water sources have to adhere to quality standards set by the jurisdiction in which the discharging occurs. For example, in the case of wastewater being discharged in the UK, the European Union sets the quality standards as part of its Water Framework Directive 2000/60/EC, which includes standards for all surface waters and groundwater, and the Urban Waste Water Directive 91/271/EEC, which provides for a range of industries mostly related to the manufacture or production of food and drink products. In the US, the Clean Water Act 1972 provides quality standards. Permits for discharge are granted by the Environment Agency in the UK and are subject to regular testing of the quality of water being discharged. Consequently, wastewater treatment is a critical unit operation of many industrial processes.

## 2.1.1 Current Treatment Methods

Current wastewater treatment unit operations can be split into three broad groups: physical, chemical and biological methods (ESCWA, 2003).

### 2.1.1.1 Physical Methods

Physical methods are, processes in which physical properties or forces are used to remove contaminants and in which no chemical or biological agents are added to the system. Screening, sedimentation and flotation are examples of such systems and they are generally employed as primary treatment protocols (Perry and Green, 1997) when it is expected that the plant effluent stream (or in cases such as sewage treatment, the inlet stream) will contain suspended solids of varying size. The major advantage of such systems is that no additional chemicals need be added in order to achieve some degree of treatment, although the major disadvantage is that physical methods in general have no means of removing dissolved compounds without the tandem use of chemical and biological processes. Ion exchange also falls into this category and its use to treat streams containing (for example) morpholine is discussed by Mishra *et al.* (1993). As well as mechanical means, this can also include physical effects such as increased temperature or radiation as a disinfectant process.

A physical technique that has become more prominent in recent years is membrane filtration (Zhou and Smith, 2002). This process involves the use of various grades of mesh through which the effluent stream flows. Contaminants are left on one side of the mesh while water passes through to the other. The process can be subcategorised based upon the grade of mesh as shown in Table 2.1.

**Table 2.1** - Categories of filtration (Richardson and Harker, 2002).

Process	Driving force	Separation size range	Examples of materials separated
Microfiltration	Pressure gradient	10 – 0.1 µm	Small particles, large colloids, microbial cells
Ultrafiltration	Pressure gradient	<0.1 µm – 5 nm	Emulsions, colloids, macromolecules, proteins
Nanofiltration	Pressure gradient	~1 nm	Dissolved salts, organics
Reverse osmosis (hyperfiltration)	Pressure gradient	<1 nm	Dissolved salts, small organics
Electrodialysis	Electric field gradient	<5 nm	Dissolved salts

### 2.1.1.2 Biological Methods

Biological processes involve the use of microorganisms to convert colloidal or dissolved organic material into gases and settleable solid material of a form that can be removed using normal physical processes. Thus biological processes are usually used in conjunction with physical and chemical processes in order to ultimately reduce the organic content of the waste stream (ESCWA, 2003).

### 2.1.1.3 Chemical Methods

Chemical methods use chemical agents to enable removal of contaminants, for example by effecting a reaction that changes the physical properties of a certain contaminant so that it can be removed by a physical method, e.g. chemical precipitation in which a coagulant such as alum, ferric chloride, etc, is added to promote the increased flocculation of finely divided solids. This results in increased separation efficiency in comparison to physical processes alone (ESCWA, 2003).

While this process implies that the coagulant is then removed along with the flocculated contaminants, the process of adding other chemical species in order to enable the removal of specific contaminants does not necessarily have this

advantage. For example, dechlorination can be achieved through the addition of activated carbon or a reducing agent removing soluble chloride ions from organochlorides but the evolved salts then need to be removed via other means.

The processes that are more recognisable as chemical processes however, include incineration, ozonation (Mishra *et al.*, 1993) and wet air oxidation (WAO) (Savage, 2009). This work is interested in these processes more than any others.

WAO is a process by which water at an elevated temperature and pressure (although below its critical point) is used as a medium in which to react mildly concentrated wastes with oxygen. WAO systems are biphasic, resulting in the reaction being mass transfer-limited, and large reactors and long retention times (>1 hour) are required to achieve substantial conversions, but a significant drawback is that refractory compounds remain in the reactor outflow. As such, WAO is often seen as an initial stage treatment step. For example, in the WAO of sewage sludges, this technology can bring about a 5-15% decrease in COD and render the sludge sterile. The sludge is then biologically treated. Such procedures can occasionally mean that oxidation at more extreme conditions may not be necessary (Mishra *et al.*, 1995).

### Incineration

Incineration, however is widespread as a treatment protocol for aqueous wastewaters and sludge, as well as for more solid wastes primarily because of its applicability to a wide range of effluent streams and its relative simplicity.

Incineration as a mass waste treatment process was developed as part of the industrial revolution with the first plant in the UK being constructed in Nottingham in 1874. Its current ubiquity stems from the fact that it is possible to achieve a 90%

reduction in volume and a 75% reduction in mass of materials going to final landfill, and that any toxic organic compounds, combustible carcinogens, biologically active materials that could affect sewage works, and pathologically contaminated materials can be rendered more suitable for final disposal, e.g. upon their landfilling if they form any part of the bottom ash of the incinerate (Petts, 1994).

Recently, specialised waste treatment facilities in Europe are investigating new kiln and energy integration technologies in order to make the process more efficient and economically and environmentally viable (Vermeulen *et al.*, 2012), however, the shortcomings of incineration currently remain readily apparent.

#### **2.1.1.4 Employed Waste Treatment Methods**

Various combinations of these different kinds of technologies in the form of trains of specific unit operations can be employed depending on the nature of the wastewater to be treated. When the effluent stream contains greater than 1% organic matter, biological treatment becomes unfeasible. However, incineration only becomes completely economically desirable when this proportion is greater than 10% (Vielcazals *et al.*, 2006) although with proportions of less than 20%, additional fuel is often required depending on the quantity of water present in the waste that would need to be vaporised (and thus would require energy) as part of the process (Dutournié *et al.*, 2007). Coupled with this sensitivity to the composition of the wastewater, incineration's tendency to only partially degrade complex components results in the potential to emit carbon monoxide, nitrogen oxides, dioxins, polychlorinated biphenyls and dibenzofurans (Sudhir *et al.*, 1998). Downstream flue-gas cleaning is therefore a necessity if the emission of acid gases, heavy metals,

PCBs, dioxins, and furans is to be avoided (Vermeulen *et al.*, 2012). Such flue-gas treatment can require the employment of other chemical reagents such as ammonia, lime, caustic soda, and activated carbon, among others. In addition to these environmental and operational factors, incineration has high capital and operating costs, requires a large excess of air and has a low thermal efficiency. These shortcomings mean that despite incineration's ubiquity, there are significant incentives to develop a more cost-effective process to treat effluent streams of organic content between 1 – 10%.

### Use of Incineration

Petts' report indicates that in 1994, the generation of incinerable wastes in the UK was as shown in Table 2.2. Clearly, there is a huge capacity for incineration in the UK and, given that most developed countries have similar per capita rates of waste, the world. A report commissioned by the World Bank in 1999 states that domestic waste generation was of the levels given in Table 2.3. Using 2001 census data to assume a UK population of 58 million people in 1999, this implies that approximately 20 million tonnes of municipal waste was produced in the UK. This is similar to that stated in Table 2.2. In the financial year 2009-10, UK households produced 23 million tonnes of household waste (Department for Environment Food and Rural Affairs [DEFRA], 2012). DEFRA suggests that this was a reduction on 2001 levels when 25 million tonnes of household waste was produced.

**Table 2.2** – UK generation of incinerable wastes ca.1994 (DEFRA, 2012).

Incinerable Wastes	Annual Arisings (million tonnes)
Agriculture	250
– Poultry litter	1
– Straw waste	13
– Carcasses	0.1
Sewage sludge (dry weight)	1
Household	20
Commercial	15
Industrial	50
‘Special’ wastes	2.7
Hazardous wastes	4
Clinical	0.4
Scrap tyres	0.4

**Table 2.3** – Municipal waste generation in 1999 (DEFRA, 2012).

Area	Waste Generation ( $\text{kg capita}^{-1} \text{yr}^{-1}$ )		Annual Growth Rate
	Range	Mean	
OECD-total	263 – 864	513	1.9%
– North America	--	826	2.0%
– Japan	--	394	1.1%
– OECD-Europe	--	336	1.5%
Europe (32 Countries)	150 – 624	345	--
8 Asian Capitals	185 – 1000	--	--
South and West Asia (cities)	185 – 290	--	--
Latin America and the Caribbean	110 - 365	--	--

All of this waste needs to be treated and, as landfill becomes less and less desirable, incineration will become more and more common, although ultimately some bottom ash continues to end in landfill. In 2006, almost 5 million tonnes of waste was incinerated in the UK at plants that accept waste from offsite (i.e. this quantity doesn't include the numerous other plants that incinerate their own wastes e.g. pharmaceutical plants, hospital incinerators, etc) (UK Environment Agency, 2012). This includes some hazardous waste and agricultural waste and indicates the order of magnitude of throughput going to incineration.

### 2.1.1.5 Other Considerations

Other important process parameters such as the extent of contaminant reduction required, energy efficiency, nature of the waste, availability and technical expertise of staff, location, availability of raw materials (fuel, water, etc), and cost are also considered when assessing how wastewater streams and other waste sources are to be treated.

Using the properties of water above its critical point as a reaction medium in the form of Supercritical Water Oxidation (SCWO) has emerged as a promising alternative to conventional waste treatment protocols.

## 2.2 Introduction to Supercritical Fluids

First, consider a mixture of gas and liquid at equilibrium conditions. Upon increasing the temperature, thermal expansion would result in the liquid phase becoming less dense. Additionally, increasing the pressure would cause the gas phase to become more dense (Bermejo and Cocero, 2006). As the temperature and pressure are raised, there will be some point - referred to on thermodynamic phase diagrams and within this work as the critical point – at which the densities of the gas and liquid phases become equal and the distinction between the two phases disappears. Above the critical point, this monophasic system is then referred to as a supercritical fluid (SCF). Consequently, any one-component fluid is defined as an SCF if its pressure exceeds the component's critical pressure,  $P_c$  and its temperature exceeds the critical temperature,  $T_c$ . This point is indicated on the phase diagram of water given in Figure 2.1 where the supercritical region is that at a higher temperature and pressure than the indicated critical point.

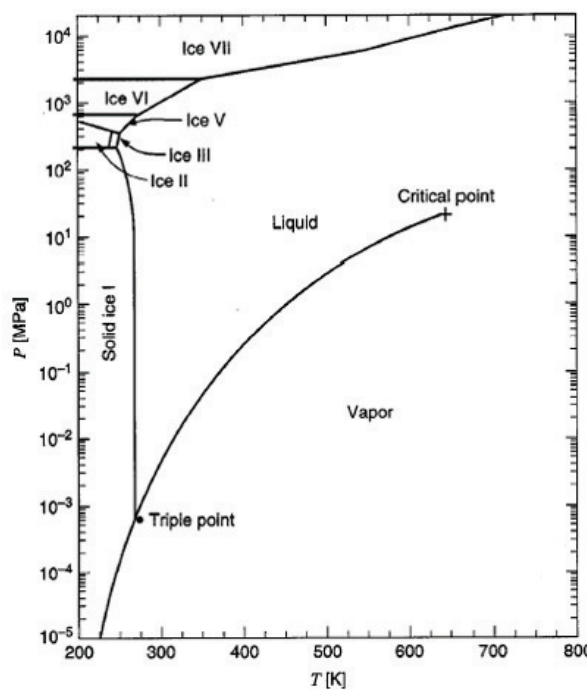


**Figure 2.1** – Phase diagram of water (Sonntag *et al.*, 2003).

Table 2.4 indicates several compounds along with their critical temperatures and pressures.

**Table 2.4** – Critical parameters of selected organic compounds.

Compound	Critical Temperature, K	Critical Pressure, MPa	Reference
Water	647.1	22.12	Kritzer and Dinjus, 2001
Carbon Dioxide	304.2	7.39	Richardson and Harker, 2002
Ethanol	514.2	6.3	Polikhronidi <i>et al.</i> , 2007
Ammonia	405.7	11.28	Needham and Ziebland, 1965
Ethane	305.4	4.88	Richardson and Harker, 2002
Ethylene	282.9	5.04	Richardson and Harker, 2002
Propane	369.9	4.25	Richardson and Harker, 2002
Benzene	562.2	4.92	Fukuda <i>et al.</i> , 2011

The densities of water at a range of temperatures as calculated by the Peng-Robinson equation of state (Lemmon *et al.*, 2012) for a number of isobaric systems

are given in Figure 2.2. The critical pressure of water is 22.12 MPa and the critical temperature is 647.1 K.

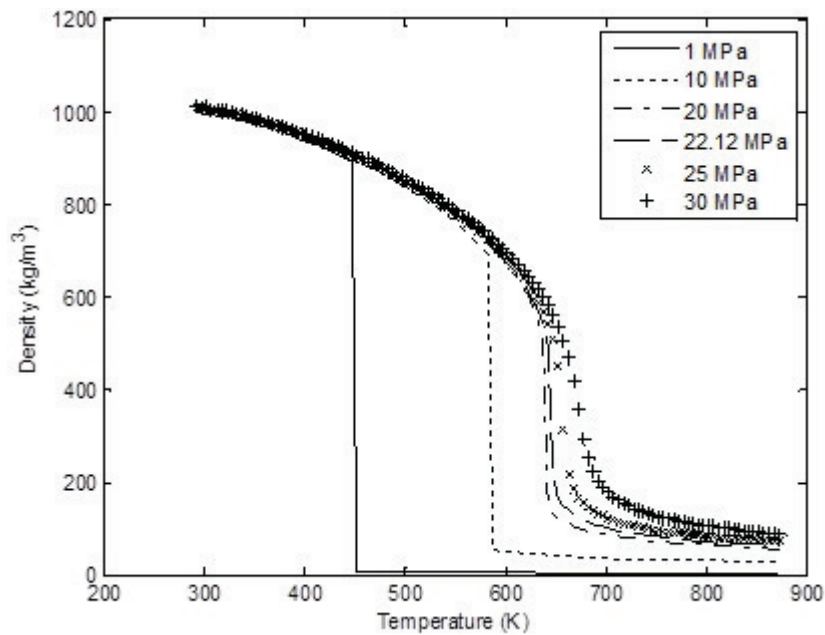


**Figure 2.2** – Density of water as a function of temperature and pressure.

Almost by definition, therefore, the density of a supercritical fluid will be somewhere between those of liquid and gaseous water at ambient pressure. In water's case at least, the density of the SCF is much closer to that of gaseous water at ambient pressure. The corollary of this is that given that the mass of any quantity of water remains the same under any conditions, a much greater volume is required to contain that same mass of water under supercritical conditions than at ambient conditions. Consequently, a compound dissolved in the water as it undergoes this transition will find its concentration in millimoles per litre (mM) reduced by the ratio of the ambient and SCW densities. The viscosity and thermal conductivity of SCW also obey a similar behaviour to that of density and are also greatly reduced with increasing temperature in an isobaric system.

The differences in physical properties between supercritical and ambient water are what make SCW a very interesting reaction medium. As the conditions exceed those necessary to allow water's transition to the supercritical state, the relative static permittivity or 'static dielectric constant' falls rapidly from 78.5 at 25°C to approximately 6 just after the critical point due to the drastically reduced number of hydrogen bonds which is a consequence of the high temperature and pressure (Bröll *et al.*, 1999).

A consequence of the reduced hydrogen bonding is that the ionic product of SCW is greatly reduced which in turn results in an approximate reversal of water's behaviour as a solvent. That is, close to the critical point, water provides a rather hospitable medium for the dissolution of non-polar organics and gases (for example, and rather pertinently, oxygen) but has great difficulty in dissolving ionic salts. Increasing the pressure to a much higher degree - e.g. at 420°C, increasing the pressure from 34 MPa to 100 MPa results in a pressure increase from 300 kg m<sup>-3</sup> to 660 kg m<sup>-3</sup> (Fujii *et al.*, 2011) - can result in an increase in density and thus a partial restoration of the fluid's ability to dissolve ionic salts. This behaviour of water is shown in Figure 2.3 for a pressure of 24 MPa.

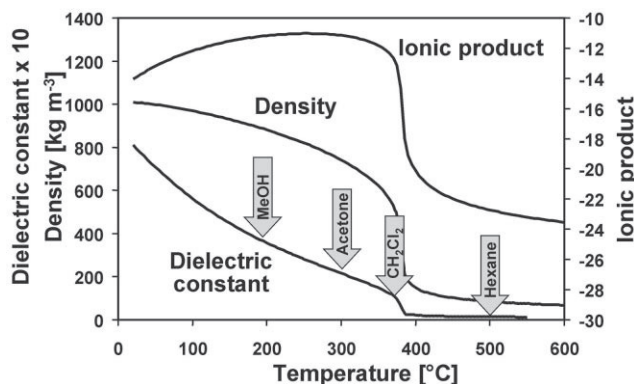


**Figure 2.3** – Density, ionic product and dielectric constant of water versus temperature at a pressure of 24 MPa (Kritzer and Dinjus, 2001).

A comparison of the physicochemical properties of various states of water is given in Table 2.5.

**Table 2.5** – Physicochemical properties of water at various states (Bröll *et al.*, 1999).

	Ambient water	Subcritical water	Supercritical water		Superheated steam
T [°C]	25	250	400	400	400
P [MPa]	0.1	5	25	50	0.1
ρ [g cm <sup>-3</sup> ]	0.997	0.80	0.17	0.58	0.0003
ε	78.5	27.1	5.9	10.5	1
pKw	14.0	11.2	19.4	11.9	-
C <sub>p</sub> [kJ kg <sup>-1</sup> K <sup>-1</sup> ]	4.22	4.86	13	6.8	2.1
η [mPa s]	0.89	0.11	0.03	0.07	0.02
λ [mW m <sup>-1</sup> K <sup>-1</sup> ]	608	620	160	438	55

## 2.2.1 Supercritical Water Oxidation (SCWO)

SCW's solvating behaviour is one of the most important design considerations when evaluating the use of SCWO as a treatment technology. The ability of SCW to form a homogeneous system of water-hydrocarbon-oxygen results in the near-elimination of mass transfer resistances and creates a very efficient environment within which oxidation can take place. Such an effect, coupled with the inherently high reaction temperatures often results in the near-complete removal (>99.99%) of waste material in short residence times of the order <10<sup>2</sup> seconds. In addition to the treatment efficiencies, another significant facet of oxidation in SCW is that even complex (high molecular weight) and recalcitrant compounds can be completely converted to benign compounds such as CO<sub>2</sub>, H<sub>2</sub>O and N<sub>2</sub>.

On the other hand, there are some operational issues that can arise due to the unique properties of SCW. It is perhaps ironic that the properties that are so advantageous when choosing to use water as the reaction medium, e.g. the solvating

ability with regard to non-polar hydrocarbons, are the same properties that are the basis of the technology's perceived disadvantages.

One problematic effect is that if aqueous feeds contain ionic salts, the transition to supercritical conditions causes these salts to precipitate. Once precipitated, the solids aggregate and can form a blockage. This effect is known as 'salt-plugging'. A similar issue arises from the presence of 'heteroatoms', i.e. atoms other than C, H, O and, to a lesser extent, N such as halogens, sulphur and phosphorus which can be converted to their mineral acids ( $\text{HF}$ ,  $\text{HCl}$ ,  $\text{HBr}$ ,  $\text{H}_2\text{SO}_4$ ,  $\text{H}_3\text{PO}_4$ ) during the oxidation process and which are potentially a source of corrosion if not neutralised. This is especially true downstream of the reactor when conditions return to subcritical levels (Marrone and Hong, 2009). These problems and their proposed solutions and/or mitigations are elaborated upon in §2.6.

### **2.2.2 Use of SCWO as a Wastewater Treatment Option**

SCWO technology effectively combines a physical and a chemical process in that the increased temperature and increased pressure create a new environment in which waste can be treated by the addition of an oxidant. However, that is where the similarity with physical processes ends – the physical change in itself does not effect any treatment, rather it provides the environment in which the chemical treatment can proceed. The chemical reaction is the most important part of the process.

The increased understanding of the chemical and engineering issues is resulting in an increasing number of pilot-scale and commercial SCWO plants being operated worldwide (Marrone, 2012). However, encouraging as this may be, the fact unfortunately remains that in an industry worth billions of dollars worldwide, SCWO

technology's market penetration remains so small as to be practically negligible and this is due to its engineering and economic issues.

For SCWO to be viable as a wastewater treatment technology, it needs to be shown that it compares favourably with existing technologies in terms of economics, energy efficiency, and process stability, and/or is either equally or, preferably, more efficient at reducing the contamination in wastewater streams.

### 2.2.3 Treatment of Other Wastes

As well as wastewater treatment, there is the potential for the application of SCWO technology to other forms of waste, in particular solid municipal waste and medical wastes. The technology has even been suggested for deployment in manned spacecraft (Webley *et al.*, 1991). In addition, because of SCWO's ability to avoid the production of noxious by-products which characterise combustion-based technologies, there is the prospect of using the technology to treat military wastes (Veriansyah *et al.*, 2005) and radioactive wastes (Sudhir *et al.*, 1998), which have the potential to generate harmful emissions if not completely degraded.

There are different engineering challenges associated with the treatment of solid wastes when compared with aqueous streams, not least the need to first dissolve the solids before they can be treated.

## 2.3 Current Research into SCWO Reactions

The investigation into the use of SCFs in chemical processes began to intensify in the 1980s (Bröll *et al.*, 1999) making it a relatively new field of engineering research. Water in its supercritical state in particular has been investigated mainly for

its use as a medium for the oxidative destruction of waste streams containing aqueous organics (SCWO) (Kritzer and Dinjus, 2001). The properties of SCW make it particularly suitable for this use in oxidation and as such, as a waste treatment technology in the form of SCWO, it competes with other oxidative processes – mainly wet air oxidation (WAO) and incineration.

Wet air oxidation is a term used when water is employed as the oxidative medium with air as the oxidant, when the temperature is high but lower than the critical point. The pressure is also heightened to avoid energy loss from evaporation, i.e. to maintain the liquid state. Water in this state is referred to as ‘subcritical’ (Li *et al.*, 1991) or on some occasions ‘high temperature liquid water’ (Savage, 2009) wherein the pressure is implied to be high as well as the temperature by the presence of liquid water, or ‘hot compressed water (HCW)’ (Kruse and Dinjus, 2007b). Compounds that have been investigated in terms of their behaviour when oxidised under WAO conditions include butyronitrile (Iyer and Klein, 1997), and more complicated molecules such as biphenol, fluorene, hexadecane and eicosane (Onwudili and Williams, 2007) in which the major intermediates were ketones and carboxylic acids, diethanolamine and morpholine (Mishra *et al.*, 1994), sebacic acid and azelaic acid (Jin *et al.*, 2008), and the oxidation of alkyl naphthalenes to carboxylic acids (Martin *et al.*, 2008).

Brunner (2009a) reviews the use of subcritical water as a reactant in a variety of hydrolysis reactions to decompose compounds such as ethyl acetate, nitriles, methylene chloride, alanine, glycine, cyanamide, dicyanamide, polyvinyl chloride (PVC), and polyethylene terephthalate. Kruse and Dinjus (2007a) offer a similar review investigating the use of subcritical water as simultaneously a reaction medium

and reactant for the decomposition broad classes of compounds including amines, amides, nitriles, and ethers. In particular, they describe esters and ethers and their tendency to form their constituent carboxylic acid and alcohol, or their constituent alcohols respectively.

A good deal of investigation has been carried out into the efficiency of the SCWO process as a treatment protocol, the mechanisms by which this process proceeds, the process' energy efficiency and economic comparisons between the use of SCWO and traditional protocols, e.g. incineration (for solid waste) as an industrial scale treatment option.

## 2.4 Treatment Efficacy, Kinetics, Mechanisms and Pathways

The SCWO of a large number and variety of compounds has been carried out. These compounds range from 'simple', e.g. short-chain aliphatic hydrocarbons, to complex, e.g. hydrocarbons with multiple aromatic groups and heteroatoms. The quantification of the kinetic parameters of the SCWO reaction of these compounds is desirable for two main reasons (Vogel *et al.*, 2003):

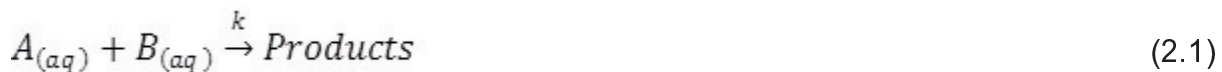
- To be able to verify the accuracy of theoretical models of SCWO processes.
- To aid the design of future SCWO reactor systems.

Evidently, it is desirable to know what happens inside the reactor in both a physical and chemical sense and to be able to model this theoretically greatly enhances the understanding of the SCWO process and informs several necessary operational considerations, especially at a larger scale of operation, e.g. process control. Ultimately however, it is the real-world benefits afforded that makes this research worthwhile. If the ultimate goal is to develop SCWO into a viable – i.e.

chemically and economically feasible – protocol for the treatment of aqueous organic wastes, then it is necessary to be able to solve the engineering issues that currently prevent the wide-scale stepping-up of the technology from lab- and pilot-scale to industrial-scale (Abeln *et al.*, 2001).

The efficacy of SCWO as a treatment protocol has been investigated for a large number of organic compounds of a variety of natures – aliphatic, aromatic, nitrogenated, non-nitrogenated, etc. These investigations also often conduct simultaneous studies into the reaction kinetics.

Most kinetics research involves the evaluation of kinetic parameters, specifically the activation energy and pre-exponential terms of the Arrhenius-type rate equation and the reaction orders of the reactants involved in the process being studied. So, for a reaction of the form:



where A and B are organic and oxidant reactants respectively and  $k$  is the reaction rate constant. Solvable equations representing this system's components can be generated, thus:

$$\frac{d[A]}{dt} = -k[A]^a[B]^b[H_2O]^c \quad (2.2)$$

where  $[A]$  represents the concentration of reactant A and so on;  $a$ ,  $b$  and  $c$  are the orders of each reactant and:

$$k = A \exp\left(\frac{-E_A}{RT}\right) \quad (2.3)$$

where A is a pre-exponential factor whose units vary depending on the order of reaction being modelled,  $E_A$  is the activation energy ( $\text{kJ mol}^{-1}$ ), R is the universal gas constant ( $\text{J mol}^{-1} \text{K}^{-1}$ ) and T is the reaction temperature (K).

Global kinetic parameters for a compound might enable the calculation of how long it should theoretically take for a given quantity of a certain compound to be completely converted to its ideal products; however, this does not paint the whole picture of what is occurring during the reaction. A molecule of methanol will not be converted directly to carbon dioxide and water upon contact with oxygen under supercritical conditions. Indeed, Brock *et al.* (1996) indicated that formaldehyde and carbon monoxide constitute major intermediates with the reaction proceeding thusly:



However, these additional two steps (vis-à-vis the inclusion of formaldehyde and carbon monoxide) are just the tip of the iceberg. The destruction of organic compounds in SCWO proceeds primarily through free radical pathways as a result of water's acting as a non-polar solvent at such conditions (Ploeger *et al.*, 2008). Such behaviour results in complex networks of reversible elementary reactions. Modelling of these networks has been undertaken (simple non-nitrogenated: Brock and Savage, 1995; Brock *et al.* 1996, simple nitrogenated: Kantak *et al.*, 1997; Benjamin and Savage, 2004) with the assumption that SCWO chemistry can be hypothesised to be similar to chemistry that may be observed in combustion reactions at typical SCWO temperatures with the caveat that adjustments must be made for the increased fluid density, increased fluid pressure and the large amount of water present.

For C<sub>1</sub> compounds, these combustion reactions are quite well understood and consequently a network of approximately 22 species (with some being radicals) and approximately 150 reversible elementary reactions can be constructed as given in appendix 1 (Brock and Savage, 1995).

The oxidation of methanol would be generally regarded as a ‘simple’ reaction inasmuch as methanol is the simplest alcohol and is a relatively small molecule. Even so, the number of reactions that should be considered in order to precisely map the global mechanism is rather large, and becomes larger when considering more complex molecules.

#### 2.4.1 Nitrogenated Compounds

Treatment efficacy and mechanisms have been investigated for nitrogenated compounds ranging in complexity from the very simple, e.g. methylamine (Benjamin and Savage, 2004), to the more complex, e.g. 2,4-dinitrophenol (Pérez *et al.*, 2004) pyridine (Sudhir *et al.*, 1999) and quinoline (Pinto, 2004). Investigations have been conducted into the oxidation of Ammonia (Segond *et al.*, 2002), acrylonitrile, acrylamide, fumaronitrile and cyanopyridine (Shin *et al.*, 2009), nitroanilines (Wang *et al.*, 1995), and hydrazine (Plugatyr *et al.*, 2011). Most investigations identify the effects of various reaction conditions on the efficacy of the process in terms of the removal of TOC (or COD) and nitrogen compounds, with some also evaluating kinetics parameters. However, some focus more deeply on the underlying reaction mechanisms, with still further papers looking at modelling the reactions on a more fundamental level.

Benjamin and Savage (2004) studied the effect of temperature and water density on the oxidation of methylamine in a batch reactor under supercritical conditions and suggested potential reaction mechanisms based on the evolved intermediates. They found that methylamine destruction proceeded via both pyrolytic and hydrolytic routes where at lower water densities the pyrolytic path dominated. At water densities higher than  $0.28 \text{ g cm}^{-3}$ , the amount of hydrolysis became more significant and increased the disappearance of methylamine. Work by the same pair (Benjamin and Savage, 2005) assesses the reaction mechanism. This analysis indicates that at most temperatures at which SCWO is performed, the reaction is initiated via hydrogen abstraction by  $\text{OH}^*$  radicals but below  $400^\circ\text{C}$  can proceed via the addition of  $\text{O}_2$  to form  $\text{CH}_3\text{NH}_2\text{O}_2$ . The abstraction reaction likely terminates via the formation of  $\text{CO}_2$ , CO and refractory  $\text{NH}_3$  but can also form  $\text{HNO}_2$ ,  $\text{N}_2\text{O}$ , HCN and (at higher temperatures)  $\text{NO}_x$  as products. They build on the work of Kantak *et al.* (1997) in which the authors present a mechanism comprising 350 different reactions including 65 different species.

Anikeev *et al.* (2004 and 2005) studied the SCWO of nitromethane, nitroethane and 1-nitropropane, and the effect of water density on the rate constant of decomposition of these compounds. They found that the oxidation rate obeyed first order kinetics and increased linearly with increasing aliphatic chain length. They also found a positive correlation between increasing pressure (between 22 and 31 MPa) and the rate constants of decomposition for all compounds.

Tsao *et al.* (1992) investigated the batch hydrolysis reactions of benzaldehyde, benzyl alcohol, benzoic acid and the more complex benzylidenebenzylamine (BBA -

$C_6H_5CH_2N=CHC_6H_5$ ) due to their appearance as intermediates in the SCWO of benzylamine (BA). The reactions were performed at 400°C, 267 bar over a period of 1 – 10 hours with the addition of  $NH_3$  in some experiments to eliminate the formation of tarry products of pyrolysis. They suggest reaction initiation routes for BA hydrolysis/oxidation based upon either the rupture of the CN single bond in an aromatic side-chain to form a radical and an alkylated aromatic or the abstraction of a hydrogen atom to form a CN double bond which can undergo oxidation or decarboxylation. Incidentally, they found that these reactions are catalysed by ammonia. They found that the presence of biphenyl and benzene (which indicate the presence of phenyl radicals) and the presence of bibenzyl, benzyl toluene and toluene (which indicate the presence of benzyl radicals) indicated that BBA was likely formed during the SCWO of BA via a benzyl radical route.

Fenuron [ $C_6H_5-NH-CO-N(CH_3)_2$ ] was oxidised at sub- and supercritical conditions by Aymonier *et al.* (2000). They found COD reductions ranging from 73.8% to 99.9% at temperatures ranging from 200°C to 540°C respectively. They found that all carbon and hydrogen was eventually converted to  $CO_2$  and  $H_2O$  and that all organic nitrogen was converted to  $N_2$ . They showed that fenuron was initially converted to nitrobenzene, nitrate, ammonia and carbonaceous intermediates and that further redox reactions then facilitated the conversion to the final products. They explain ammonia's conversion to  $N_2$  at this relatively low temperature (despite its well-known refractory nature) by redox reaction between ammoniacal nitrogen and nitrate ions.

Kililea *et al.* (1992) studied the SCWO of feeds containing urea and nitrate/nitrite mixtures at 600°C and 23 MPa, and found that nitrogen was converted to N<sub>2</sub> or N<sub>2</sub>O and that gaseous NO<sub>x</sub> compounds were not formed. Their kinetic analysis indicates that reactions in which gaseous NO<sub>x</sub> compounds would be expected to form as products are of the order 10<sup>12</sup> times slower, indicating that SCWO is greatly unfavourable to the production of these compounds.

Sudhir *et al.* (1999) found that conversions of pyridine in excess of 99% could be obtained at temperatures as low as 370°C (marginally sub-critical) in the presence of 10 mg of platinum catalyst in the form of Pt-doped gamma alumina.

One further compound is worthy of mention in this section, but rather than being a ‘nitrogenated organic’, it is the simplest azane, ammonia. Clearly, ammonia contains no carbon, but it is nonetheless widely investigated. Ammonia is produced in most nitrogen-containing waste streams, especially raw and partially-treated waste sludges, as a by-product of hydrolysis (Ploeger *et al.*, 2007; Goto *et al.*, 1999; Kililea *et al.*, 1992). Ammonia has the potential to be (and is) formed in the SCWO of nitrogenated organics as an intermediate (Pinto, 2004). It is a refractory material that is recalcitrant once formed, and difficult to destroy at relatively mild conditions, e.g. close to the critical point of water. Indeed, ammonia generally requires temperatures in excess of 600°C to undergo observable conversions at residence times common to continuous SCWO (i.e. less than 60 s) (Ploeger *et al.*, 2007). Work from Ploeger’s group (Ploeger *et al.*, 2006) indicated that for small concentrations of ammonia of the order of 1 mM, temperatures of 680°C would only result in conversions of 20% in residence times under 10 s, a set of conditions that would routinely return high

conversion rates for less refractory compounds. It was only after increasing the temperature to 700°C that more satisfactory conversions were observed for the same conditions - of the order of 60%. Kililea *et al.* (1992) found that when treating urea at 690°C, ammonia was formed as a by-product but only 41% of the intermediate ammonia was subsequently destroyed. Segond *et al.* (2002) investigated the SCWO of ammonia in an isothermal tubular reactor at high temperature (530 - 630°C) at a range of stoichiometric oxidant ratios. They found that near-complete removal of ammonia was obtained at a temperature of 600°C, pressure of 24.5 MPa, stoichiometric ratio of 1.5 and residence time of 30 s.

The investigation of the use of co-oxidant fuels as an aid to ammonia conversion is discussed in §2.4.4.

The effect of pressure on the hydrolysis of butyronitrile at subcritical temperatures was investigated by Iyer and Klein (1997). They found that the reaction terminated at the production of butanamide, butanoic acid and ammonia and developed a four-step autocatalytic rate model with kinetic parameters for the disappearance of butyronitrile where the autocatalyst is the product, butanoic acid.

A summary of the experimental conditions and some kinetic parameters are given in Table 2.6 below.

**Table 2.6** – Summary of kinetic parameters of selected nitro-organic compounds.

Compound	T K	P MPa	C <sup>o</sup> --	SR --	Time <sup>a</sup> 3 - 30	A $M^{(1-y)} s^{-1}$	E <sub>A</sub> $kJ mol^{-1}$	X --	Reference (1 <sup>st</sup> author)
Acrylonitrile	572-825	25	0.27- 2.1M	0.3- 2.5	3 - 30	$6.1 \times 10^3$	$66.33^{y4}$	0.16 – 0.97	Shin (2009)
BBA	673	26.7	17%	0	1-10 h	--	--	> 0.95	Tsao (1992)
Benzyl Alcohol	673	26.7	17%	0	1-10 h	--	--	0.99	Tsao (1992)
Benzaldehyde	673	26.7	17%	0	1-10 h	$1.6 \times 10^{10}$	$179.1^{y2}$	0.25 – 0.99	Tsao (1992)
Benzoic Acid	673	26.7	17%	0	1-10 h	--	--	0.45 - 1	Tsao (1992)
Butyronitrile <sup>*†</sup>	603	12-25	3.8%	0	0-3 h	$k_1: 0.01-0.12^{y2}, k_3^{y3}: 40-280$	$40-280$	Iyer (1997)	
2,4-Dinitrophenol	742-813	24.5	2.4%	0-2	0 - 25	--	--	0.93 - 1	Pérez (2004)
Fenuron	481-813	25	0.3%	1.3	20-400	--	--	0.74 - 0.99	Aymonier (2000)
Hydrazine <sup>†</sup>	473-725	25	<1000 ppm	0	0 - 100	$19 \times 10^3$	$70.24^{y1}$	--	Plugatyr (2011)
Methylamine	659-773	25	4 - 78mM	0	2 h	$1.3 \times 10^6$	159	0.04-0.45	Benjamin (2004)
Nitromethane	683	23-31	37mM	2.3	0 - 130	$k: 0.055 - 0.0169^{y1}$	$\sim 0.35$	Anikeev (2004/5)	
Nitroethane	683	22-31	29mM	2.9	0 - 130	$k: 0.0052 - 0.0124^{y1}$	$\sim 0.71$	Anikeev (2004/5)	
1-Nitropropane	683	23-32	22mM	3.8	0 - 130	$k: 0.0059 - 0.0142^{y1}$	$\sim 0.79$	Anikeev (2004/5)	
Pyridine <sup>†‡</sup>	643-663	24.2	2mM	13	3.25	--	--	0.5 - 1	Sudhir (1999)
Quinoline	753-923	5-30	0.1- 0.4mM	0.7- 10	4 - 9	$2.7 \times 10^{13}$	$226^{y1}$	0.08 - 1	Pinto (2004)
Ammonia <sup>a</sup>	923-963	23	--	--	--	--	--	0.41 - 0.9	Kililea (1992)
Ammonia	805-873	14-25	0.6 - 9.4mM	0- 9.6	20-120	$4 \times 10^8$	$166^{y5}$	--	Segond (2002)

<sup>o</sup> Percentages are weight percent.<sup>a</sup> Residence times in units of seconds unless stated.<sup>\*</sup> Butyronitrile destruction proceeds via 4-step reaction.  $k_1$  and  $k_3$  describe disappearance of butyronitrile. No conversion data.<sup>†</sup> Partially subcritical conditions<sup>‡</sup> Pt-alumina catalyst – conversion decreased with increasing catalyst particle size

k Specified reaction rate constants

y1,y2,y3 reaction order 1, 2, 3 respectively (contributes to units of A in table)

y4 order of reaction 1.26 with respect to acrylonitrile TOC and 0 with respect to O<sub>2</sub>,

y5 order of reaction with respect to ammonia and oxygen are 0.9 and 0.06 respectively.

a With auxiliary fuel and formed from decomposition of urea.

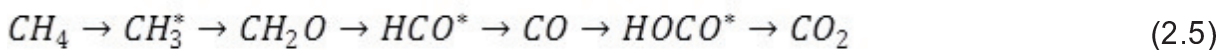
## 2.4.2 Non-nitrogenated Compounds

Kinetic properties have been investigated for the oxidation of a very large number of compounds including: methane (Savage *et al.*, 1998), ethanol (Schanzenbächer *et al.*, 2002), phenol (Pérez *et al.*, 2004), 2,4-dichlorophenol (Lee and Gloyna, 1990), acetic acid (Meyer *et al.*, 1995; Aymonier *et al.*, 2001) polychlorinated biphenyls (Hatakeda *et al.*, 1999),.

Non-nitrogenated compounds constitute the majority when considering those whose oxidation under supercritical conditions has been investigated. A very large number of these compounds can be found in industrial waste streams and as such, their investigation in terms of SCWO has usually primarily been undertaken in order to ascertain whether the waste streams in which these components can be found could be treated via SCWO technology and, if they can, whether the treatment could be practicable on a large scale.

Investigations into some of the simplest hydrocarbons, methane (Sato *et al.*, 2004; Savage *et al.*, 1998), methanol (comprehensive review by Vogel *et al.*, 2005; Fujii *et al.*, 2011) and formaldehyde (Osada *et al.*, 2004) have been carried out on numerous occasions in both batch and continuous reactor configurations in an attempt to completely understand the kinetics. In the majority of cases, it was found that methane conversion is positively correlated with temperature, oxidant ratio, feed concentration and residence time (reaction time for batch operations).

The global reaction for methane can be somewhat condensed to the following main pathway:



where the transitions are facilitated via reaction with radical species (primarily OH<sup>\*</sup>) and O<sub>2</sub>. Brock and Savage (1995) and Savage *et al.* (1998) indicate further routes between CH<sub>3</sub><sup>\*</sup> and CH<sub>2</sub>O that incorporates species such as CH<sub>3</sub>OO<sup>\*</sup>, CH<sub>3</sub>OOH and CH<sub>3</sub>O formed via reaction with HO<sub>2</sub><sup>\*</sup> radical and O<sub>2</sub> due to fuel-lean conditions. Similar mechanism terms to those seen in the oxidation of methane have been found in the oxidation of methanol (Dagaut *et al.*, 1996; Savage *et al.*, 1998) where

methanol is converted to formaldehyde and then eventually to  $\text{CO}_2$  with the dynamics of methanol, formaldehyde, CO and  $\text{CO}_2$  indicated in Figure 2.4 for conditions in Table 2.7, where the solid lines are 1<sup>st</sup> order model predictions.

**Table 2.7** – Conditions for the SWCO of MeOH (Brock *et al.*, 1996).

Temperature, °C	Pressure, bar	Oxidant	$[\text{MeOH}]_0$ mM	$[\text{O}_2]_0$ mM	$[\text{H}_2\text{O}]_0$ M	Residence Time, s
570	246	$\text{H}_2\text{O}_2$	0.65	3.46	4.16	0.1 – 0.8

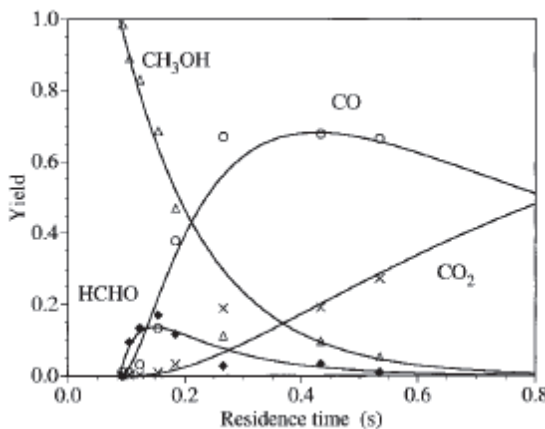


**Figure 2.4** – Dynamics of methanol, formaldehyde, CO and  $\text{CO}_2$  in the SCWO of methanol (Brock *et al.*, 1996).

Brock and Savage's (1995) paper indicates that detailed kinetics modelling of C<sub>1</sub> compounds was predicated on a mechanism that comprised 22 species and 148 elementary, reversible, free-radical reactions between these species, the stipulation for inclusion being that compounds should contain either zero or one carbon atoms along with oxygen and hydrogen. Atmospheric chemistry and combustion literature was used to provide kinetic parameters and were incorporated in a set of 22 differential equations, which could be solved in numerical engines. Similar models

were used by Fujii *et al.* (2011) to explain an observed increase in methanol conversion rate with increasing water density, indicating the importance of water concentration at very high pressures (up to 100 MPa) in the creation of the OH\* radical.

The removal of formaldehyde in a batch reactor was performed by Osada *et al.* (2004). At 400°C, a water density of 0.5 g cm<sup>-3</sup> and a reaction time of 30 minutes, 90% removal of formaldehyde was observed. The reaction progressed further in terms of fewer liquid intermediates (CH<sub>3</sub>OH, HCHO) when the density was reduced to 0.17 g cm<sup>-3</sup>.

Lee and Gloyna (1990) investigated the oxidation of acetic acid in a batch reactor and compared the use of hydrogen peroxide and molecular oxygen as the oxidant. They investigated temperatures of 400, 450 and 500°C, and oxidant ratios of 1, 2, 3, 4 and 5 times those required by stoichiometry were investigated at 450°C. They also investigated two particular densities: 0.15 and 0.35 g ml<sup>-1</sup> and reaction times between 5 – 30 minutes. Under isothermal conditions, these would correspond to pressures of approximately 30 and 46 MPa respectively (NIST). They found that acetic acid conversion increased with temperature and residence time with rapid conversion occurring at the beginning of the reaction. H<sub>2</sub>O<sub>2</sub> was much more efficient an oxidant, likely due to production of OH\* radicals. At a density of 0.15 g ml<sup>-1</sup>, 400°C and a reaction time of 5 minutes, H<sub>2</sub>O<sub>2</sub> was 8 times as efficient an oxidant as O<sub>2</sub>. An acetic acid conversion of 97.5% was achieved with H<sub>2</sub>O<sub>2</sub> at 500°C, 0.15 g ml<sup>-1</sup> and at a reaction time of 10 minutes. At the same conditions but at a reaction time of 30 minutes, O<sub>2</sub> only managed to facilitate a conversion of 64.3%. Increasing the oxidant

ratio for H<sub>2</sub>O<sub>2</sub> only had an effect at levels of up to 300% oxidant. They conclude that a change in density only caused a very small increase in the conversion and was thus defined as negligible in comparison to the other effects, however at 400°C and for reaction times of 15 and 30 minutes, this increase was 12.6 and 9.5% respectively. It was unclear why such an increase was classified as negligible. Aymonier *et al.* (2001) treated the same compound in a quasi-adiabatic tubular reactor in three experiments (labelled A1, A2 and A3, which is the order of data stated hereafter) at an initial temperature of 400°C, 25 MPa and residence times of 43.2 s, 26.4 s and 24.6 s. The change in residence time was a function of changing oxidant (H<sub>2</sub>O<sub>2</sub>) delivery flowrate with the organic flowrate remaining constant (where the concentration of the acetic acid at the reactor inlet was thus 3.35%, 3.92% and 4.90% (w/w) respectively). They reported conversions of 30.5%, 98.4% and 96.9% respectively, however, rather than to discuss treatment efficiency or reaction kinetics, the experiment was performed to assess the heat of reaction. The nature of the reactor meant that the exothermic oxidation reaction caused temperature profiles within the reactor as indicated in Figure 2.5 that resulted in peak temperatures of 438°C, 558°C and 568°C respectively.

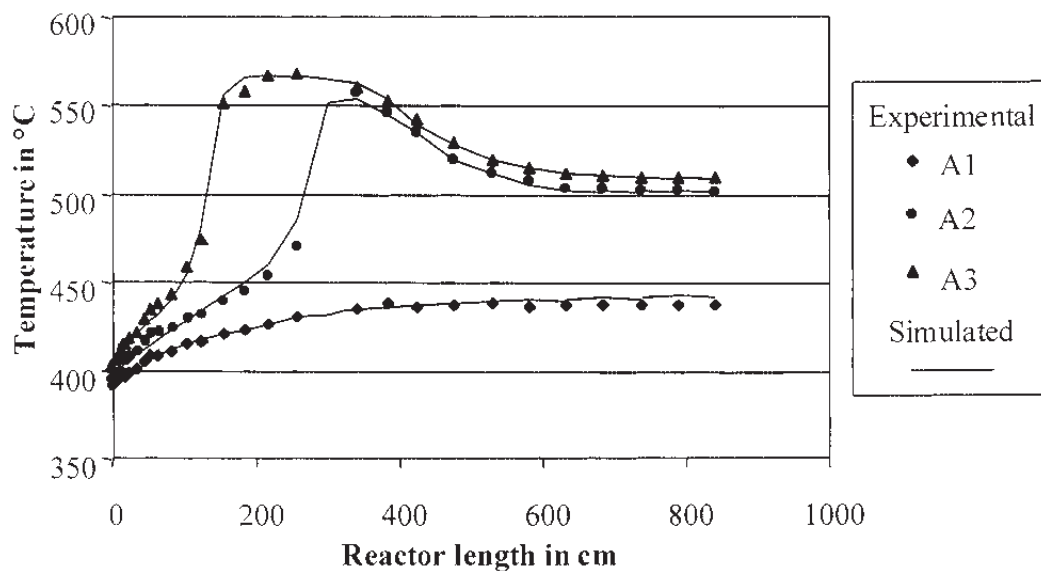


**Figure 2.5** – Temperature profile in quasi-adiabatic tubular reactor during SCWO of acetic acid (Aymonier *et al.*, 2001).

The plot indicates that the 2 experiments with the higher acetic acid concentrations managed to exceed a temperature threshold that resulted in much higher reaction rates and subsequently much higher conversions. The data from these experiments allowed the calculation of the heat of reaction as  $-925 \text{ kJ mol}^{-1}$ . Two-dimensional CFD modelling of heat transfer in a tubular reactor immersed in a fluidised sand bath was conducted by Moussiére *et al.* (2007) in the two stage SCWO reaction of dodecane where acetic acid is an intermediate. They found that the reaction inlet temperature greatly influenced the reaction rate.

The oxidation of phenol has been a relatively popular investigative route to traverse due to phenol's ubiquity in industrial wastewater streams (Thornton and Savage, 1990), and the facts that it is one of the simplest aromatic compounds and has a functional group (OH). Research in this area therefore has applicability to the study of phenol's oxidation kinetics and the use of phenol as an analogue compound

both for industrial waste streams and for intermediate compounds formed during the oxidation of more complex compounds. The SCWO of phenol in both a tubular reactor (Thornton and Savage, 1990; Fourcault *et al.*, 2009; Pérez *et al.*, 2004; Oshima *et al.*, 1998) and in a batch reactor (Koo *et al.*, 1997) has been investigated at a variety of temperatures, pressures, oxidant ratios and residence times. Some experiments have also been conducted at subcritical temperatures.

Thornton's work indicated a variety of phenol conversions ranging from 0 – 20% when the pressure was subcritical, the phenol feed concentration was very small, or when there was a large oxygen deficit (e.g. 15% of that required by stoichiometry). The conversion approached 100% at high residence times, high oxidant ratios, and/or high temperatures. Varying combinations of these conditions also resulted in varying conversions between these extremes. Residence time, reactor temperature, reactor pressure and oxidant ratio were all shown to be positively correlated with the phenol conversion. These effects with regard to temperature, residence time and oxidant ratio were also seen in Pérez *et al.*'s work. They concluded that the feed concentration had little effect on phenol removal. The effect of reactor pressure was not investigated.

Thornton's work indicated that a multitude of organic intermediates were formed during the reaction with some identified using gas chromatography-mass spectroscopy (GC-MS) that were larger than the original phenol molecule. These ranged from bi-substituted phenols (i.e. where another hydroxyl group had been substituted into the benzene ring, e.g. catechol (2-substitution), resorcinol (3-substitution), hydroquinone (4-substitution)), to m-phenoxyphenols, dibenzofuran and

2,2-biphenol. The variety of hydroxyl-substituted species would be consistent with a mechanism predicated on the hydroxyl radical. Other intermediates included various carboxylic acids ranging in complexity from formic acid to succinic acid and maleic acid, p-benzoquinone and carbon monoxide. Plots of some intermediates during oxidation with conditions of  $380^{\circ}\text{C}$ ,  $278\text{ atm}$ ,  $250\text{ ppm}$  phenol and 250% excess oxygen were given as shown in Figure 2.6.

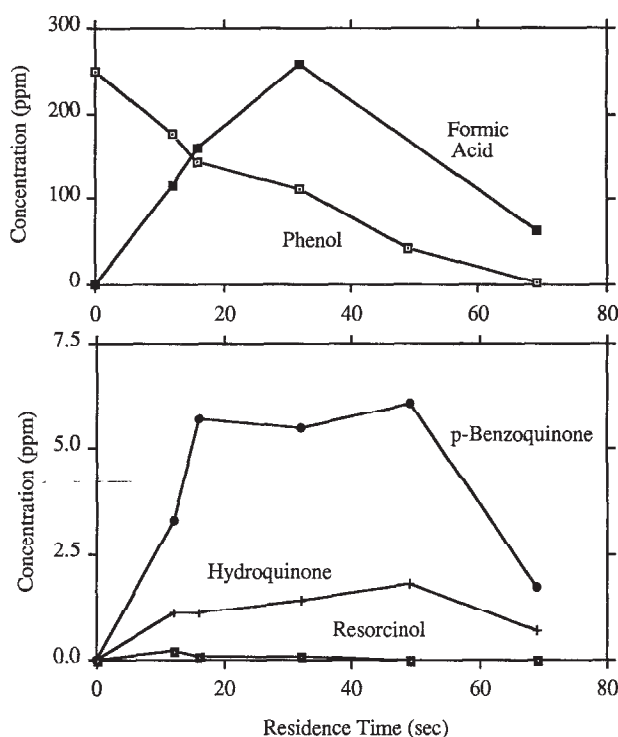


**Figure 2.6** – Variation of selected phenol oxidation with time (Thornton and Savage, 1990).

The fact that the phenol concentration consistently decreases whereas the concentrations of the other compounds increase to a maximum and then decrease indicates the prevalence of parallel sets of series reactions. The only intermediate specified in Pérez' group's work was carbon monoxide. Koo *et al.* (1997) assert that the oxidation of phenol is likely initiated and propagated by parallel reactions in which  $\text{O}^*$  reacts with both phenol and water in their system in which they use gaseous

oxygen as an oxidant. Upon the atomic oxygen radical's reaction with water, OH\* radicals are formed as follows.



These newly-formed OH\* radicals are also free to react with phenol. Thus as well as the reaction being parallel in terms of O\*, it is also parallel in terms of phenol, thus:



However, the rate constant of equation 2.6 is smaller than those of equations 2.7 and 2.8 by a factor of about 10<sup>2</sup> and gas phase combustion chemistry suggests that the splitting of O<sub>2</sub> to O\* radicals proceeds very slowly relative to the consumption of O\* (Tsang and Hampson, 1986) implying that other interactions may also be driving the oxidation reaction in terms of the initiating radical formation.

Thornton *et al.* (1990)'s work indicates that a variety of potentially complex molecules should form as intermediates after these two radical precursors, however, aside from the calculation of kinetic parameters of these kinetic parameters via regression from previous work, they make no further analysis of intermediate reaction products. Thornton's paper also analysed the liquid effluent for trace amounts of corrosion products. In their apparatus, the high temperature sections were made of Hastelloy C-276 and type-316 stainless steel was used for the other sections. They detected iron, chromium and cobalt. Iron and chromium are present in both alloys. They note that nickel, the primary metal in Hastelloy was not detected, but concluded that relatively low levels of corrosion may have been occurring.

Koo *et al.* (1997) found that the conversion of phenol varied between 11 – 99% corresponding primarily with the residence time range of 12 – 120 s. However, the phenol conversion was also positively correlated with oxidant ratio and temperature. They calculated the reaction order of phenol to be unity, indicating that increasing reaction rate is positively correlated to increasing phenol concentration. Koo's group's work also investigated the effect of system pressure. The effect of pressure is often difficult to separate from the effect of density. Possible explanations for this are that water participates directly as a reactant or that changes in the water concentration change the total system pressure, due to water being by far the majority component in the system (thus the partial pressure is only slightly less than the system pressure). Inert helium gas was used to change the reactor pressure. The results indicated that the system pressure had no clear influence on the reaction rate. This effect is partially corroborated by work by Thornton *et al.* (1990) in which increasing the pressure also increased the final phenol conversion, but the initial rate at which this conversion occurred remained largely constant. Oshima *et al.* (1998) found from experiments at temperatures close to the critical point that the phenol oxidation reaction was almost first order in phenol and order 0.48 with respect to the oxidant.

A summary of the experimental conditions and some kinetic parameters are given in Table 2.8 below.

**Table 2.8** – Summary of kinetic parameters of selected organic compounds.

Compound	T K	P MPa	C <sup>o</sup> --	SR --	Time <sup>^a</sup>	A $M^{(1-y)} s^{-1}$	E <sub>A</sub> $kJ mol^{-1}$	X --	Reference (1 <sup>st</sup> author)
Acetic Acid	748-873	24.6	1- 2mM	1-5.5	3.7-10	$7.9 \times 10^9$	$168^{y1}$	0.08 - 1	Meyer (1995)
Ethanol	706-667	24.6	1mM	0.5-1	2-12	$1.3 \times 10^{11}$	$164^{y1}$	0.02-0.17	Schanzenbächer (2002)
Methane	673	20-35	0.3M	0.03	30-110	--	--	0.5%- 2.3%	Sato (2004)
Methanol									Brock (1996)
Phenol	666-778	25	2.7% -4% 250-	0-36	29-61	--	--	0.25 - 1	Pérez (2004)
Phenol	573-699	19-28	1000 ppm	1-4	4-110	303	$51.8^{y2}$	0 - 1	Thornton (1990)
Phenol	653-713	19-27	828 ppm	1-17	10-100	$89 \times 10^3$	$99.6^{y1}$	0.1 - 0.95	Koo (1997)

<sup>o</sup> Percentages are weight percent.<sup>a</sup> Residence times in units of seconds unless stated

y1,y2, reaction order 1, 2 respectively (contributes to units of A in table)

### 2.4.3 Heteroatom-containing Compounds

The investigation of organic compounds containing heteroatoms is an important facet to the assessment of the suitability of SCWO technology as a waste treatment protocol. The ideal SCWO reaction scheme of organics comprising solely carbon, hydrogen and oxygen results in the production of CO<sub>2</sub> and H<sub>2</sub>O. However, the inclusion of heteroatoms such as chlorine and sulphur can be a little more problematic. Domestic and industrial waste streams frequently include compounds containing heteroatoms and so their fate in the SCWO process has been investigated in order to determine both the ability of the technology to break down these components and the fate of the heteroatoms themselves. The compounds that these species form during treatment are not as benign as the products that arise when heteroatoms are absent and as such, the fate of these atoms should be assessed in order to ascertain whether it is necessary or desirable to treat the product streams

further such that they will adhere to standards as detailed in §2.1. Commonly-investigated organo-heteroatoms are chlorine, e.g. in the form of chlorobenzene (Svishchev and Plugatyr, 2006), 2-chlorophenol (Lin and Wang, 2001), 2,4-dichlorophenol (Lee and Gloya, 1990), and sulphur, e.g. in the form of thiodiglycol (Lachance *et al.*, 1999); Veriansyah *et al.*, 2005).

The SCWO of thiodiglycol (TDG –  $[\text{HOC}_2\text{H}_4]_2\text{S}$ ) was investigated by Veriansyah *et al.* (2005). They chose TDG both because it is a refractory product of the hydrolysis of HD mustard, a vesicant (blister agent) (Munro *et al.*, 1999) and because it has the same C-S bond arrangement and similar density of HD mustard, which is the chlorinated version of TDG. The structural similarity to HD mustard means that the treatment of TDG could be seen as analogous to the destruction of this harmful chemical agent. Rather than focusing on the kinetics of TDG disappearance, they monitored the kinetics of the sulphur heteroatom by observing the total organic carbon (TOC) removal because it follows that if all TOC is removed, no organic sulphur can remain.

The results indicated that after SCWO treatment in a continuous flow tubular reactor at a pressure of 25 MPa, for the temperature range of 397 - 617°C, at an oxidant excess of up to 4.4 times stoichiometry, and for residence times of 9 – 40 seconds, TOC conversions were >90%. This conversion was in excess of 99.99% for temperatures in excess of 600°C. Figure 2.7 indicates the removal of TOC for TDG with increasing residence time as a function of temperatures up to 500°C.

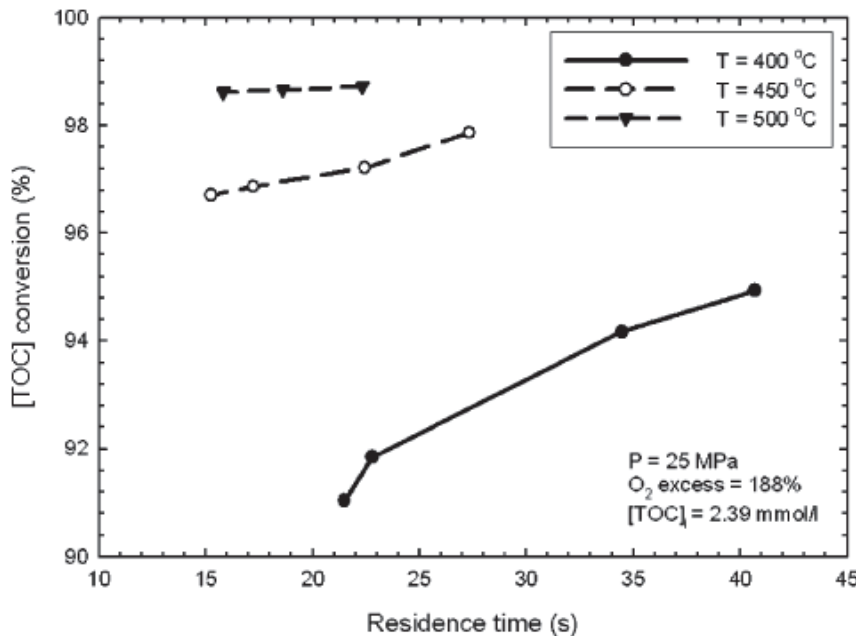


**Figure 2.7 – TOC removal during SCWO of TDG (Veriansyah *et al.*, 2005).**

From the data acquired, it was shown via model that for the more extreme conditions, i.e. for temperatures above 600°C and an oxidant concentration of 150% of that required by stoichiometry, >99.99% could be achieved in residence times less than 30 s. The sulphur-containing waste products detected were sulphuric acid ( $\text{H}_2\text{SO}_{4(\text{aq})}$ ) in the liquid phase and hydrogen sulphide ( $\text{H}_2\text{S}$ ) in the gas phase. Sulphur balances indicated that at least 95% of all sulphur was accounted for in these two compounds. Comments on the potentially corrosive effect of the acidic compounds in the reactor effluent on the process hardware were beyond the scope of the paper. Lachance *et al.* (1999) found that the SCWO of TDG was likely to result in complete conversion to  $\text{CO}_2$ ,  $\text{H}_2\text{O}$ , molecular sulphur and some sulphates within seconds at temperatures as low as 400°C. The formation of sulphates would imply the formation of sulphuric acid as a product but no comment on the engineering issues pertaining to the formation of this salt was made.

The oxidation of polychlorinated biphenyls (PCBs) was investigated by Hatakeda *et al.* (1999) and Izsaki *et al.* (1990 – as described by Mishra *et al.* (1995)) although Izsaki's group's work was at subcritical conditions where the hydrolysis was assisted with the addition of a 20% NaOH solution resulting in near complete PCB conversion at 30 minutes residence time. Hatakeda's group oxidised 3-chlorobiphenyl (3-PCB), a mono-substituted biphenyl and Kanechlor KC-300, of which the average molecular weight of 266.5 Da indicated that between three and four chlorine atoms were present in each compound, with assay tending towards trichlorinated biphenyl. Oxidation reactions were performed in both batch- and continuous-reactor systems at supercritical conditions. Within the batch system, a comparison of H<sub>2</sub>O<sub>2</sub> and pure O<sub>2</sub> as the oxidant was also conducted. At 400°C, 30 MPa and 5 minutes residence time it was found that the conversion of 3-PCB using hydrogen peroxide and oxygen was 95% and 20% respectively. This indicated that it was likely that the oxidation of 3-PCB proceeded via a free-radical mechanism initiated by the presumed decomposition of H<sub>2</sub>O<sub>2</sub> to OH\* radicals. When a reaction temperature of 450°C and a residence time of 30 minutes were the conditions, the 3-PCB conversion was increased to 99.999% when using H<sub>2</sub>O<sub>2</sub> while with O<sub>2</sub> the conversion did not exceed 40%. H<sub>2</sub>O<sub>2</sub> was used in all continuous-reactor experiments and it was found that at 400°C and 30 MPa, >99% of 3-PCB was oxidised within 10.7 – 101.7 s and >99% of KC-300 was converted within 11.8 – 12.2 s. An experiment at 56% of oxidant stoichiometry indicated that approximately 22 reaction intermediates are generated (and potentially destroyed) during the reaction, with m-chlorobiphenyls, biphenyl, other chlorinated aromatics, chlorinated dibenzofurans, dibenzofuran and acetophenone among the intermediate by-products. Chlorine in these systems is

converted to HCl which becomes  $\text{HCl}_{(\text{aq})}$  when the conditions are favourable for solubility. As such, the reactor was made of Hastelloy C-276 in order to minimise the effect of corrosion. Analysis of the effluent indicated that minute quantities of iron, nickel, molybdenum, chromium and cobalt were present. All of these metals are present in Hastelloy C-276 indicating that some surface corrosion had occurred. This can be compared with the work of Thornton and Savage (1990) where they oxidised phenol, i.e. without chlorine substitution. They saw much less corrosion, despite some reaction intermediates that would have been analogous to those seen in Hatakeda's group's work. This difference in corrosion rates is very likely to be due to the presence of the chlorine heteroatom.

Sun *et al.* (2007) investigated the dechlorination of o-chlorophenol (o-CP) in SCW. As already stated, the SCWO of chlorinated compounds can be very problematic due to complications arising from corrosion, and although work investigating the effect of the addition of catalysts containing  $\text{Cu}^{2+}$  and  $\text{Li}^+$ ,  $\text{Na}^+$ ,  $\text{K}^+$ ,  $\text{Ca}^{2+}$ ,  $\text{Fe}^{2+}$  and  $\text{Fe}^{3+}$  on the conversion of chlorinated compounds (Sun *et al.*, 2007) impregnated on various zeolite structures (Lin and Wang, 2001) showed that the formation of unwanted intermediates including polycyclic aromatics was reduced, the corrosion issues remained very severe. Consequently, Sun *et al.* (2007)'s work focused particularly on introducing an initial dechlorination step prior to the oxidation reaction. They found that the introduction of potassium- or sodium-based alkalis (from potassium hydroxide, potassium carbonate, sodium hydroxide and sodium carbonate) facilitated dechlorination of o-CP through 2 pathways: hydrolysis (replacement of –Cl with –OH) and hydrodechlorination (removal of –Cl group through a radical mechanism) as shown in Figure 2.8 producing catechol and

resorcinol (1,2- and 1,3-diphenol – from hydrolysis) and phenol (from hydrodechlorination).

They concluded that a dechlorination step involving the addition of an alkali before the oxidation reaction could reduce the corrosion problems experienced by the SCWO of chlorinated compounds. They found that potassium alkalis promoted dechlorination better than sodium alkalis.

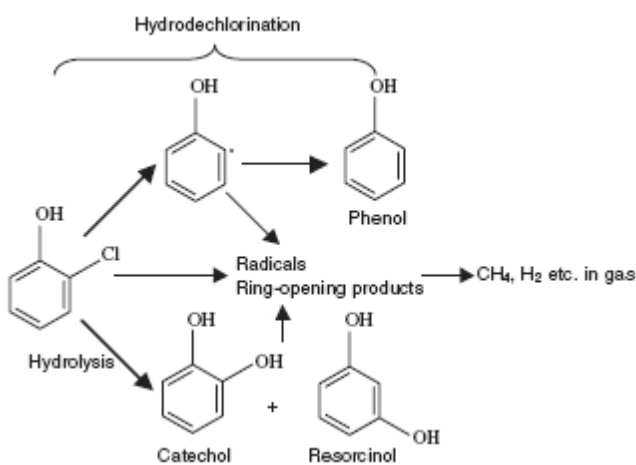


**Figure 2.8** – Dechlorination reaction pathways (Sun *et al.*, 2007).

They don't however comment on the fate of metal chloride salts, the precipitation of which they acknowledge as a terminator of the free-radical reaction chain. The issues surrounding salt precipitation are discussed in §2.6.1 but suffice to say that salt-plugging problems could potentially occur in any dechlorination step and the chloride salts in the product stream would have to be removed via another unit operation before the dechlorinated organics could be passed to the oxidation step.

A summary of the experimental conditions and some kinetic parameters are given in Table 2.9 below.

**Table 2.9** – Summary of kinetic parameters of selected heteroatom-containing organic compounds.

Compound	T K	P MPa	C <sup>o</sup> --	SR --	Time s	A $M^{(1-y)} s^{-1}$	E <sub>A</sub> $kJ mol^{-1}$	X --	Reference (1 <sup>st</sup> author)
2,4-Dichlorophenol	450-500	30-36	0.2%	1-5	45-120	--	--	0.34-1	Lee (1990)
Polychlorinated Biphenyl	473-723	30	0.9%	0.5-2	11-101	--	--	0.63-1	Hatakeda (1999)
Thiodiglycol	670-890	25	1.8-21mM	1.1-4.4	9-40	$1.6 \times 10^2$	$41.53^{y1}$	0.94-1	Veriansyah (2005)

<sup>o</sup> Percentages are weight percent.

y1 reaction order 1.1 (contributes to units of A in table)

#### 2.4.4 Co-oxidation Reactions

The term ‘co-oxidation reaction’, as far as this work is concerned, describes systems in which there are two or more organic species that are oxidised simultaneously. That said, aqueous feed mixtures that have more than three distinct organic components will be termed ‘complex wastes’ and will be discussed in §2.5. This is because the more complex a waste becomes in terms of the number of components, the more the investigation of its oxidation can be deemed analogous to the oxidation of an industrial wastewater. It is thus useful to deal with these investigations separately.

Co-oxidation reactions have been investigated for a variety of reasons. Some are for the investigation of basic feasibility of SCWO when the complexity of the organic feed rises above that of simple single-component solutions, some for the investigation of the removal of specifically recalcitrant compounds such as ammonia (Ploeger *et al.*, 2007; Oe *et al.*, 2007; Ploeger *et al.*, 2008), some to investigate the addition of a fuel as an aid to the oxidation reaction, and some to verify that models

that were formulated to simulate the more simple systems, e.g. for C<sub>1</sub> containing compounds, are accurate for more complex systems, such as for methane/methanol mixtures (Savage *et al.*, 2000) in which the models created contain terms for both compounds and therefore should be able to predict their dynamics during co-oxidation.

As described in §2.4.1, ammonia has been studied often and is one of the more refractory and recalcitrant compounds studied. Its popularity as a compound of investigation stems from the fact that it is evolved in almost all SCWO involving a nitrogenated organic but is usually only partially destroyed after it is generated unless the conditions are extreme. The formation of ammonia is the rate limiting step in the overall oxidation of nitrogen (Webley *et al.*, 1991). The addition of simple aliphatic organics to the reaction system in order to investigate the effect on ammonia destruction has been increasingly carried out since about 2007. Methanol (Oe *et al.*, 2007; Webley *et al.*, 1991), ethanol (Ploeger *et al.*, 2007; Ploeger *et al.*, 2008) and isopropyl alcohol (Cocero *et al.*, 2000; Bermejo *et al.*, 2008) have all been investigated as auxiliary fuels. The addition of methanol can be very beneficial to the oxidation of ammonia, however there are induction periods that must be taken into account. Webley *et al.* (1991) added methanol to ammonia. In two experiments, the temperature was 530°C and the pressure was 24.58 MPa, the C/N fractions were 0.81 and 0.77 and the residence times were 6.7 s and 9.5 s respectively. This work found that the NH<sub>3</sub> conversion did not exceed 7.0%. However, Oe *et al.* (2007) ran several experiments at temperatures in excess of 560°C and residence times in excess of 60s at varying C/N fractions and found that the conversion of ammonia was in excess of 99.85% in all cases except when no methanol was added, when it

was 97.2%. They suggest that for the first 10 seconds, the conversion of methanol allows the building of a pool of radical species and CO which both feature in the oxidation mechanism for ammonia. After this period, the rate of ammonia conversion is able to increase due to the presence of these assistive species.

A similar conclusion is reached in work by Ploeger *et al.* (2007 & 2008) in which they use ethanol as an auxiliary fuel in a tubular reactor. They found that NH<sub>3</sub> conversion increased with increasing temperature and initial ethanol concentration with maximum conversion of 75% at 700°C, 241 bar, 6.4 s residence time and with 95% of the oxidant required for complete oxidation of all ammonia and ethanol.

The use of isopropyl alcohol (Cocero *et al.*, 2000) as an auxiliary fuel for ammonia oxidation was found to aid conversion. Optimal conditions for ammonia conversion were found to be 25 MPa, 43 s residence time and reaction temperature of 570-600°C at which the maximum ammonia removal of 99% and minimum concentration of nitrites and nitrates were observed. The conversion of ammonia was greater than 98% regardless of the initial feed concentration of ammonia. Cocero's group's work indicated that at temperatures in excess of 670°C resulted in the detection of NO<sub>x</sub> in the gaseous product. This result was partially in agreement with Kililea *et al.* (1992) in which an investigation into the oxidation of urea showed that the production of NO<sub>x</sub> is unfavourable at temperatures of 600°C or lower.

As well as the oxidation of ammonia, Cocero's group's work also used isopropyl alcohol as an auxiliary fuel for the oxidation of aniline, acetonitrile and pyridine. They found that the maximum conversions of N and TOC and the optimal conditions at which these conversions were achieved were similar to those seen during the oxidation of ammonia, indicating that regardless of the types of molecules

and nitrogen bonds, similar results could be achieved via SCWO when isopropyl alcohol was employed as an auxiliary fuel. Bermejo *et al.* (2008) have also used isopropyl alcohol as an auxiliary fuel for the SCWO treatment of feeds with a high concentration of ammonia (up to 7 wt.%). They found that complete removal of ammonia was possible at all concentrations up to this highest value with stoichiometric air input and at residence times of 40 s. The temperatures necessary to effect the highest possible ammonia conversions increased with increasing feed ammonia concentration from 710°C at 1 wt.% to 780°C at 7 wt.%. These temperatures also yielded the lowest concentrations of nitrate and acetic acid, indicating the most advantageous oxidation conditions. It was noted after conducting simulations that the observed reaction rate was faster than those quoted in literature. This effect was attributed to either: enhancing of reaction by IPA and associated radicals, catalytic effect of the Ni-alloy from the Inconel 625 reactor, or the geometry of their reactor (cool-wall continuous-flow packed-bed) eliminating the induction time. They state this third reason to be the most probable.

#### **2.4.5 Treatment of Specific Wastes**

Some wastes exist for which there is currently no satisfactory industrial treatment. Spent ion exchange resins are an example of such a waste (Leybros *et al.*, 2010). Ion exchange resins are used in nuclear power plants to remove radioactive contaminants from wastewater streams and to reduce corrosion (IAEA, 2002). As such, these resins become radioactive. They are currently disposed of via combustion, which although having adequate treatment rates and decontamination factors in terms of the level of radioactivity, is not a completely satisfactory solution due to the necessity of employing gas treatment unit operations downstream of the

incinerator to prevent the emission of harmful substances including radionuclides such as Caesium-137 and Ruthenium-106. Leybros' paper investigated the use of SCWO as a treatment for these resins. They measured the TOC removal of the resins to be between 95-98% and found that the most complex components (e.g. the polystyrenic structures) were degraded into simpler compounds such as benzoic acid, phenol and acetic acid. However, some nitrogen-containing heterocyclic compounds remained undegraded. Sulphur present in the feedstock was converted into sulphate ions. Unfortunately, their work is ambiguous as to whether the industrial resins that they treated contained radionuclide contaminants and, if they did, what the fate of these radionuclides was. It is implied that SCWO provides a very promising treatment option to the resin structure, which could result in the elimination of the need to employ incineration. As a result of the removal of this unit operation, radionuclide emission to the atmosphere could be reduced and the waste stream from the treatment of these resins could undergo more targeted treatment to address the radioactivity-oriented issues.

## 2.5 Treatment of More Complex Wastes

As well as the investigation of the reaction kinetics of single-component oxidations and bi- and tri-component co-oxidations, there has also been lab- and pilot-scale research into what happens when multi-component real waste samples are treated using SCWO.

The lab- and pilot-scale treatment of these real wastes is very important in assessing the potential efficacy of SCWO as a treatment protocol when applied to industrial-scale operations. The quantification of the removal of TOC, COD, nitrogen

compounds and other species of interest allows predictions on the efficiency of the treatment but the ability to constantly monitor the apparatus allows the identification of engineering issues that may occur at the reaction conditions such as extensive corrosion.

The SCWO of a dyehouse wastewater has been investigated at lab-scale at a temperature range of 400-600°C and a residence time range of 8 – 16 s (Sögüt and Akgün, 2010). The wastewater that they treated was from a Turkish textile drying plant and contained several complex coloured dye compounds - most of which were multi-ring aromatics - dimethyl cocobenzyl ammonium chloride as a surfactant and acetic acid as a pH regulator. The reactor feedstocks were the samples as supplied, i.e. without dilution, although these were of relatively low concentration (TOC: ~860 mg litre<sup>-1</sup>; total nitrogen: ~118 mg litre<sup>-1</sup>). Some trace metals (in decreasing concentration: calcium, iron, lead and chromium) and solids (~0.5 g litre<sup>-1</sup>) were also present in the feedstock. The case study mentions no engineering issues apart from to say that solid particles managing to progress far enough downstream are caught by a filter placed before the BPR. No corrosion or plugging problems were reported, even though the potential would have been present due to chloride, phosphate and methyl-bisulphate ions in the feed. Presumably, solid particles that they described as being caught by a filter upstream of the BPR would also have the potential of agglomerating and eventually forming an obstruction. The work makes no mention of the rate of build-up that was experienced at these filters, nor does it comment on whether solid particles downstream of the reactor would be expected at an industrial scale.

TOC removal efficiencies ranged from 92% - 100% with the effect being positively correlated with increasing temperature. Significant TOC removals of up to 93.8% were also achieved at a higher still temperature of 650°C via thermal degradation (i.e. without oxidant addition). The removal efficiencies quoted under SCWO coupled with the lack of engineering problems reported indicates that SCWO is a promising treatment protocol for dyehouse wastewaters.

Pilot-scale SCWO of semi-synthetic cutting fluids (Biocut® and Servol®) has been carried out at the University of Cádiz using H<sub>2</sub>O<sub>2</sub> as an oxidant in the temperature range of 400–500°C, pressure of 25 MPa and oxidant excess. The oils were originally composed of water, mineral or synthetic oils, tensioactives and other additives, which are usually anticorrosion compounds. The concentration of these components varied between the two fluids. When used in the metalworking industry, these oils are diluted in-situ with deionised water, forming an emulsion which dissipates heat from the cutting interface, eventually generating a complex oily, aqueous waste after long use (Sánchez-Oneto *et al.*, 2007). The elemental composition of the two oils as provided in their paper was as shown in Table 2.10.

**Table 2.10** – Composition of cutting oils (Sánchez-Oneto *et al.*, 2007).

Elemental Analysis (wt.% dry basis)	Biocut®	Servol®
C	70.10 ± 0.42	45.56 ± 3.99
H	16.54 ± 2.61	17.75 ± 0.57
N	0.26 ± 0.05	3.22 ± 0.28
S	0.36 ± 0.04	0.28 ± 0.01
Others (rest to 100%)	12.74	33.19
COD (g O <sub>2</sub> g <sup>-1</sup> conc. Cutting fluid)	2.264 ± 0.041	3.105 ± 0.031

Since the current treatment methods of these oils (evaporation, filtration, phase separation) are either inefficient or environmentally unsound, SCWO was

investigated as a treatment protocol. As well as investigating the treatment efficiency, the kinetics of the oxidation reaction were also studied. They found that the TOC removal increased with increasing temperature up to 97.0% for Biocut® and 97.9% for Servol® at residence times of 34 s and 9.7 s respectively. They also showed that the TOC removal kinetics for Servol® obeyed a pseudo-first order model of the form:

$$-r_{TOC} = -\frac{d[TOC]}{d\tau} = 4.851 \times 10^5 \exp\left(-\frac{90,300}{RT}\right) [TOC] \quad (2.9)$$

Whereas for Biocut® a two-stage model was required of the form:

First step:

$$-r_{TOC} = -\frac{d[TOC]}{d\tau} = 9.257 \times 10^5 \exp\left(-\frac{90,300}{RT}\right) [TOC] \quad (2.10)$$

Second step:

$$-r_{TOC} = -\frac{d[TOC]}{d\tau} = 5.905 \times 10^5 \exp\left(-\frac{106,900}{RT}\right) [TOC] \quad (2.11)$$

The first stage corresponded to a fast elimination where most of the organics were oxidised, followed by the second step where the rest of the compounds were slowly oxidised. Experimental data for their system implied that the demarcation between the two regimes occurred at approximately 15 – 20 s residence time. These models only apply to oxidant-excess systems.

They conclude that SCWO would be an effective protocol for the treatment of cutting fluids in terms of its ability to degrade the waste, but that its economical suitability is difficult to assess. This is partially due to the fact that alternate oil

formulations would have to have their kinetics parameters separately assessed, and partially due to the fact that operational costs of SCWO are influenced by the ability to recover energy from the process. This is not feasible for more diluted aqueous wastes (with a heating value less than  $930 \text{ kJ kg}^{-1}$ ), which don't produce effluent temperatures high enough to allow preheating the feeds to the required temperature. Thus the heat-exchanger service fluid would have to be heated via other means, reducing the energy efficiency of the process as a whole (Sánchez-Oneto *et al.*, 2007).

## 2.6 Treatment Problems and Reactor Design

As touched upon in §2.2.2, scaling up to industrial treatment requirements introduces engineering and constructive challenges that aren't necessarily impinged upon in the SCWO of single compounds or dual compound co-oxidations. Complex waste mixtures frequently contain heteroatoms that are the source of precipitation and corrosion problems. In addition to this, dissolved oxygen at such high temperatures will also attack non-corrosion-resistant piping.

Figure 2.9 indicates the plant positions of, extent of, and main causes of these problems in the SCWO process:

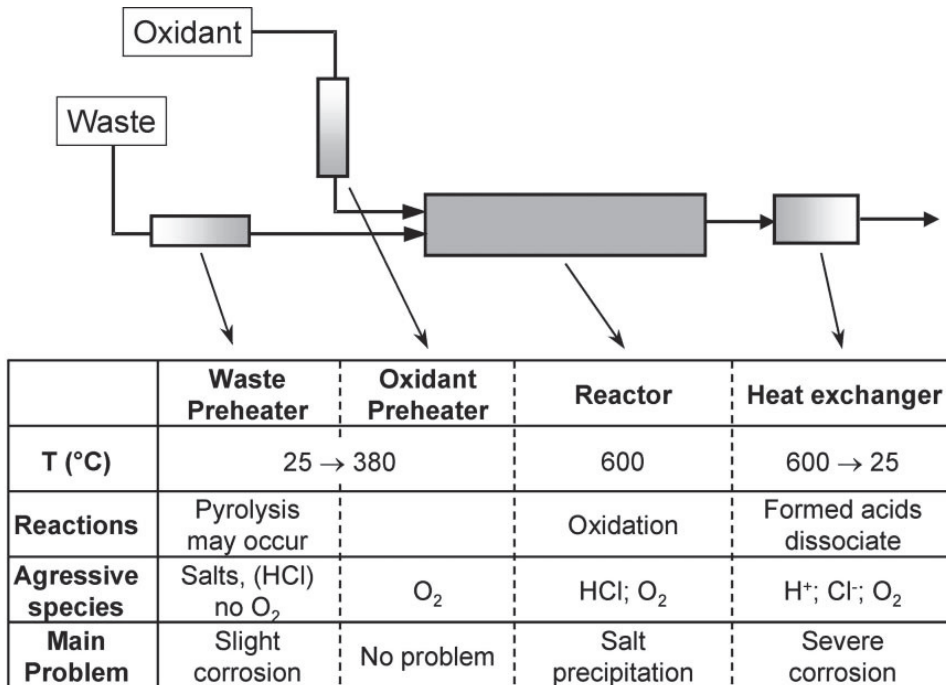


**Figure 2.9** – Location of potential engineering issues associated with SCWO (Kritzer and Dinjus, 2001).

### 2.6.1 Salt Plugging

As water becomes ‘low-density’ SCW (that is, SCW relatively close to its critical pressure), its ability to dissolve most salts decreases dramatically. At room temperature, water can dissolve approximately  $100 \text{ g litre}^{-1}$  of most salts but as a low-density SCF, this is reduced to  $1 - 100 \text{ ppm}$  (Kritzer and Dinjus, 2001) i.e. a reduction in solvability of a factor of  $10^3 - 10^5$ . Thus if salts are present in the organic feed, either as a natural constituent of the waste or as a result of the neutralisation of acids in order to reduce the possibility of corrosion, then they can form a fine-crystalline, slimy “shock precipitate”, which can coat internal surfaces resulting in fouling that can significantly reduce heat transfer from/to external surfaces (Brunner, 2009b; Bermejo and Cocero, 2006). Such fouling can cause losses of operating

efficiency of varying degrees depending on where the effect occurs, for example the fouling of heat transfer surfaces in the cooler would reduce the heat transfer efficiency and would require the increased delivery of service fluid to achieve the desired reduction in product temperature. The salts may also agglomerate resulting in the blockage of transport lines and/or the reactor. This can happen even at high flow velocities (Calzavara *et al.*, 2004).

It is not possible to eliminate this problem by chemical means and so physical and engineering solutions have been investigated by several groups. Kritzer and Dinjus (2001) state the following concepts as potential solutions to this problem:

- **Increasing the pressure of the supercritical solution:**

Increasing the pressure will increase the solution density, which has the effect of enhancing the solubility of salts. Unfortunately however, this increased solubility isn't discriminatory and as such, the solubility of metal-protecting oxides on the walls of the reactor is also increased. This can result in corrosion of the reactor since attacking species such as acids and bases will have their dissociation increased by the increased density.

- **Introduction of a “mobile surface” onto which precipitating salts may settle**

The mobile surface may consist of a slurry of particles or a recirculating fluidised bed providing a very large surface area onto which any precipitating particles may adhere (Whiting and Metha, 1996). Kritzer and Dinjus' (2001) assessment of this method however is that it may in reality only be able to provide a delaying effect and that salt plugging may still eventually occur.

- **Other novel reactor concepts in which salts are not permitted to settle at the walls or agglomerate**

These concepts generally involve the utilisation of subcritical zones within which the salts are able to be dissolved. This area has received a good deal of attention and several reactor designs have been built and tested (Marrone *et al.*, 2004).

- Reverse flow tank reactor with brine pool
- Transpiring wall reactor with a variety of methods for introducing the transpiration concept
- Reactor with catalytic absorption/reaction on solid phase
- Reversible flow tubular reactor

A detailed list of patents pertaining to reactors and processes designed to reduce the salt precipitation problem can be found in Marrone's (2004) paper.

Perhaps the most common of these novel reactor concepts is the 'transpiring wall reactor'. In this type, a porous wall is situated just inside the reactor shell creating a thin layer into which clean transpiring water can be pumped. This water can be sub- or supercritical (though when supercritical, it should be less than the reaction temperature) and provides a protective film, which prevents the deposition of salt films on the reactor surface. A diagram of a TWR is given in Figure 2.10 below.

As can be seen from the diagram, a shell of water at the edge of the reactor prevents deposition. The porosity normally takes the form of a shell of sintered 'platelets' etched with specific patterns which result in a three-dimensional network of channels when combined to form the liner (Marrone *et al.*, 2004). This can be seen a little more clearly in Figure 2.11.

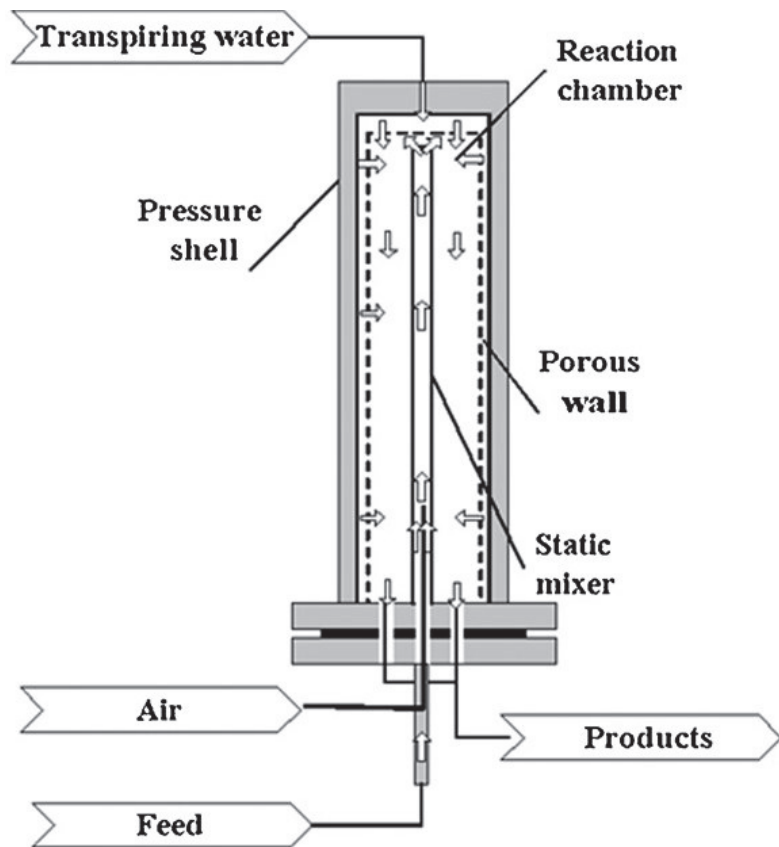


**Figure 2.10** – Diagram of Transpiring Wall Reactor (Bermejo *et al.*, 2011).

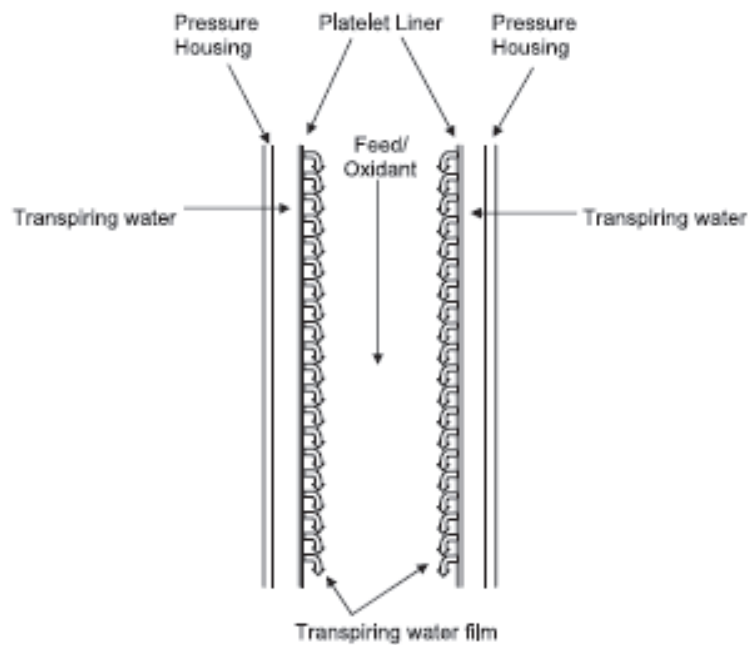


**Figure 2.11** – Liner schematic of Transpiring Wall Reactor (Marrone *et al.*, 2004).

The TWR is a promising concept and investigation is currently on-going into its long-term performance, however, one issue is that a separate supply of transpiring water is required. This secondary supply also has to be raised to a high temperature (although not necessarily past the critical point) which will increase costs relating to operation and control on a full-scale plant.

Long-term investigations as to the performance of technologies designed to reduce the salt precipitation burden in full-scale treatment plants are still being performed but all seem to be less than ideal (Kritzer and Dinjus, 2001). They even go so far as to say that despite SCWO's potential, it may be better to combine the technology with conventional salt-removal methods such as reverse osmosis in order to generate a waste stream feed with a much lower salt content that would therefore be more conducive to treatment in a SCWO reactor.

## 2.6.2 Corrosion

Corrosion of the reactor materials is the second of the two major hindrances to the utilisation of SCWO at industrial scale. Even without taking into account the reaction that is being attempted, the aggressively oxidative conditions can have a damaging effect on the construction materials.

Sun *et al.* (2009) investigated the oxidation of type-316 stainless steel under supercritical conditions with a constant feed of oxidant in the form of H<sub>2</sub>O<sub>2</sub>. SS316 is a very common construction material and they found that as the temperature of the autoclave in which they conducted the experiments was increased, so too did the mass of the SS316 plate that they had exposed to the oxidising atmosphere over a

period of up to 250 hours – up to  $\sim 0.75 \text{ mg cm}^2$  increase on a sample of surface area  $6.625 \text{ cm}^2$  after 250 hours at  $500^\circ\text{C}$  as seen in Figure 2.12.

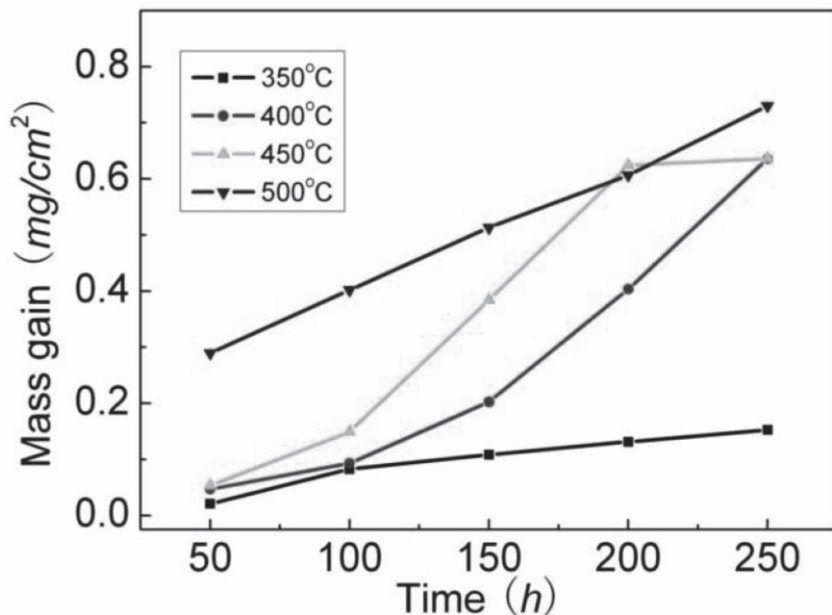


**Figure 2.12** – Mass gain of stainless steel due to oxidation at various temperatures and exposure times (Sun *et al.*, 2009).

The mass increase was attributed to the oxidation of the SS316 plate surface. X-ray diffraction data also shows the presence of iron and chromium oxides after 250 hours, with the number of peaks increasing with increasing temperature as shown in Figure 2.13, indicating that at different temperatures, different species are formed from the corrosion of SS316.

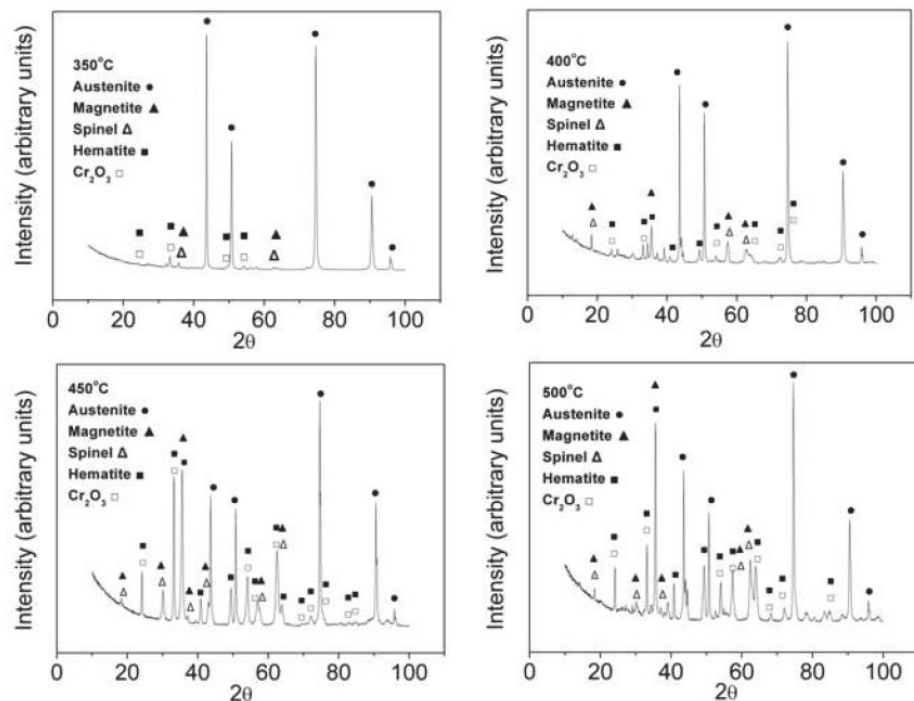


**Figure 2.13 – XRD patterns from 316 SS exposed to SCW for 250 hours at various temperatures (Sun *et al.*, 2009).**

As well as these initial corrosion issues in the reactor, corrosion effects caused by the chemistry of the reactor feed solution can also be exhibited within the reactor and further downstream in the SCWO process resulting in the potential to damage downstream unit operations such as cooling systems, pressure control hardware and gas-liquid separation systems.

The formation of films of ‘shock precipitates’ on the walls of the reactor as described above can cause ‘microenvironments’ between the wall and the salt film in which corrosion can be especially severe even if steps are taken to mitigate acid production through the addition of neutralising bases to the feed (Hodes *et al.*, 2004). This makes the investigation of new reactor concepts even more important in that a mitigation of the salt precipitation issues also has the potential to reduce the

incidence of formation of these ‘microenvironments’ and thus reduce the level of corrosion caused by them.

The production of acids as part of the oxidative process from heteroatoms that enter as part of the complex feed becomes a problem when the reactor effluent is subsequently returned to subcritical conditions. After the super- to subcritical transition, the dissociation of acid compounds increases, resulting in piping downstream of the reactor being exposed to aggressive corrosive species. This effect also has the potential of occurring within the reactor if the pressure is increased in order to try to solve the salt plugging issue. Such effects are clearly undesirable due to their causing:

- the inevitable need for maintenance in the form of hardware replacement.
- the reduction in process efficiency in affected unit operations, e.g. when the pipe walls in the heat exchanger corrode causing a loss of efficiency.
- the potential need to separate any metal salts formed from the corrosion of the apparatus from the reactor products.

It would seem that simply choosing a material resistant to corrosion from which to manufacture the reactor may not be a viable solution due to inconsistencies in the resistance of different alloys when exposed to different acidic species (Kritzer and Dinjus, 2001). For example, stainless steel 316 can be used between 300 - 550°C outside of the extremes of pH (although the attacking of the material under the hostile conditions will eventually be observed as indicated in Figure 2.13) but is very susceptible to attack by  $Cl^-$  ions (Bermejo and Cocero, 2006) so low (or preferably zero) concentrations of this ion are extremely desirable, whereas titanium alloys have

very high resistance to HCl at all temperatures but are vulnerable to  $\text{H}_2\text{SO}_4$  and  $\text{H}_3\text{PO}_4$  at temperatures above 400°C (Boukis *et al.*, 1998) and are mechanically vulnerable to creeping at high temperatures (Bermejo and Cocero, 2006).

Nickel alloys such as Inconel 625 and Hastelloy also provide some protection against corrosion, but this protection can depend on the process conditions. In neutral conditions, nickel alloys give high resistances to corrosion at very high temperatures. This protection diminishes in acid conditions however. Additionally, there exists an optimum window of electrochemical potential outside of which dissolution of a protective oxide layer can occur. The metal that forms the protective oxide layer in these alloys (and stainless steel) is usually chromium and the oxidation state of chromium governs its solubility. Cr(III) (occurring under optimum conditions) confers good protection, Cr(II) and Cr(VI) are soluble. Increasing temperature favours the formation of the stable Cr(III) (Bermejo and Cocero, 2006).

## 2.7 Current State of Industrial SCWO Technology

SCWO at an industrial scale can by no means be regarded as a widespread technology. Table 2.11 indicates the commercially designed SCWO treatment facilities that were in existence in 2006.

**Table 2.11 – SCWO facilities ca. 2006 (Bermejo and Cocero, 2006; Veriansyah and Kim, 2006).**

Company	Licenses	Large-scale plants	Application
MODAR	Organo, University of Tokyo	Nissetsu Semiconductor, Japan (const. Organo)	Semiconductor manufacture wastes (non-operational –moved to Tokyo 2002)  University waste (since 2002)
MODEC	Organo, Hitachi, NGK	None	Pharmaceutical wastes, pulp and paper mill wastes, sewage sludge
General Atomics	Komatsu, Kurita, Waste Industries	U.S. Army Newport Chemical Depot, Newport, IN	Nerve agents, chemical agents, explosives, shipboard wastes, rocket propellant
Foster-Wheeler	--	U.S. Army Pine Bluff Arsenal, AR (op. Sandia National Labs)	Smokes and dyes, chemical agents and explosives, shipboard wastes (non- operational)
EcoWaste Technologies	Chematur	Huntsman Chemical, Austin, TX	Oxygenated and nitrogenated hydrocarbons
		Johnson-Matthey, Brimsdown, UK	Spent catalyst (recover PGMs and destroy organic contaminants)
Chematur	Shinko Pantec	Japan (constructed by Shinko Pantec)	Municipal sludge
SRI International	Mitsubishi Heavy Industries	Japan	PCBs, chlorinated wastes
Hydro-processing	--	Harlingen Wastewater Treatment Plant No. 2, Harlingen, TX	Mixed municipal and industrial wastewater sludge
Hanwha Chemical	--	Nambae Chemical Corp. Korea	Wastewater from DNT/MNT plant and Melamine plant

However, as of 2012, of the plants given above only the General Atomics and SRI International plants are still in operation, with the University of Tokyo facility undergoing remodelling (Marrone, 2012). There are a further four plants that are currently operational as shown in Table 2.12.

**Table 2.12** – Additional operational SCWO facilities as of 2012 (Marrone, 2012).

Company	Licenses	Large-scale plants	Application
SuperWater Solutions	--	Florida (pilot-scale), full-scale expected in 2013	Wastewater sludge
Supercritical Fluids International (SCFI)	--	Cork, Ireland	Wastewater, drinking water sludge
Innoveox	--	Arthez-de-Béarn, France	Hazardous industrial waste
Hanwha Chemical	--	Seoul, Republic of Korea	Toluene diisocyanate (current operating conditions are subcritical)

Marrone's paper indicates that twenty-one companies have operated SCWO facilities at some point in time, with only six still operational. These six are: General Atomics, SRI International, Hanwha Chemical, SuperWater Solutions, Supercritical Fluids International (SCFI) and Innoveox. The majority of plants stopped operating due to engineering issues as opposed to business or contractual issues, however the currently-operating companies have plans to install up to nine further plants.

The fact that the construction of these additional plants are being planned by companies that are currently operating SCWO treatment technologies is a cause for cautious optimism that the technology may now be able to treat volumetric throughputs more comparable to those being treated by 'conventional' technologies without succumbing to failure from physicochemical effects of the SCWO process.

### 2.7.1 Energy Efficiency

SCW provides certain advantages in terms of attempts to maximise the energy efficiency of the oxidation process. The monophasic nature reduces mass transfer limitations upon the mixing of the two supercritical reactant streams wherein the

reactants are brought into close molecular contact, resulting in a very efficient oxidation process.

Because the temperatures and pressures that are required in order to maintain supercritical conditions are high, the process on a large-scale inevitably has the potential to be energy-intensive. Consequently, if the use of SCWO is to become widespread, then there is a great deal to be gained by making the process as energy efficient as possible. Initially, steps toward energy integration can take a relatively simple form, for example the using of the hot reactor effluent to preheat the feed streams reduces the need to employ energy-intensive electricity- or gas-powered heaters to the extent that would be required if no integration was employed.

A good deal of SCWO research has been conducted using isothermal reaction conditions in which the tubular reactor rig (including preheaters) is either immersed in a fluidised sand bath, e.g. in the Department of Environmental Systems at the University of Tokyo, or placed in a furnace (as in investigations described in this work). A significant drawback of these ‘immersion’ methods is that it inherently requires a large amount of energy to maintain the reaction temperature. Unfortunately, a good deal of this energy will ultimately be lost to the atmosphere. In addition, the exothermic nature of the oxidation could serve to increase the temperature inside the reactor, but the isothermal conditions act to cool the reactor contents and quench any runaway temperature increase. Consequently, at larger scales, it is much more common to operate rigs adiabatically, as with pilot plants at the University of Cadiz, the Massachusetts Institute of Technology, and the University of Valladolid, and to work to retain the energy through adequate insulation and manipulation of the exothermic process.

Figure 2.14 shows the reactor of the AquaCritox® process operated by SCFI as an example of a large scale SCWO process that ideally operates under adiabatic conditions and suggests the possibility of operating under autothermal conditions.



**Figure 2.14 – AquaCritox® Reactor (SCFI).**

The insulation incorporated in the tubular pilot plant reactor at the University of Cadiz allows the exothermic reaction to heat the reactor stream from 400°C at the injection point to 550°C at the reactor exit (Fourcault *et al.*, 2009). Cocero *et al.* (2002) found that in operations using their pilot plant's continuously operating statically mixed reactor, self-sufficient oxidation can be achieved by using feed streams with an energy content of at least 930  $\text{kJ kg}^{-1}$ . They list some C<sub>6</sub> compounds in solution with water that could fulfil this condition: 2 wt.% n-hexane, 2.4 wt.% 1-hexanol or 3.2 wt.% hexanoic acid. This would result in reaction temperatures above 650°C at 23.0 MPa and removal efficiencies greater than 99.95% were reached.

Cocero *et al.* (2002) published an analysis of the energy that would be expected to be released from reaction. This energy release directly affects the sustainability of the reaction temperature and will therefore inform the preheating and the required flowrate of any necessary auxiliary fuel for the oxidation of more complex wastes. They suggest that at 400°C and 25 MPa, the heat of reaction can be expressed as:

$$-\Delta H_r = 415n + 107m - 193f \quad (2.12)$$

where n, m, and f are the number of carbon, hydrogen and oxygen atoms respectively. This equation estimates the heats of reaction of acetic acid and methanol to be  $-872 \text{ kJ mol}^{-1}$  and  $-650 \text{ kJ mol}^{-1}$  respectively where experimentally-derived values are  $-870 \text{ kJ mol}^{-1}$  and  $-670 \text{ kJ mol}^{-1}$  respectively. These equate to errors of 0.3% and 3% respectively and they quote a maximal error of  $\pm 4\%$ . This is lower than the  $-925 \text{ kJ mol}^{-1}$  reported by Aymonier *et al.* (2001) at similar conditions.

Further manipulation of the reaction conditions can be undertaken in an attempt to reduce the high feed temperature requirement to something a little closer to ambient temperature. The concept of a hydrothermal flame can be employed in order to drastically increase the efficiency of the reactor and reduce the necessary preheating burden. When the temperature is higher than that required for autoignition, oxidation in SCW will take place in the form of flames, where a flame can be considered as a ‘surface’ of nominally constant temperature at which the oxidation reaction occurs. The advantages over a ‘flameless’ process include (Augustine and Tester, 2009):

- Reactions can be completed over a timescale of milliseconds, which is even smaller than those of conventional SCWO.
- Higher temperatures (600-700°C) arising from the exothermic nature of the reaction improve the possibilities for energy recovery by utilising the waste's heat of reaction further downstream.
- Reactants can be injected directly into the flame once it has been established and stabilised. Furthermore, the reactants can be introduced to the flame at much-reduced or even ambient temperatures, which greatly reduces the need for feed preheating or, in the case of ambient injection, could remove the need entirely. Clearly, this would greatly reduce the necessary energy input, with the subcritical conditions of the feed injectors resulting in the avoidance of the standard problems of salt-plugging and corrosion in the preheater tubes.

In simple tubular reactors, total TOC removals could be obtained for residence times less than 0.5 s but this behaviour was only observed for injection temperatures above 370°C – almost at water's critical point. Tubular reactors narrower than ¼ inch external diameter and packed reactors presented worse results (Bermejo *et al.*, 2011).

Vessel reactors such as a transpiring wall reactor (TWR) have been shown to be more successful than simple tubular reactors at maintaining a steady, stable hydrothermal flame with an injection temperature close to room temperature (Bermejo *et al.*, 2011). Work at ETH Zurich found that the oxidation of methanol in a TWR proceeded to over 99.9% within residence times of 50 – 100 ms under hydrothermal flame combustion (Wellig *et al.*, 2005). The ETH rig can be seen in Figure 2.15 below.

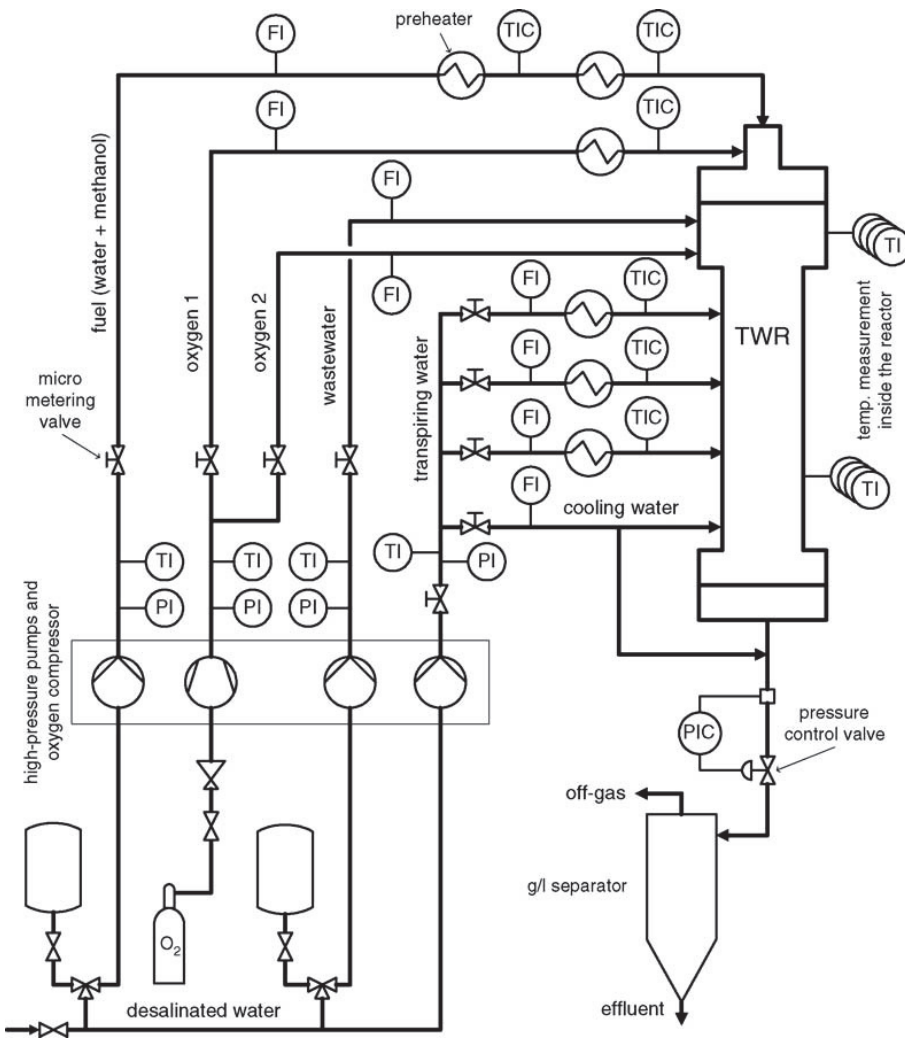


**Figure 2.15** – TWR operating in a hydrothermal flame regime (Wellig *et al.*, 2005).

This work included fuel (aqueous methanol) injection temperatures below the critical point for 11 wt.% methanol and the injection temperature could be reduced to below 100°C by increasing this mass proportion to 27 wt.%. Experiments in this work used ‘simulated wastewater streams consisting of either desalinated water (0% waste) or 6 wt.% methanol. Essentially, cold waste could be injected posterior to the flame, with heating to the reaction temperature occurring near-instantaneously upon contact with the flame surface and the subsequent exothermic reaction working to maintain the temperature of the flame region. In the ETH Zurich rig, no preheating of

the wastewater to be treated occurs. Consequently this means that the TWR, as well as already reducing the previously discussed salt precipitation and corrosion issues that are prevalent during the SCWO of heteroatom-containing feeds, can also be operated in such a way as to greatly reduce the energy requirement. Clearly, in a self-sustaining regime such as oxidation using a hydrothermal flame, the need to use any residual heat in the product stream to increase the temperature of the feed is much reduced. Indeed, although the oxygen feed and an auxiliary fuel will need to be preheated (with the duty depending on the fuel proportion), the waste feed could be fed to the reactor at ambient temperature once a stable flame has been established. This leaves the energy left in the product stream to be utilised for other purposes. These purposes will vary in accordance with the type of reactor that is being employed – for example, in a TWR, the transpiring water will need heating to some optimum point, which is likely to be between 40-250°C and the transpiring water mass flux can amount to over 65 wt.% of the bulk mass flow rate. Once the reactor product stream leaves the combustion zone, the temperature will begin to drop as heat is lost to the transpiring water. However, the energy from the outlet stream could be recovered to some of these preheating operations. In the ETH rig, the outlet stream is currently quenched using cooling water rather than integrated with other streams, however they have identified the opportunities for future efficiency increases in this vein.

## CHAPTER 3 – EXPERIMENTAL APPARATUS AND PROTOCOLS, AND ANALYTICAL TECHNIQUES

### 3.1 Components and construction of experimental rig

The experimental rigs that were used to undertake the experimental work for this project were designed and built by the author. Two different rigs were built: one for investigating single-stage oxidation and a second for investigating multi-stage oxidation. The design of the multi-stage experimental rig was informed by a tubular reactor produced by the author's supervisor in Japan. A general process flowsheet for the SCWO rig is shown in Figure 3.1 with more focused schematics for the rigs used for each series of experiments being presented in later chapters as Figures 4.1 and 5.1. In Figure 3.1, the red lines indicate streams at supercritical conditions, the blue lines indicate streams that are highly pressurised but at ambient temperature, and the black lines indicate streams at ambient conditions.

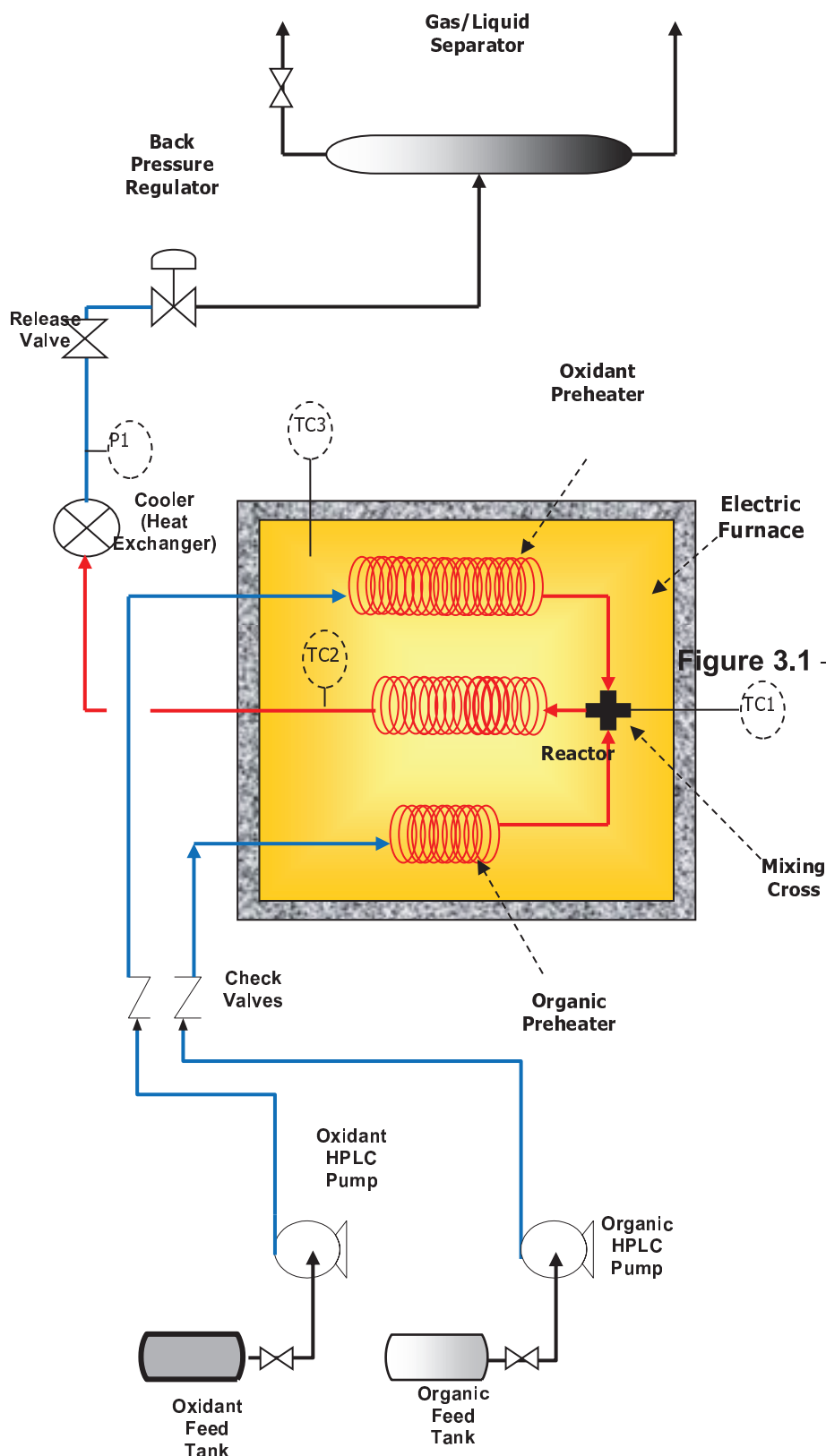


Figure 3.1 – General flowchart of S

This process flowchart is largely applicable to all SCWO processes incorporating tubular reactors. The specific rigs used in this work were tailored to accommodate the specific oxidant requirements, specifically a single-stage oxidation and a multi-stage oxidation. The difference between the single-stage configuration and the multi-stage configuration was that there was a secondary oxidant preheater coil. This coil could be connected to one of three entry ports resulting in the ability to inject the second oxidant feed 25%, 50% or 75% of the way along the reactor length. The single-stage configuration was largely similar to Figure 3.1 above.

The different sections of the reaction rig will be described below where all piping is type 316 stainless steel unless otherwise stated.

### 3.1.1 Oven

The oven that was employed in order to achieve the desired reaction temperature was a medium-sized, air-driven furnace (AEW, Hampshire). The layout of the oven, along with indications of the reactor situated within it can be seen in Figure 3.2. The only access port to the oven was a small chimney as shown on Figure 3.3 where the dotted line represents the frame onto which the reactor rig was attached and placed inside the oven. The solid outer line represents the interior dimensions of the oven itself and the 10 cm diameter circular aperture represents the chimney into which and from which all input and output lines enter and leave the oven interior. All dimensions are in centimetres.



**Figure 3.2** – View of the reactor inside the oven.

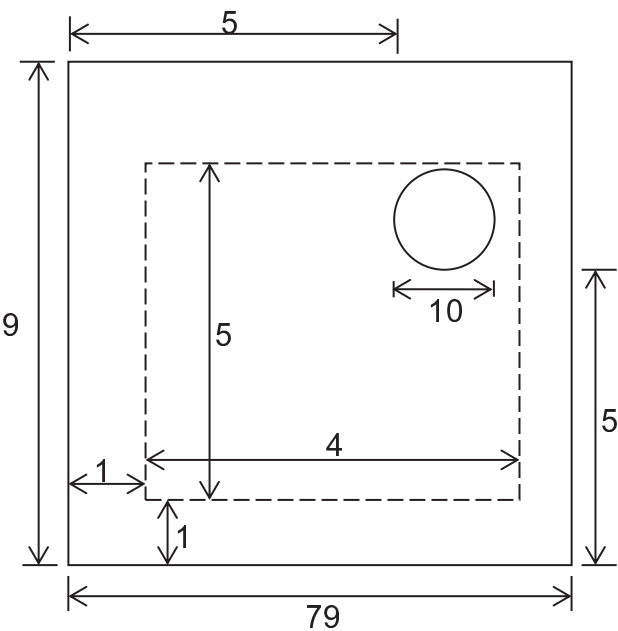


**Figure 3.3** – Plan view of the oven where the circular aperture is the only entry/exit point to/from the heating cavity.

The location and depth of the chimney (and by extension the length of piping required to take the reactor effluent from the hot zone to the cooler) was a deciding factor in several aspects of the reactor configuration, e.g. the definition of ‘reactor length’.

The oven controlled its temperature via a PID controller (initially *West 4100* and later *West 6100* due to the short-circuiting and failure of the *West 4100* model) with an ambient oven temperature reading provided by an integral K-type thermocouple). The oven temperature setpoint was adjusted after assessing the temperature in the reactor at any particular time via the thermocouples connected to the reactor – in particular the thermocouple monitoring the reactor inlet temperature.

### 3.1.2 Reagent Storage

The organic and oxidant feed solutions were prepared and stored in 2 *litre* brown glass Winchester bottles. The concentration of the organic solution prepared always depended on the desired reaction conditions, but the oxidant solution that was prepared was always 30 *ml* of 35% (w/w) H<sub>2</sub>O<sub>2</sub> (*Sigma*) as delivered, added to and dissolved in 2 *litres* of distilled and deionised water, which corresponds to a concentration of 174 millimoles per litre (*mM*). This relatively low concentration of oxidant was chosen to try to minimise the possibility of the H<sub>2</sub>O<sub>2</sub> decomposing in the stock bottle. The oxidant was also stored under ice in a further attempt to avoid decomposition. The relative flowrates of the organic and oxidant solutions were then adjusted to provide the required reaction conditions.

### 3.1.3 Pumps

The reagents were delivered using Jasco PU-2086 Plus High Pressure Liquid Chromatography (HPLC) pumps. These pumps had maximum deliverable flowrates of 20 *ml/min* that could be incremented to the microlitre level. One pump was used to deliver the organic solution and either one or two pumps were used to deliver the oxidant solution depending on which oxidant configuration was being employed. The pumps are depicted in Figure 3.4.

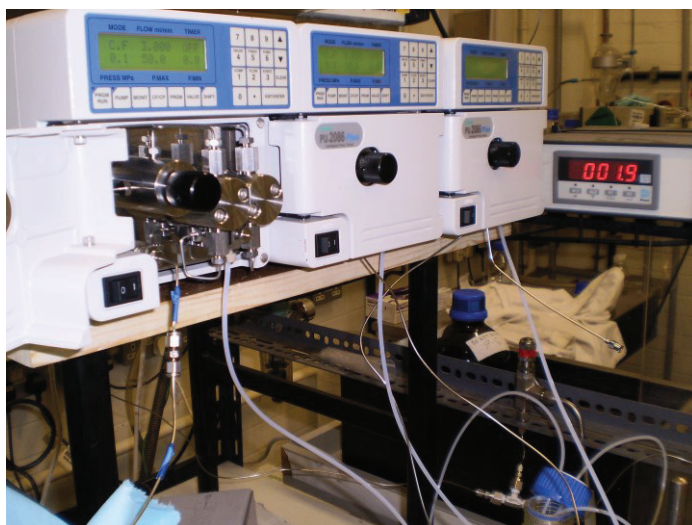


**Figure 3.4** – Pumps used to deliver reactants inc. pressure transducer display.

### 3.1.4 Preheating Coils

The reactants were preheated separately in 1/16" o.d. pipes (Swagelok) to the desired reaction temperature before being combined at the inlet of the reactor. The preheater pipes were required to be long enough to be able to ensure that:

- The reactants were preheated to the desired temperature at all possible flowrates
- All hydrogen peroxide in the oxidant stream decomposed to oxygen and water.

As such, the organic and oxidant preheaters employed were 6 m and 12 m in length respectively. Kinetics data for the decomposition of H<sub>2</sub>O<sub>2</sub> (Tsang and Hampson, 1986) established that at the temperatures investigated, H<sub>2</sub>O<sub>2</sub> decomposed rapidly (< 2 s).

### 3.1.5 Reactor

The reactor was built from 1/16" o.d. pipes (*Swagelok*) and was 12.4 m in length. In order to make the reactor configuration slightly more flexible and to render changing the configuration slightly simpler, a 12 m length of piping was connected to a 0.15 m length at the beginning of the reactor and a 0.25 m length at the end of the reactor resulting in the 12.4 m total length. This was done to ensure that when changing the configuration, only relatively inexpensive, straight connecting unions had to be disconnected and re-connected.

The reactor rigs were mounted on a moveable frame as seen in Figure 3.2, which allowed a little more structure to the apparatus. This was especially valuable when performing delicate manipulation to the flexible piping, which could be rather awkward work.

#### 3.1.5.1 Temperature Measurement and Profiles

The entry of the reactor was connected to the south port of a cross union (*Swagelok*) to which the organic and oxidant preheater pipes were also attached via the east and west ports. A K-type stainless steel 316-sheathed thermocouple (*TC Direct*) was connected to the north port. The end of the reactor was attached to a tee-shaped union (*Swagelok*), to the perpendicular port of which was attached another thermocouple of identical specification. The piping between these two unions was the

length defined as the ‘reactor length’ because after the tee-shaped union, the product stream left the oven via the exit port in its ceiling and its temperature could not be guaranteed to be at the desired reaction temperature. As such, it was possible or even likely that some reaction may have continued until the product stream was quenched by the temperature decrease experienced upon passage through the cooler unit, but the length available for this was limited to approximately 5% of the reactor length.

The temperatures that were measured by the thermocouples attached to the rig and floating inside the oven were logged by a TC-08 USB Data-logger (*Pico Technology*).

Figure 3.5 gives an example of the reactor’s temperature profiles during a run, where the reactor inlet ( $T_i$  – solid line) was held as close to the required reaction temperature as possible. This trace shows five experiments run consecutively over a four and a half hour period. The first hour (not shown) constitutes the initial start-up transient. It is assumed throughout this work that the reactor can be approximated to be isothermal in nature due to the oven’s constant temperature environment and the narrowness of the piping, however the difference in outlet and inlet temperature shown in Figure 3.5 indicates a potential flaw in this assumption. Because of this, calculations of the possible temperature increases in purely adiabatic conditions were performed. These corresponded to a potential 3 - 14°C increase for the single-stage configuration and up to 27°C increase for the multi-stage configurations. Conditions conducive to a higher DMF conversion resulted in a higher potential adiabatic temperature rise. The conditions shown in Figure 3.5 for a residence time of 10 s had the potential to show a temperature increase of 14.8°C. The upper plot shows  $T_i$

(solid line),  $T_o$  (dashed line) and the oven temperature measurement (dash-dot with noise). The lower plot shows the difference between  $T_i$  and  $T_o$  where a positive value indicates  $T_o > T_i$ . The fact that the measured temperature at the outlet was less than 1°C greater than that at the inlet implies that (at least for lower flowrates), an isothermal assumption is workable.

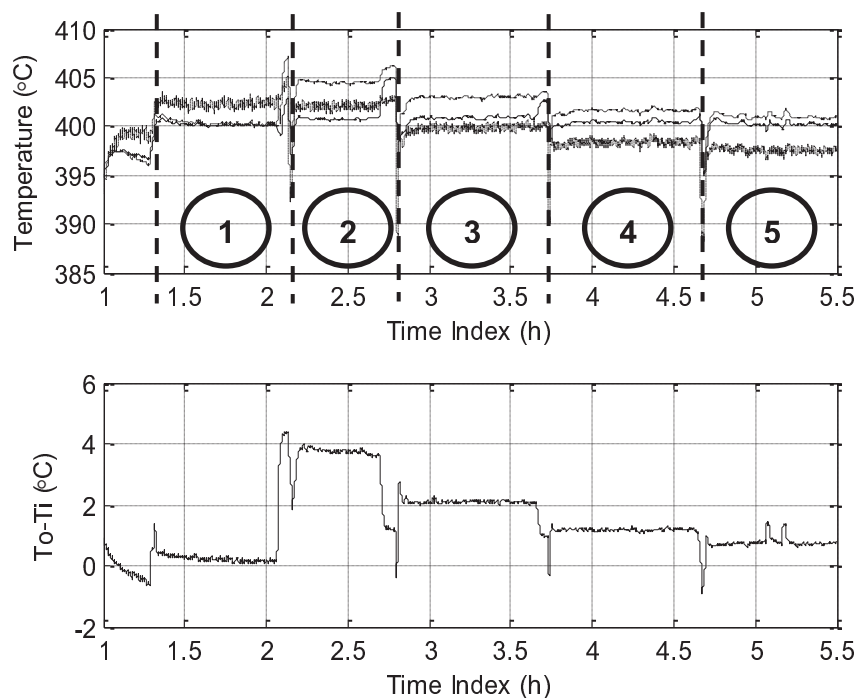


**Figure 3.5** – Temperature logs at 400°C at 2, 4, 6, 8 and 10 s residence time (sections 1 – 5 respectively) for the multi-stage configuration.

### 3.1.5.2 Multi-stage Configuration

The multi-stage oxidation configuration was of a very similar layout to that described above, with the exception that an additional oxidant preheater, identical to the primary oxidant preheater was attached to a secondary injection port via a tee-shaped union. No additional instrumentation (e.g. additional thermocouples) was available when using this configuration.

### 3.1.6 Cooler

In order to quench the reaction and bring the temperature of the product stream back to an ambient level, a water-cooled countercurrent heat exchanger was designed, built (*Chemical Engineering Workshop*) and connected to the product stream exit piping emerging from the ceiling port of the oven. Figure 3.6 shows a diagram of the cooler.

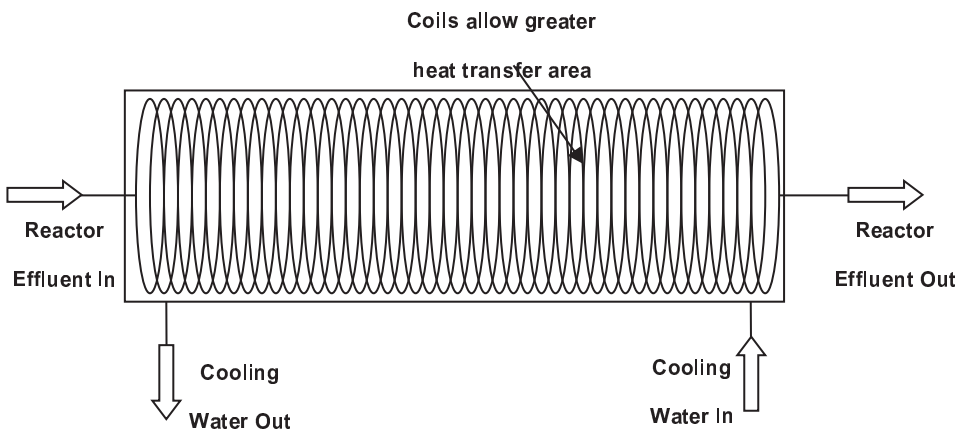


**Figure 3.6** – Diagram of effluent stream cooler.

The cooler consisted of a coil of 1/16" o.d. piping of length 3 m situated inside a stainless steel cylindrical shell, which was approximately 3" in radius and sealed via welding. Two connecting ports for the service water were welded to the outer shell, one at each end. The cooler operated in a countercurrent configuration and returned the reactor products to ambient temperature. Cold water at approximately 15°C was used as the service fluid, with the assumption that the service fluid flow was high enough to maintain a constant wall temperature on the inner piping. The cooler is depicted in Figure 3.7, where hot reactor effluent enters laterally from the left hand side.



**Figure 3.7 – Cooler module.**

### 3.1.7 Pressure Sensing and Control

The pressure in the rig was controlled by way of the use of a BP-66 manual back-pressure regulator (BPR - GO Inc.). The regulator allowed pressure control up to 10,000 *psi* (68.8 MPa), well in excess of the desired experimental pressures of 25 MPa. A digital pressure transducer (*Druck*) was mounted just after the cooler and the desired pressure upstream of the BPR could be achieved by adjusting the regulator and monitoring the pressure reading – i.e. there was no automatic means of controlling the reactor pressure and thus close monitoring of the reactor pressure reading was important both to maintain the desired pressure and to quickly diagnose any potential problems. Downstream of the BPR, the system was at ambient pressure. All experiments were carried out at a nominal reactor pressure of 250 bar. However, because the pressure transducer was downstream of the reactor and cooler, frictional pressure drop meant that the pressure in the reactor was marginally higher than that indicated by the sensor.

Pressure drop could be calculated by using a correlation for the friction factor,  $\varphi$  which is a function of the Reynolds number and the pipe roughness, and equation 3.1 which is the Darcy equation (Coulson *et al.*, 1999):

$$\Delta P = 4\varphi(Re, \varepsilon) \frac{L}{D} \rho(T, P) \bar{u}^2 \quad (3.1)$$

Quality assurance data pertaining to the SS-316 pipes provided by Swagelok indicated that the piping could be approximated to a smooth pipe. This meant that given the density and Reynolds number ranges seen for all experiments, the friction factor would be between 0.003 and 0.0055 for the reactor section in the single-stage configuration. Evaluating the pressure drop for each experiment results in a calculated pressure drop of 0.08 – 1.75 MPa, indicating that the maximum pressure at the reactor inlet was 26.75 MPa. At residence times in excess of 2 s, the reactor pressure drop was generally around 0.5 MPa, thus for over 80% of experiments, the maximum pressure experienced in the reactor was approximately 25.5 MPa.

Opinion is somewhat divided as to whether or not small variations in the pressure close to the critical point affects the reaction rates to any appreciable degree. However, on balance, the greater weight of research suggests that higher pressures are required before the effects are seen, and at any rate, the pressure losses amount to a small proportion of the desired reaction pressure (< 2% in most cases, and up to a maximum of 7% at the upper bounds of density and flowrate). The pressure drop range of 0.08 – 1.75 MPa would correspond to a water density increase from that expected at the reactor inlet of between 0.9% (at 400°C) and 8.6% (at 550°C), which could correspond to a similar increase in the concentration of DMF being fed to the reactor. The vast majority of experimental conditions would exhibit

this lower bound and only the very high temperature experiments would approach the upper bound. As such, the effect of a pressure gradient across the reactor was not considered in the treatability and kinetics analysis.

The total pressure drop over the rig between the pumps and the pressure transducer was more difficult to calculate due to the temperature differences and differing preheater lengths, but using upper bound values yields a maximum pressure drop of 6 MPa, although the actual values are likely to be lower than this. Indeed, observations of the manometers built into the pumps indicated that the maximum pumped pressures for the highest flowrates were of the order of 30 MPa, implying that the pressure drop over the system was a maximum of 5 MPa with most flow conditions yielding more conservative pressure drops over the whole apparatus of around 2.5 MPa. Again, it is emphasised that this drop doesn't indicate a descent into subcritical regimes as supercritical pressures were measured at the pressure transducer downstream of the reactor.

In order to ensure that the rig adhered to both the University of Birmingham's safety regulations and the ratings on several of the rig's components, a pressure relief valve (*Swagelok*) set to vent the product stream if the pressure exceeded 285 bar.

### 3.1.8 Gas-Liquid Separator, Sampling and Gas Flow Measuring

Downstream of the BPR, the final part of the rig was a gas/liquid separator. This consisted of a long glass tube of diameter 50 mm (*University of Birmingham School of Chemistry Glassblowing Workshop*) into which the product stream (now at ambient conditions) flowed. This tube allowed the separation of the gas and liquid

phases. The liquid phase left the tube via an on-off valve from which liquid samples could also be taken.

The gas phase left via a 1/8" o.d. pipe (*Swagelok*), which was connected to a two-way valve. From here, the gas could either be sampled or directed to a glass tube with 5 ml graduations into which a detergent bubble could be introduced. The rate at which such a bubble rose could be recorded and from this, the flowrate of the gaseous product calculated. The gas-liquid separator is shown in Figure 3.8, where the reactor effluent enters from the top through the thinner of the two pipes.

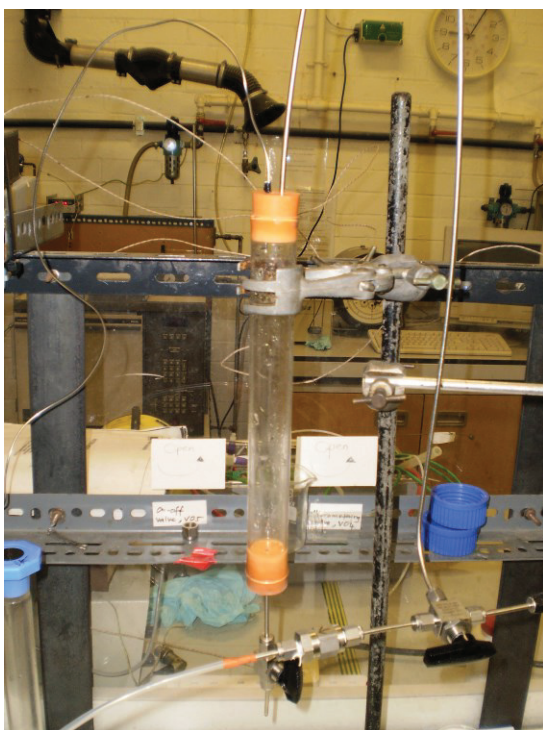


**Figure 3.8 – Gas-liquid separator.**

Gas samples were taken both by gas syringe and by a liquid displacement technique (as a back-up). The gas syringe samples were analysed immediately and constituted the primary measurement of the composition of the gaseous product. The

liquid displacement technique involved filling a serum bottle with distilled and deionised water and sealing it with a rubber stopper (*Sigma*).

## 3.2 Experimental Protocol

### 3.2.1 Generic Experimental Protocol

The SCWO treatment protocol takes a largely universal format across most research with the only differences occurring when considering either to use a batch (Goto *et al.*, 1999) or continuous operation (e.g. Cocero *et al.*, 2002) and deciding which source of oxygen to use, either air (e.g. Cocero *et al.*, 2000), molecular oxygen (e.g. Perez *et al.*, 2004), other gas mixtures such as a 40/60% O<sub>2</sub>/N<sub>2</sub> split (e.g. Moussiére *et al.*, 2007) or H<sub>2</sub>O<sub>2</sub> solution (e.g. Sánchez-Oneto *et al.*, 2007).

In batch operation, the reactants are fed to the reactor, compressed and heated to the required temperature. Once the required reaction time has elapsed, the temperature and pressure are returned to ambient conditions. Samples of gas and liquid products are then taken and analysed.

In continuous operation, which usually involves a tubular plug flow reactor, but can involve a packed bed or other kind of reactor, the reactants are separately compressed and heated to the required conditions and then combined at the reactor inlet. After the reactor, the effluent is cooled, decompressed and again, samples taken and analysed.

### 3.2.2 Experiment and Sampling

The reactor and preheaters were heated to the desired reaction temperature while distilled and deionised water was pumped through the whole apparatus at a

cumulative flowrate of 5 ml/min. The rig was pressurised slowly as the temperature rose and as the temperature approached the desired setpoint, the pump flowrates were adjusted to those that would result in the residence time required for the experiment. This ensured that when the pump feeds were changed from water to the reagents, no flowrate change would be necessary and thus the reactor would take much less time to return to its equilibrium temperature.

When the temperature and pressure of the rig were stable, the feeds were switched from distilled water to the organic and oxidant reagents. Once the reagents were fed to the reactor, the apparatus was allowed to stabilise for 15 – 30 minutes to ensure that the product stream entering the gas-liquid separator was representative of the stream leaving the reactor at the reaction conditions.

The reactor pressure was constantly monitored to ensure both that the reaction conditions were maintained and that no drop in feed inflow went unnoticed. The temperature at the reactor inlet and outlet was logged every second by the PicoLog software. The signal from a thermocouple monitoring the ambient oven temperature was also logged at the same interval. This allowed a further check of the accuracy of the oven's temperature control system.

The flowrate of the liquid effluent was also checked frequently and logged for each experiment, particularly prior to sampling. The combination of pressure, temperature and liquid flowrate data was used both to calculate parameters (liquid flowrate especially) and to ensure the steady state operation of the reactor. At each sampling, gas samples and liquid samples were taken and gas flowrates and liquid flowrates were recorded.

After all samples and measurements at a particular set of conditions had been obtained, the option was available to adjust the reagent flowrates to provide different residence times in order to conduct additional experiments. If no further experimentation was required, the apparatus was shut down by turning off the oven, opening the oven vent and switching the reagent flow back to distilled water.

The rig was then allowed to cool gradually while the pressure was also reduced gradually as the temperature fell. Gradual cooling and pressure reduction was important to ensure that the components within the oven did not undergo any undue physical or thermal stress, which thus ensured that the lifetime of the apparatus could be maximised.

It took approximately between 3 – 5 *hours* to conduct one experiment (investigating one residence time) depending on the time needed to heat up and cool down the apparatus, which in turn was dependent on the reaction temperature required. Each additional residence time to be investigated at the reaction conditions, took an additional time of between 40 – 60 *minutes*. This was again dependent on the reaction conditions as higher desired residence times resulted in the necessity to afford the reactor longer to reach an equilibrium state and required more time to acquire samples due to the inherently lower flowrates that occurred when investigating these longer residence times.

### 3.3 Analysis Techniques

The analysis of the experimental samples was performed in order to assess and to quantify the extent of destruction of the organic species and the generation

and destruction of any intermediate compounds including nitrogen-containing species.

What follows is a description of the analytical methods that were employed.

### 3.3.1 Total Organic Carbon (TOC)

The total organic carbon (TOC) content of liquid samples was quantified for each experiment in order to calculate the effect of changing various experimental parameters on the destruction of TOC.

The TOC content of each sample was evaluated via analysis in a Shimadzu TOC-5050A analyser fed by a Shimadzu ASI-5000 autosampler. In order to calculate the TOC content, the analyser determined the total carbon (TC) content and inorganic carbon (IC) content of each sample.

#### 3.3.1.1 Total Carbon (TC)

The total carbon (TC), as the name suggests, is the total quantity of carbon in a particular sample and is comprised of both organic and inorganic carbon. The TC content of a sample was evaluated by injecting up to 100  $\mu\text{l}$  of said sample into a combustion tube, which was filled with oxidation catalyst (platinum), heated to 680°C and through which a carrier gas (moistened high-purity air) was flowing at a flowrate of 150 ml min<sup>-1</sup>. The sample was combusted within the tube to form CO<sub>2</sub>. This CO<sub>2</sub> was the product of oxidising the organic carbon contained within the sample. The carrier gas, which contained the product from the TC combustion tube, was then passed through the IC reaction vessel – the reaction that takes place here will be described when discussing the IC determination in §3.3.1.2 below.

Upon leaving the IC reaction cell, the carrier gas is cooled and dried in a dehumidifier, passed through a halogen scrubber and into a sample cell set in a non-dispersive infrared gas analyser (NDIR) where CO<sub>2</sub> is detected. A peak is generated and its area calculated by a data processor. This area is proportional to the TC concentration in the sample. This value is converted into a concentration in milligrams per litre (*ppm C*) by comparing it against three internal calibration curves that were generated by preparing a standard solution and then diluting this standard using distilled and deionised (zero grade) water to obtain several samples of varying concentrations.

### 3.3.1.2 Inorganic Carbon (IC)

The IC content of a sample was determined by injecting the sample, which was either taken directly from a sample vial in the case of an IC-only determination or which consisted of the carrier gas from the combustion tube in the case of a TC determination, into the IC reaction chamber whereupon any inorganic carbon reacted with 25% (w/w) phosphoric acid solution to produce CO<sub>2</sub>. Only inorganic carbon (e.g. in the form of carbonates and other inorganic salts) decomposes upon contact with the acid solution. The quantity of CO<sub>2</sub> was again determined by NDIR. This value was converted into a concentration in milligrams per litre by comparing it against three internal calibration curves that were generated by preparing a standard solution and then diluting this standard using zero grade water to obtain several samples of varying concentrations.

The high concentration standard solutions had a limited shelf life of approximately two months. As such, whenever re-calibration was necessary, new

standards were prepared on each occasion, with dilutions of this new standard solution providing the range of concentrations necessary to obtain the calibration curves.

### 3.3.1.3 Total Organic Carbon (TOC) Determination

Once the TC and IC of each sample had been quantified, TOC was determined by the simple relationship.

$$TOC = TC - IC \quad (3.2)$$

### 3.3.2 Gas Chromatography – Thermal Conductivity Detector (GC-TCD)

All gas samples were analysed to quantify the presence of gaseous species in the reactor effluent once returned to ambient conditions. An Agilent 6890 gas chromatograph with a thermal conductivity detector attached was employed to which a CRT1 column (*Alltech Gases*) was connected. The column was capable of detecting N<sub>2</sub>, O<sub>2</sub>, CO<sub>2</sub>, CO and CH<sub>4</sub>. Helium was used as the carrier gas as it was clearly not expected to form any part of the reactor effluent stream. The GC-TCD analysis program used for each determination is given in Table 3.1.

**Table 3.1** – GC-TCD conditions and program parameters.

<b>Column: CTR I (Alltech) 1.82 m x 6.35 mm outer, 1.82 m x 3.175 mm inner</b>	
Carrier gas	Helium
Carrier gas flowrate	65 ml/min
Detector reference gas	Helium
Detector gas flowrate	65 ml/min
Make-up gas flowrate	2 ml/min
Detector temperature	250°C
Injection temperature	50°C
Injection volume	1 or 2 ml (injection loop was changed)
Oven temperature (isothermal)	33°C
Program duration	15 mins

### 3.3.3 Nitrogen Species Analysis

Because DMF is a nitrogenated species, it was necessary to test the liquid samples for various nitrogen-containing species in an effort to approximately evaluate the fate of nitrogen within the reactor.

The liquid samples were evaluated photometrically using Spectroquant® spectrophotometric cell tests (Merck) to generate a coloured sample, the concentration of which was determined using a Nova 60A Spectrophotometer (Merck) as shown in Figure 3.9.



**Figure 3.9** – Merck Spectroquant® Nova 60A Spectrophotometer used for nitrogen analysis (Merck Millipore).

Tests to evaluate the concentrations of ammonium nitrogen ( $N\text{-NH}_4$ ), nitrate ( $NO_3^-$ ), nitrite ( $NO_2^-$ ) and the total nitrogen (TN) were used. However, due to the cost of these tests, only one determination was performed for each experiment and this was carried out at a residence time of 6 seconds. This time was chosen due to the fact that at some conditions (in particular at the highest temperatures) 6 seconds was the maximum feasible residence time due to the increased fluid volume (a corollary of the decreased density) and the fixed reactor volume. Higher residence times

resulted in the Reynolds Number indicating a laminar flow regime. It was desirable for the N-content to be comparable across all conditions and thus the residence time of 6 seconds was selected. Due to the high cost of the cell tests, a second determination was only performed if an obviously erroneous result was obtained. The determinations were performed as described below.

### 3.3.3.1 Ammonium Nitrogen

It was considered likely that ammonia would have the potential to be formed during the oxidation process and it is known as a particularly recalcitrant species (Killilea *et al.*, 1992). Thus, analysis of the quantity of ammonium nitrogen present in the forms of the ammonium ion ( $NH_4^+$ ) and ammonia ( $NH_3$ ) was performed.

In order to determine the concentration of ammonium nitrogen, a 100  $\mu$ l sample of the liquid reactor effluent was added to a reaction cell containing an alkaline solution in which the ammonium nitrogen is present almost entirely as ammonia due to the pH-dependent equilibrium between the ammonium ion and ammonia. In this cell, ammonia reacts with hypochlorite ions to form monochloramine. Monochloramine in turn reacts with substituted phenol to form an indophenol derivative which is blue in colour. The intensity of this colour is related to the concentration of ammonia in the sample and is determined photometrically (*cell test manual*).

### 3.3.3.2 Nitrate Ion

Depending on the reaction conditions, it was possible that nitrate ions ( $NO_3^-$ ) could be formed along a few as oxidation products. In order to determine the

concentration of nitrate ions, a 0.5 ml sample of the liquid reactor effluent was added to a reaction cell containing a mixture of sulphuric acid and phosphoric acid. To this solution, 1 ml of 2,6-dimethylphenol was added which reacts with nitrate ions under acidic conditions in order to form 4-nitro-2,6-dimethylphenol which is pink in colour. The intensity of the colour is related to the concentration of nitrate ions in the effluent sample and is determined photometrically (*cell test manual*).

### 3.3.3.3 Nitrite Ion

Depending on the reaction conditions, it was possible that nitrite ions ( $NO_2^-$ ) could be formed along as an oxidation product. In order to determine the concentration of nitrite ions, 5 ml of reactor effluent was added to a reaction cell containing a powder reagent consisting of sulfanilic acid and N-(1-naphthyl)ethylenediamine dihydrochloride. In the subsequently formed acidic solution, nitrite ions react with the sulfanilic acid to form a diazonium salt. This salt subsequently reacts with N-(1-naphthyl)ethylenediamine dihydrochloride to form an azo- dye which is red-violet in colour. The intensity of the colour is related to the concentration of nitrite ions in the effluent sample and is determined photometrically (*cell test manual*).

### 3.3.3.4 Total Nitrogen

The initial concentration of DMF in the reactor feed was known and consequently the initial concentration of nitrogen in the feed could also be calculated. In order to quantify the nitrogen yield, the quantity of nitrogen remaining in the liquid effluent was determined using a total nitrogen (TN) cell test.

In order to determine the concentration of nitrogen, 1 *ml* of the liquid reactor effluent was diluted with 9 *ml* of distilled and deionised water in an empty cell. Pre-prepared oxidising agents were added to the solution and mixed thoroughly, after which the cell was transferred to a thermoreactor and heated to 120°C for one hour. The digestion with the oxidising agents resulted in all organic and inorganic nitrogen being converted to nitrate ions. The digested sample was then allowed to cool to ambient temperature. Once the cooling was complete, 1 *ml* of the digested sample was added to a reaction cell containing a mixture of phosphoric acid and sulphuric acid. In addition, 1 *ml* of 2,6-dimethylphenol (DMP) was added to this cell and mixed vigorously. The nitrate ions react with the DMP to form 4-nitro-2,6-dimethylphenol which is pink in colour. The intensity of the colour is related to the concentration of nitrate ions in the test sample and is thus related to the concentration of nitrogen in the effluent sample, which is determined photometrically (*cell test manual*).

### 3.3.4 Gas Chromatography – Flame Ionisation Detector (GC-FID)

All liquid samples were analysed in order to quantify the removal of DMF from the waste as well as to track the evolution and destruction of intermediate compounds. An Agilent 6850 gas chromatograph with a flame ionisation detector attached was employed to which an Agilent DB-Wax column was connected. The conditions at which the analysis was conducted (column gas flowrates, oven temperature programs, etc) are given in Table 3.2 below.

**Table 3.2** – GC-FID conditions and program parameters.

<b>Column: Agilent DB-Wax (122-7032E) 30.0 m x 250 µm x 0.25 µm</b>	
Carrier gas	Helium
Carrier gas flowrate	0.1 ml/min
Combustion gases	Air and Hydrogen
Combustion gas flowrate	500 ml/min and 30 ml/min respectively
Split flowrate	Splitless operation
Detector temperature	260°C
Injection temperature	200°C
Oven temperature program	1 min @ 50°C; ramp = 20°C/min; 12.5 mins @ T <sub>max</sub> =180°C
Misc. program	Needle wash (zero grade water) prior to and post-injection
Total program duration	20 mins

Analysis of a number of samples of known DMF concentration allowed the creation of a calibration curve from which the DMF concentration of liquid samples taken from experiment could be evaluated. A linear relationship between DMF concentration and peak area was observed.

### 3.3.5 Gas Chromatography – Mass Spectroscopy (GC-MS)

For the oxidation of real wastes, liquid samples were analysed using gas chromatography with a mass spectrometer. The waste samples that were provided were said to be reasonably complex solutions and as such, as well as assessing the TOC content in order to quantify how the reaction had progressed on a global scale, mass spectroscopy was also performed in order to find out which components had been treated most effectively and, potentially what intermediate compounds had been formed by the SCWO of the multi-component feedstock.

This analysis was performed by the School of Chemistry and due to the cost involved with sending these samples to be analysed, only feed samples and samples

at the maximum residence time were analysed using this technique. The hardware used for this analysis was a gas chromatograph (*Shimadzu*) coupled with a time-of-flight (TOF) electron impact (EI) mass spectrometer (GCT). The method indicating the conditions at which the analysis was conducted was found by preliminary analysis using GC-FID (also conducted by the School of Chemistry).

The cost of this analysis per sample was very high and this high cost was the reason that GC-MS analysis was not performed on liquid samples taken from the SCWO of DMF.

When GC-MS analysis was performed, the mass spectra of the compounds with the highest concentrations were provided. On average, spectra from between 5 – 15 specific compounds were provided for each sample analysed. From these spectra, an assessment of the identity of each component (or a judgment on the likely form of a component, e.g. ether, carboxylic acid, aromatic compound, etc) was carried out.

## 3.4 Calculation of Parameters

### 3.4.1 Thermophysical Properties

The wide range of temperatures and pressures inherent to the SCWO process mean that no assumptions of constant density, volume, viscosity, or specific heat capacity can be made and consideration of the state and conditions of water must be made when using these properties for calculations.

As the experimental systems are over 99% water, and given the lack of thermodynamic data for DMF-water systems, the physicochemical parameters for the

DMF-Water system were assumed to be equal to those of pure water. This approximation to the physicochemical properties of water was also assumed when considering the complex waste feeds as described in chapter 6.

The thermophysical properties were obtained using NIST's online chemistry webbook (Lemmon *et al.*, 2009-2012) which calculates a number of properties of pure water at various temperatures and pressures, including density, viscosity, specific heat capacity, and thermal conductivity..

### 3.4.2 Volumetric Flowrate Changes

The HPLC pumps would deliver a constant volumetric flow at ambient temperature (298 K) and a pressure of 25 MPa. Using the fluid density, this could be converted to a mass flowrate and it was assumed that this mass flowrate remained constant. However, due to the density changes as the temperature was increased, the volumetric flowrate changed in order to maintain a constant mass flowrate such that the relationship between two flowrates,  $F_1$  and  $F_2$  at two different points with different temperatures and pressures was:

$$F_2 = \frac{\rho(T_1, P_1)}{\rho(T_2, P_2)} F_1 \quad (3.3)$$

### 3.4.3 Reynolds Number

It was required that all experiments be conducted with the fluids in the turbulent regime. As such, it was important to be able to calculate the pipe Reynolds number for each experiment. The equation for Reynolds number is:

$$Re = \frac{\rho \bar{u} D}{\mu} \quad (3.4)$$

However, as described in §3.4.1 and §3.4.2 the density and viscosity of the fluid and the velocity of its flow will change with varying temperature and pressure. As such, the equation is more accurately written:

$$Re(T, P) = \frac{\rho(T, P)\bar{u}(T, P)D}{\mu(T, P)} \quad (3.5)$$

### 3.4.4 Pécllet Number

The Pécllet number is the ratio of the rate of bulk transport to the rate of conductive or diffusive transport. This number is defined for both energy transport and mass transport in equations 3.6 and 3.7 respectively (Coulson et al., 1999):

$$Pe_e = RePr = Re \frac{C_p(T, P)\mu(T, P)}{k(T, P)} \quad (3.6)$$

$$Pe_m = ReSc = Re \frac{\mu(T, P)}{\rho(T, P)D_m(T, P)} \quad (3.7)$$

Values of the energy and mass transport Pécllet numbers were much greater than unity for all experimental conditions, indicating that reactor conditions could be assumed to be acting as plug flow.

### 3.4.5 Residence Time

The residence time of the reaction was defined as the time needed for one reactor volume of fluid to completely pass through the reactor at reaction conditions. In other words, the residence time,  $\tau$  is related to the reactor volume ( $V_r$ ) and the volumetric flowrate at reaction conditions ( $v_{sc,0}$ ) as shown in equation 3.6:

$$\tau = \frac{V_r}{v_{sc,0}} \quad (3.8)$$

### 3.4.6 Oxidant Delivered and Stoichiometric Ratio

The quantity of oxidant required was based on the molar and volumetric flowrates of the organic feed at the particular reaction conditions and the stoichiometric ratio of the particular experiment, in which the total molar flowrate of oxidant was the product of the molar flowrate of oxidant required to achieve ideal stoichiometry and the oxidant ratio. The stoichiometric ratio was defined as follows:

$$SR = \frac{([oxidant]/[organic])_{initial}}{([oxidant]/[organic])_{stoichiometric}} \quad (3.9)$$

In this system, a stoichiometric ratio (or sometimes ‘oxidant ratio’ for simplicity) of unity indicates that the amount of oxidant delivered was exactly the amount necessary for ideal stoichiometric conversion. Consequently, SR>1 indicated an oxygen excess and SR<1 indicated an oxidant deficit.

### 3.4.7 Concentration at Reaction Conditions

The concentration of the reactants at reaction conditions will be different from the concentrations when they are prepared at ambient conditions due to the temperature-dependent nature of density and, consequently, volume. The initial organic concentration ( $[organic]_i$ ) and oxidant concentration ( $[oxidant]_i$ ) will be reduced at supercritical conditions and this was taken account of by incorporating the ratio of densities at ambient and reaction conditions, molar flowrates and volumetric flowrates. Consequently, the initial concentrations of organic and oxidant at the reactor inlet ( $[organic]_0$  and  $[oxidant]_0$  respectively) was determined.

### 3.4.8 Product Yields

The yields of various products, where calculated took the following general forms.

$$\text{Carbon yield} = \frac{\text{moles } C_{\text{product}}}{\text{moles } C_{\text{initial}}} \quad (3.10)$$

$$\text{Nitrogen yield} = \frac{\text{moles } N_{\text{product}}}{\text{moles } N_{\text{initial}}} \quad (3.11)$$

where ‘moles  $C_{\text{product}}$ ’ and ‘moles  $N_{\text{product}}$ ’ are the moles of carbon and nitrogen respectively in the individual components in the product and ‘moles  $C_{\text{initial}}$ ’ and ‘moles  $N_{\text{initial}}$ ’ are the number of moles of carbon and nitrogen respectively in the initial feed.

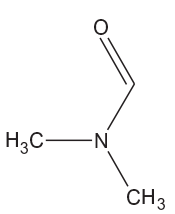
### 3.5 Risk Assessments

Assessments of the hazards of operation at high temperatures and pressure, the use of potentially harmful chemicals in the form of DMF, hydrogen peroxide, and the complex industrial wastes, and the general hazardous natures involved in laboratory work were carried out and are provided in appendix 2.

## CHAPTER 4 - SINGLE-STAGE SUPERCRITICAL WATER OXIDATION OF DIMETHYLFORMAMIDE

### 4.1 The Oxidation of Dimethylformamide

As described in §2.4.1, nitrogenated organics are commonly found in wastewater streams from a wide variety of industrial processes. Despite this, the majority of SCWO research has involved the treatment of non-nitrogenated organics. As such, an analysis of the SCWO of a nitrogenated organic compound would be valuable to the field. Furthermore, an analysis of the SCWO of such a compound in differing reactor configurations such that would be able to offer differing oxidant injection profiles would be of even greater novelty, being that such research was even less common. This approach will be discussed in chapter five.

Structure	
Formulae	C <sub>3</sub> H <sub>7</sub> NO or (CH <sub>3</sub> ) <sub>2</sub> NCHO
Molecular Mass	73.09 g mol <sup>-1</sup>
Boiling Point	153.1°C
Miscibility with Water	Completely Miscible
C.A.S. Number	68-12-2

Dimethylformamide (DMF) was chosen as the compound to be investigated as an analogue of a nitrogenated organic waste pollutant. Some physical and chemical data pertaining to the structure and properties of DMF are provided in Table 4.1.

DMF is the doubly methyl-substituted relation of the simplest amide, formamide. It is

**Table 4.1** – Properties of DMF

miscible with water in all proportions, meaning that solutions could be formulated and maintained at ambient conditions for the duration of the experiment.

DMF is used primarily as an industrial solvent in the manufacture of fibres, films and surface coatings, to facilitate the easy spinning of acrylic fibres, to produce wire enamels, and as a crystallisation medium in the pharmaceutical industry (US Environmental Protection Agency, 2007). It is also employed commercially as a solvent in vinyl resins, adhesives, pesticide formulations, and epoxy formulations; for purification and/or separation of acetylene, 1,3-butadiene, acid gases, and aliphatic hydrocarbons; and in the production of cellulose triacetate fibres and pharmaceuticals (Long *et al.*, 2001).

The reasons for the selection of DMF were twofold. Firstly, as described above, its use in industry is widespread and as such, the investigation of the SCWO treatment of this compound would provide an insight of the potential applicability of SCWO technology to these DMF-containing wastewater streams.

Secondly, DMF is a relatively simple nitrogenated organic in the sense that it has a relatively low molecular mass and is no part of the molecule is aromatic in nature. As such, as well as being able to assess the global process efficiency by considering TOC analysis data, DMF's likely reaction mechanisms in the SCWO process can be estimated via the determination of the likely reaction products, for example, by correlation with kinetic data obtained from experiment, literature and from analogous elementary gas-phase combustion reactions.

## 4.2 Experimental Setup

The reactor apparatus used for this single-stage oxidation work was the construction as described in §3.1 and as shown in Figure 4.1, where the two reactants were preheated separately, mixed at the reactor inlet, and then, downstream of the reactor, the reactor exit stream was quenched and cooled to ambient temperature, depressurised, and separated into gas and liquid components.

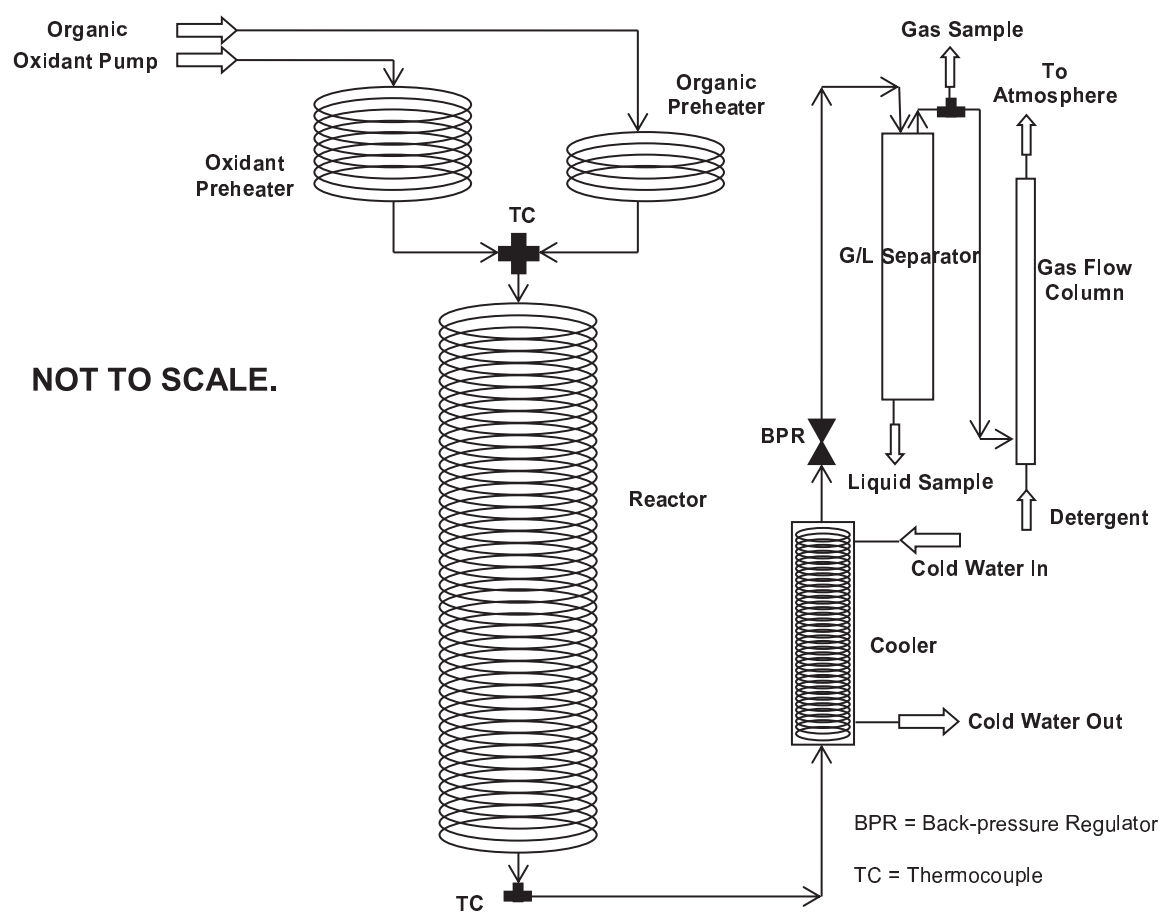


**Figure 4.1** – Reactor schematic indicating the single-stage oxidation rig.

The reactor was 12.4 m in length for the majority of experiments, but was 12.54 m in length for some others due to the need to replace some piping. When piping was cut and new sections transplanted, slight changes in length were

inevitable. The reactor residence time calculation was based upon the section of the reactor between the inlet and outlet thermocouples as described in §3.1.5. This length in which the temperature could be controlled corresponded to 94.7% of the length of piping in which the two reactants exist together upstream of the cooler. Any reaction is assumed to occur within the defined reactor length, but it should be noted that if the temperature is maintained between the outlet thermocouple and the cooler, residence times could potentially be ~5% greater than those reported.

Where possible, multiple experiments at different residence times were conducted consecutively for each permutation of temperature, initial feed concentration and oxidant stoichiometric ratio.

### 4.3 Effect of System Parameters

If SCWO technology is to penetrate the mainstream wastewater treatment market to any appreciable extent, it is necessary to fully understand the SCWO process with particular reference to the effect on the rate of reaction and chemical dynamics. Such understanding informs the development of more efficient processes, thus making the technology more attractive for long-term use. For these reasons, the effect of several process operational variables on the treatability of DMF has been investigated and the results presented below.

#### 4.3.1 Experimental Programme

The effects of temperature, feed concentration, oxidant ratio, and residence time on the treatability of DMF in solution with water under supercritical conditions upon exposure to oxygen were investigated. The default conditions for this process

was to maintain the temperature at 400°C, to make up a solution of DMF of 10 mM at supercritical conditions, and to deliver the stoichiometric quantity of oxygen required, i.e. the stoichiometric ratio was 1.

The range of temperatures that were investigated was 400-550°C. The reaction temperature has a significant effect on the dynamics of all chemical species being generated and consumed within this system through the Arrhenius term in the reaction rate constants and as such, the investigation of a wide range of temperatures was desirable. The range stated above was almost the largest feasible given that it was desirable to ensure that the lowest temperature was sufficiently far from the critical point transition. The upper limit of the temperature range available for investigation was governed purely by the limits of the laboratory hardware. The temperature control system on the oven had a nominally proportional-integral-derivative (PID) format but age commuted this to essentially on-off operation. As such, at the top of its rated range (650°C), the oven's controller could not limit the fluctuations in the ambient temperature to within  $\pm 2^\circ\text{C}$  as required. The limit of 550°C was therefore chosen as the highest oven temperature at which the reactor inlet temperature could confidently be expected to remain constant.

The concentration of the DMF solutions that were prepared prior to each experiment were based on their concentration upon injection to the reactor, i.e. at supercritical conditions. For example a DMF concentration of 10 mM immediately prior to injection at 400°C and 250 bar would correspond to a concentration of 59.1 mM in the stock at ambient temperatures. Organic solutions were prepared such that the concentration at supercritical conditions varied between 5 and 20 mM with most experiments having a 10 mM organic stream injected.

Oxidant ratios between 0.5 and 5 were investigated at varying temperatures and initial conditions, and residence times were set between 2 s and 10 s where the higher residence times were possible whilst still maintaining turbulent flow through the reactor. The experimental conditions are summarised in Table 4.2.

**Table 4.2** – Experimental conditions for single-stage oxidation of DMF

Experiment	Temperature K	Pressure bar	DMF Concentration mM	Oxidant Ratio -	Residence Time s
VA-VD	400 – 550	250	10	1	2 – 10
VE-VH	400	250	5 – 20	1	2 – 10
VI-VP	400	250	10	0.5 – 5	2 – 10
VQ-VS	400	250	5 – 15	3	2 – 10
VBR,VT-VW	450 (VBR), 500	250	10 (VBR) 2 – 15	3	2 – 10

#### 4.3.2 Effect of Reactor Pressure

The effect of reactor pressure was not specifically investigated – i.e. no experiment sets were planned in which the pressure was varied whilst the other parameters were held constant. Experimental conclusions in the literature with regards to the effect of pressure are somewhat contradictory and as such future investigations into the effect of pressure, with particular reference to the probable contribution to the dynamics of the radical pool would likely be profitable.

#### 4.3.3 Effect of Residence Time

The effect of residence time on the dynamics of various species (DMF, TOC, TC, nitrogen species, etc) was investigated. For all investigated combinations of temperatures, concentrations and oxidant ratios, the pumps were set so that residence times of between 2 s and 10 s would be delivered. For the most part,

residence times of 2, 4, 6, 8 and 10 s were investigated. As described in §4.3.4, the higher residence times could not always be reached as the condition of the preservation of turbulent flow had to be met. At the other end of the scale, residence times below 2 s were usually unfeasible due to such pump flowrates being required to be higher than the upper limit of  $20 \text{ ml min}^{-1}$ . In general at  $400^\circ\text{C}$ , residence times between 1.4 s and 19 s were possible, although for times in excess of 10 s the low liquid flowrates required made the experiments unfeasible to perform.

It was expected that yields of DMF, TOC and TC would decrease with increasing residence time. This follows from the knowledge that as long as there is available oxidant and associated reacting radical species, the oxidation reaction is favourable. Increasing residence time increases the time at which the reactants are together under the reaction conditions and thus, given that no research seems to suggest that lower Reynolds numbers hinder the reaction, the higher the residence time, the more conversion of these key species would be expected. Indeed, it follows that due to the lack of mass transfer limitations, given a sufficiently long reactor (and thus a sufficiently high residence time) one would expect the yields of DMF and TOC to be reduced to zero. Figure 4.2 shows the removal of DMF, TOC and TC at temperatures of  $400$  and  $500^\circ\text{C}$ . As is ubiquitous in previous research, there was a clear positive dependence of the removals of DMF, TOC and TC with residence time for all reaction conditions.

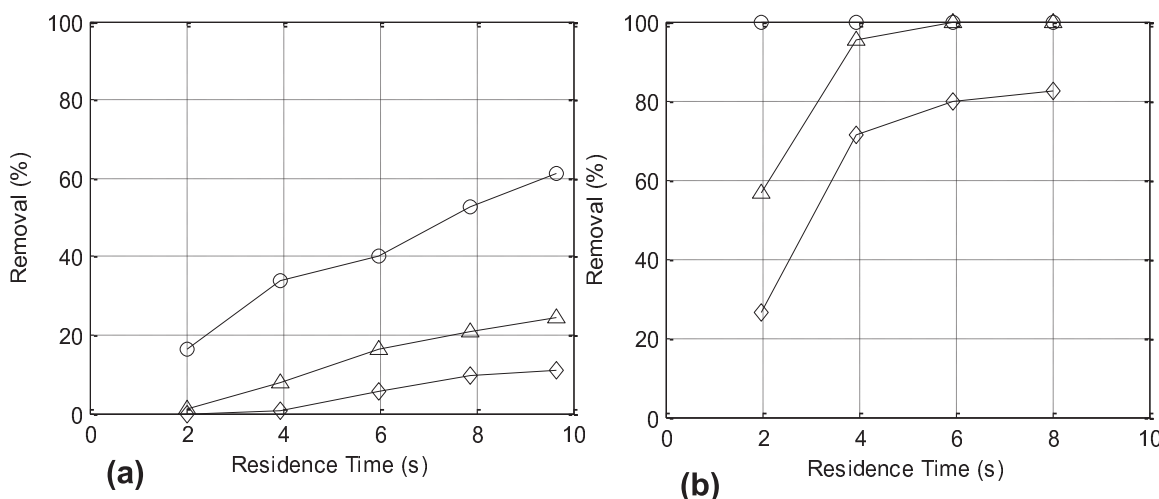


**Figure 4.2** – DMF (O), TOC ( $\Delta$ ) and TC ( $\diamond$ ) removal as a function of residence time for temperatures of 400°C (a) and 500°C (b). [DMF]<sub>feed</sub> of 10 mM and oxidant ratio of 1.

#### 4.3.4 Effect of Temperature

The effect of varying temperature on the carbon and nitrogen yields was investigated. The idea that the reaction kinetics will follow an Arrhenius-type rate law is ubiquitous in the literature. Given this assumption, one would expect that the reaction rate constant would increase with increasing temperature, resulting in correspondingly reduced carbon yields (higher TOC conversions) in the liquid products as the temperature was raised.

The temperature of the reaction was set to 400, 450, 500 and 550°C whilst the organic concentration and stoichiometric ratio were held constant at 10 mM and 1 respectively. For each of these temperatures, several oxidation experiments were carried out at residence times up to 10 s where this was possible after taking the Reynolds number of the flows into account in order to ensure that conditions were

turbulent at all times. Temperatures in excess of 550°C could not be investigated due to the maximum rating of the oven.

Figure 4.3 displays the removal of carbon in the liquid fractions at 2.0 s, 5.9 s and 7.8 s as functions of temperature. The figures show that as expected, there is a positive dependence of the removals of DMF, TOC and TC on the reaction temperature. Interestingly, it appears that at very low residence times (~ 2 s), the removals of DMF, TOC and TC could be approximated to have a linear relationship with temperature. Extrapolating this behaviour implies that the x-axis would be crossed very close to the critical point indicating that the supercritical state of water is critical to facilitating the oxidation of DMF at such low residence times. In comparison, WAO of analogous compounds generally need residence times of the order of minutes to generate appreciable conversions.

There were near complete removals of TOC at temperatures in excess of 500°C and residence times in excess of 6 s. At a residence time of 7.9 s, 98% of TOC was removed at 450°C indicating that providing the reactor can be made long enough, temperatures lower than 500°C would be sufficient for complete removal of TOC. Generally these observations agree with all of those seen in numerous sources in the literature, and with what would be expected for Arrhenius-type kinetics where DMF and TOC removals show a positive dependence on reaction temperature.

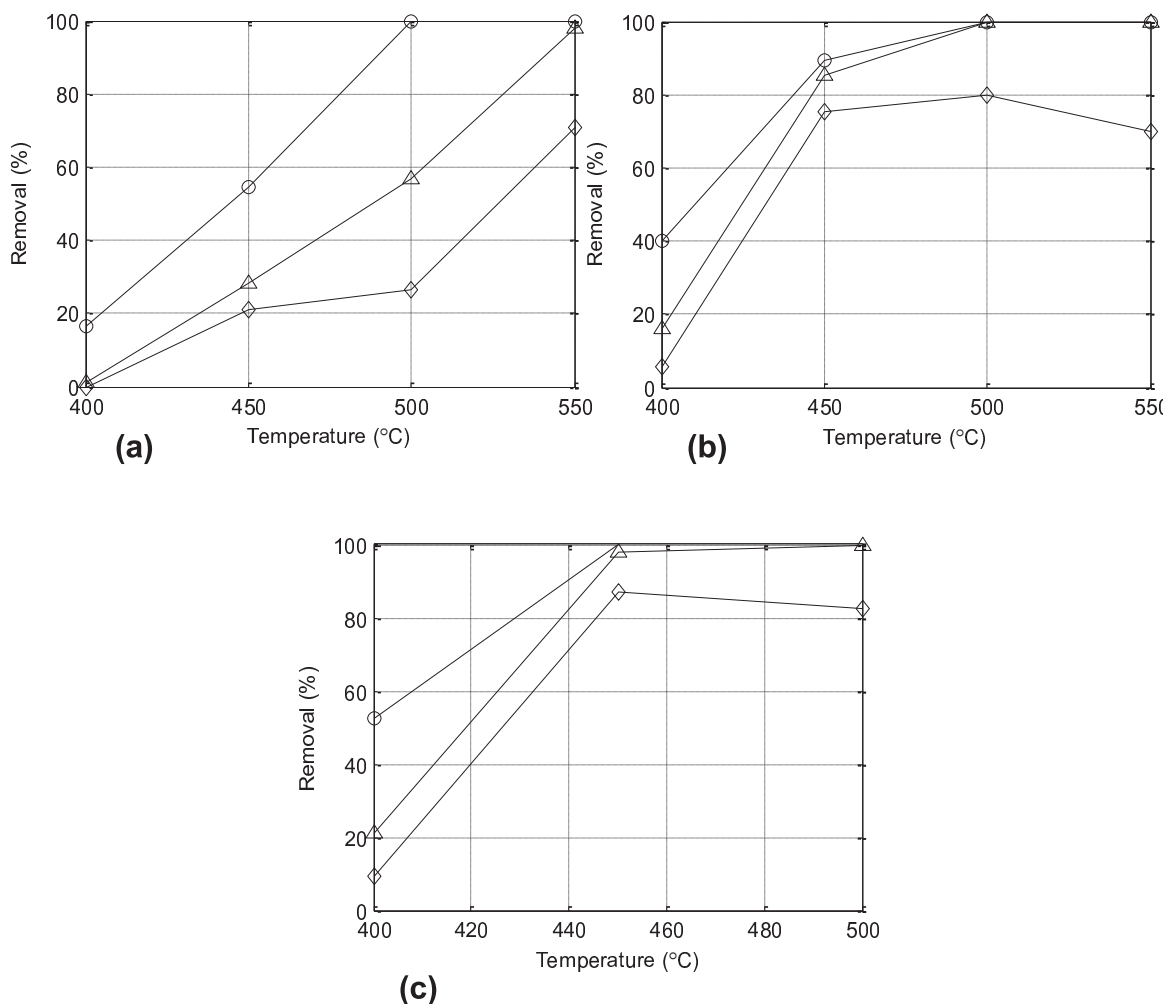


**Figure 4.3** – Removal of DMF (O), TOC ( $\Delta$ ) and TC ( $\diamond$ ) as a function of temperature for a residence time of 2.0 s (a), 5.9 s (b), and 7.9 s (c), and  $[DMF]_{feed}$  of 10 mM.

At a residence time of 5.9 s, the level of carbonaceous species removal increased rapidly between 400-450°C, behaviour that is also seen in the higher residence time plot (Figure 4.3c). TC removals for 2 experiments (550°C and 5.9 s; 500°C and 7.9 s) were slightly reduced in comparison to what would follow from the previous points in the plot (Figure 4.3b and Figure 4.3c). Increased yields of IC were found for these particular experiments indicating that higher temperatures and/or

longer residence times at these higher temperatures could be facilitating an increased conversion of DMF to IC products.

The carbon fraction yields as a function of temperature for a residence time of 5.9 s are given in Figure 4.4. It is clear that as the temperature increases, the yields progress further towards CO<sub>2</sub> and inorganic carbon (IC) being the major products. It is likely that the inorganic carbon exists in the form of carbonate and hydrogencarbonate ions that can exist in soluble equilibrium with water once the reactor products are returned to a subcritical state.

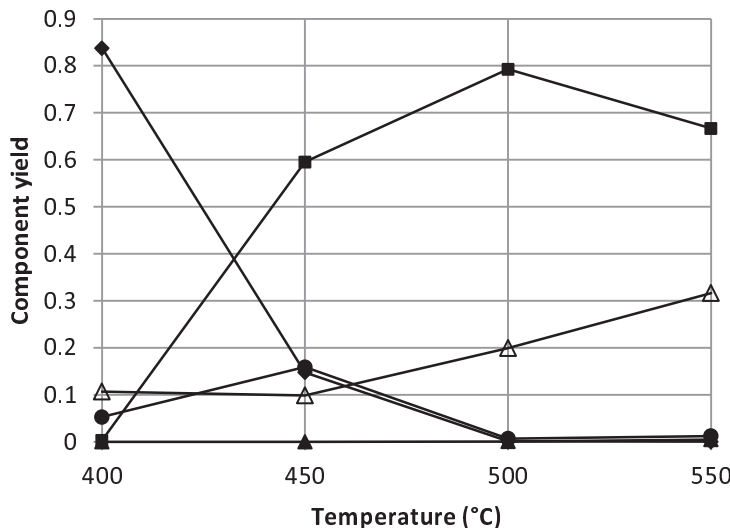


**Figure 4.4** – Carbon fraction yields as a function of temperature at a residence time of 5.9 s: TOC (♦), IC (Δ), CH<sub>4</sub> (▲), CO (●), CO<sub>2</sub> (■).

At 500°C and 550°C, the rate of the conversion reaction of CO to CO<sub>2</sub> was high enough such that the selectivity of CO<sub>2</sub> approached 1. Very small quantities of methane (yield ~ 0.4%) were detected in the gaseous products at the highest temperatures, indicating the presence of interactions between CH<sub>3</sub>• and other organic radicals (CH<sub>3</sub>O• [loss of hydroxyl hydrogen], CH<sub>2</sub>OH• [loss of methyl

hydrogen],  $\text{HCO}\cdot$ ) as suggested in the mechanism reported by Brock and Savage (1995). It is likely that any surviving methane was produced in the last stages of the reaction, just prior to quenching because it has the potential to be destroyed rapidly in contact with many radicals, in particular with the non-organic radicals denoted by  $\text{H}\cdot$  ( $k \sim 10^7 \text{ litre mol}^{-1} \text{ s}^{-1}$ ),  $\text{O}\cdot$  ( $k \sim 10^8 \text{ litre mol}^{-1} \text{ s}^{-1}$ ), or  $\text{OH}\cdot$  ( $k \sim 10^9 \text{ litre mol}^{-1} \text{ s}^{-1}$ ) (Brock and Savage, 1995). The presence of methane could also indicate the relative lack of such radical compounds at these latter stages, or a lack of adequate mixing such that these species are not brought together as often as would be desired. Nitrogen fraction yields are presented in Figure 4.5.

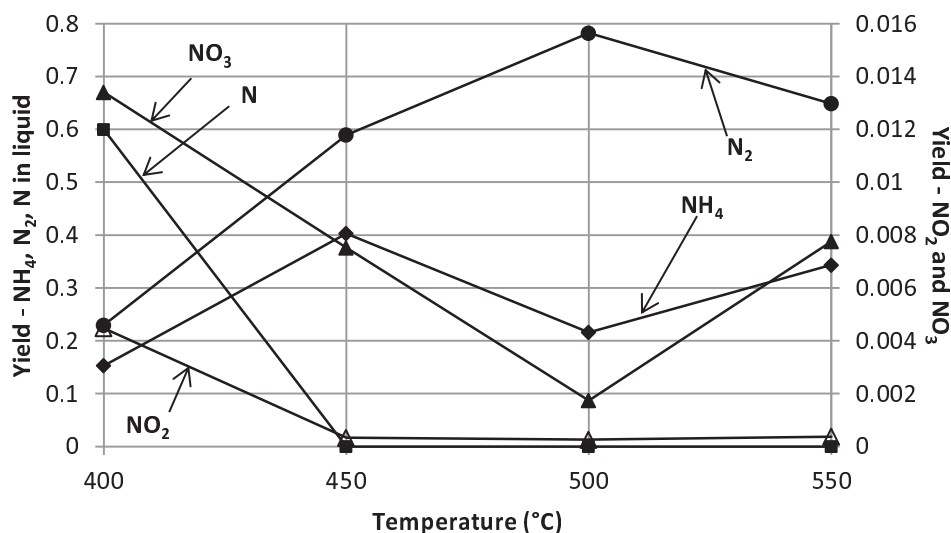


**Figure 4.5** – Nitrogen fraction yields as a function of temperature at a residence time of 5.9 s. Right y-axis:  $\text{NO}_2^-$  (Δ),  $\text{NO}_3^-$  (▲); Left y-axis:  $\text{NH}_4^+$  (◆),  $\text{N}_2$  (●), other N in liquid (■).

Gas samples were taken via injection into a water-filled serum bottle and although every attempt was made to ensure that no contamination occurred, frequent contamination of the gas samples with atmospheric air was observed. As such, the

assumption was made that all nitrogen not present in the liquid product was to be found in the gaseous product in the form of diatomic nitrogen.

The ammonia yield increased with temperature from 400 to 450°C, with less being produced at 500°C and 550°C. It is frequently reported that any ammonia being formed is not subsequently decomposed to any great degree at temperatures below 650°C. However at higher temperatures investigated, almost all DMF and TOC was removed, but ammoniacal nitrogen yields were below 50%. Further analysis will be given in §4.4.4, but suffice it to say that detailed kinetics analysis of the SCWO of methylamine (Benjamin and Savage, 2005) suggest that the fate of nitrogen for the end of the DMF oxidation would be about 75% biased towards the formation of ammonia for the branches in which methylamine is formed, but analysis of the fate of fenuron [ $C_6H_5-NH-CO-NH(CH_3)_2$ ] (Aymonier *et al.*, 2000) suggest that at temperatures between 500°C and 550°C a redox reaction between  $NH_4^+$  and any of the  $NO_3^-$  ion present can form diatomic nitrogen and water, although it is unlikely that enough nitrate was produced to make such a branch significant. As such, it seems that at higher temperatures, the DMF decomposition was either slightly biased toward a route that was unfavourable to the formation of ammonia, or that ammonia decomposition has occurred to some extent.

#### 4.3.5 Effect of DMF Concentration

When considering an Arrhenius-type rate expression, the rate of reaction is a function of the concentration of DMF raised to some power, notated as 'a' in the analysis in §4.4. As such, oxidation runs were conducted at various organic feed concentrations at 400°C and 500°C. The investigated DMF feed concentrations were

5, 15 and 20  $\text{mM}$  at 400°C (with 10  $\text{mM}$  already having been investigated as part of the temperature runs), and 2, 5, 10 and 15  $\text{mM}$  (no 20  $\text{mM}$ ) at 500°C. Generally, selection of concentration range is subject to the oxidant flow constraints required in order to supply stoichiometric oxygen. Operating at higher temperatures can also affect the chosen concentrations due to flow conditions being affected by varying fluid density.

The removal of DMF, TOC and TC as a function of the feed concentration of DMF is shown in Figure 4.6 (SR = 1), Figure 4.7 (SR = 3) and Figure 4.8 (oxidant excess and temperature of 500°C). A comparison of each combination of conditions on the removal of DMF is presented in Figure 4.9 for residence times of 2 s and 6 s. The rate of removal of DMF and TOC was found to have a positive dependence on the feed concentration of DMF, both for stoichiometric additions of oxidant and at conditions of oxidant excess. At a 6 s residence time, DMF removal ranged from 28% at 5  $\text{mM}$  feed concentration to 56% at 20  $\text{mM}$  feed concentration. If one considers the concentrations in the reactor, rather than in the feed, this corresponds to a strong reliance of removals on concentration where 5 and 20  $\text{mM}$  in the feed correspond to 2 and 2.9  $\text{mM}$  in the reactor respectively for a stoichiometric ratio of unity. Thus, for an additional millimoles of DMF per litre of reactor content at injection (from 5  $\text{mM}$  to 20  $\text{mM}$  feed), double the DMF conversion is seen after 6 s.

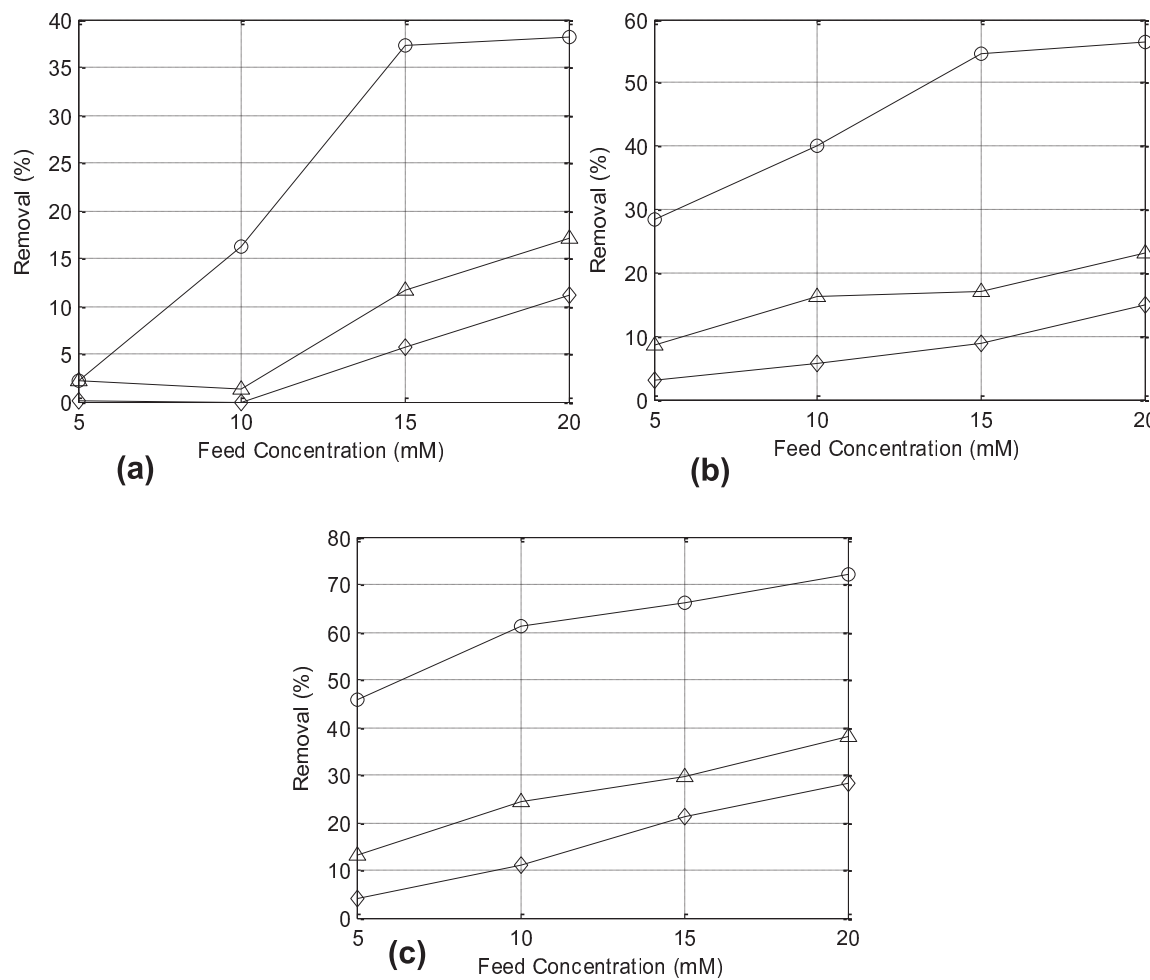


**Figure 4.6** – Removal of DMF (O), TOC ( $\Delta$ ) and TC ( $\diamond$ ) against DMF feed concentration at  $400^{\circ}\text{C}$ , SR of 1, and residence times of 2 s (a), 6 s (b) and 10 s (c).

This behaviour was also observed with the TOC removal at a reaction temperature of  $500^{\circ}\text{C}$  and oxidant excess at low residence times (2 s) where it ranged from 72% at 5 mM to over 95% at 15 and 20 mM. For residence times higher than this for these conditions, complete removals of TOC and DMF were observed.

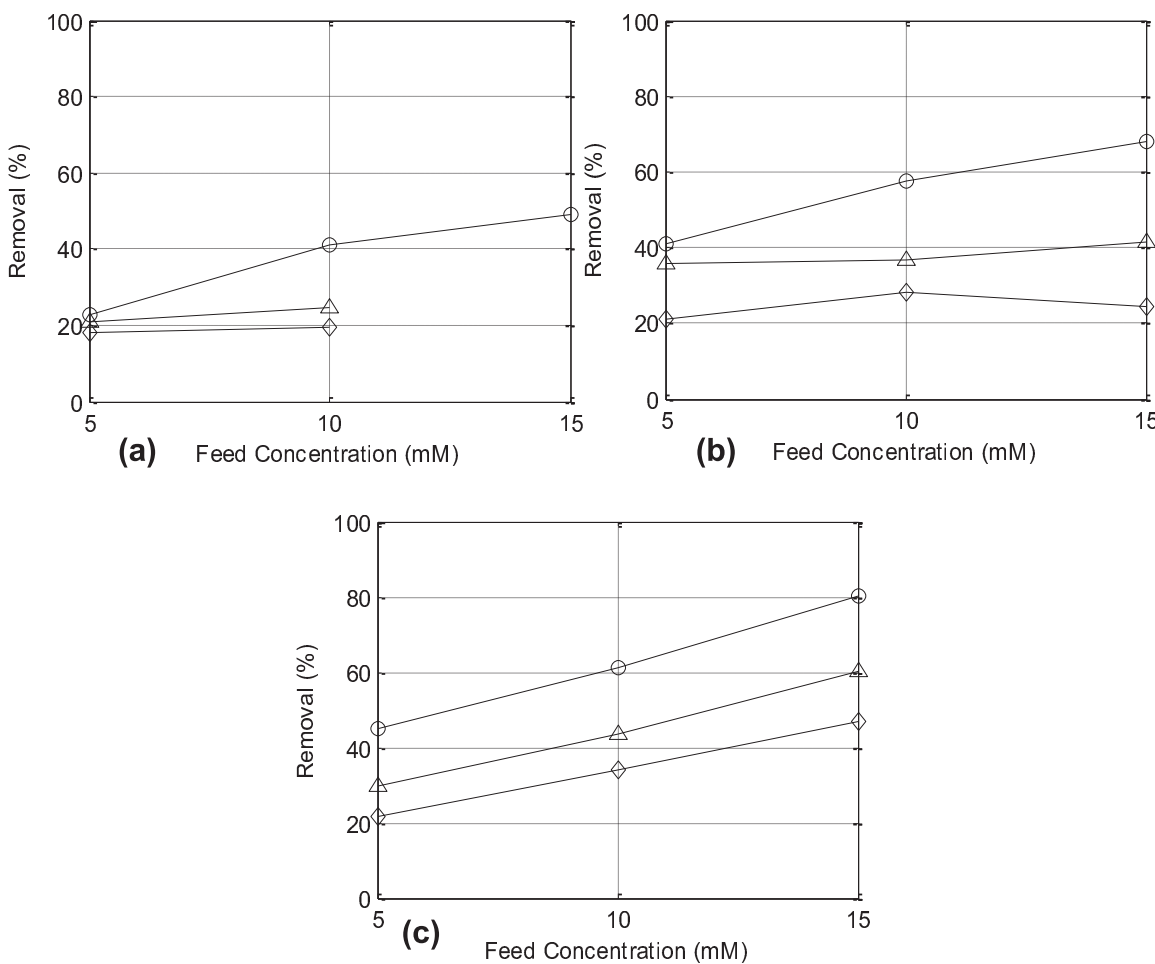


**Figure 4.7 – Removal of DMF (O), TOC ( $\Delta$ ) and TC ( $\diamond$ ) against DMF feed concentration for a temperature of 400°C, SR of 3, and residence times of 2 s (a), 6 s (b) and 10 s (c).**

The DMF and TOC removals for the experiments at excess oxidant were higher than those where the quantity of oxidant delivered is stoichiometric. Some studies indicated that the concentration of the excess oxidant had no effect on the rate of reaction, i.e. that the order of reaction with respect to oxygen is zero (Sánchez-Oneto, 2007), but this elevation in rate at a higher oxidant ratio indicates that this reaction order may not be zero. This effect is even more pronounced when one considers that the oxidant ratios were varied (at constant feed concentration)

and as such the concentration in the reactor would have been further reduced for the oxidant-excess scenario. Thus the dependence of DMF and TOC removals on the oxidant ratio could be construed to be even higher. This will be visited further in §4.4.

As was established in §4.3.4, increasing the reaction temperature greatly increases the rate of reaction and thus the degree of removal. This effect dominated for experiments conducted at oxidant excess and high temperature. DMF removal at 500°C and oxidant excess was always greater than 99.99%, while TOC removal matched this at a residence time of 6 s. For a residence time of 2 s, the TOC removal rises with increasing feed DMF concentration as would be expected from the above observations, as does the TC removal, both to a greater extent than at 400°C and without an excess of oxidant.

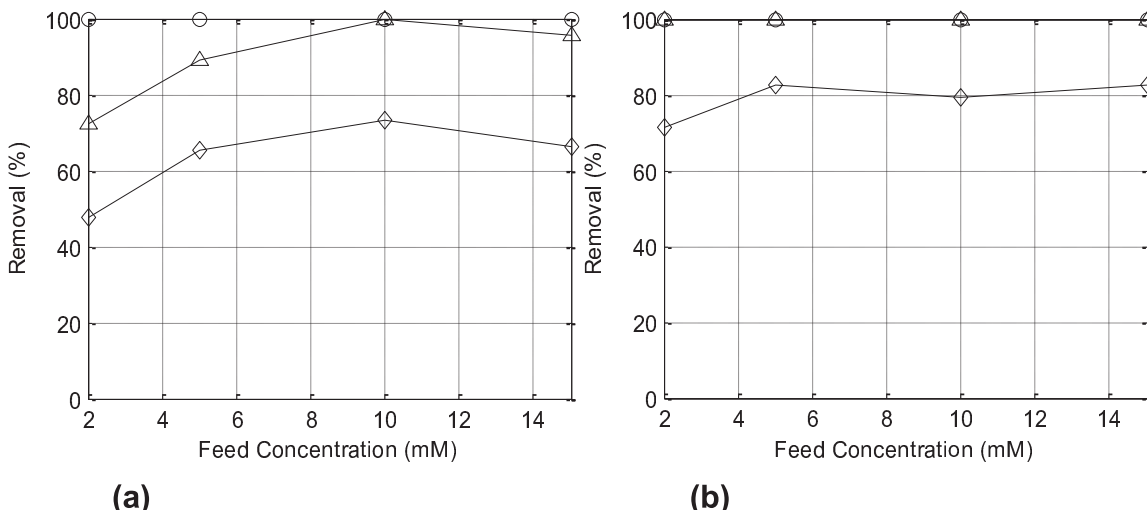


**Figure 4.8** – Removal of DMF (O), TOC ( $\Delta$ ) and TC ( $\diamond$ ) as a function of DMF feed concentration for a temperature of 500°C, SR of 3, and residence times of 2 s (a) and 6 s (b)

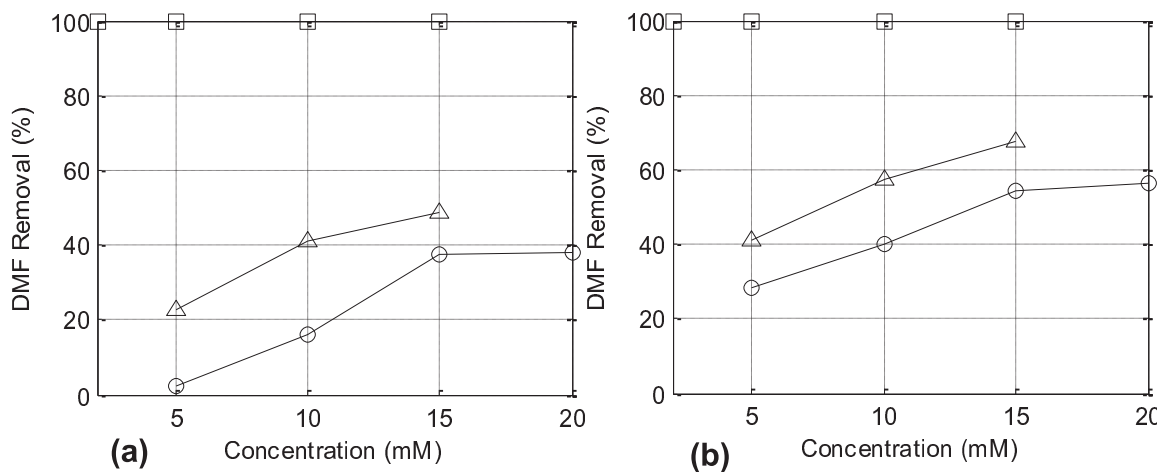


**Figure 4.9** – DMF removal as a function of concentration at residence times of 2 s (a) and 6 s (b) for (temperature/SR): 400°C / 1 (O), 400°C / 3 ( $\Delta$ ), 500°C / 3 ( $\square$ ).

The carbon and nitrogen fraction yields, provided in Figure 4.10 and Figure 4.11 indicate that the main products are CO<sub>2</sub>, IC and N<sub>2</sub>, along with unreacted DMF and its associated TOC. No methane was detected in the gaseous products.

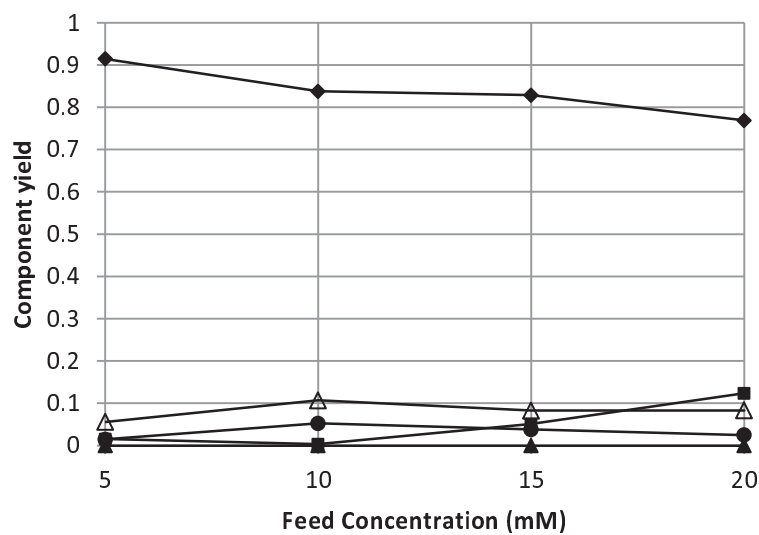


**Figure 4.10** – Carbon fraction yields as a function of concentration at a residence time of 5.9 s: TOC (◆), IC (Δ), CH<sub>4</sub> (▲), CO (●), CO<sub>2</sub> (■).

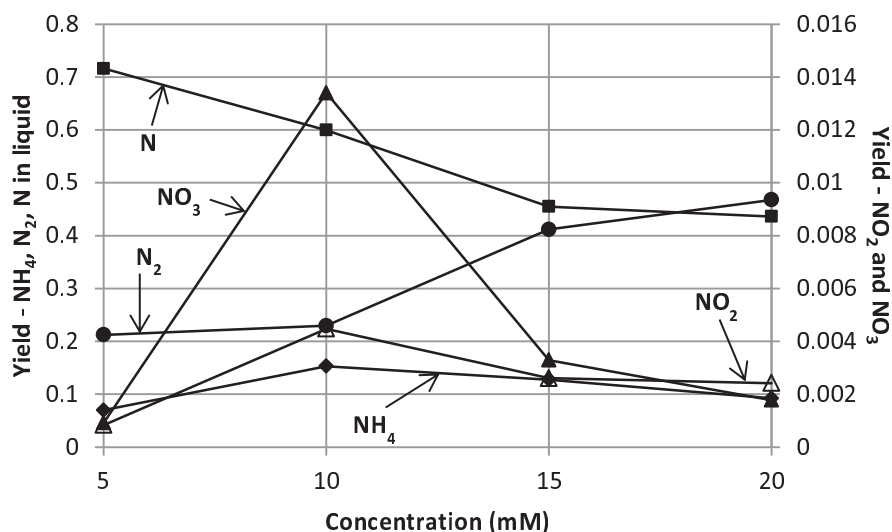


**Figure 4.11** – Nitrogen fraction yields as a function of concentration at a residence time of 5.9 s. Right y-axis:  $\text{NO}_2^-$  ( $\Delta$ ),  $\text{NO}_3^-$  ( $\blacktriangle$ ); Left y-axis:  $\text{NH}_4^+$  ( $\blacklozenge$ ),  $\text{N}_2$  ( $\bullet$ ), other N in liquid ( $\blacksquare$ ).

The yields of nitrite and nitrate generally didn't exhibit a great dependence on concentration, nor did the yields of IC and CO, indicating that if the concentration was increased further, the expected yields of  $\text{CO}_2$  and  $\text{N}_2$  would be even greater. The yield of ammoniacal nitrogen decreased slightly as the feed concentration of DMF was increased, in opposition to the DMF conversion. The ammonia yield could have remained relatively low (at approximately 15% - which corresponds to between 18% and 38% of the nitrogen present in non-organic products) either by progression of the reaction along a route non-conducive to the production of ammonia, or by the offsetting of any ammonia production by decomposition via reaction with CO, an increased amount of which is presumably produced as an intermediate of the ultimate oxidation of methanol and methylamine (which also form as intermediates as is discussed in §4.4.4). An interaction with CO is one feature of why co-oxidations of

ammonia with an auxiliary fuel can show markedly increased removals of ammonia than in systems without the co-fuel and may be a system that is occurring here at higher concentrations, although a study by Oe *et al.* (2007) suggests that the temperature employed herein may not be high enough for this effect to be appreciable. The implication of this is that ammonia production as well as decomposition could be inhibited at lower temperatures in comparison to the higher yields observed at higher reaction temperatures.

In contrast, at 400°C and at oxidant excess, the IC yield shows a positive dependence on DMF concentration; with the main products aside from liquid organics clearly being CO<sub>2</sub> and IC (Figure 4.12). A very small amount of methane was detected at the lowest concentration.

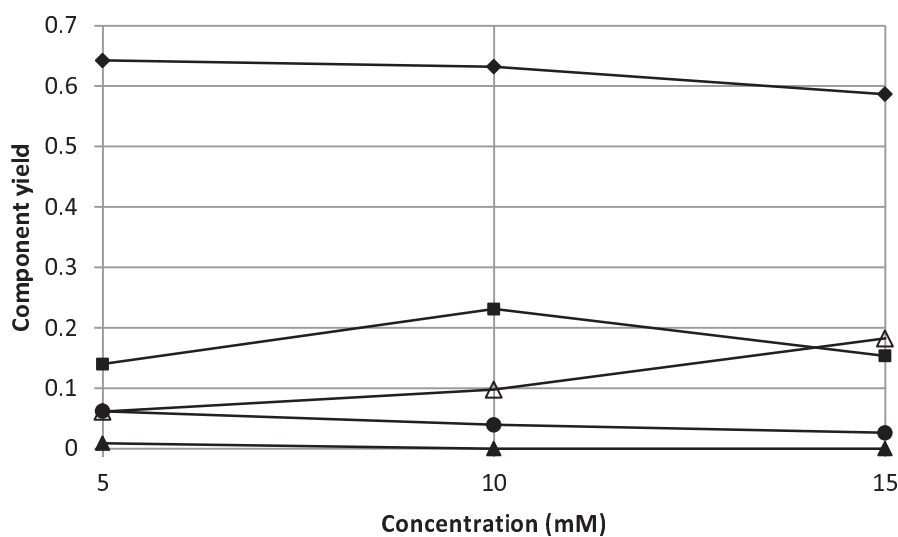


**Figure 4.12** – Carbon fraction yields as a function of concentration at a residence time of 5.9 s (SR = 3): TOC (◆), IC (Δ), CH<sub>4</sub> (▲), CO (●), CO<sub>2</sub> (■).

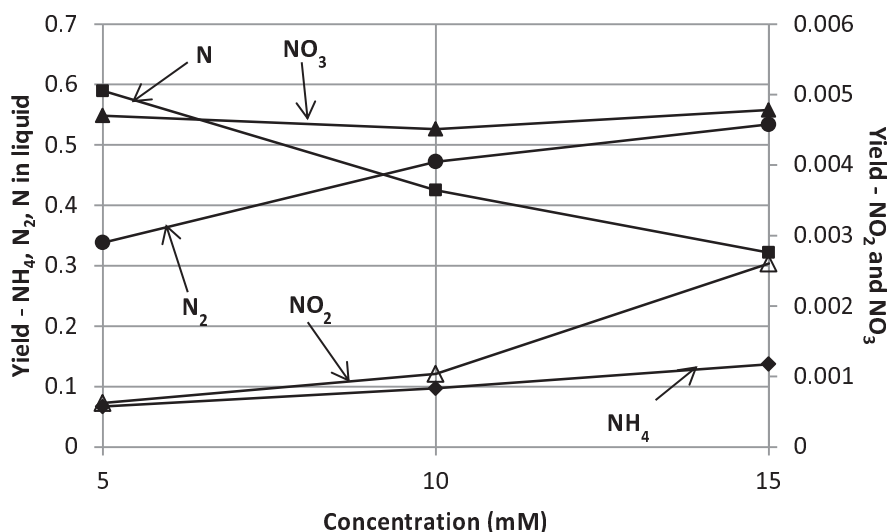
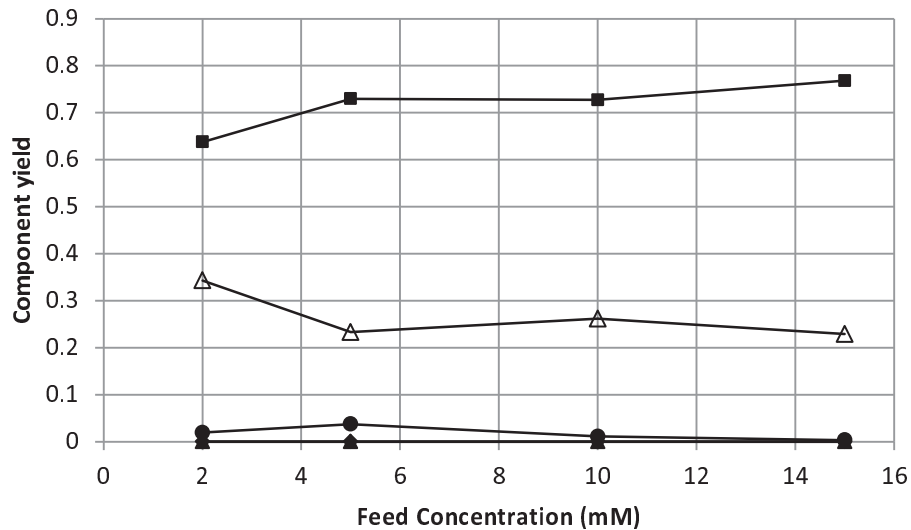


**Figure 4.13** – Nitrogen fraction yields with concentration at residence time of 5.9 s (SR = 3).

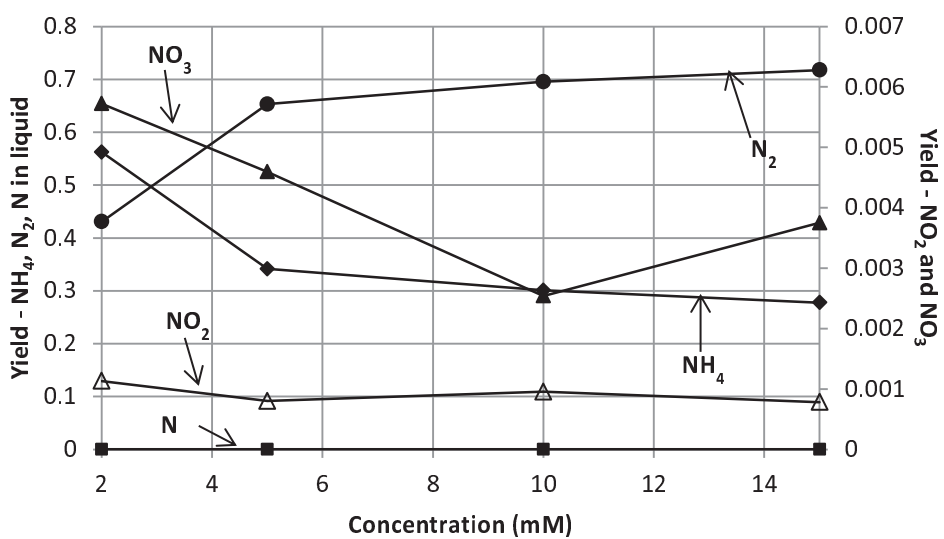
Right y-axis:  $\text{NO}_2^-$  ( $\Delta$ ),  $\text{NO}_3^-$  ( $\blacktriangle$ ); Left y-axis:  $\text{NH}_4^+$  ( $\blacklozenge$ ),  $\text{N}_2$  ( $\bullet$ ), other N in liquid ( $\blacksquare$ ).

Figure 4.13 indicates the nitrogen fraction yields at 400°C and oxidant excess. The ammonia yield showed a positive dependence on DMF feed concentration, increasing from 6% to 13% when the DMF feed concentration is increased from 5 to 15 mM. Such a behaviour contrasts slightly with the relatively constant ammonia yields seen at stoichiometric oxidant. This is likely to be purely down to the increased removal of DMF, although this behaviour wasn't overtly apparent in the stoichiometric oxidant system. If the difference is due to the mechanism, there is the potential for oxidant excess to cause faster oxidation down the non-nitrogenated organic branches (methanol oxidation) resulting in fewer interactions between ammonia and other reactive intermediate components, facilitating a greater ammonia yield. Nitrate and nitrite yields were very low (<0.5%) and as the yield of organic nitrogen decreases, the yield of  $\text{N}_2$  increases (both trends occur with increasing DMF feed concentration).

Finally, Figure 4.14 and Figure 4.15 indicate the carbon and nitrogen fraction yields at 500°C and oxidant excess.



**Figure 4.14** – Carbon fraction yields as a function of concentration at a residence time of 5.9 s ( $T = 500^{\circ}\text{C}$ , SR = 3): TOC (◆), IC (Δ), CH<sub>4</sub> (▲), CO (●), CO<sub>2</sub> (■).



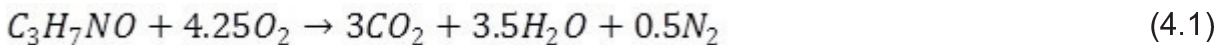
**Figure 4.15** – Nitrogen fraction yields with concentration at residence time of 5.9 s ( $T = 500^{\circ}\text{C}$ , SR = 3). Right y-axis:  $\text{NO}_2^-$  (Δ),  $\text{NO}_3^-$  (▲); Left y-axis:  $\text{NH}_4^+$  (◆),  $\text{N}_2$  (●), other N in liquid (■).

The yield of organic carbon in the liquid was reduced to zero at this temperature as discussed above and a corollary of this was that the yield of organic-bound nitrogen was also reduced to zero. There was a positive dependence of the CO<sub>2</sub> yield on the DMF concentration at the expense of the IC fraction indicating that the higher initial DMF concentration could affect the radical dynamics such that the formation of IC was less favourable.

Even less nitrate and nitrite was formed as a result of the increase in temperature, hence N<sub>2</sub> and ammonia were the only significant nitrogen products. The ammonia yield seemed to have a negative dependence on DMF concentration which became less obvious as the concentration increased past 5 mM. This trend is opposite to that observed with oxidant excess at 400°C indicating that temperatures in excess of 500°C could assist in the decomposition of ammonia. Benjamin and Savage (2005a) studied the SCWO of methylamine in a tubular Hastelloy flow reactor and quantified the ammonia yield. They found that the presence of methylamine had an enhancing effect on the oxidation of ammonia (which was formed from the breakdown of methylamine) at 500°C and that ammonia oxidation was also catalysed by the walls of the reactor (Hastelloy is a Nickel-based alloy). The enhancing effect of methylamine would be applicable in the work described herein, given that methylamine is a breakdown product of trimethylamine and dimethylamine, which in turn are formed from DMF (see §4.4.4).

### 4.3.6 Effect of Oxidant Ratio

The ideal form of the complete oxidation of dimethylformamide is given by:



The effect of the stoichiometric ratio of oxidant to DMF was investigated by varying this ratio between 0.5 and 5, i.e. from half that needed for complete oxidation to five times such a quantity, at a temperature of 400°C, pressure of 250 bar and an injected organic concentration of 10 mM. Figure 4.16 indicates the removal of DMF, TOC and TC for varying stoichiometric ratios at a residence time of 5.9 s.

The removal of all forms of carbon increased with increasing the oxidant ratio in excess of the stoichiometric value. The stoichiometric ratio's effect on DMF removal started to become less important for SR > 3. It was rather obvious that there was some unexpected behaviour with regard to these results. As shown in §4.3.5 the removals of these fractions are sensitive to the DMF concentration. However, although the concentration of DMF in the feed was maintained at a constant level, the increased oxidant to organic flow ratio required to adjust the molar oxidant ratio whilst maintaining the correct residence times resulted in dilutions of the organic stream at reaction conditions. I.e. although the molar flowrates remained as desired, the concentration differed between runs.

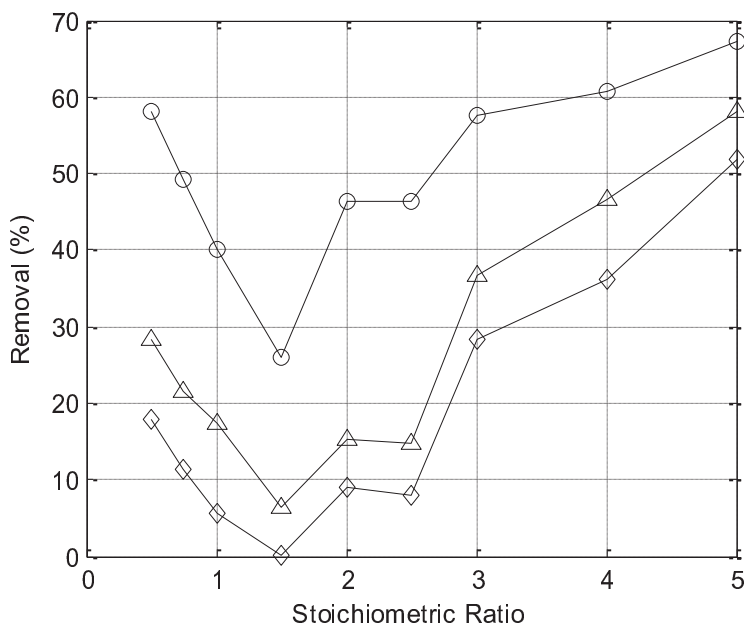


**Figure 4.16** – Removal of DMF (O), TOC ( $\Delta$ ) and TC ( $\diamond$ ) against SR ( $\tau = 5.9$  s) at a temperature of 400°C.

For a constant feed concentration, the concentration inside the reactor would have been highest at the lowest stoichiometric ratio and would have decreased as the stoichiometric ratio increased. Figure 4.17 indicates the change in DMF concentration at the reactor inlet for a constant feed concentration as stoichiometric ratio increased and also shows the effect of these changing parameters on DMF removal at a constant temperature. It can be seen that for  $SR \leq 1.5$ , the DMF removal decreases with the effectively decreasing concentration, but that after this point the DMF conversion increases with oxidant ratio.

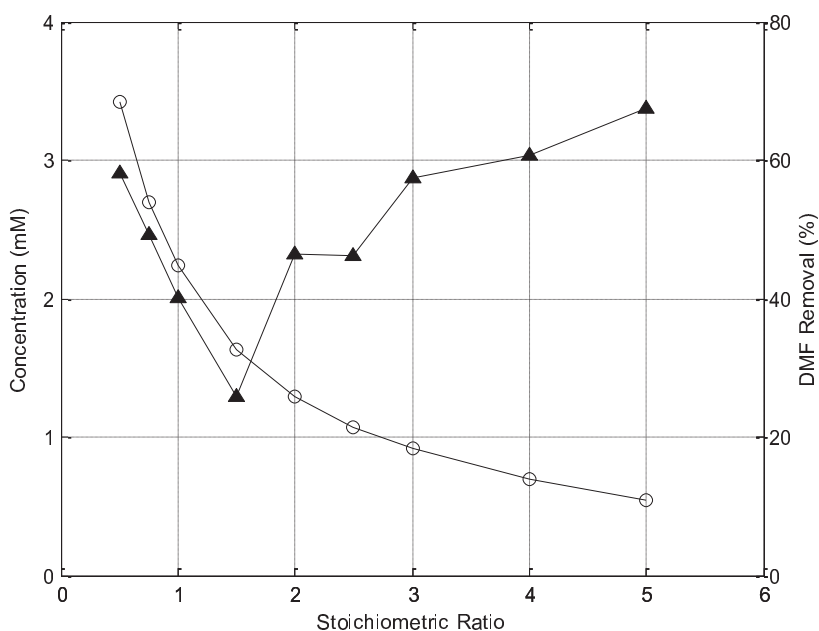


**Figure 4.17** – DMF removal vs SR ( $\blacktriangle$ ) and concentration/SR relationship (O) at  $400^{\circ}\text{C}$  and a residence time of 5.9 s.

Given the establishment that the DMF removal at identical times increases with increasing concentration, it is clear that the DMF removal has a positive dependence on the stoichiometric ratio for the range investigated, although the effect of this dependence seemed to be diminishing at the upper end of the stoichiometric ratios investigated ( $\text{SR} \rightarrow 5$ ).

Carbon and nitrogen fraction yields are presented in Figure 4.18 and Figure 4.19, where the dotted lines indicate the reactor concentration changing with SR normalised such that 3.4 mM represents 1 on the primary y-axis..

The yields of IC,  $\text{CO}_2$  and  $\text{N}_2$  generally increased with increasing oxidant ratio, largely correlating with the increased removals of DMF and TOC. CO yield remained between 2% and 4% in most cases, with IC and  $\text{CO}_2$  yields rising to 10% and ~45%

respectively at the highest SR. N<sub>2</sub> yield decreased from 37% to 18% with decreasing reactor temperature until the SR rose above 1.5 and this effect began to dominate. No methane was detected in the gaseous products. Ammonia yields remained roughly constant indicating that the reactor temperature and the feed concentration of DMF are more important factors with regard to the dynamics of ammonia. Nitrate and nitrite concentrations were generally below 0.6%, although nitrate yields were higher than this around an SR of unity and seemed to follow the reverse pattern to N<sub>2</sub>: increasing as the concentration reduced up to a SR of 1.5 and then reducing with increasing SR.

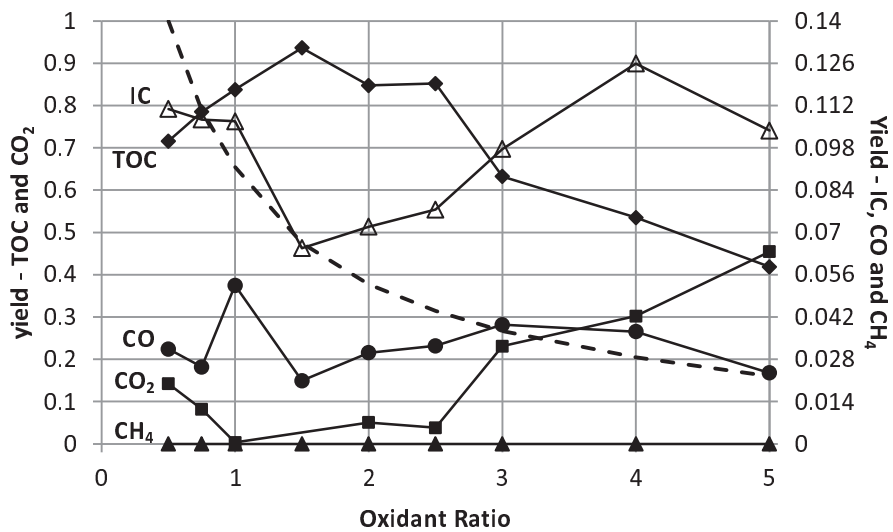


**Figure 4.18** – Carbon fraction yields as a function of SR at a residence time of 5.9 s (T = 500°C, SR = 3): TOC (◆), IC (Δ), CH<sub>4</sub> (▲), CO (●), CO<sub>2</sub> (■).

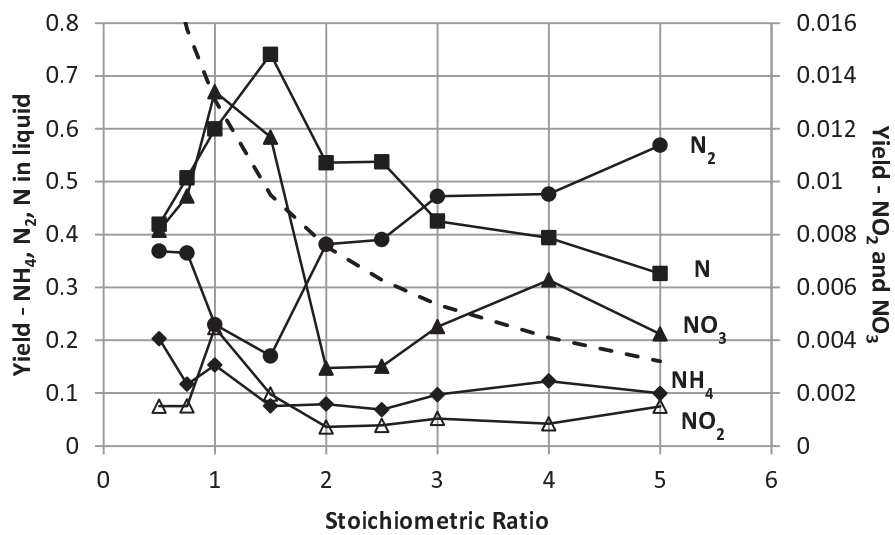


**Figure 4.19** – Nitrogen fraction yields against SR at a residence time of 5.9 s. Right

y-axis:  $NO_2^-$  (Δ),  $NO_3^-$  (▲); Left y-axis:  $NH_4^+$  (◆),  $N_2$  (●), other N in liquid (■).

#### 4.4 Global Kinetics of DMF Oxidation

The measured concentrations of DMF and TOC at specific residence times for each set of reaction conditions can be used to develop some kinetics models of the global oxidation reaction, regarding both the conversion of DMF and the disappearance of TOC.

The oxidation reaction was assumed to follow an Arrhenius-type rate law of the form:

$$-\frac{d[DMF]}{dt} = A \exp\left(\frac{-E_A}{RT}\right) [DMF]^a [O_2]^b [H_2O]^c \quad (4.2)$$

where A is the pre-exponential factor ( $M^{1-a-b-c} s^{-1}$ ),  $E_A$  is the activation energy of the reaction ( $J mol^{-1}$ ), T is the reaction temperature (K), R is the universal gas constant ( $J mol^{-1} K^{-1}$ ), and a, b and c are the reaction orders with respect to DMF, O<sub>2</sub> and H<sub>2</sub>O respectively.

This section will discuss the models and associated assumptions that were used in order to calculate values for the kinetic parameters in equation 4.2, and will then present values of the kinetic parameters calculated using each model. Finally, the likely mechanism of the DMF oxidation reaction will be briefly outlined.

#### 4.4.1 Derivation of Kinetics Models

The global kinetics of the SCWO of DMF inside a tubular reactor can be modelled by combining equation 4.2 with some simplifying assumptions and substituting the result into the plug-flow design equation (equation 4.3). Plug flow was assumed due to the non-laminar flow regimes indicated by  $Re > 2100$  and Péclet numbers indicating that the diffusive transport rates were dwarfed by the advective (bulk system) transport rates (cf. §3.4.4).

$$\frac{\tau}{[DMF]_0} = \int_0^{X_{DMF}} \frac{dX_{DMF}}{-r_{DMF}} \quad (4.3)$$

A ubiquitous assumption with regard to kinetic analyses in the literature is that the rate of reaction is completely independent of the concentration of water due to the system being approximately 99% water and the variation in this value from the

products of reaction being essentially negligible. That is, the reaction order with respect to water,  $c$ , can be set to zero.

Several of the experimental runs were performed with an excess of oxidant and another common assumption when considering such a system is that given that the oxidant is in excess, its concentration will not affect the reaction rate. That is, that the reaction order with respect to  $O_2$ ,  $b$ , can initially be set to zero while in addition, the ‘unchanging’ concentration means that when evaluating the rate (and hence the conversion) at any particular time, one can initially consider the oxidant concentration to be the initial concentration. Later, evaluations of non-zero values of  $b$  would be made given that an oxidant excess of three times that of stoichiometry was possibly not quite high enough to ultimately merge this effect inside a pseudo-first order reaction rate constant, requiring considerations of stoichiometry to be made.

Finally, a further assumption that the rate of reaction is a linear function of the concentration of the organic reactant, i.e. that the reaction order with respect to the organic,  $a$ , can be set to unity, is also often made initially, resulting (in combination with the above assumptions) in a pseudo-first order system. Some published reaction orders for different molecules are shown in Table 4.3.

**Table 4.3** – Reaction orders of selected organic compounds.

Compound	Molecular Weight ( $g\ mol^{-1}$ )	Order	Reference
Methanol	32.04	1	Brock <i>et al.</i> (1996)
Phenol	94.11	0.85 – 1.04	Thornton and Savage (1990); Pérez <i>et al.</i> (2004)
Benzaldehyde	106.12	1.5 – 2	Tsao <i>et al.</i> (1992)
Thiodiglycol	122.19	1.02 (TOC Removal)	Veriansyah <i>et al.</i> (2005)

#### 4.4.1.1 Pseudo-first Order System

From the assumptions given above, for a pseudo-first order system, the rate expression contracts to:

$$\frac{d[DMF]}{dt} = A \exp\left(\frac{-E_A}{RT}\right) [DMF] \quad (4.4)$$

which can be inserted into the equation 4.3 and solved for  $X_{DMF}$  to yield:

$$X_{DMF} = 1 - \exp(-kt) \quad (4.5)$$

where  $k$  is the reaction rate constant. Clearly this equation can also be used to solve for the reaction rate constant when using experimentally observed DMF conversions, thus:

$$k = -\frac{1}{\tau} \ln(1 - X_{DMF}) \quad (4.6)$$

The  $-\ln(1 - X_{DMF})$  term will sometimes be written as  $\ln[1/(1 - X_{DMF})]$ . These forms are equivalent.

#### 4.4.1.2 Non-unity Organic Reaction Order

If there were systems in which the reaction order with respect to DMF could not be approximated to unity, a slightly more complicated solution of the design equation is required. The reaction rate expression is reduced to:

$$\frac{d[DMF]}{dt} = A \exp\left(\frac{-E_A}{RT}\right) [DMF]^a \quad (4.7)$$

Incorporating this into the PFR design equation and solving for  $X_{DMF}$  produces the following result:

$$X_{DMF} = 1 - (1 + (a - 1)k\tau[DMF]_0^{a-1})^{1/(1-a)} \quad (4.8)$$

#### 4.4.1.3 Non-zero Oxidant Reaction Order

If it becomes apparent that the reaction is not zero order with respect to the oxidant concentration, i.e. that even if the oxidant is in large excess, its concentration still affects the reaction rate, further elaboration of equation 4.7 and its solution, equation 4.8 are required. For systems in which the oxidant is in excess, one would be able to assume that the oxidant concentration at any time could be approximated to the initial oxidant concentration. As such, the reaction rate expression:

$$\frac{d[DMF]}{dt} = A \exp\left(\frac{-E_A}{RT}\right) [DMF]^a [O_2]^b \quad (4.9)$$

can be incorporated into the PFR design equation, whilst considering that for every mole of DMF requires 4.25 moles of  $O_2$  to completely oxidise, yielding:

$$k\tau[DMF]_0^{a-1} = \int_0^{X_{DMF}} \frac{dX_{DMF}}{(1 - X_{DMF})^a \left( \frac{[O_2]_0}{[DMF]_0} - 4.25X_{DMF} \right)} \quad (4.10)$$

This equation could be solved iteratively. Equations 4.2 – 4.10, in conjunction with the experimental data, should be sufficient to evaluate the reaction orders  $a$  and  $b$ , and subsequently, either graphical methods or a Matlab regression model can be used in order to evaluate the kinetic parameters,  $E_A$  and  $A$ .

#### 4.4.1.4 Matlab Regression Model

There would be two ways that Matlab could be used to solve equation 4.2 for  $X_{DMF}$ . One can either input two simultaneous equations describing the DMF and oxygen consumption rates into Matlab with the inbuilt solving functions being invoked to solve for  $X_{DMF}$ , or one can consider that the concentration of oxidant will change in a very specific way if one assumes that the ideal stoichiometric reaction as shown in equation 4.1 is what will occur globally. In this case, one can assume that for every mole of DMF destroyed, 4.25 moles of  $O_2$  will be consumed and use the values for the reaction orders that will be derived in §4.4.2 and §4.4.3 when solving. As such, asking Matlab to solve equation 4.11 and using the result to calculate a rate constant which can subsequently be used in a minimisation function to calculate the kinetic parameters is a more convenient way to ultimately solve for  $X_{DMF}$ .

$$\text{Integral Function} = \int \frac{dX_{DMF}}{(1 - X_{DMF})^a \left( \frac{[O_2]_0}{[DMF]_0} - 4.25X_{DMF} \right)^b} \quad (4.11)$$

This model would not require an assumption of oxidant excess and would be able calculate  $X_{DMF}$  for all supercritical reaction conditions if the initial concentrations of DMF and  $O_2$  were known.

Fitting the data derived using these different model types to the experimental data has allowed the calculation of the parameters  $E_A$  and  $A$  from the reaction rate equation. The following sections include the results of these analyses.

#### 4.4.2 Pseudo-first Order Approximation

As indicated in Table 4.3, reaction orders for organic compounds treated using SCWO frequently approximate to unity. Investigating the reaction rate parameters for organic systems frequently invokes an assumption of pseudo-first order kinetics when the quantity of oxidant delivered is in excess of that required by stoichiometry. This assumption is also invoked in more complex systems, e.g. the oxidation of cutting oils (Sánchez-Oneto *et al.*, 2007) where the order with respect to COD is set to unity.

A check of whether or not a first order assumption is valid can be performed graphically as an analogue to equation 4.6. Plotting  $\ln(1 - X_{DMF})$  against the residence time should yield a straight line, with a gradient of  $-k$ .

Data for experiments conducted with the oxidant in excess were plotted with an example of two different temperatures (400°C and 450°C) shown in Figure 4.20, where each series corresponded to experiments in which the temperature and feed DMF concentrations were identical. The series all showed a good approximation to a first order system, suggesting that the reaction order with respect to DMF (and TOC) is close to unity.

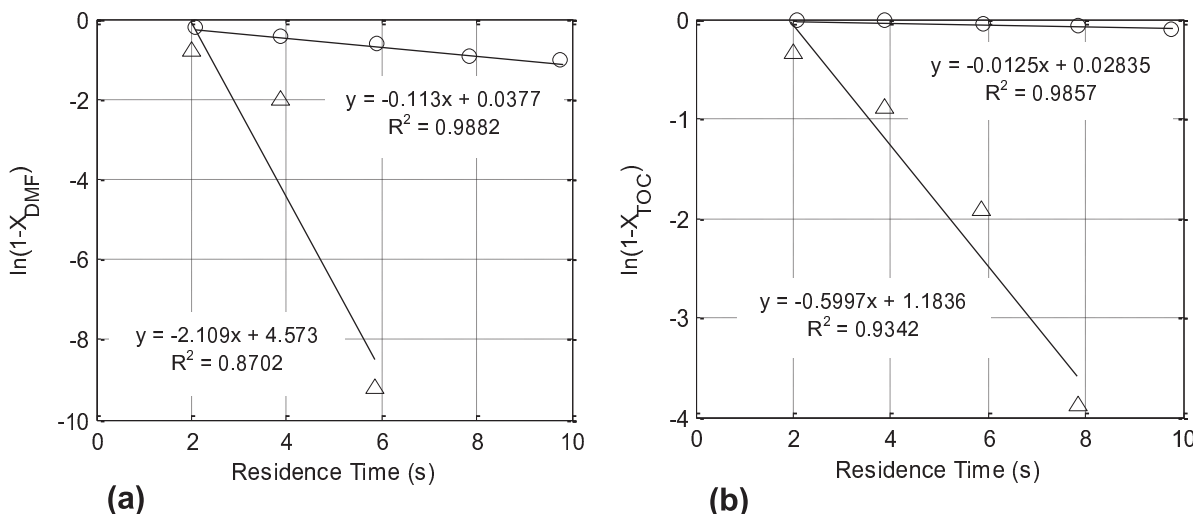


**Figure 4.20** – Natural logarithms of  $(1-X_{\text{DMF}})$  (a), and  $(1-X_{\text{TOC}})$  (b) versus residence time for experiments at  $400^{\circ}\text{C}$  (O) and  $450^{\circ}\text{C}$  ( $\Delta$ ).

Arrhenius plots were created, incorporating each of the 57 experiments where the oxidant was in excess. These experiments were conducted at temperatures of  $400^{\circ}\text{C}$ ,  $450^{\circ}\text{C}$  and  $500^{\circ}\text{C}$  and feed DMF concentrations between 5 and  $15 \text{ mM}$  with residence times between 2 and 10 s. This plot can be seen in Figure 4.21a, with the corresponding plot for the TOC removal provided in Figure 4.21b.

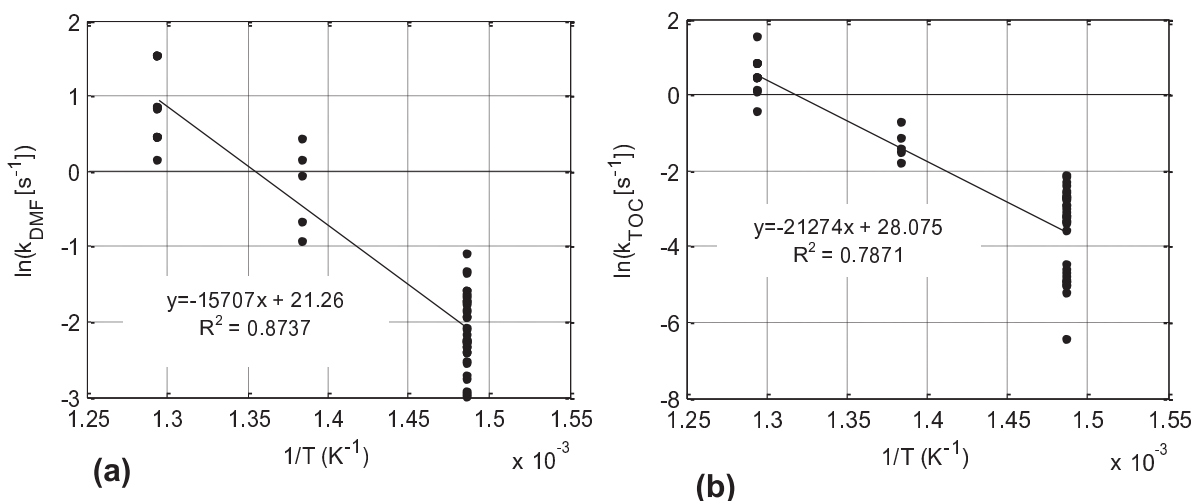


**Figure 4.21** – Arrhenius plots for DMF (a) and TOC (b)

A straight line through these points was used to calculate an activation energy and pre-exponential factor assuming pseudo-first order kinetics. The value of  $E_A$  was found to be  $131 \text{ kJ mol}^{-1}$  and the value of  $A$  was  $1.7 \times 10^9 \text{ s}^{-1}$ . Thus, the following version of equation 4.4 was obtained for the rate expression:

$$\frac{d[DMF]}{dt} = 1.71 \times 10^9 \exp\left(\frac{-130588}{RT}\right) [DMF] \quad (4.12)$$

It can be seen that there is some degree of variation in the  $\ln(k)$  data points for each temperature, especially at  $400^\circ\text{C}$ . Although individual experimental data indicated that a pseudo-first order model fitted the data reasonably well (though not perfectly), the spread of these points indicates that this is unlikely to be the best representation of this data. For the oxidant term to be adequately absorbed into the rate constant term, these points should be much closer. Assessment of the oxidant effect is presented in §4.4.3.

It was noticed that the highest rate constants for a specific series of experiments (identical temperatures, identical concentrations) were exhibited at the lowest residence times. Given that the reaction is propagated via a free radical chain reaction, this could indicate that the dynamics of the radical pool (or their ability to react with the DMF) could be sensitive to the flow conditions. Hence an assumption that the reactor behaves identically for all flowrates given that the flow is turbulent due to the plug flow conditions in the reactor is likely to be too sweeping a generalisation due to these potential mixing effects. As such, investigation into the mixing conditions present upon injection would be a useful future research avenue.

Optimisation of any injection system in order to enhance the development of the radical pool, and thus increase the reaction rate constant, would increase the efficiency of the SCWO process.

A similar analysis was performed for the TOC removal resulting in an activation energy of  $175 \text{ kJ mol}^{-1}$  and a pre-exponential factor of  $1.2 \times 10^{12} \text{ s}^{-1}$ .

In addition, upon observation of Figure 4.20, one can notice that an induction time exists for this system, where a straight line through each set of points will cross the x-axis at a non-zero residence time. This is a common effect in SCWO systems that are propagated via free-radical chain reactions due to the need to build up a sufficient supply of radical species before the reaction can proceed. Incorporating these induction times into the model and calculating a theoretical conversion based on the Arrhenius parameters gave the parity plot in Figure 4.22. Although the trend for this plot is in the correct direction, there are several underestimated points (below the  $45^\circ$  lines) indicating that a pseudo-first order model is unlikely to describe the system perfectly.

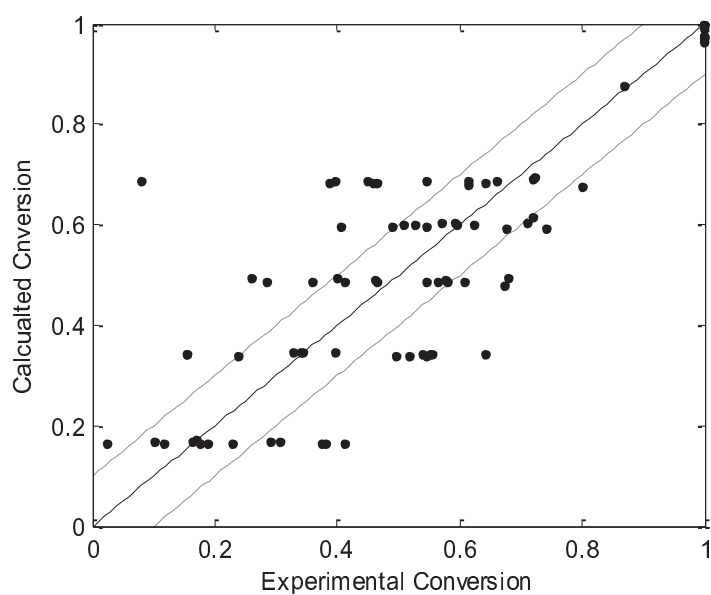


**Figure 4.22** – Parity plot of DMF conversion for pseudo-first order model.

#### 4.4.3 Global Power Law Models

It was observed in §4.3.6 that when the oxidant was in excess ( $SR > 1$ ), increasing the oxidant ratio still effected an increase in DMF and TOC removals. Consequently, the reaction order with respect to oxygen,  $b$ , is likely to be non-zero. In order to evaluate  $b$ , one can consider a modified version of equation 4.9. It has already been established that a fit for the data at  $a = 1$  yields a straight line and so equation 4.9 could be written as:

$$\frac{d[DMF]}{dt} = A \exp\left(\frac{-E_a}{RT}\right) [DMF][O_2]^b \quad (4.13)$$

Substitution into the PFR design equation and solving with the assumption that although the concentration of oxidant affects the reaction, the concentration can be assumed to be unchanging ( $[O_2] = [O_2]_0$ ), yields equation 4.14:

$$\ln\left(\frac{1}{(1 - X_{DMF})}\right) = k\tau [O_2]_0^b \quad (4.14)$$

Consequently, plotting  $\ln[1/(1 - X_{DMF})]$  against the residence time for each series for which the reaction conditions are identical will yield a straight line with the gradient of the slope equal to  $k [O_2]_0^b$ . Three example series are indicated in Figure 4.23.

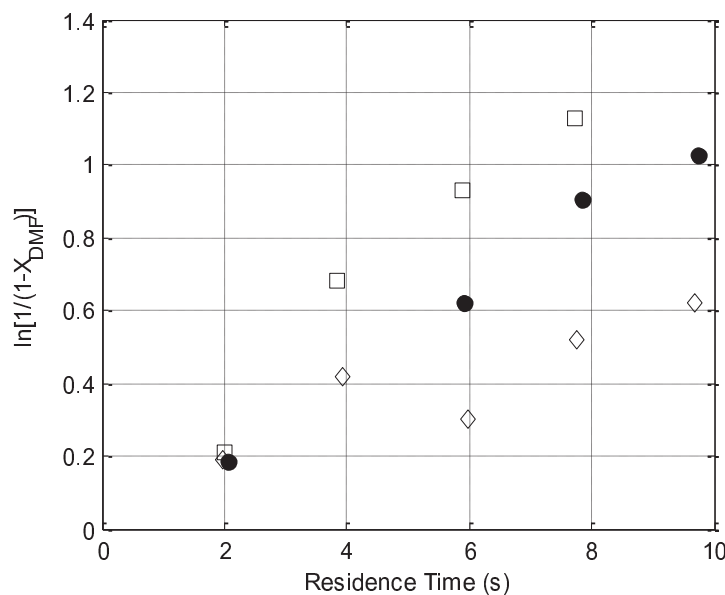


**Figure 4.23** – Normalised DMF removal as a function of residence time at SR of 1.5 ( $\diamond$ ), 2.5 ( $\bullet$ ) and 4 ( $\square$ ).

If the natural logarithm of  $k[O_2]_0^b$  is taken, this group can be rewritten as:

$$\ln(k[O_2]_0^b) = \ln(k) + b\ln([O_2]_0) \quad (4.15)$$

Subsequently, in order to evaluate the reaction order, a graph of the gradients of Figure 4.23 versus  $\ln([O_2]_0)$  was obtained and is indicated in Figure 4.24.

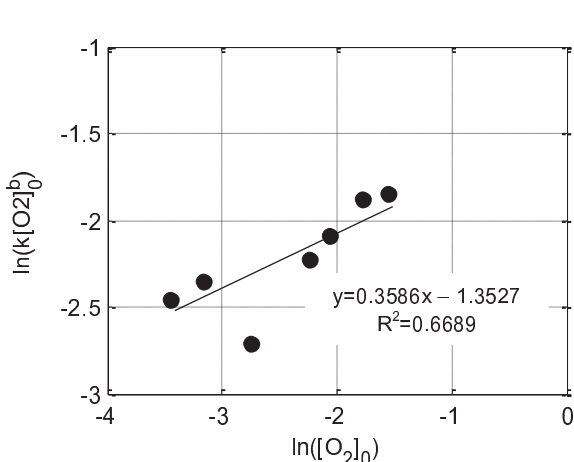


**Figure 4.24** – Gradient of Figure 4.23 as a function of  $\ln([O_2]_0)$ .

The gradient of a straight line through these points is equal to  $b$  and the intercept of the y-axis is equal to  $\ln(k)$ . The order with respect to the oxidant was found to be 0.36. The rate constant indicated by this plot was

approximately  $0.26 \text{ litre mol}^{-1} \text{ s}^{-1}$ , which is slightly greater than that indicated in Figure 4.20a where only the DMF (and not the oxidant) was taken into account. Similar analyses were performed for the TOC removal indicating that the order with respect to oxygen was 0.35. Once  $b$  had been evaluated, equation 4.14 could be rearranged to solve for  $k$ :

$$k = \ln\left(\frac{1}{(1 - X_{DMF})}\right) \frac{1}{\tau} \frac{1}{[O_2]_0^{0.36}} \quad (4.16)$$

Values of  $k$  were then used to find the Arrhenius parameters for this non-integral order system, where  $E_A$  was  $140 \text{ kJ mol}^{-1}$  and  $A$  was  $4.8 \times 10^{10} \text{ litre}^{0.36} \text{ mol}^{-0.36} \text{ s}^{-1}$  yielding:

$$\frac{d[DMF]}{dt} = 4.8 \times 10^{10} \exp\left(\frac{-140432}{RT}\right) [DMF][O_2]^{0.36} \quad (4.17)$$

Solving this equation and using it to calculate DMF conversions while incorporating induction times generates the parity plot given in Figure 4.25. This model shows much less of an underestimate for some points, indicating that incorporating the effect of the oxidant concentration into the solution much better describes this system. Incidentally, programming Matlab to calculate Arrhenius parameters using a minimising function based on the reaction temperature (see Appendix 4, Pinto (2004)) yields an activation energy of  $176 \text{ kJ mol}^{-1}$  and a pre-

exponential factor of  $2.6 \times 10^{13} \text{ litre}^{0.36} \text{ mol}^{0.36} \text{ s}^{-1}$ . These parameters result in a very marginal improvement on the fit of the data points (sum of square differences of 1.27 as opposed to 1.29).

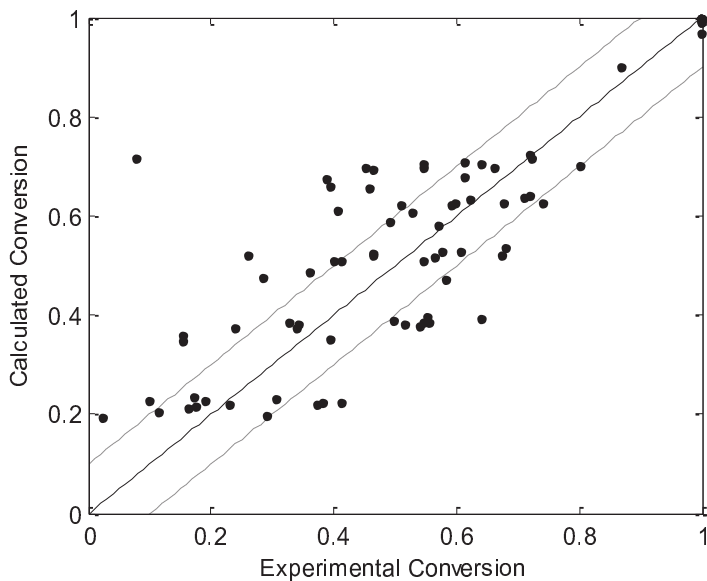


**Figure 4.25** – Parity plot of DMF conversion when incorporating oxidant reaction order.

#### 4.4.4 Proposed Reaction Mechanisms

Water in the supercritical state acts as a non-polar solvent due to its greatly reduced dielectric constant, ion product, and hydrogen-bonding capability. As such, the oxidation of organics in SCW proceeds primarily through free radical pathways (Brock and Savage, 1995; Ploeger *et al.*, 2008). In order to derive such models, comparisons have frequently been drawn between SCWO and combustion models that are comprised of networks of elementary reactions that include radical species. SCWO modelling can take similar forms and even though assumptions are made in their derivation, they are necessary for the understanding of the dynamics of the

radical species due to the direct measurement of these radical species being unfeasible during SCWO (Brock *et al.*, 1996; Ploeger *et al.*, 2008). Brock *et al.*'s paper (1996) details the radical reaction of methanol indicating that the following generic scheme is available:



where R represents a stem of a neutral compound (either aliphatic or aromatic, e.g. CH<sub>3</sub>O- in the case of methanol) and Q a part of a radical compound (e.g. -CH<sub>2</sub>O in the case of methanol) that becomes neutral upon removal of a hydrogen atom upon interaction with a hydroxyl radical. QH<sup>·</sup> can also react with O<sub>2</sub> to form the hydroperoxyl radical thus:

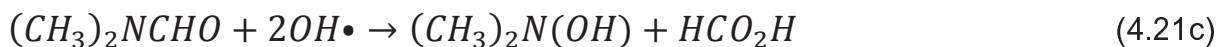
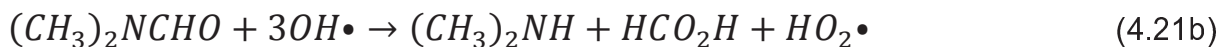


The hydroperoxyl radical can then 'recycle' the oxidant capacity by forming hydrogen peroxide which then decomposes homolytically to two hydroxyl radicals as in the following scheme (Brock *et al.*, 1996):



DMF is a nitro-centric molecule and as such, there are two primary carbon atoms (-CH<sub>3</sub> groups) and a secondary carbon atom (-HC=O group). In the oxidation reaction, the DMF molecule can be attacked at various places by hydroxyl radical. The three C-N bonds are the likeliest locations of attack, with the radical substitution

reaction favoured at the secondary carbon atom (Darwent, 1970; Atkins, 1996; Pinto, 2004). This implies that the following reactions are likely to be the initial substitution reactions of DMF (notated as  $(CH_3)_2NCHO$  in an attempt to better demonstrate the removal of specific functional groups):



Further hydroxyl radical attacks would then follow on the nitrogenated species and the formic acid groups. Substitution of OH in  $(CH_3)_2N(OH)$  from equation 4.21c with  $CH_3\cdot$  yields trimethylamine (TMA) as an intermediate. No GC-MS analysis was available so the definitive identification of TMA in the reaction products was not possible; however its formation as an intermediate was less favourable due to the necessary removal of  $CH_3$  from a DMF molecule initially (attack of primary, less substituted, carbon).

From these initiation reactions, one could suggest the direction in which the reaction might then proceed as shown in Figure 4.26 and Figure 4.27. A simplified global reaction mechanism showing the major pathways is shown in Figure 4.28. Complex interaction with radical species would yield some reasonably exotic, short-lived radical groups as well as the simpler, more stable components. Indeed, with the network for the oxidation of methanol comprising some 150 reactions, one would expect the oxidation of DMF to be expressed in a far greater number of reactions if it were to be described completely. However, one can appreciate that the main branches of such a mechanism could approximate to those below.

#### 4.4.4.1 Trimethylamine

TMA is formed when the CHO group of DMF is substituted with a CH<sub>3</sub> group. Clearly, in order for this to occur, a CH<sub>3</sub>• radical needs to be formed. This occurs by its substitution with a hydroxyl radical from the DMF molecule. The removal of the CHO group is also facilitated by hydroxyl radical substitution. This formation is shown in Figure 4.26. Other intermediates evolved during the formation of TMA will include (Pinto, 2004; NIST):

- formic acid,
- N-hydroxymethylformamide
- N-hydroxydimethylamine.

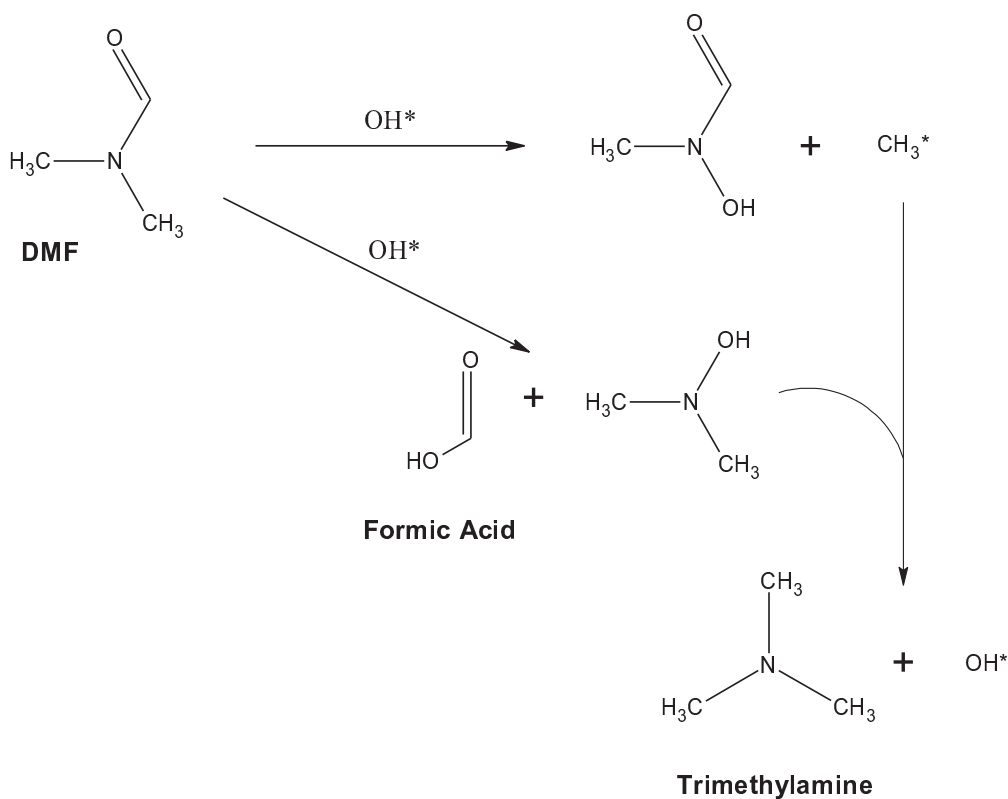
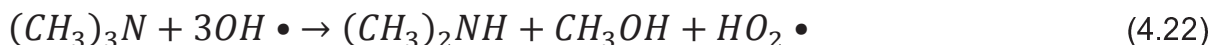


**Figure 4.26** – Formation of Trimethylamine via radical substitution of DMF.

#### 4.4.4.2 Dimethylamine

Dimethylamine can be formed via several routes, but the most important are directly from DMF and TMA themselves. TMA can be attacked by hydroxyl radicals once formed and a CH<sub>3</sub> group re-abstracted to form methanol:



In addition, the CHO group can be removed from DMF and replaced with a hydrogen atom instead of an OH group, liberating a formic acid group. This route is shown in Figure 4.27.

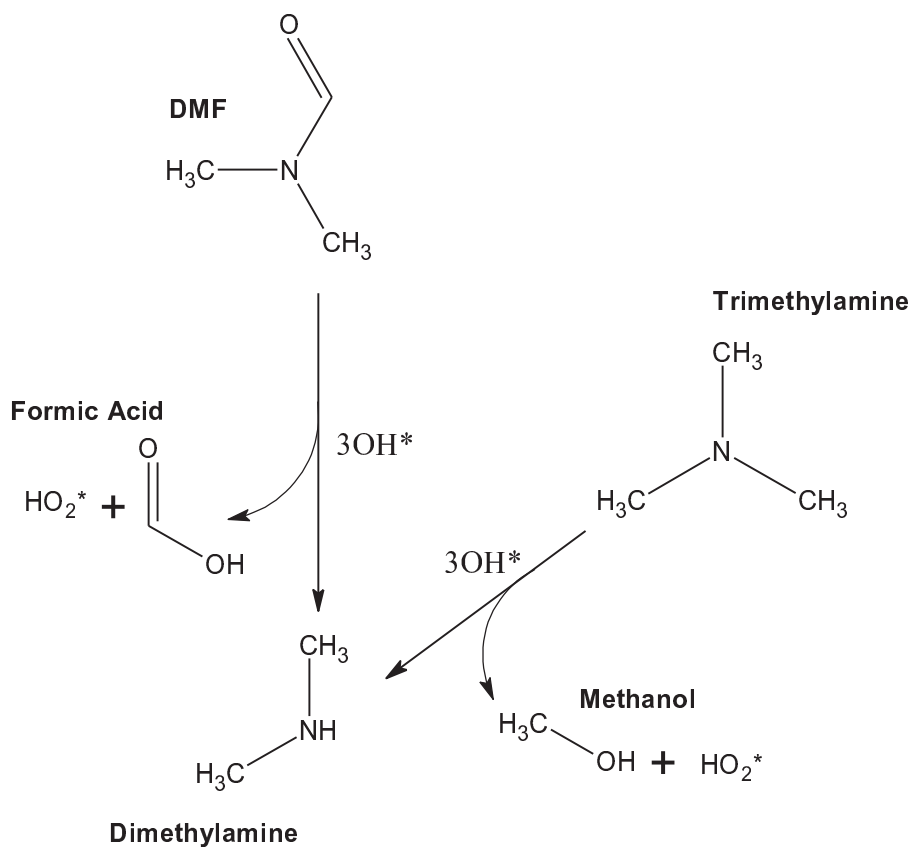


**Figure 4.27** – Formation of dimethylamine from radical substitution of DMF and TMA.

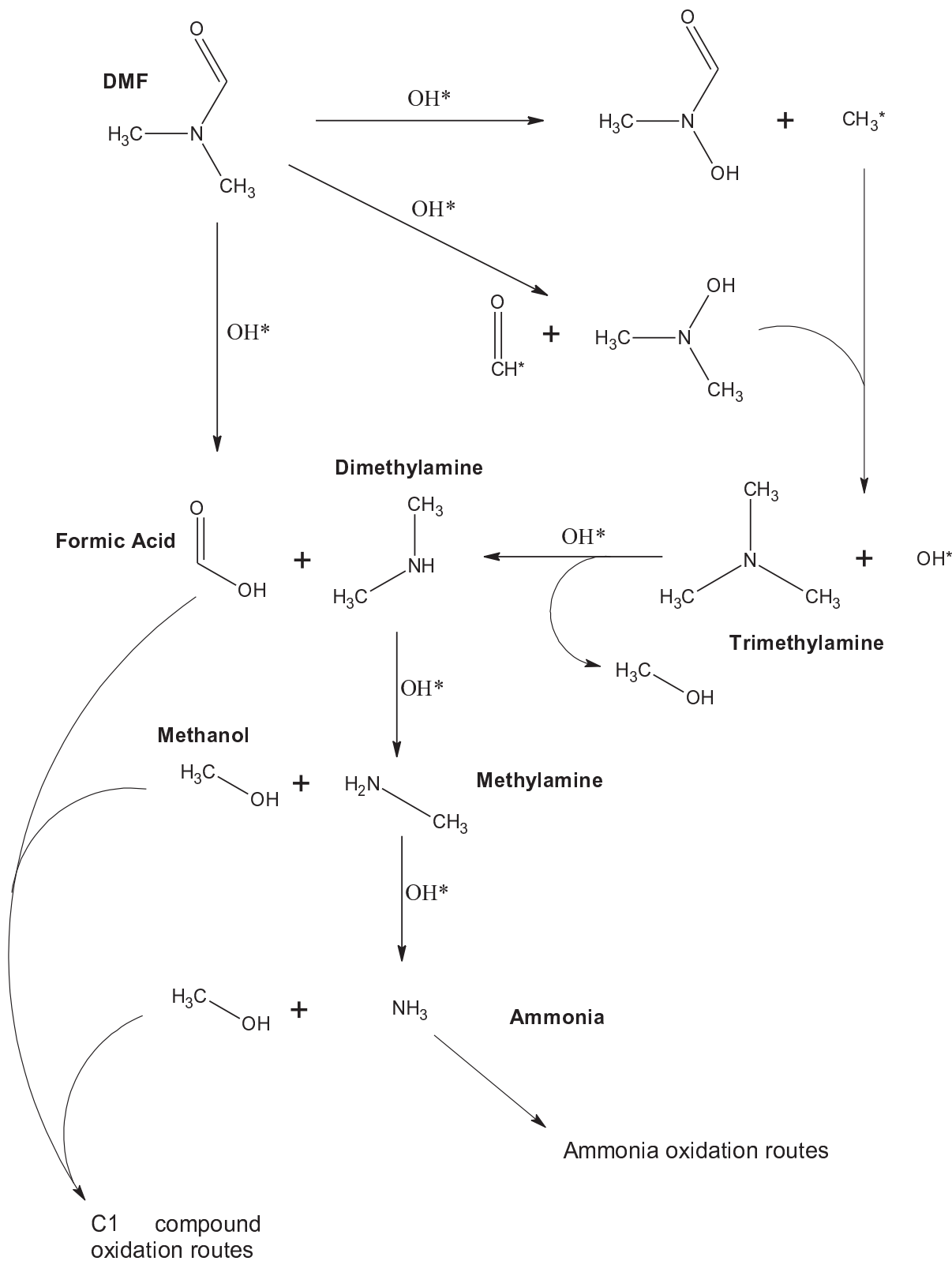
#### 4.4.4.3 Methylamine

Once formed, dimethylamine can then be converted to methylamine by a similar mechanism to conversion of TMA to DMA. Abstraction of a CH<sub>3</sub> group by OH• to yield methanol is very possible and there are few other options available given that at some point, the last C-N bond must be broken. When the N is bonded to only one carbon, the likely form that the compound will take is MA. Formamide is also a possible intermediate, but the OH• attack is more prevalent on the secondary carbon, rather than on the primary methyl groups, making progression along this branch less favourable.

Once formed, methylamine is most likely to be attacked in one of two ways. Either a hydrogen will be abstracted resulting in the CH<sub>3</sub>NH• radical, or (as is more likely) reaction with O<sub>2</sub> and OH• will result in the formation of formamide which will readily convert to ammonia (Benjamin and Savage, 2005). The ammonia formation is discussed in the next section. The CH<sub>3</sub>NH• radical reacts with O<sub>2</sub> as follows:

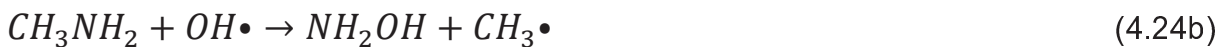


where the products from equation 4.23a will ultimately end up being converted to CO, CO<sub>2</sub>, NO, NO<sub>2</sub> and/or N<sub>2</sub>O depending on the reaction conditions, and the H<sub>2</sub>CNH from equation 4.23b can form HCN. This route is unfavourable in the ratio 1:7 (Benjamin and Savage, 2005). It was not possible to detect any of these species using the gas product analysis available for this work and as such, the extent to which these routes are favoured was not possible to quantify.

**Figure 4.28 – DMF SCWO reaction mechanism.**

#### 4.4.4.4 Ammonia Yields

In order for ammonia to be formed, the substituted groups bonded to the nitrogen atom of DMF (and, subsequently, trimethylamine (TMA), dimethylamine (DMA), and/or methylamine (MA)) must be replaced during reaction with radicals. Therefore, if one considers the destruction of one potential intermediate, MA, via free-radical attack, it is feasible that there could be multiple outcomes:



where these are just some of the possibilities and there are many other routes from  $\text{CH}_3\text{NH}_2$ ,  $\text{NH}_2\cdot$  and  $\text{NH}_2\text{OH}$  that could potentially yield ammonia. The implication from this is that for nitrogen that is liberated from an organic molecule, there are several routes that can be taken to proceed to an ultimate stable product, and for those routes that don't lead to ammonia, the nitrogen is likely to be converted to  $\text{N}_2$  and leave as part of the gaseous product. However, for routes that include ammonia, further oxidation is unfavourable at low energies (i.e. temperatures below 650°C). The slightly reduced yields of ammonia at temperatures in excess of 450°C could indicate that equation 4.24c is less favourable and that  $\text{NH}_2\cdot$  is a more common intermediate at higher temperatures.

The required energy to break the N-H bond in ammonia ( $\text{NH}_3$ ) is much higher than that required to break a C-N (for example in MA), explaining its recalcitrance once formed (Darwent, 1970). However, the energy to break an N-H bond within

amidogen (an ammonia-type radical,  $\text{NH}_2\bullet$ ) is lower than that which is required to attack ammonia, and the required energy is lower still for NH (almost similar to that of C-N) which is applicable for the combination and abstraction scheme given below (Ploeger *et al.*, 2008):



Therefore, the assumption is that once  $\text{NH}_2\bullet$  is formed, it is oxidised further to gaseous products; however, the degree of formation of ammonia is very much dependent on the specific reaction conditions as described in §4.3.

## 4.5 Summary

The SCWO of dimethylformamide was conducted at a variety of reaction temperatures, DMF feed concentrations, oxidant ratios and residence times. The reaction temperature was identified as the variable that had the greatest effect on the removals of DMF and TOC. Complete removals of DMF were observed at 450°C for residence times in excess of 6 s, with less than 2 s residence time required for temperatures in excess of 500°C. Removals of TOC in excess of 95% were observed at residence times of 4 s and higher for temperatures of 500°C and higher. Near-complete TOC removals were observed at residence times of 4 s at temperatures of 550°C. Experiments into the effect of varying the DMF feed concentration at 500°C were identical in terms of their DMF removal being in excess of 99.99% for all. Ammonia yields were highest at a temperature of 450°C and were roughly unchanged at temperatures in excess of this for a DMF concentration of 10 mM. For a large oxidant excess at high temperature, increasing the concentration caused an

obvious decrease in ammonia yield, which was potentially attributable to side reactions involving the intermediate, methylamine.

DMF and TOC removal rates indicated a positive dependence on the feed concentration of DMF as expected from the assumption of an Arrhenius-type reaction rate model. Ammonia yields at 400°C increased with increasing DMF feed concentration indicating an increased rate of formation but a diminished propensity for destruction.

Reaction rate expressions were developed for the oxidation of DMF. The reaction orders were found to be 1 for DMF and 0.36 for the oxidant, with the reaction order with respect to water assumed to be zero. The parameters of the reaction rate constant were evaluated, with the pre-exponential factor being calculated to be  $4.8 \times 10^{10} \text{ litre}^{0.36} \text{ mol}^{-0.36} \text{ s}^{-1}$  and the activation energy being evaluated as 140 kJ mol<sup>-1</sup>.

# CHAPTER 5 – MULTI-STAGE SUPERCRITICAL WATER OXIDATION OF DIMETHYLFORMAMIDE

## 5.1 Experimental Setup

The implementation of a multi-stage configuration required modification to both the reactor hardware and experimental protocol. By its very definition, multi-stage reaction required the use of a secondary oxidant injection port. Rather than just splitting the oxidant stream in two, control over the proportion of oxidant delivered to each port was required and as such, this secondary injection required the use of an additional HPLC pump as well as an additional oxidant preheater as described in §3.1.5.2 and as shown in Figure 5.1.

When considering the proportion of oxidant to be injected at each port, the global reaction conditions formed the basis of the calculation. The global reaction stoichiometry was used to calculate the total quantity of oxidant that would be delivered to the reactor and once this quantity had been determined, it would be divided between the two ports according to the particular experiment that was being conducted. For example, if  $20 \text{ ml min}^{-1}$  of oxidant were to be delivered at the ratio 75:25, then 75% of the total flowrate ( $15 \text{ ml min}^{-1}$ ) would be delivered via the primary port (at the beginning of the reactor) and 25% of the total flowrate ( $5 \text{ ml min}^{-1}$ ) via the secondary port.

As shown in Figure 5.1, there were three potential secondary oxidant injection points at 25%, 50% and 75% of the total reactor length from the beginning of the

reactor, i.e. the secondary injection was placed approximately 3 m, 6 m, and 9 m along the reactor length (downstream of the inlet). The primary injection port was unchanged throughout all experiments, i.e. there was always oxidant injected with the organic feed. The separate tubes that are notated ‘reactor one’, ‘reactor two’, ‘reactor three’ and ‘reactor four’ on the diagram were not considered completely separate for the purposes of analysis. Instead, any coils prior to the secondary injector were considered one reactor and similarly, any coils downstream of the secondary injector were also considered one reactor.

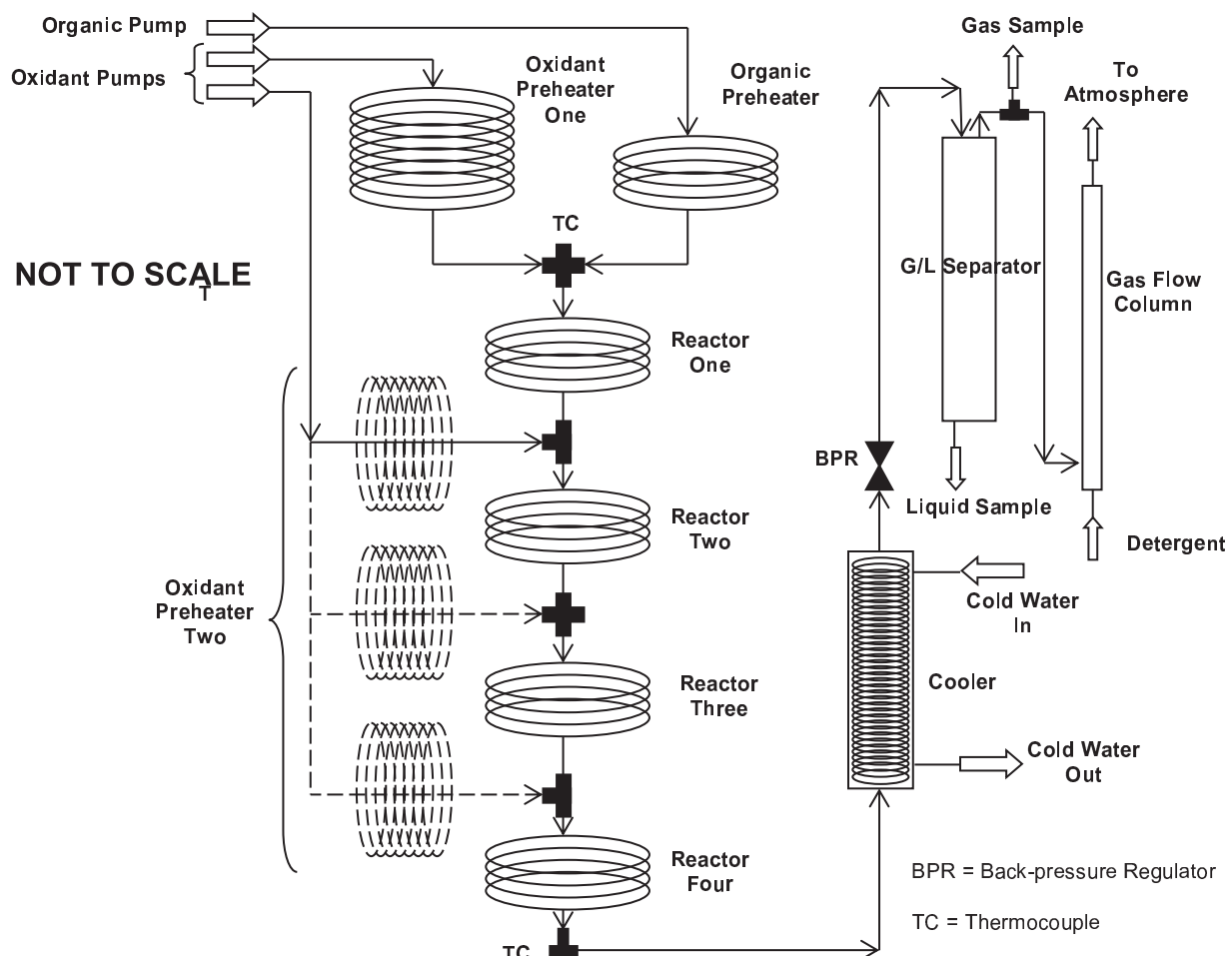


**Figure 5.1** – Reactor schematic indicating the multi-stage oxidation rig.

As was the case for the single-stage configuration, the reactor was allowed fifteen minutes to reach equilibrium after adjusting pump flowrates in order to achieve different residence times. This was to ensure that any product samples that were taken would be properly representative of the oxidation reaction at the intended conditions.

## 5.2 Initial Multi-stage Experimental Runs

The single-stage configuration had a large number of potential reaction conditions when considering that there were a high number of permutations pertaining to temperature, organic feed concentration, oxidant ratio, and residence time. Clearly, when considering a multi-stage configuration, a similar degree of permutations with regard to temperature, organic feed concentration and oxidant ratio are again possible while further permutations are available due to simultaneously being able to vary both the proportion of the oxidant delivered to each port and the location of the secondary feed port. Thus, the three additional configurations were coupled with the five different injection ratios that were to be investigated: 75:25, 67:33, 50:50, 33:67, 25:75, where the ratios convey the ratio of the percentage of oxidant injected at the inlet to the percentage of oxidant injected at the secondary port. This resulted in a fifteen-fold increase in the range of experimental conditions in comparison to those that were investigated for the single-stage configuration.

Consequently, it was decided that a sensible way of investigating the multi-stage process would be to select a temperature, organic feed concentration, and oxidant ratio and to hold these constant whilst varying both the location of the

secondary oxidant injection port and the proportion of oxidant injected to each port.

Table 5.1 indicates the conditions that were studied in these initial experimental runs.

**Table 5.1** – Multi-stage SCWO experimental conditions for varying oxidant injection configurations and ratios.

Expt #	Second Injection	Injection ratios	Feed [DMF] <sub>sc</sub> mM	T °C	P bar	Oxidant Ratio	Residence Time, s
AA – AE; AR – AV	6 m	75:25 – 25:75					
AF – AJ; AW – AAA	9 m	75:25 – 25:75					
AK – AP	3 m	75:25 – 25:75	10	400	250	1	2 – 15
SA, VA, AQ	None	100:0					

For each of these experimental runs, GC-FID, TOC, nitrogen species and GC-TCD analyses were conducted. The TOC data allowed the calculation of TOC removal and a subsequent assessment of which set of conditions resulted in the most advantageous TOC removal efficiency.

### 5.2.1 Implications of the Multi-stage Configuration

There are several implications of a multi-stage configuration when compared to a single-stage configuration that should be considered before conducting the experiments.

Firstly, due to the fact that for all of these experiments, the total quantity of oxidant, was held constant, an assumption of ideal oxidation would result in all of the experiments tending towards the same levels of DMF and TOC removal at the longest residence times, however it is the effect of both the formation of different intermediates and of the oxidant ratio at specific parts of the reactor to which it was

hoped that these experiments could allude. For example, in splitting the oxidant in a 25:75 ratio, a large oxidant deficit would be experienced by the organic feed in the first section of the reactor before this was remedied by the secondary oxidant feed. It was assumed that any differences in the global kinetics that were becoming manifest in the DMF removal, TOC removal, nitrogen species dynamics, etc, could be thus attributed to the varying oxidant injection.

Secondly, any temperature increase due to the exothermic oxidation reaction (that had not been nullified by the ambient oven temperature before the second oxidant stream was injected) would be reversed by the injection of more oxidant at the desired reaction temperature. That is, one would expect a lower overall increase in temperature between the inlet and outlet thermocouples than for the single-oxidant configuration, even taking into account the fact that the near-isothermal oven conditions should cool any exothermic behaviour back towards the base temperature.

Finally, any comparison between theoretical prediction and experimental data points must be derived such that the final model conversions are at the residence time of the data point to be compared. This is because the secondary injection will always occur a certain distance upstream of the reactor outlet and as such, if, for example, a prediction is obtained for a residence time of 10 s, the simulated removal values at 6 s in that same scenario would not be comparable to the experimental removals at a residence time of 6 s.

### 5.2.2 Effect of Residence Time

Residence times in this chapter are defined as the time that the organic feed spends inside the reactor. Because of the possible configurations of the reactor, not all oxidant will be present in the reactor for the entire defined residence time. In addition, the residence times prior to and after the secondary injection will clearly differ (even when the secondary injection is at half of the reactor length) due to the differences in length and the greater total mass flowrate of fluid downstream of the secondary injector than upstream of it.

When investigating the oxidant configurations, the organic feed stream was subjected to reactor residence times between 1.9 and 14.4 s. Of these, the residence times pertaining to the first section of each reactor (i.e. prior to the secondary injection) ranged between 0.6 and 12.5 s. It was not possible to take liquid samples after the ‘first’ reactor section and as such comparisons between the products before and after the secondary injection was not possible.

The removals of DMF and TOC as a function of reactor residence time for each injection percentage and for each injector position are shown in Figure 5.2 and Figure 5.3 respectively.

These figures show primarily that – as would be expected – as the time at which the organic feed is exposed to oxidant under supercritical conditions increases, the removals of both DMF and TOC also increase. They also indicate that in general there are reasonably close groupings of data points for the removal of DMF and TOC for each injector position. This would be as expected given that globally, each experiment had identical conditions in terms of the reactor temperature, the feed

concentration of DMF and the total amount of oxidant that was injected. However, there is also clear variation between the data points for each specific configuration. This is especially true in Figure 5.2a where there is the greatest variability in data points. This could be due to the secondary injector providing a near-immediate disruption to the establishment of the reactor flow regime after the initial injection.

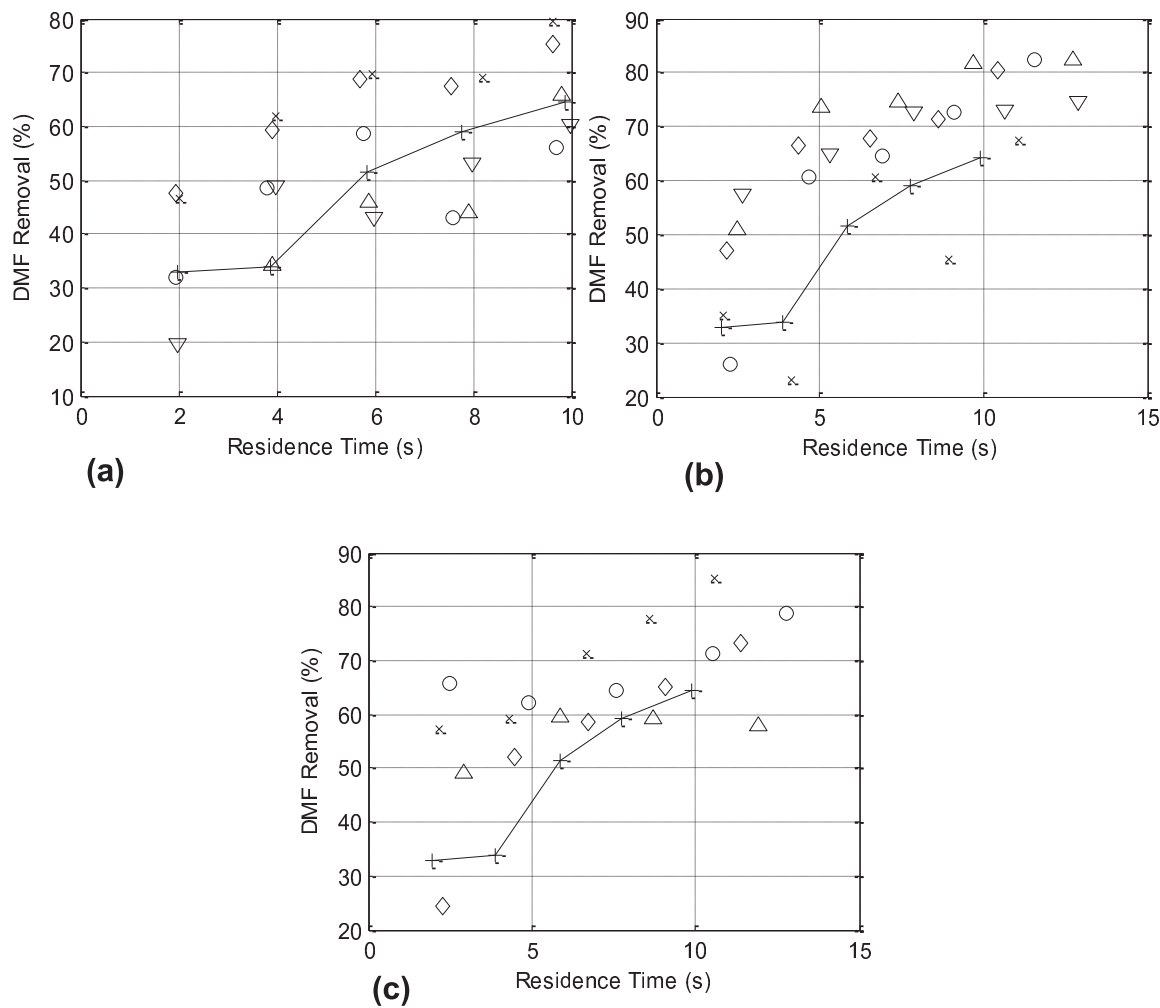


**Figure 5.2** – DMF removal for multi-stage SCWO – varying secondary injection (3 m downstream (a), 6 m (b), 9 m (c)) at 400°C, 250 bar, SR = 1, [DMF]<sub>feed</sub> = 10 mM for injection ratios: 75:25 (x), 67:33 (◊), 50:50 (O), 33:67 (Δ), 25:75 (▽), 100:0 (-+-).

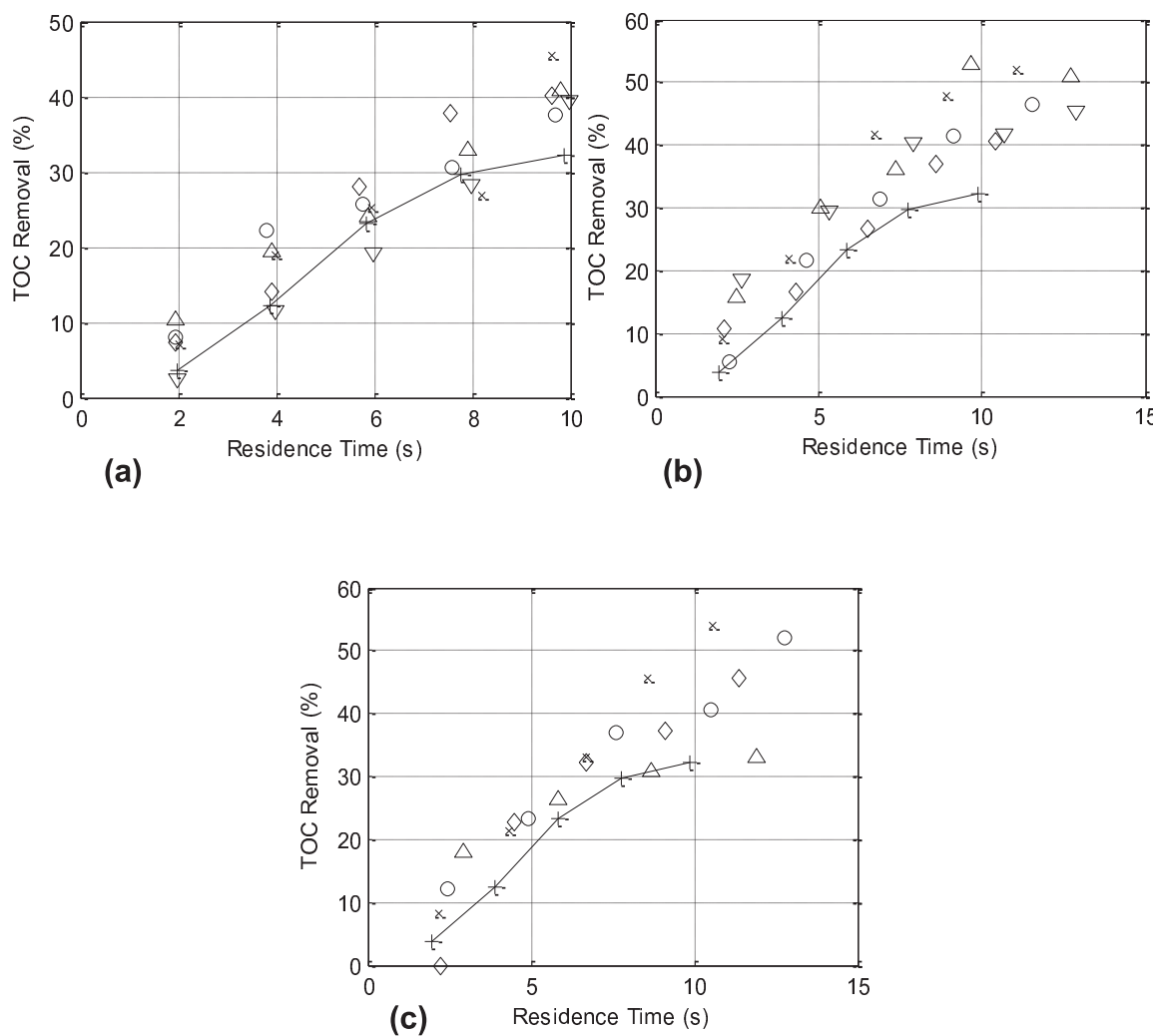


**Figure 5.3 – TOC removal for multi-stage SCWO – varying secondary injection (3 m downstream (a), 6 m (b), 9 m (c)) at 400°C, 250 bar, SR = 1, [DMF]<sub>feed</sub> = 10 mM for injection ratios: 75:25 (x), 67:33 (◊), 50:50 (O), 33:67 (Δ), 25:75 (▽), 100:0 (---).**

The data also shows clearly that the multi-stage reactor configurations result in higher DMF and TOC removals than the single-stage configuration (as indicated by the solid lines). Such an indication is interesting because it shows that the manipulation of the distribution of oxidant throughout the reactor could allow the optimisation of the removal of DMF (and TOC in general), thus resulting in the ability to optimise the quantity of oxidant that would be necessary to perform the oxidation.

This would in turn potentially enable the process to be made more efficient, and thus more environmentally and economically viable. In addition, multiple injections of oxidant would allow better manipulation of the reactor's temperature distribution, which although not a great concern for the apparatus employed in this work due to the oven's isothermal nature, is of interest in larger-scale plants due to their operation in quasi-adiabatic regimes in which the exothermic nature of the reaction necessitates more delicate temperature control.

### **5.2.3 Effect of Varying Injector Position and Injection Proportion**

The treatability of the DMF-water system with three injector positions and five oxidant injection ratios (effectively six when counting the single-stage oxidation) was investigated.

Figure 5.4 displays the DMF, TOC, and TC removals seen in these experiments as a function of the percentage of oxidant injected via the primary port but at a specific reactor residence time of 6 s. The removals were compared to those exhibited by oxidations run under similar conditions but in a single-stage configuration.

Although one would expect that globally there may not be a huge discrepancy between removals, given that the total quantity of oxidant delivered with respect to the organic is identical in each case, it can be seen from this data that with varying secondary oxidant injection port and primary injection percentage, the conversions of DMF, TOC and TC do show differences to those that are exhibited for a single-stage oxidation. In general, there are differences in removal of up to 10 percentage points

for different injection profiles for TC and TOC, and in some cases, an even greater deviation from the single-stage oxidation for DMF removal.

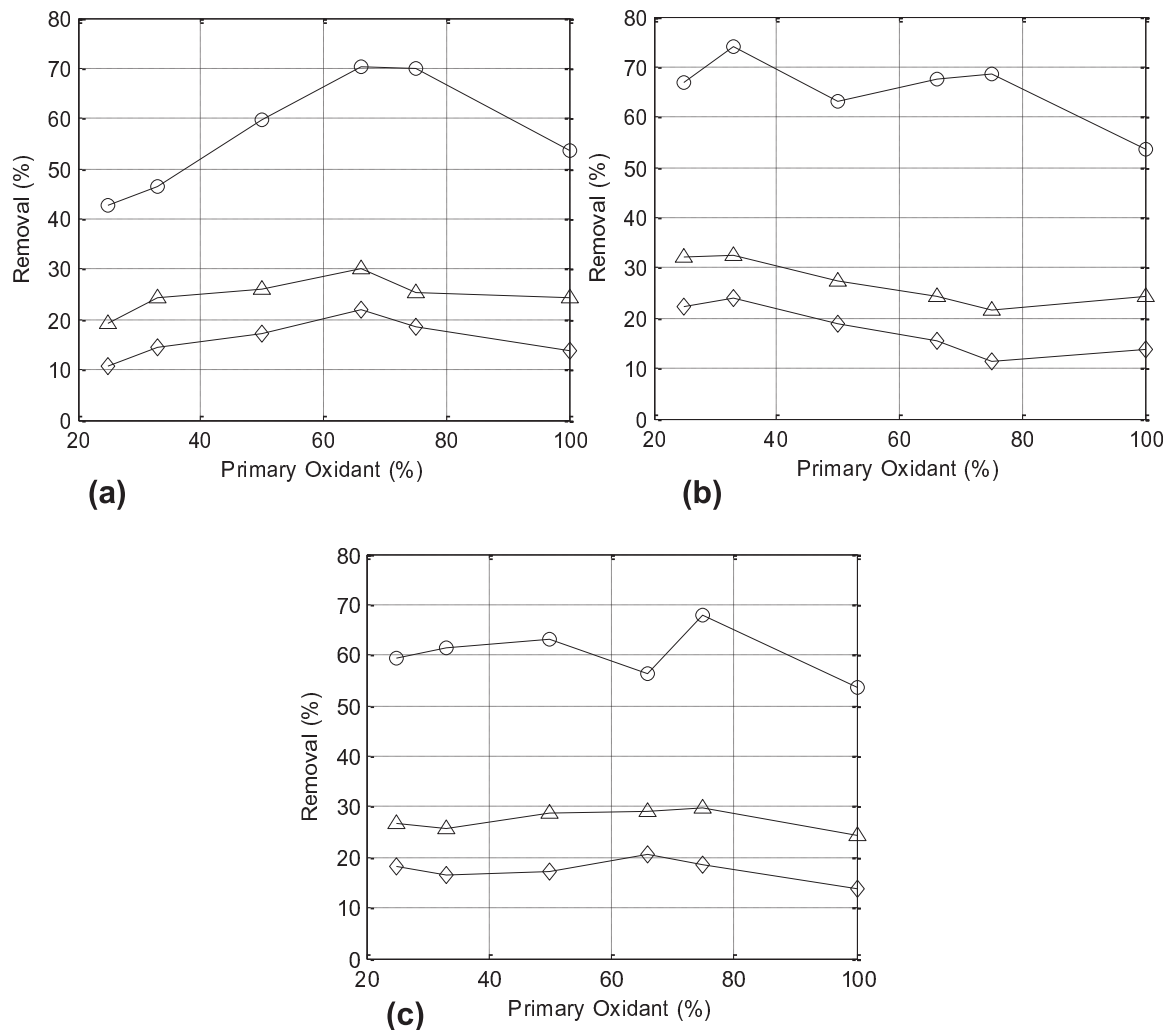


**Figure 5.4** – Removals for multi-stage SCWO with varying secondary injection points (3 m downstream (a), 6 m (b), 9 m (c)) at 400°C, 250 bar, SR = 1, [DMF]<sub>feed</sub> = 10 mM, and τ=6 s: DMF (O), TOC (Δ), TC (◊).

The situations wherein the secondary oxidant was delivered towards the extremes of the reactor initially show a slight increase in TOC conversion with decreasing primary oxidant proportion. This then reverses, with TOC conversion decreasing as the primary oxidant percentage is reduced further. For the central

injection, an increase in TOC removal is observed with decreasing primary oxidant injection throughout.

The increases in performance for some configurations when compared to the single-stage oxidation configuration could be attributed the fact that two injection points allow for the generation of two ‘separate’ radical pools which, when coupled with two opportunities for radial mixing, allow for greater organic-oxidant contact resulting in increased removals. There are markedly lower conversions for the 3 m downstream injection with low primary injection percentages. The TOC conversions for these conditions are lower than analogous conversions (similar oxidant percentages) with downstream injections at greater lengths. This could indicate that the radical pool had not built to a great enough degree at the start of the reaction before the plug-flow regime was established for the removals to match those expected for single-stage oxidation. The relative lack of radial mixing then could not afford as much reaction opportunity as with other configurations. At higher residence times (for example as seen in Figure 5.7a), this effect is less noticeable, indicating that slower transit times may afford greater opportunity for the radical pool to build, causing a more extensive oxidation before the secondary injection.

A clearer comparison between the injector positions for the removals of TOC and DMF can be seen in Figure 5.5. A good degree of variability can be seen when comparing the three traces with the 9 m injector position outperforming the 3 m injector with regards to TOC removal, with the performance of the 6 m injector seeming to depend more strongly on the proportion of oxidant injected at each point. Where DMF removal is concerned, there was more variability on the part of the 3 m injector, with the 9 m injector the most consistent, and being shadowed by the 6 m

injector. This is most likely due to variation in the radical dynamics or differing temperature profiles due to the differing secondary oxidant injection point.

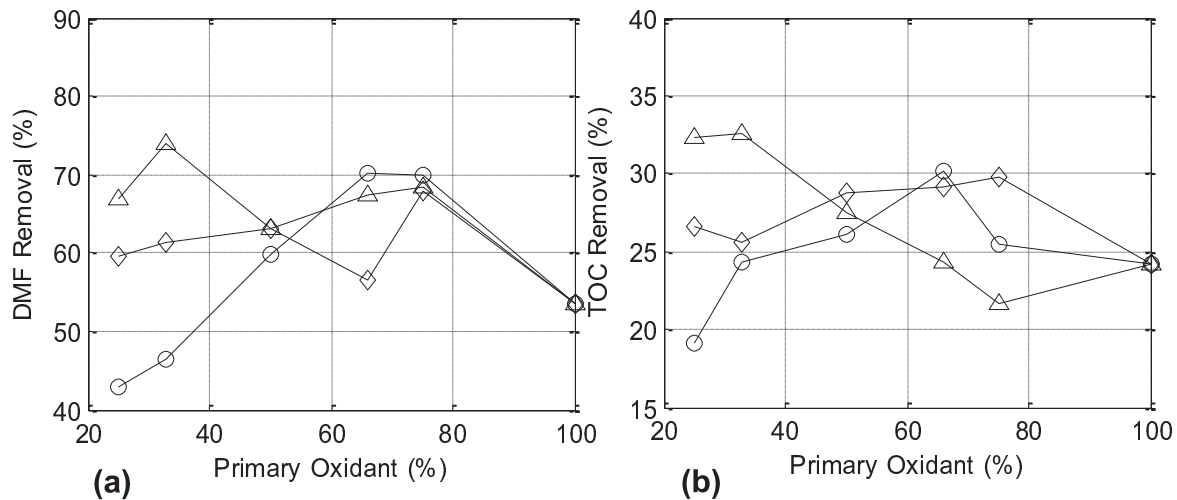


**Figure 5.5** – DMF (a) and TOC (b) removals as a function of primary oxidant proportion at a residence time of 6 s: Secondary injectors at 3 m (O), 6 m ( $\Delta$ ) and 9 m ( $\diamond$ ).

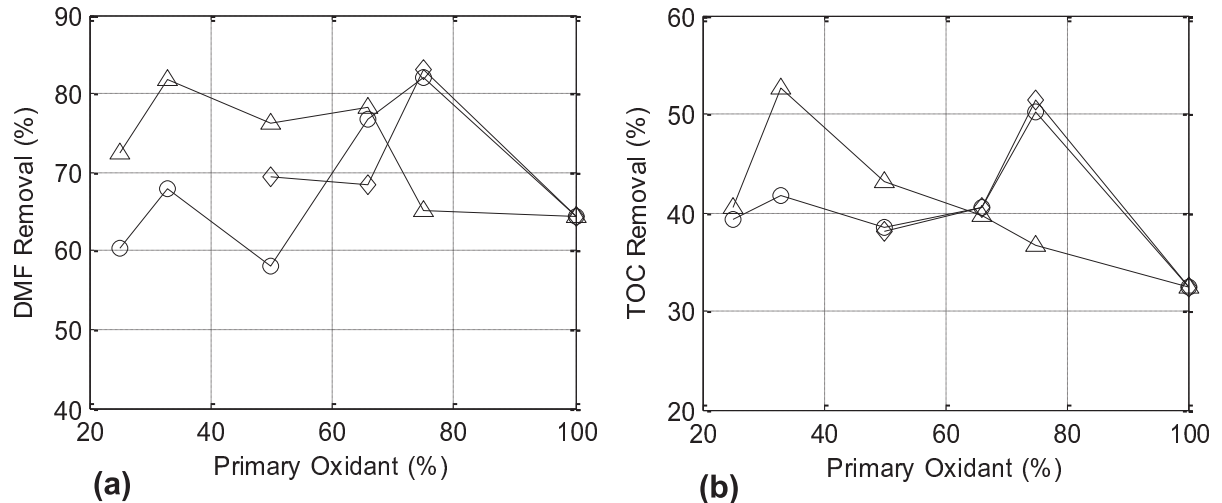


**Figure 5.6** – DMF (a) and TOC (b) removals as a function of primary oxidant proportion at a residence time of 10 s: Secondary injectors at 3 m (O), 6 m ( $\Delta$ ) and 9 m ( $\diamond$ ).

Figure 5.7 shows similar data to that depicted in Figure 5.4 but for an increased residence time of 10 s.

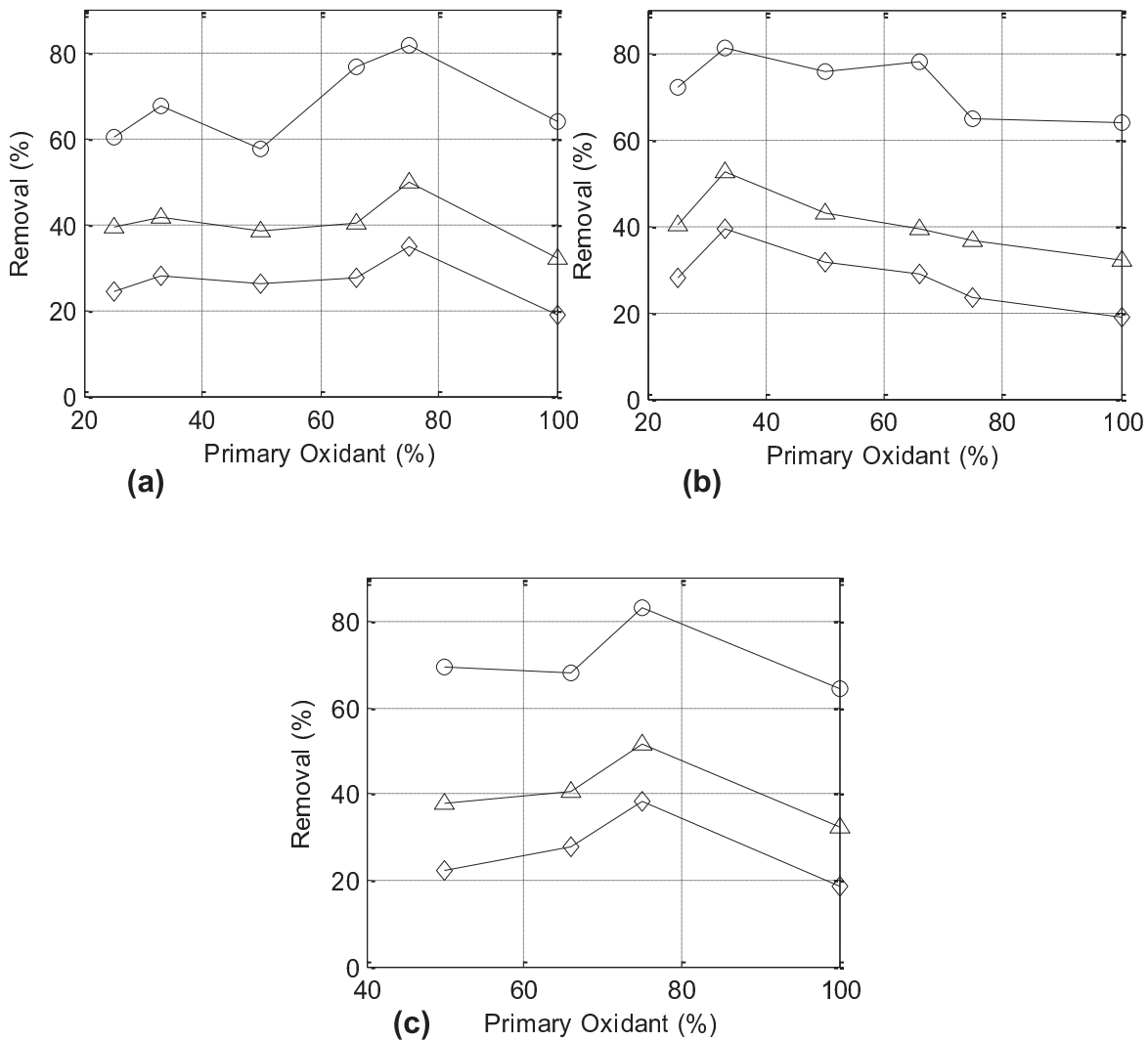


**Figure 5.7 – Removals for multi-stage SCWO with varying secondary injection points (3 m downstream (a), 6 m (b), 9 m (c)) at 400°C, 250 bar, SR = 1, [DMF]<sub>feed</sub> = 10 mM, and τ = 10 s: DMF (O), TOC (Δ), TC (◊).**

These plots show a near-universal improvement in TOC and TC removal when compared to single-stage configurations with profiles for DMF removal being similar to those observed for residence times of 6 s indicating that the conversion of DMF to

other (potentially ‘simpler’) organic compounds happens quite rapidly. Again, for a secondary injector position of 6 m, there was a marked pattern wherein TOC and TC removal increased with decreasing primary oxidant injection percentage until the lower value at 25% initial injection. The decreased reactor transit speeds enabled the two oxidant exposure points and the associated radical generation profiles to have a greater effect on the oxidation of the organic stream.

Again, clearer comparisons between the injector positions’ effects on the TOC and DMF removals can be seen in Figure 5.6 indicating that the 3 m and 9 m injectors had similar performance with regard to TOC removal and that the 9 m injector could perform better with regard to DMF removal. The 6 m injector was more efficient with regard to DMF removal and performed generally equal to or better than the other configurations with regard to TOC removal.

Initial data indicated that injecting 75% of the oxidant via the primary port, with the remainder injected 6 m downstream of the inlet would give the greatest increase in performance over the single-stage configuration. Consequently, this configuration was focused upon in experiments investigating the effect of varying temperature, feed DMF concentration, and oxidant ratio. However, after more detailed analysis, it became apparent that although DMF removals were superior to those seen in single-stage oxidations, they were slightly inferior to some other tested configurations, with TOC removals also being slightly inferior to other configurations. However, the data gained from investigating the effect of parameter variations on carbon and nitrogen fractions of this multi-stage configuration in comparison to a single-stage configuration would still be extremely useful.

Figure 5.8 and Figure 5.9 show the removals of DMF and TOC with total residence time for all instances in which 66% and 33% of the total oxidant have been injected in the primary port.

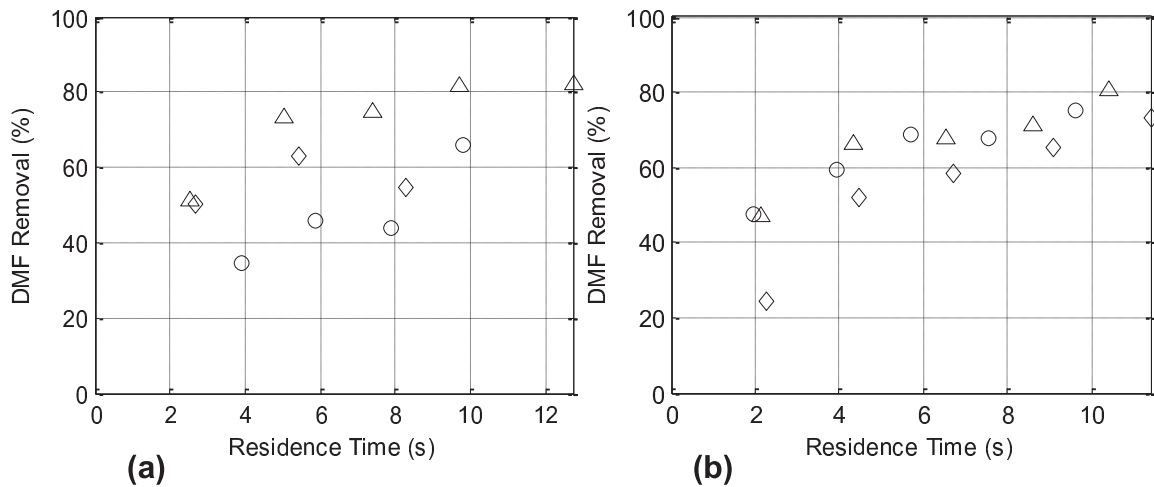


**Figure 5.8** – DMF traces for all cases at 33% (a) and 66% (b) primary oxidant injection, where the traces are: secondary injector 3 m (O), 6 m ( $\Delta$ ), and 9 m ( $\diamond$ ) downstream.

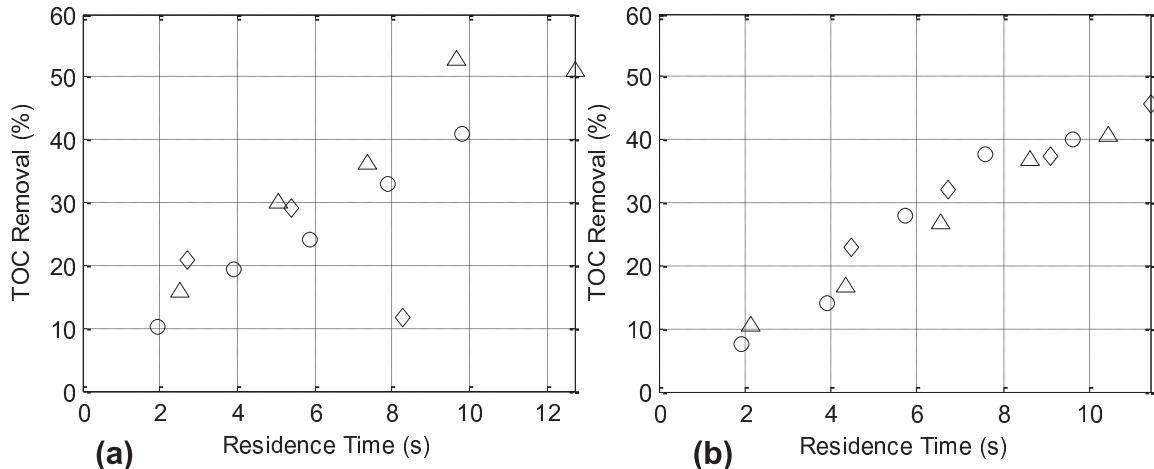


**Figure 5.9** – TOC traces for all cases at 33% (a) and 66% (b) primary oxidant injection, where the traces are: secondary injector 3 m (O), 6 m ( $\Delta$ ), and 9 m ( $\diamond$ ) downstream.

For TOC removal, the data points are reasonably well grouped along similar trends in both plots. Indeed, similar effects were also seen in the analysis of data points taken from 75% and 50% primary injection experiments. Overall though, the profiles start to separate as the proportion of oxidant injected at the inlet decreases. For DMF removal, a similar effect is observed for 66% primary injection, although this is less true for the 33% primary injection case. These data imply that the location of the secondary injector is of lesser importance when compared to the effect that the proportion of oxidant injected via each port has on the removals.

Figure 5.10 indicates the yields of nitrogenous compounds when compared to the primary oxidant percentage, and varying with secondary injector location. Although every attempt was made to make the gas sampling syringes airtight, samples were almost always contaminated within some quantity of atmospheric air, which would clearly inflate the quantity of N<sub>2</sub> present in such a sample. As such, the quantity of N<sub>2</sub> in the gaseous product was evaluated by assuming complete closure of the nitrogen balance with the assumption that all other nitrogen was present in the liquid effluent. In reality, this assumption is not ideal considering the fact that under certain conditions (higher temperature, higher oxidant ratio) N<sub>2</sub>O can be formed along the ammonia oxidation pathway, however, at the conditions investigated during these primary experiments, this effect is a lot less prevalent. The majority products were ammonia and molecular nitrogen, in a similar vein to the single-stage configuration.

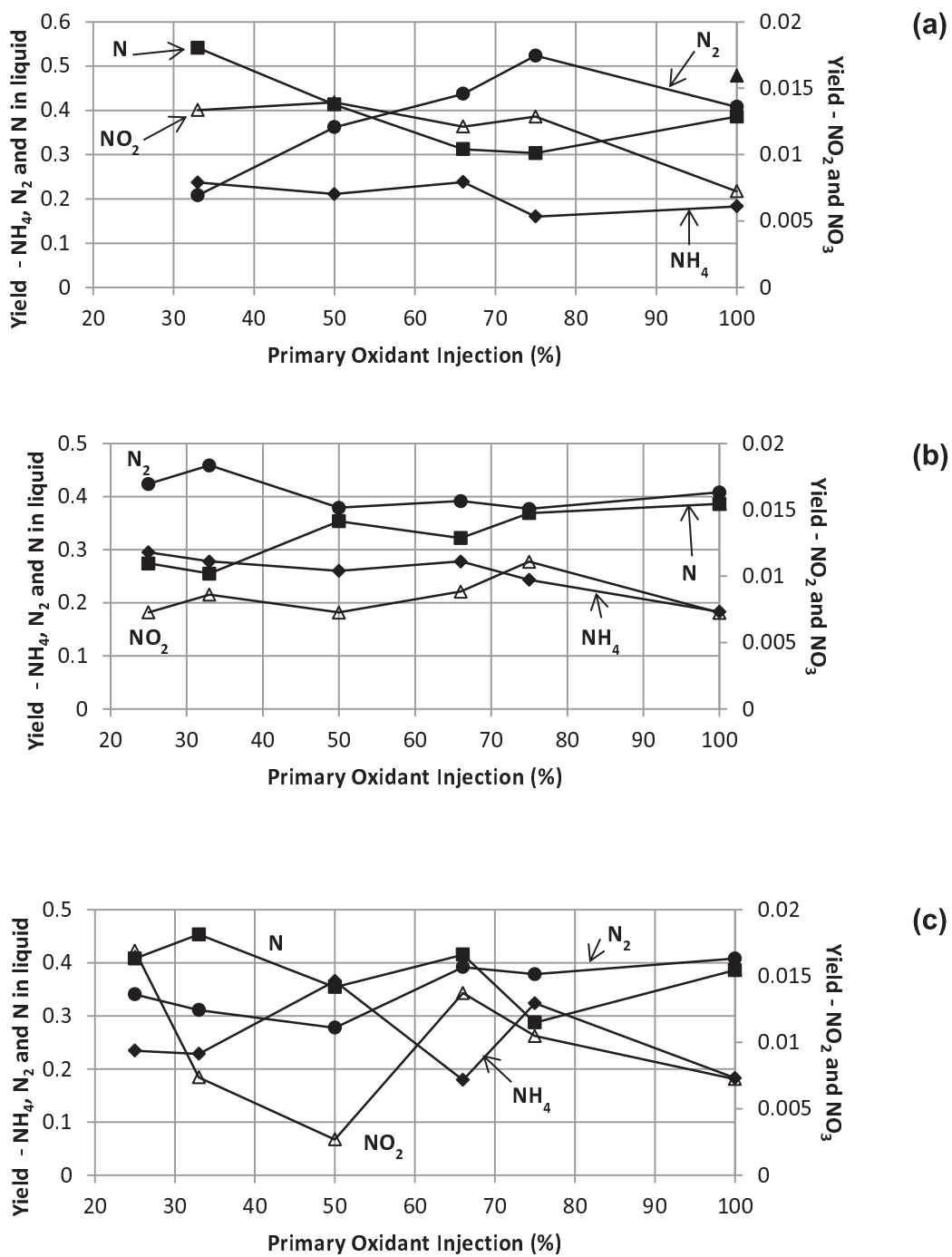


**Figure 5.10** – Nitrogen fraction yields as a function of primary oxidant proportion at a residence time of 6 s and 2<sup>nd</sup> injector location of 3 m (a), 6 m (b) and 9 m (c) downstream of the inlet. Right y-axis:  $NO_2^-$  ( $\Delta$ ),  $NO_3^-$  ( $\blacktriangle$ ); Left y-axis:  $NH_4^+$  ( $\blacklozenge$ ),  $N_2$  ( $\bullet$ ), other N in liquid ( $\blacksquare$ ).

In general it was seen that ammonia yield increased slightly as primary oxidant percentage decreased, indicating that ammonia could have been formed during the initial phase in which the oxidant ratio was in a relative defect. This subsequently-formed ammonia would then remain in the liquid product due to the difficulty in effecting its oxidation at such low temperatures. Ammonia's yields in these experiments were generally greater than those seen for single-stage systems at similar conditions. This is very likely to be a result of the differing oxidant and radical distributions. This particular aspect is a disadvantageous facet of the multi-stage oxidation configuration, given that the formation of ammonia is an unwelcome side-reaction and once formed, ammonia is unlikely to be removed unless the temperature is in excess of 650°C. However, the increased ammonia yield may just be an indicator of the improved conversion of DMF. In either case, downstream processing of the ammonia content would still need to be considered upon scale-up.

Nitrite yields steadily increased with decreasing initial oxidant percentage for the 3 *m* configuration, but were roughly constant at the 6 *m* configuration although lower than the 3 *m* scenario (~0.8% compared to ~1.3%). This could indicate that nitrite is formed at higher specific oxygen concentrations further along the reactor from intermediates formed in an oxidant-defective environment in the 3 *m* case. It would appear that this effect is not facilitated in the 6 *m* case. However, nitrite yields in the 9 *m* case are quite erratic. Disregarding the points for 50% and 33% injection shows behaviour for the nitrite yield that is amalgamated between the other 2 configurations – an upward trend with decreasing primary oxidant injection, with yields rising from ~0.7% to ~1.7%. The data for the 9 *m* configuration could imply that the nitrogen product yields for this configuration are very sensitive to disruption to the

oxidant and radical profile that occurs toward the end of the reactor and further investigation would be required to map this. No nitrate determinations were made for these experimental runs.

#### 5.2.4 Summary

The results of the initial multi-stage oxidation experiments implied that this configuration could result in a higher degree of removals of DMF and TOC when compared to single-stage oxidation reactions.

It seemed that the distribution of oxidant in terms of the proportion injected via each port is a more important factor when considering the treatability of the organic stream than the position of the secondary oxidant injector, although the lower the percentage of oxidant injected via the primary port, the more effect the secondary injector position had. The 6 m downstream injector seemed to exhibit the greatest DMF and TOC removals in these low initial injection cases, likely due to the longer residence time available after the secondary injection in comparison to the 9 m injection, with the additional benefit of a longer residence time prior to this secondary injection when compared to the 3 m injection. For the 3 m injector, it was likely that the radical pool was unable to build up to the necessary level before more oxidant was added.

It was noted that ammonia yields were consistently higher for the multi-stage configurations when compared to those seen in the single-stage configuration.

### 5.3 Focused Multi-stage Experimental Runs

After assessing the performance of the reactor with varying oxidant flow proportions and varying secondary oxidant feed port locations, it was decided to focus on a configuration that placed the secondary oxidant feed at 50% of the total reactor length with an oxidant split that involved delivering 75% of the required oxidant via the primary port and the remaining 25% through the secondary port. This was convenient due to the fact that this allowed the system to be modelled as two similar plug flow reactors in series with similar residence times through each ‘half’, but the major reason for selecting this configuration was that initial experimentation indicated that this configuration may yield the highest TOC conversion. However, after further analysis it became apparent that although this was true for shorter residence times, it was not the case for all times. However, there are advantages in comparing the single-stage data to a configuration that exhibits similar behaviour at the control conditions ( $400^{\circ}\text{C}$ ,  $10\text{ mM}$ , SR = 1) so that any differences at the varied conditions would be more apparent.

The reaction conditions for this configuration were investigated in a similar manner to the experiments in chapter 4. A range of temperatures, feed concentrations and oxidant ratios were investigated for a similar range of residence times as indicated in Table 5.2.

**Table 5.2** – Multi-stage oxidation experimental conditions (fixed configuration – T, [DMF]<sub>feed</sub>, SR variation).

Expt #	Second Injection	Injection Ratio	[DMF] <sub>feed</sub> mM	T °C	Oxidant Ratio	P bar	Residence Time, s
BA – BC	6 m	75:25	10	450 – 550	1	250	2 – 6 (8,10)
BD – BG	6 m	75:25	5 – 30	400	1	250	
BH – BM	6 m	75:25	10	400	0.5 – 3	250	
BN – BP	6 m	75:25	2 – 15	400	3	250	2 – 10

### 5.3.1 Effect of System Pressure

In a similar vein to the work presented in chapter four, the effect of system pressure on the treatability of DMF and TOC, and the dynamics of specific components was not investigated. Future experimentation in this regard would employ an automated back-pressure regulator to better maintain control of the reactor pressure. The data presented herein was obtained in the system with the pressure controlled using an analogue regulator as described in §3.1.7 with close monitoring ensuring that the pressure was never allowed to stray from the 250 bar setpoint.

### 5.3.2 Effect of Temperature

The effect of varying the temperature of the reactor on the carbon and nitrogen yields was investigated. The oxidation was performed at temperatures of 400, 450, 500 and 550°C, at a pressure of 250 bar, at a DMF feed concentration of 10 mM, and at an oxidant ratio of unity. Although it would have been desirable to conduct these experiments at a similar range of residence times as those during the screening experiments, temperatures in excess of 450°C resulted in it being unfeasible to set residence times in excess of 6 s due to the decreased density

resulting in increased fluid volumes for a fixed reactor volume. This resulted in a decreased capacity for the delivery of flowrates small enough to ensure residence times in excess of 6 s.

As described in §3.1.5, temperatures at the inlet and outlet of the reactor were monitored using thermocouples and the PicoLog data acquisition software. It was not possible for a thermocouple to be placed incident to the secondary oxidant injector and as such a separate temperature measurement at this point was not obtained. As such, it was assumed that the oven's internal environment was completely isothermal and that this consequently provided a constant wall temperature for the reactor sections and preheater pipes. In addition, it was assumed that the pipe walls were sufficiently thin that any exothermic reaction would be unable to significantly raise the temperature of the reactor stream in transit due to heat loss through the walls of the reactor, i.e. when the reaction elevated the reactor stream's temperature to a level in excess of that at the oven's internal environment, heat would be lost to the surroundings, reducing the reactor temperature. The difference between the reactor inlet and outlet temperatures was always less than 5°C during oxidation runs, indicating that although temperature rises may occur, particularly at the secondary injection point (see §5.4.3), the product stream always returned to the programmed reaction temperature.

As would be expected to follow from an assumption that the removal kinetics of DMF and TOC follow an Arrhenius-type rate law, the DMF and TOC conversions increased with increasing temperature. Figure 5.11 indicates the removals of DMF, TOC and TC as a function of the reaction temperature for residence times of 2 s and 6 s.

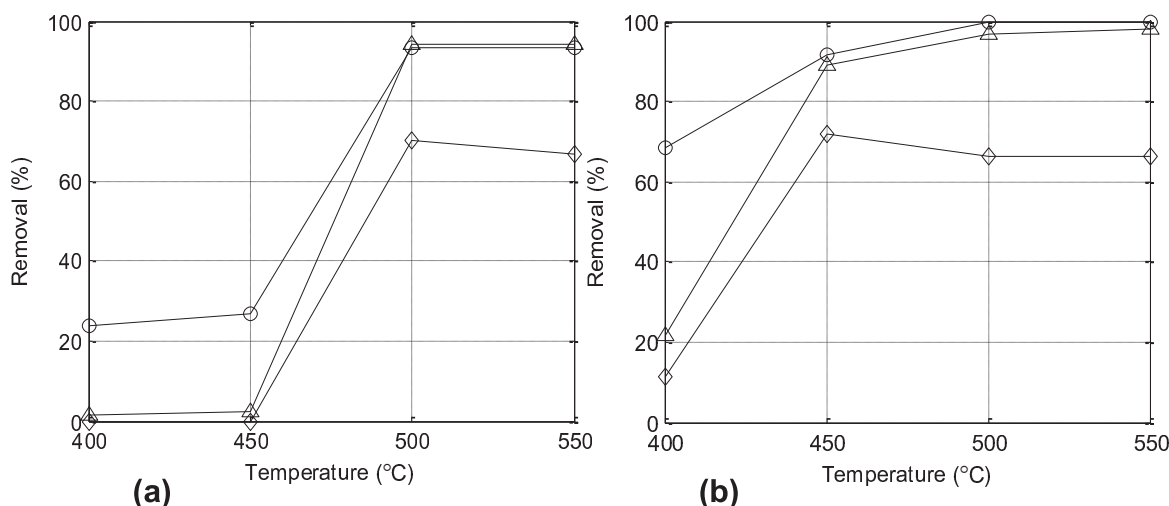


**Figure 5.11** – Removals of DMF (O), TOC ( $\Delta$ ) and TC ( $\diamond$ ) as a function of temperature for  $[DMF]_{sc} = 10\text{ mM}$ , SR = 1 and  $\tau = 2\text{ s}$  (a) and 6 s (b).

Removals of DMF in excess of 99.99% and TOC in excess of 95% were observed at temperatures in excess of 500°C for residence times of 6 s. Data at lower residence times at the higher temperatures also displayed similar removals (e.g. in excess of 94% TOC removal at 2 s residence time), whereas at 450°C the TOC removal at a similar residence time is less than 5%. This indicates that between 450 and 500°C a transition point occurs between low and high DMF and TOC removals even at this low residence time. The increase in removal could be linked to a decrease in the induction time, which could in turn be ascribed to the hydrothermal flame effect seen in some investigations at analogous reactor temperatures (Bermejo *et al.*, 2011). The removals at a residence time of 6 s and a temperature of 450°C were also very high. This could be explained by the additional time allowing the radical chain reaction to proceed to a much greater extent, resulting in an apparent

conversion transition lying between 400 – 450°C instead of between 450 – 500°C as with the 2 s residence time runs. Another possibility is that the exothermic reaction increased the temperature of the fluid such that a hydrothermal flame surface could develop. However, without much more stringent mapping of the temperature profile or CFD simulations, this cannot be confirmed; indeed, the isothermal nature of the oven environment make this less likely to be the case. Whatever the explanation, it appears that as long as the residence time is sufficient, TOC and DMF removals in excess of 90% can be achieved at temperatures of 450°C and near total removals can be achieved at temperatures in excess of 500°C. The concentrations of these compounds in the liquid products at these conditions were certainly below the detection limits of the TOC analyser and GC-FID respectively.

The results for temperatures in excess of 400°C were very similar to the removals observed for the single-stage configuration indicating that as far as treatability is concerned, the reaction temperature is by far the most critical process parameter. This result is widespread in the literature. One slight discrepancy between the two configurations was that for a temperature of 450°C (prior to any potential flame ignition point) the multi-stage configuration indicated that removals of DMF and TOC were higher than those of the single-stage configuration by about 3% for residence times in excess of 6 s, but below this level, the multi-stage oxidation performs less well than the single-stage configuration. Indeed, whereas at 450°C in the single-stage SCWO the DMF removal is greater than 50% and the TOC and TC removals were above 20%, in the multi-stage configuration the DMF removal was below 30% and TOC and TC removals were still very low. This is likely due to the

lower concentration of oxidant at the initial part of the reactor for the multi-stage configuration and could result in a greater induction time.

Figure 5.12 shows the yields of the major carbon-containing compounds at a residence time of 5.8 s, indicating that depending on the temperature, each component of TOC, IC, CO and  $\text{CO}_2$  could be defined as a majority product. The yields of TOC and  $\text{CO}_2$  had mirroring behaviours as they exhibited negative (TOC) and positive ( $\text{CO}_2$ ) dependences on temperature.

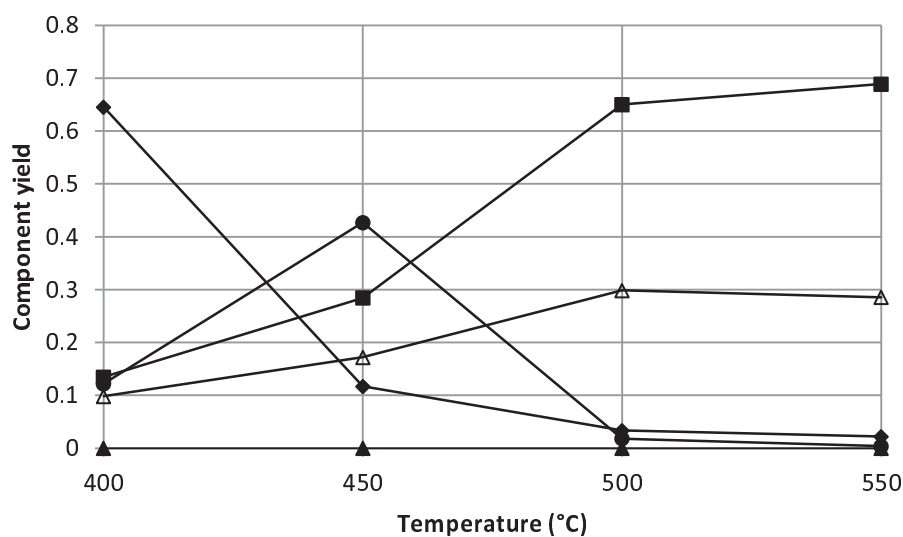


**Figure 5.12 – Carbon fraction yields as a function of temperature at a residence time of 5.8 s: TOC (♦), IC (Δ),  $\text{CH}_4$  (▲), CO (●),  $\text{CO}_2$  (■).**

The profile of TOC with temperature was similar to that for the single-stage oxidation, although the removal of TOC at 400°C was higher for the multi-stage configuration. However, the maximum removal of TOC observed was 98% at 550°C, slightly lower than that seen for the single-stage oxidation. Carbon monoxide was the majority component yield at 450°C (~43%), with the gaseous product yields

amounting to 71% of the total carbon. At lower temperatures the CO yield is higher for the multi-stage configuration indicating that although a higher degree of TOC removal is observed, the oxygen-deficit conditions initially limit the subsequent conversion to CO<sub>2</sub>. This effect is eliminated at higher temperatures.

At higher temperatures, the CO yield reduces to less than 2% at 500°C and 0.4% at 550°C, less than the single-stage configuration (~0.7% and ~1.2% respectively). This indicates that the secondary injection could cause a higher degree of contact between CO and oxidising radicals conducive to the conversion to CO<sub>2</sub> and IC. No methane was detected in the gaseous product for any temperature.

In a similar vein to the single-stage oxidations, the yields of IC showed a positive dependence on temperature, peaking near to 30% at 550°C, similar to the single-stage configuration.

The nitrogen component yields are indicated in Figure 5.13. The ammonia yield was highest at 450°C, with the fraction reducing at higher temperatures. The increased ammonia yield at 450°C in comparison to the single-stage configuration (58% as opposed to 40%), is likely to be due to the similar partial oxidant defect effect that caused an increase in CO yield. This could have caused a greater selection of a route that produced ammonia rather than a more readily oxidised N-species (e.g. amidogen, NH, etc). The very low removals of ammonia observed in the literature at temperatures lower than 650°C, seem to imply that the reduction in ammonia yield at higher temperature is likely to be due to a reduced rate of formation, rather than a removal of ammonia after formation.

Nitrate and nitrite yields were less than 2% in all cases. The yields of both of these compounds decreased as the reactor temperature increased.

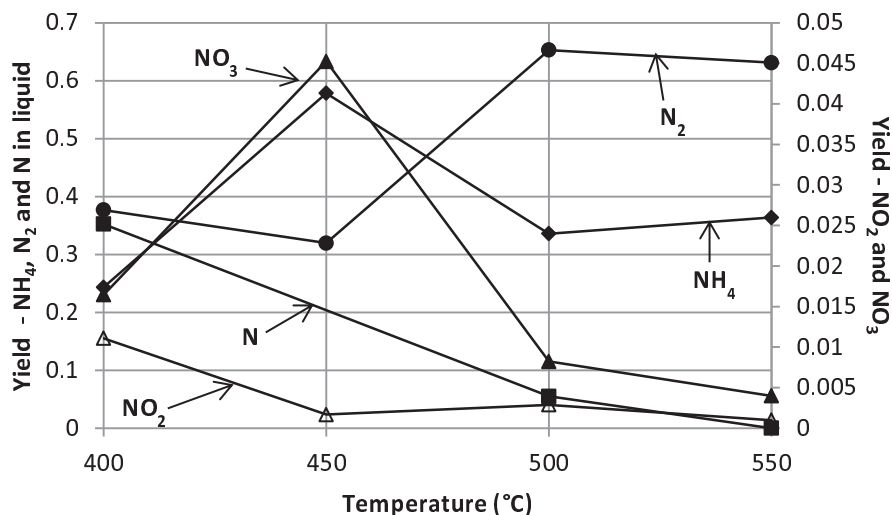


**Figure 5.13** – Nitrogen fraction yields as a function of temperature at a residence time of 5.8 s. Right y-axis:  $\text{NO}_2^-$  ( $\Delta$ ),  $\text{NO}_3^-$  ( $\blacktriangle$ ); Left y-axis:  $\text{NH}_4^+$  ( $\blacklozenge$ ),  $\text{N}_2$  ( $\bullet$ ), other N in liquid ( $\blacksquare$ ).

In general, the higher the temperature of reaction, the less difference there is between the single- and multi-stage oxidations, although at 450°C (interestingly, a temperature just below the autoignition temperature of DMF, and as such a point that would be pertinent to the ignition of a hydrothermal flame) discrepancies in the yields of CO and ammonia were observed. As such, it seems that if any advantages of the multi-stage configuration with regard to treatability are to be utilised, lower reaction temperatures would be necessary, which may be desirable if lower energy costs were a design priority.

### 5.3.3 Effect of Organic Concentration

The effect of the organic concentration at the feed on the TOC conversion was investigated for stoichiometric systems ( $\text{SR} = 1$ ) and systems with the oxidant in

excess ( $SR = 3$ ). The reactor temperature, pressure and range of residence times were held constant at  $400^{\circ}\text{C}$ ,  $250\text{ bar}$  and  $2 - 10\text{ s}$  respectively. Organic feed solutions were made up such that the target concentration of DMF in the feed at supercritical conditions would be  $5, 10, 15, 20$  and  $30\text{ mM}$ . DMF, TOC and TC removals are displayed in Figure 5.14. The removals of DMF, TOC and TC show a positive dependence on inlet feed concentration. When adjusted and plotted for the initial organic concentration inside the reactor, there is a clear upward trend in the removals of TOC and TC. It was not possible to conduct experiments at higher inlet feed concentrations whilst maintaining the investigated residence times in the apparatus investigated here due to the even higher quantities of oxidant that would be required to maintain the stoichiometric ratio.

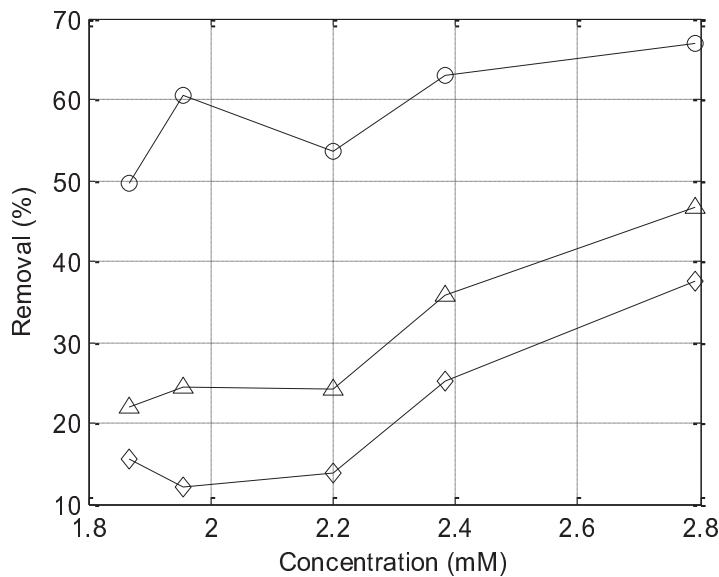


**Figure 5.14** – Removal of DMF (O), TOC ( $\Delta$ ) and TC ( $\diamond$ ) as a function of organic concentration at a residence time of 6 s.

A comparison with the single-stage configuration is shown in Figure 5.15. It can clearly be seen that greater removals are seen for the multi-stage configuration for otherwise identical conditions in terms of temperature, oxidant ratio and residence time. It would appear then, that the removal of TOC and DMF could be optimised by controlling the distribution of oxidant, were the organic feed concentration to be fixed.

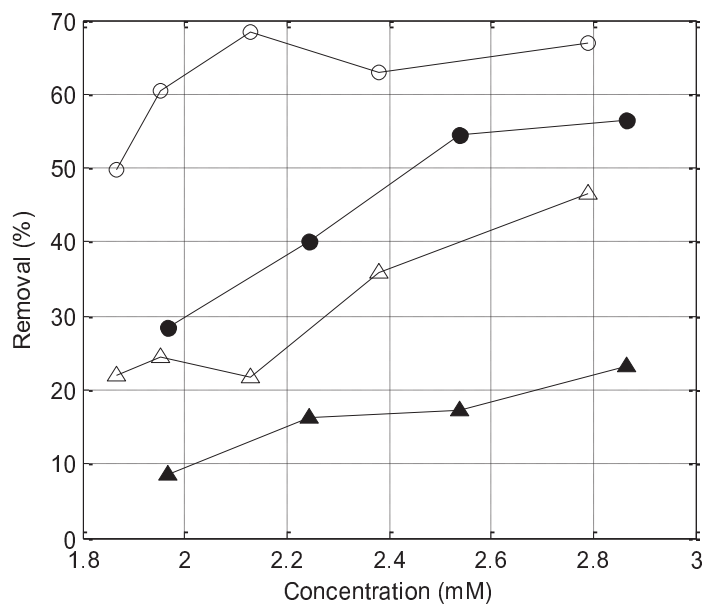


**Figure 5.15** – Comparison of DMF (O) and TOC ( $\Delta$ ) removals as a function of initial reactor concentration for multi- (white markers) and single-stage (black markers) configurations ( $400^{\circ}\text{C}$ , SR=1).

The effect of reactor concentration on the carbon and nitrogen fraction yields is displayed in Figure 5.16 and Figure 5.17 respectively. The major carbonaceous products were TOC and  $\text{CO}_2$ , with TOC exhibiting a negative dependence on reactor concentration and  $\text{CO}_2$  exhibiting the opposite. In general, the IC yield appeared independent of concentration and the CO yield did not rise above 15% indicating that

at these conditions, the rate of formation of CO was never much greater than the rate of consumption. No methane was detected in the gaseous products.

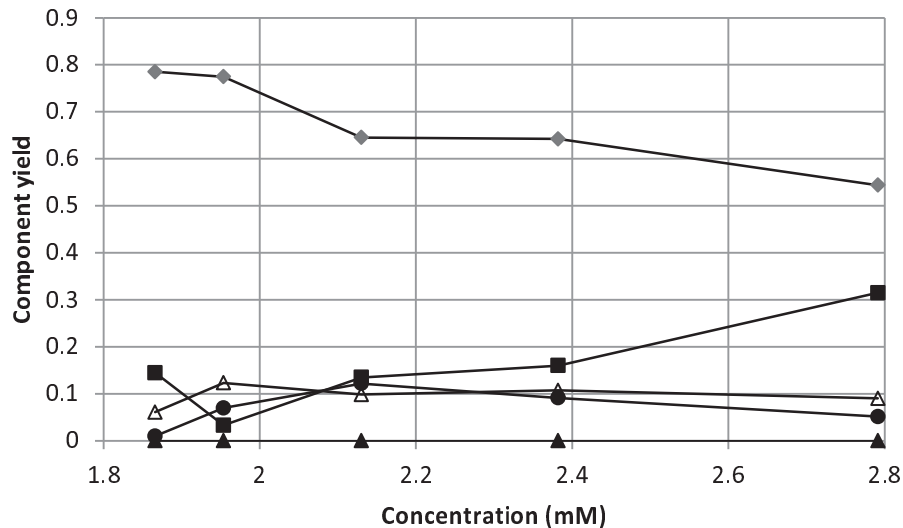


**Figure 5.16** - Carbon fraction yields as a function of concentration at a residence time of 6 s: TOC (♦), IC (Δ), CH<sub>4</sub> (▲), CO (●), CO<sub>2</sub> (■).

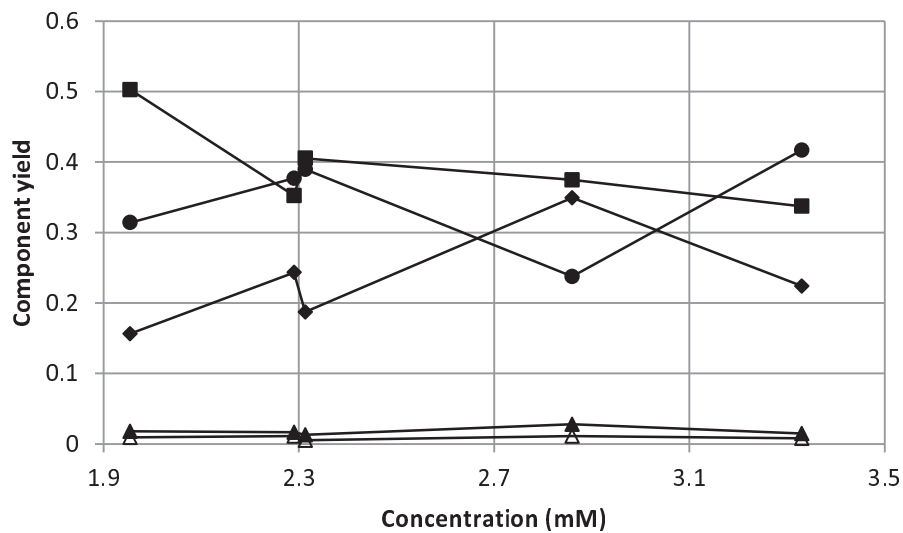


**Figure 5.17** – Nitrogen fraction yields as a function of concentration at a residence time of 6 s.  $\text{NO}_2^-$  (Δ),  $\text{NO}_3^-$  (▲),  $\text{NH}_4^+$  (♦), N<sub>2</sub> (●), other N in liquid (■).

Ammonia yield showed a positive dependence trend on the inlet feed concentration, increasing from 16% at 5 mM to 34% at 30 mM (31% to 56% of non-organic nitrogen products respectively). Again, these ammonia yields were higher than those observed for the single-stage configuration as shown in Figure 4.11, indicating that although the oxidant optimisation would benefit the TOC and DMF removal efficiencies, the initially oxidant-lean conditions resulted in formation of ammonia that was refractory at these relatively mild conditions. It seemed that over the concentration range investigated, the nitrite yield was largely insensitive to the concentration, being maintained at about 1%. Nitrate yields were marginally increased by increasing the inlet organic concentration from 1.8% at 5 mM to 2.8% at 30 mM corresponding to between 3.5% and 4.4% of all non-organic nitrogen in the product.

#### 5.3.4 Effect of Oxidant Ratio

The range of oxidant ratios investigated was such that the oxidation reaction was conducted under both oxidant excess and oxidant deficit conditions. This range spanned oxidant ratios of 0.5 – 3. Such a range allowed both the attempted re-evaluation of some reaction kinetics parameters and an assessment of the operational benefits of particular oxidant ratios when considering the optimum conditions to be employed when conducting SCWO on an industrial scale. The oxidant ratio was varied whilst maintaining other conditions similar to those seen in previous sections: a reactor temperature of 400°C, an organic feed concentration of 10 mM, a reactor pressure of 250 bar and a residence time range of 2 – 10 s.

Due to the split-oxidant nature of the investigations, the oxidant ratio varied in both series reactors. For all select experiments, the oxidant was split in a 75:25 ratio, meaning that for globally stoichiometric conditions, the oxidant ratio in the first reactor would be 0.75. If global oxidant excess conditions were required, the ratio would have to be greater than 1.33 for the oxidant ratio in the first PFR to also be in ‘excess’. Due to the impossibility of determining the composition of the reactor stream at the exit of the first PFR (in terms of both organic and nitrogenated compounds, and the oxidant), the results presented below defined the oxidant ratio to be the global stoichiometric ratio. The residence time is defined as previously: the total time at which the organic stream was exposed to supercritical conditions.

The removals of DMF, TOC and TC as a function of the global stoichiometric ratio for residence times of 6 s and 10 s are given shown in Figure 5.18.

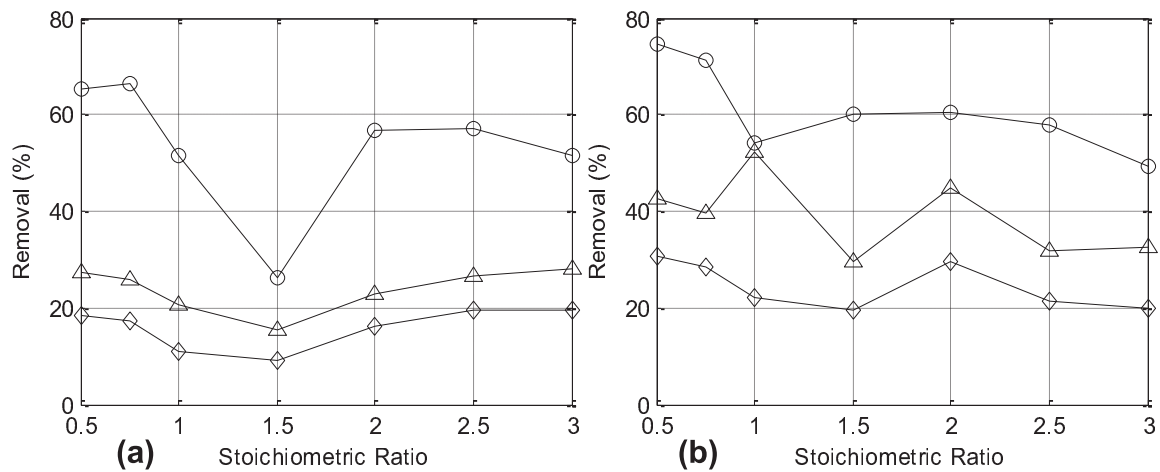


**Figure 5.18 – DMF (O), TOC ( $\Delta$ ) and TC ( $\diamond$ ) removals as a function of SR at a residence time of 6 s (a) and 10 s (b).**

The data indicates that the DMF removal was sensitive to the oxidant ratio at values below 1.5, but not above this level. The variation in DMF removal at the higher oxidant ratios could also be explained by the decreasing concentration at the inlet as indicated in Figure 5.19 for a residence time of 6 s.

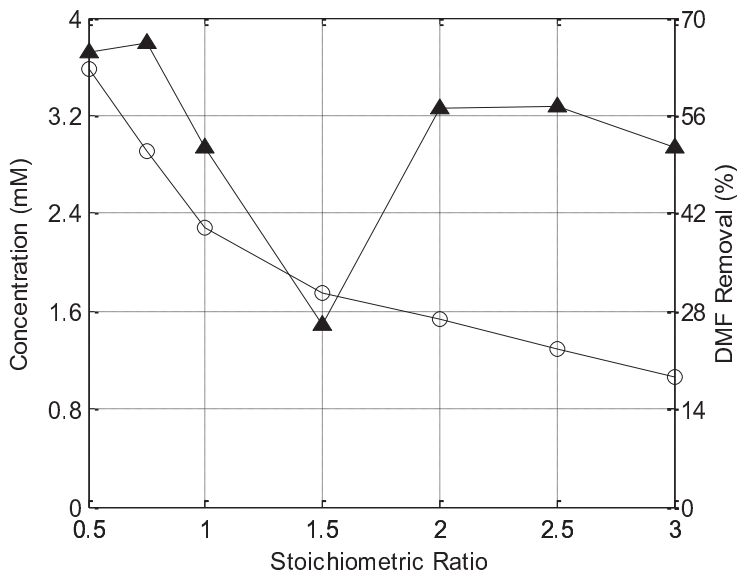


**Figure 5.19** – DMF removal (▲) as compared to the relationship between concentration and SR (○).

Although there was a large decrease in the DMF yield at an SR of 1.5, Figure 5.19 shows that initially this followed a reduction in the concentration. When the oxidant ratio increased above this value, the DMF conversion recovered to ~56% where it seemed subsequently insensitive to an increasing oxidant ratio.

The carbon and nitrogen fraction yields as a function of oxidant ratio are indicated in Figure 5.20 and Figure 5.21, where the dashed lines indicate a concentration normalised to the reactor concentration at a stoichiometric ratio of 0.5 (3.6 mM). Figure 5.20 indicated that increasing the stoichiometric ratio above 2 did

not have a great effect on the carbon fraction yields aside from the TOC yield starting to increase again at the highest stoichiometric ratio due to the effective concentration at the reactor inlet decreasing further. The IC yield started to increase very marginally at the same point.

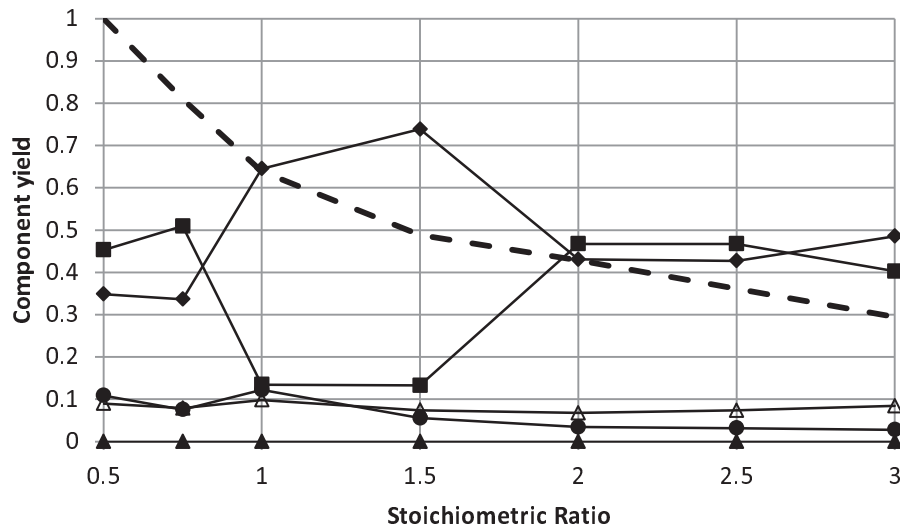


**Figure 5.20** – Carbon fraction yields as a function of SR at a residence time of 5.8 s: TOC (♦), IC (Δ), CH<sub>4</sub> (▲), CO (●), CO<sub>2</sub> (■).

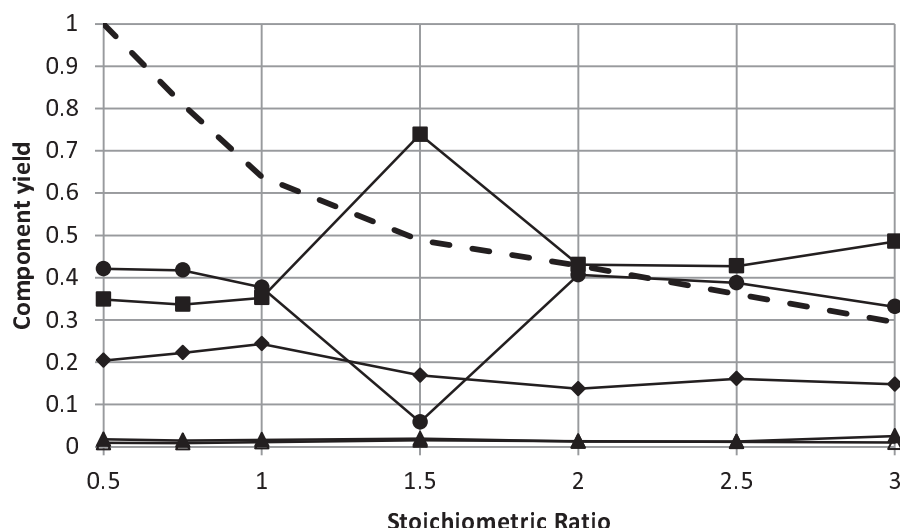


**Figure 5.21** – Nitrogen fraction yields as a function of SR at a residence time of 5.8 s.  
 $\text{NO}_2^-$  (Δ),  $\text{NO}_3^-$  (▲),  $\text{NH}_4^+$  (♦),  $\text{N}_2$  (●), other N in liquid (■).

Figure 5.21 shows that the ammonia yield decreased slowly with increasing oxidant ratio. Such an effect could be explained by the excess oxidant resulting in an increased concentration of hydroxyl radicals that could force an elevated rate of subsequent destruction of ammonia after formation. As well as the simpler mechanism of  $NH_3 \rightarrow NH_2^* \rightarrow NH \rightarrow N_2$  facilitated by the OH• radical (Ploeger *et al.*, 2008), Oe *et al.* (2007) suggest that the following mechanism could also describe this process:



The reactions in the work were derived from combustion chemistry and are elemental reactions, hence increases in the concentration of the hydroxyl radical (OH•) would encourage conversion of ammonia to an ultimate product of N<sub>2</sub>O. The same work indicates that a reaction of N<sub>2</sub>O with OH• to form N<sub>2</sub> would only occur at an appreciable rate at temperatures of almost 900°C. Work by Benjamin and Savage (2005a) on the oxidation of methylamine indicates that even at temperatures as low as 390°C with oxidant ratios of 1.5 and higher, 8% of ammonia could be converted to nitrogen products, assuming that all nitrogen must proceed via an ammoniacal intermediate (not necessarily complete molecular ammonia). The implication of this is that provided that the oxidant ratio is high enough, some ammonia that is formed as an intermediate could be decomposed to N<sub>2</sub> (and N<sub>2</sub>O) later. Work by Fujii and

Oshima at the University of Tokyo (personal communication, October 2011) indicated that for a co-oxidation between an organic compound (in this case methanol) and ammonia, selectivity toward N<sub>2</sub>O is increased at higher oxidant ratios, but this cannot be ascertained in this work due to both the inability of the TCD column to detect N<sub>2</sub>O when the experiments were performed, and the lack of GC-MS data to potentially indicate the presence of these specific N-based intermediates in the liquid effluent. Further investigation into this reaction under multi-stage configurations will incorporate GC-MS analysis in order to identify – qualitatively at least – specific neutral and radical intermediates.

### 5.3.5 Effect of Residence Time

Almost without exception, it was shown that the DMF and TOC removal increased with increasing residence time although there were limitations, for example as shown in Figure 5.22 at temperatures in excess of 500°C there was very little dependence of the conversion of TOC on the residence time with the conversion profile for these experiments almost approximating to a straight line. This indicated that almost all conversion happens very quickly with the reaction with regards to TOC then ceasing. A similar effect was observed for the DMF yields, with over 93% of DMF removal occurring within 2 s for temperatures in excess of 450°C.

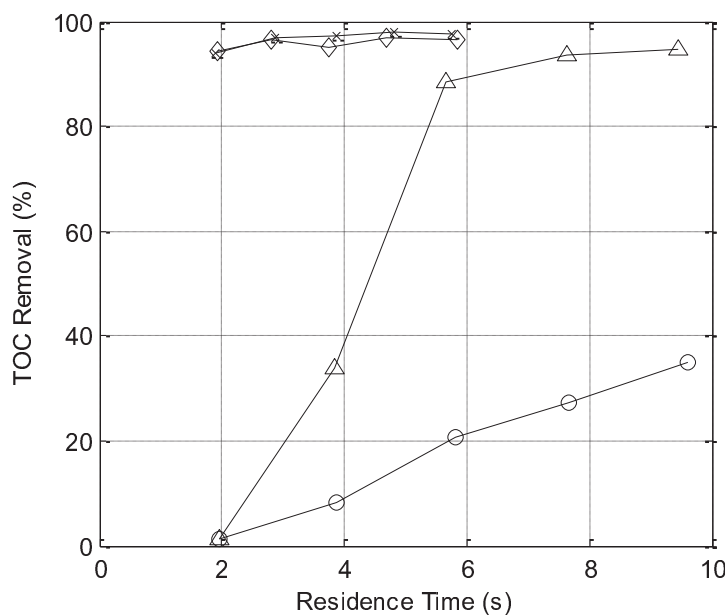


**Figure 5.22** – TOC removal as a function of residence time at 400°C (O), 450°C (Δ), 500°C (◊) and 550°C (x).

At higher oxidant ratios ( $SR = 3$ ), the residence time had a much diminished effect. Although increases in TOC conversion with increasing residence time were still observed, the effect was much less apparent as with lower oxidant ratios. This indicated that for these situations where the oxidant ratio was in great excess, the majority of the TOC conversion occurred within two seconds.

Studies (Wellig *et al.*, 2005; Augustine and Tester, 2009; Bermejo *et al.*, 2011) that include investigations into the initial mechanisms of the SCWO reaction suggest that there could be a variety of chemical effects to explain rapid conversions for very high temperatures and high oxidant ratios. Investigations into hydrothermal flames display similar timescales for rapid conversions (of the order of 0.5 s) although these systems usually exhibit very high conversions at these very short timescales, which could be argued for at temperatures in excess of 500°C if the temperature and

oxidant injection conditions are suitable for the creation and stabilisation of a flame surface. Hydrothermal flames have been observed at temperatures above the autoignition temperature of the investigated organic compound. The autoignition temperature of DMF is 455°C which implies that conditions could potentially be sufficient for the formation of a hydrothermal flame for the experiments where the reaction temperature was 500°C and 550°C, however, the limits of DMF in air are 2.2% - 16% (v/v) (IPCS, 1990). Although for some conditions, when the DMF concentration was compared purely to the oxygen concentration, the result would lie inside this range, water is by far the most dominant component (well over 99% by volume) and this implies that even at the maximum oxidant excess investigated, the local environment at the reactor inlet was unlikely to have a high enough oxygen concentration to encroach into a regime conducive to a hydrothermal flame. Generally, research into hydrothermal flames has focused on systems in which an auxiliary fuel (methanol, ethanol, isopropyl alcohol, etc) has been employed as an aid to the oxidation – a condition that is not replicated in the experiments described in this work. It is worth noting however, that research by Wellig *et al.* (2005) into the formation of hydrothermal flames in a transpiring wall reactor introduced a methanol solution as both the organic feed and auxiliary fuel where methanol was delivered to a flame surface maintained by methanol oxidation and was thus a system that was almost tantamount to a single component system (discounting the oxidant). This would imply that DMF could similarly form such a flame without an auxiliary fuel under the right conditions. In order to be certain that such an effect is present, further investigation would be necessary using a rig with which it is possible to achieve much lower residence times than are possible with the current rig.

A further test as to whether a flame has been formed would be to attempt to lower the organic injection temperature once the reaction has begun (and thus the hypothetical flame has been established) and to monitor the subsequent effect on the TOC conversion. However this investigation would be more easily carried out in a pseudoadiabatic reactor rather than the isothermally operating rig described herein, particularly because it has been found by Bermejo *et al.* (2011) that tubular reactors with internal diameters lower than  $\frac{1}{4}$  inch are less successful at maintaining a flame while reducing the organic feed injection temperature and with the isothermal configuration, it is difficult to preheat the organic feed to a temperature different to that at which the reactor is being maintained.

## 5.4 Kinetics Analysis

### 5.4.1 Application of Single-stage Model to Series PFRs

The multi-stage oxidation reaction was initially modelled as two plug flow reactors in series, because when one considers that each oxidant stream is separate, and not just two parts of one global quantity, this is how the reactor appears. Some of the oxidant is injected with the DMF solution at the inlet of ‘reactor one’, and the products of this reaction in conjunction with more oxidant act reagents injected into ‘reactor two’. This process can be represented by the following global series reactions:



The oxidant (B) is notated as two separate reactants ( $B_1$  and  $B_2$ ) to differentiate from the notion that there may just be two parallel reactions in B – the oxidant added for the second PFR is an entirely new reactant added to the products leaving the first PFR. In reality, many initial and intermediate components will participate in numerous reactions, in both a series and parallel manner, but at this stage, only the simple scheme shown above will be considered as part of an evaluation of the global dynamics of DMF.

Using the reaction kinetic parameters derived from chapter 4's results, predictions for the removal of DMF for the multi-stage oxidation were made using the Matlab program shown in appendix 5. Identical parameters were used for both series PFRs, resulting in identical rate constants. However, the inputs of the second PFR were recalculated from the outputs of the first to take into account both the additional oxidant, and the supplemental dilution effect of the water in which the oxidant is delivered. A parity of plot of these calculated conversions against the experimentally obtained values is given in Figure 5.23, with the kinetic parameters used recapped in Table 5.3.

**Table 5.3** – Model parameters used to generate Figure 5.23.

Parameter	Symbol	Value
DMF Order	$a$	1.00 [–]
Oxidant Order	$b$	0.36 [–]
Activation Energy	$E_A$	140.432 [ $\text{kJ mol}^{-1}$ ]
Pre-exponential Factor	$A$	$4.8 \times 10^{10} [\text{litre}^{0.36} \text{mol}^{0.36} \text{s}^{-1}]$

In general, for the multi-stage system, it seemed that the parameters used resulted in an underestimate of the experimental conversions. Breakdowns of

different sets of data are presented in Figure 5.24 (variation of injector locations and proportions) and Figure 5.26 (variation of temperature, concentration, oxidant ratio and concentration at oxidant excess).

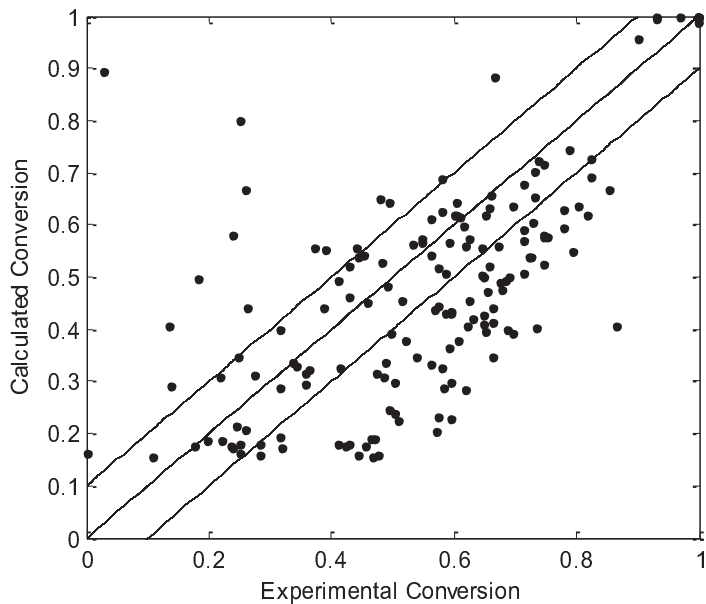


**Figure 5.23** – Parity plot of calculated and experimental conversions for all multi-stage experiments undertaken based on rate parameters calculated in chapter 4.

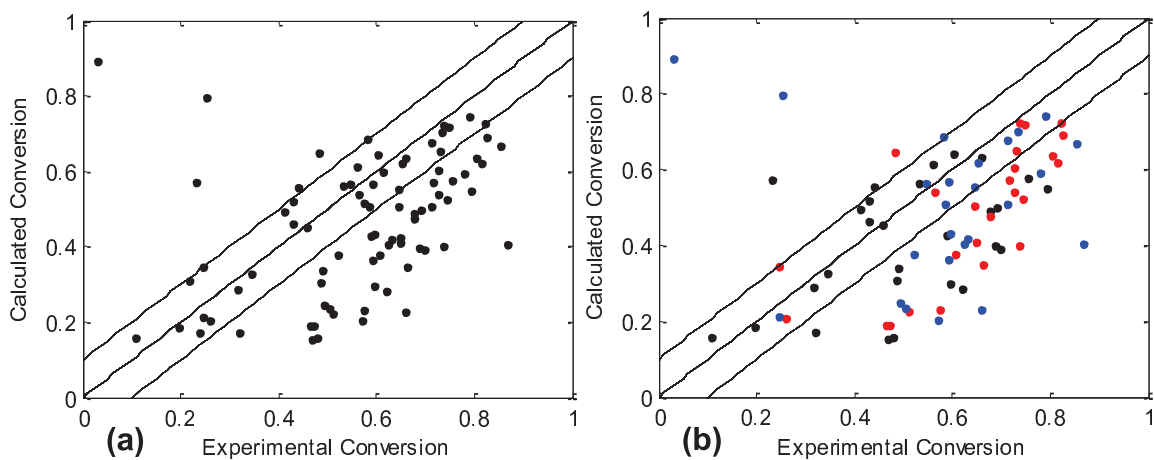


**Figure 5.24** – Parity plots for oxidant location and proportion experiments: all (a), and separated by injector location (b), indicating injector at 3 m (black), 6 m (red) and 9 m (blue).

As Figure 5.24a shows, the majority of the underestimated data points in Figure 5.23 originated from the experiments in which the secondary injector location and proportions were varied at a reaction temperature of 400°C, DMF feed concentration of 10 mM and a global stoichiometric ratio of 1. An interesting effect can be seen when consulting Figure 5.24b. The instances in which the secondary oxidant was injected 3 m downstream of the reactor inlet (black dots; and thus can be most easily compared to the single-stage configuration described in chapter 4) are those which were generally best predicted by the model. It was noticeable that the lower the amount of oxidant that was injected through the primary injector, the more accurate the model prediction for this 3 m injector configuration. This could be attributable either to variation in mixing effects or to an increasing residence time in the first PFR with decreasing primary oxidant proportion that was inevitable in order to expose the DMF to the same sets of total residence times for each configuration.

The other configurations showed a great degree of variability in their predictions, generally falling into an underestimate. These discrepancies are very likely to be due to the increased degrees of mixing provided by the additional injector and the different distribution of radicals that this will cause. The result of any enhancement of the radical pool generation could well be that the reaction order with respect to the oxidant could decrease. Indeed, reducing  $b$  to 0.25 results in a large shift of the data in Figure 5.24a up the y-axis as shown in Figure 5.25.

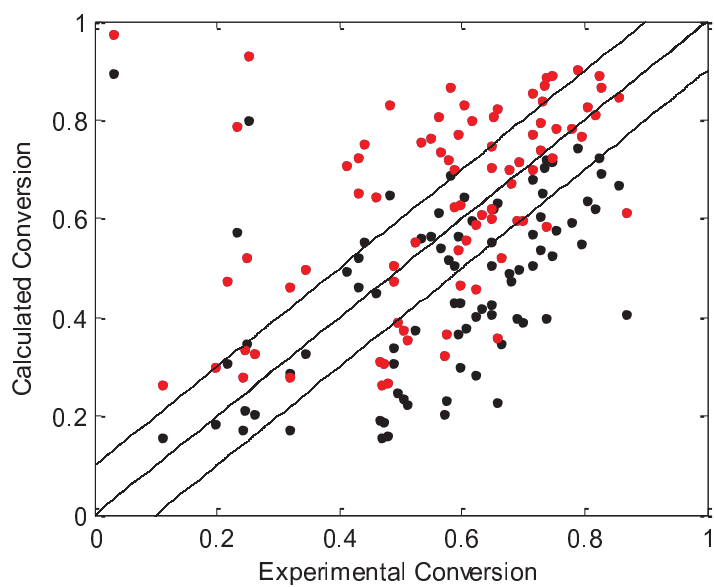


**Figure 5.25** – Parity plot for data in Figure 5.24 for oxidant reaction order of 0.36 (black) and 0.25 (red).

Figure 5.26 shows that the experiments in which the temperature and stoichiometric ratio were elevated resulted in much less of an underestimate of the experimental data. For these instances, the higher temperature effect dominates (Figure 5.26a), or the progression of the chain reaction was more similar to that which would be seen for a single-stage reaction (Figure 5.26c and the upper points in Figure 5.26d).

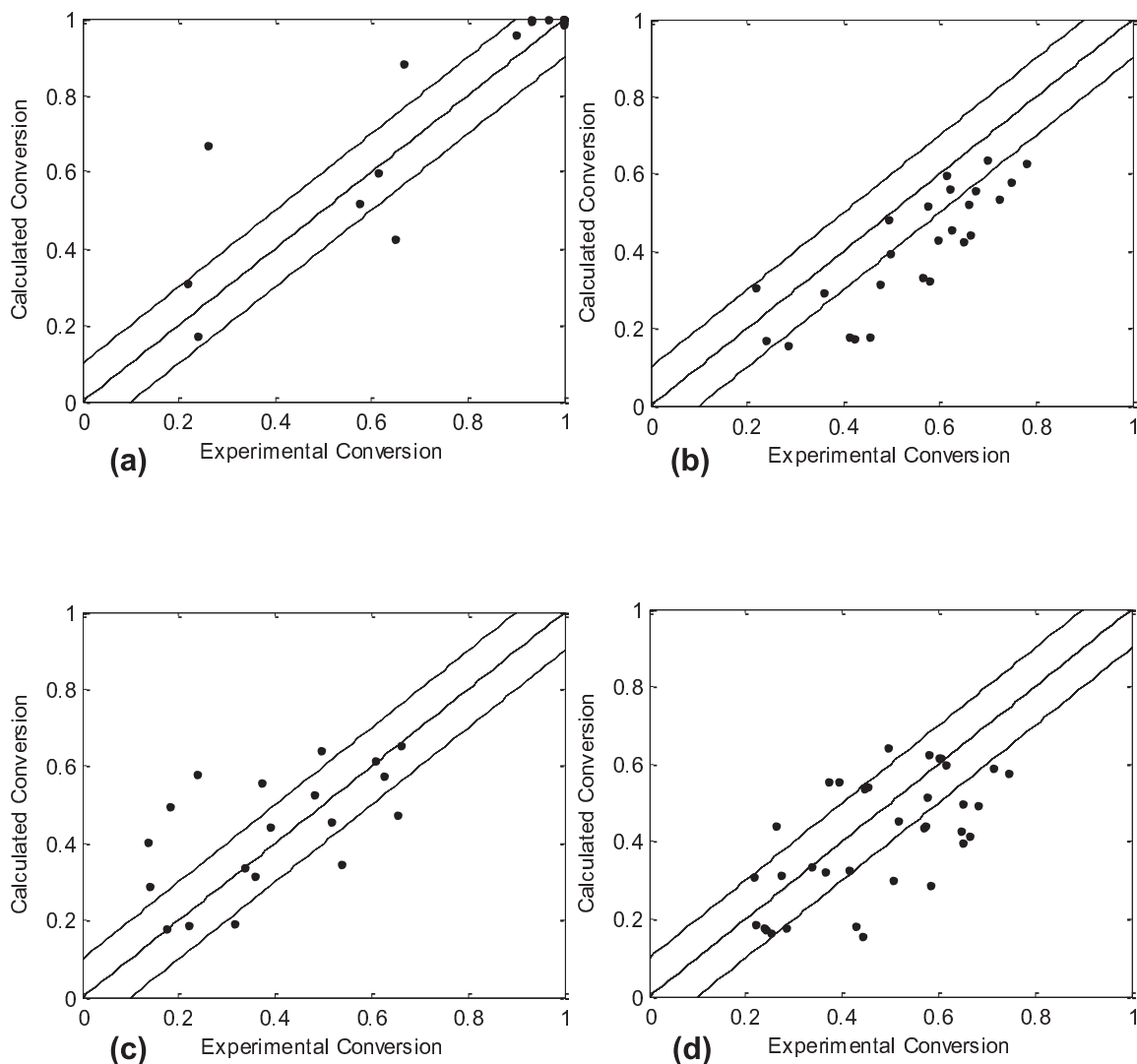


**Figure 5.26** – Parity plots for 75% oxidant delivered through the primary port and the secondary injector 6 m downstream for varying: temperature (a), concentration ( $SR = 1$ ; b), concentration ( $SR = 3$ ; c) and stoichiometric ratio (d).

However, at lower temperatures and global stoichiometric ratios approaching unity, the DMF conversions exhibited by the multi-stage configurations seemed to out-perform those predicted. This is likely to be due to the different radical dynamics and additional radial mixing zones introduced by the secondary oxidant. The radical dynamics will be changed by the sudden influx of  $O_2$  and hydroxyl radicals disrupting

any chemical equilibrium that might have formed. This enabled the formation of new species by drastically increasing the local OH<sup>•</sup> concentration (and thus the local reaction rates) for the species whose consumption relies on this precursor (DMF, TMA, DMA, MA, methanol, etc).

#### 5.4.2 Optimisation of Kinetic Model

The model was shown to predict the global DMF removal well at some specific conditions, generally where the effect of a certain condition (high temperature, high oxidant ratio) dominated the reaction and made it analogous to the single stage reaction. However, at lower temperatures and with global oxidant ratios of unity or below, the single-stage model under-predicted the DMF conversions that were observed during experiment.

Further work on describing this system will focus on the solution of partial differential equations to evaluate the removal of DMF and TOC along the length of both stages of the reactor. Following this, a more accurate model could be developed by being able to quantify:

- The radical dynamics, the complexity of which is greatly increased by the addition of the secondary oxidant. Induction time quantification would also be served by this analysis, where currently any induction time is ignored (resulting in an over-prediction of experimental conversions for some conditions).
- The temperature profile along the reactor. The temperature was shown to be higher at the outlet of the reactor than at the inlet, despite the reactor wall temperature being held essentially constant. Given that the

reaction kinetics follow and Arrhenius-type law, this temperature profile, particularly the expected sharp increase in temperature after the secondary injection will greatly affect the oxidation. Not being able to incorporate this effect in the models described above is likely a major source of the under-prediction seen in Figure 5.26b and Figure 5.26d.

Performing additional experiments in an adiabatically operating reactor would allow the validation of models that also incorporate the exothermic heating effects.

#### 5.4.3 Operation of Multi-stage Reactor

The employment of a multi-stage reactor configuration presents a slightly different set of engineering challenges than those present for the operation of a single-stage PFR.

The reactor in this work was approximated to isothermal due to the constant temperature in the oven's ambient atmosphere; however temperature trace data indicated that the assumed constant wall temperature wasn't always successful in negating the temperature increase effected by the exothermic reaction. The example temperature trace in Figure 3.5 indicated the temperature measurements for experiments at a residence time of 2, 4, 6, 8 and 10 seconds (from left to right) at a temperature of 400°C, feed concentration of 10 mM and global oxidant ratio of 1. The increases in outlet temperature for the 4 s experiments onwards are caused by the exothermic nature of the reaction, with the effect attenuated somewhat at higher residence times due to the ambient conditions having more opportunity to cool the reactor product before exiting the reactor (due to lower flowrates).

It was very likely that the temperature increase was tempered by the approximately isothermal nature of the reactor, however the employment of an isothermal regime when utilising a tubular reactor on an industrial scale would be impractical and undesirable due to the high energy costs that would be incurred. As such, an adiabatic reactor would be considered.

Studies by Portella *et al.* (2007) showed that during the oxidation of  $1 \text{ kg h}^{-1}$  methanol in an adiabatically-operating tubular multi-stage reactor at  $430^\circ\text{C}$ , temperature spikes of  $620^\circ\text{C}$  and  $700^\circ\text{C}$  were observed at the two respective additional oxidant injection points. The temperature then decreased downstream of these points due to thermal losses as shown in Figure 5.27.

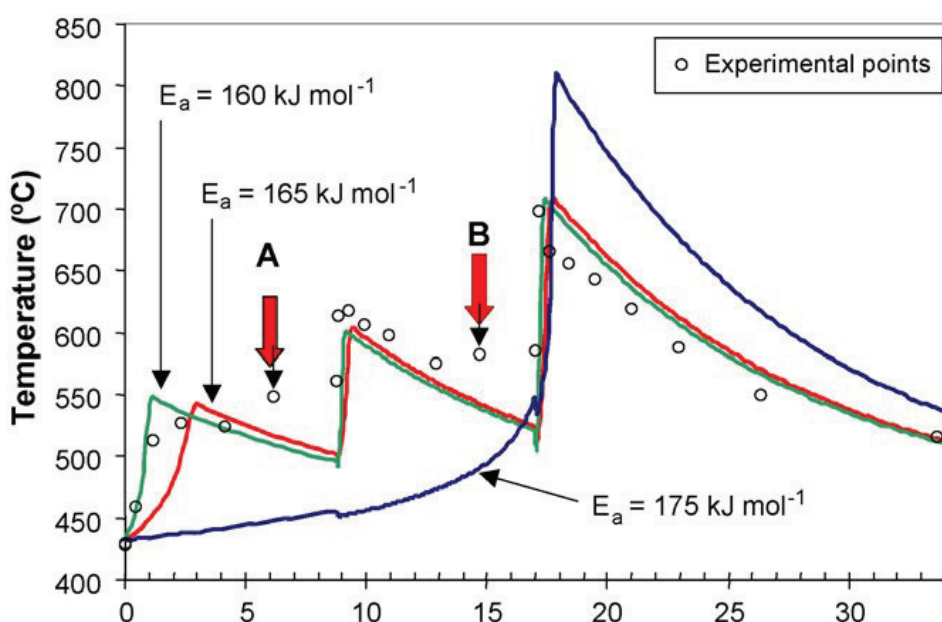


**Figure 5.27 – Temperature profile in adiabatic multi-stage SCWO of methanol**

(Portella *et al.*, 2007).

A and B indicate data points not predicted accurately, which are explained by axial heating after oxidant injection, which was not accounted for in their simulation.

The oxidant injections were 24%, 20% and 56% of stoichiometry into the first, second and third points respectively.

These temperature spikes were lower than what were observed by the same group for a single-stage oxidation in which the entire stoichiometric amount of oxidant was injected at the reactor inlet. However, simulation indicated that for a better-insulated reactor, much higher temperatures than the reactor could withstand (ca. 875°C) would be attained, due to the dramatic temperature increase upon oxidant injection. As such, temperature control in an industrial-scale adiabatic multi-stage reactor is likely to be a key operational consideration. Consequently, the optimisation of several variables (temperature, energy efficiency, TOC/COD removal, etc) in order to ideally control the reaction will be a critical future simulation challenge and would tie directly into the work both presented here and being conducted in Spain.

## 5.5 Summary

It was determined that splitting the required amount of oxidant and delivering different proportions at the reactor inlet and at another secondary position resulted in TOC and DMF removal efficiencies greater than those seen for single-stage reactor configurations at 400°C in a large number of proportion/position permutations. Varying concentration and oxidant ratio showed that the multi-stage configuration performed better than the single-oxidant configuration in terms of the removal of DMF and TOC. As such, there would appear to be the potential for optimisation of the SCWO process by controlling the injection of oxidant into different parts of the reactor.

Ammoniacal nitrogen yields were observed to be higher for multi-oxidant configurations. It would therefore be beneficial to conduct experiments investigating the effect of oxidation with an alcohol co-fuel on the ammonia yield. The SCWO oxidation of ammonia proceeds via a network that can include CO. Therefore, multi-injection of the co-fuel as well as the oxidant could also provide beneficial effects in limiting some formation of CO to the latter stages of the reactor, where it could facilitate the removal of ammonia.

If the beneficial effect of a multi-stage oxidation is to be properly quantified in future, further investigation into the generation and consumption of intermediates as functions of both time and reactor length will be required. Coupling such an analysis with an analysis of the temperature distribution of an adiabatically-operating reactor would provide very useful information about exactly what is occurring in different parts of the reactor.

Eventually, in order to completely understand the multi-stage oxidation process, the above analysis could be coupled with an in-depth chemical kinetics model. Such a model would require the derivation of equations governing the dynamics of hundreds of species (the exact number of which depending on the chosen model compound(s)). The SCWO of methanol or ethanol will result in 150 – 250 reactions corresponding to up to 50 distinct components. A nitrogenated compound such as methylamine, DMF, acetonitrile or quinolone (an N-aromatic) could potentially result in thousands of separate reactions involving hundreds of intermediates.

A simulation providing a true optimisation of the reactor configuration would need to predict the dynamics of the radicals at specific points well, and progress towards the development of such a model would be one of the logical future directions for this work.

## CHAPTER 6 – SCWO OF REAL INDUSTRIAL WASTE AND INDUSTRIAL-SCALE TREATMENT EVALUATION

### 6.1 Specifications of the Waste Samples

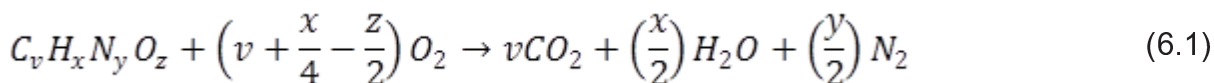
Six waste samples were provided for treatment. No COSHH data for these samples were provided, although hazard symbols indicating a corrosive behaviour (along with pH values indicating weakly acidic and weakly alkaline samples) were present. Due to the lack of COSHH information extra PPE precautions, such as the use of a facemask in addition to the usual labcoat, safety glasses and gloves, were employed when handling the samples. Very little information in terms of the identification of either the chemical components that comprised each sample or the concentration of such components within each sample was provided, and as such before the reaction conditions could be decided upon, it was necessary to do some preliminary analysis of the samples. It was particularly necessary to quantify their TOC content so the quantity of oxidant that should be supplied to the reactor could be calculated. Therefore, the samples were diluted by a factor of 20 and a TOC determination was performed. The dilution was performed in an attempt to ensure that the TOC determination was as accurate as possible due to the fact that the high-concentration calibration curve spanned 100 – 1000 ppm. Although a good linear relationship was present for this calibration (and thus the curve can feasibly be extrapolated upwards of 1000 ppm), it was desirable for the dilution to result in a TOC determination underneath this calibrated upper bound, or as close to this limit

as possible whilst being able to maintain sensible reaction conditions in terms of volumetric flowrates and oxidant ratios. The concentration of TOC in the diluted feedstock used in the experimental runs was as indicated in Table 6.1 where each undiluted sample was diluted with distilled and deionised water by a factor of 20 apart from E134 and E135, which were diluted by a factor of 40 due to their being over three times as concentrated than the other samples.

**Table 6.1** – Feed concentrations of organic reactant after dilution.

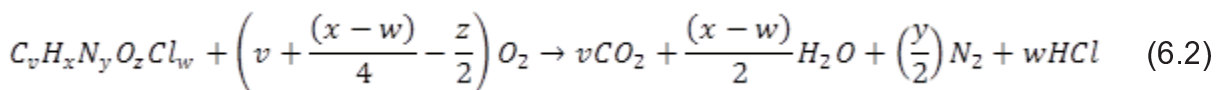
Waste Sample	Diluted [TOC] <sub>Stock</sub> (ppm)
T105	674
E72	1498
E95	869
E134	4946
E135	2178
NE	1740

The general oxidation equation for organic compounds with no heteroatoms can be represented as shown in equation 6.1 if it is assumed that the oxidation ideally results in all reactants being converted to carbon dioxide, water, and molecular nitrogen.



It was explained upon receipt that the samples had a generally similar component makeup to each other but that the concentrations of each component within each sample could differ greatly – a statement that was found to be true with regard to some samples, but not necessarily others. As well as this information, the only other data given was some assay data. However, this data proved to be practically useless due to the labels on the samples being in no way similar to the

identifiers in the assay data and due to there being more entries in the data file than there were samples. The only useful information was an indication that some of the samples may have contained trace amounts of dissolved phosphorus (either organic or as an inorganic phosphate salt), and sulphate and chloride salts. These were likely to be salts of calcium or magnesium due to these two elements' specific mention in the assay data. Including these species in a general equation very quickly renders it rather complicated, but including chlorine atoms in the organic molecule and assuming that it is all converted to hydrogen chloride (HCl) yields the following equation:



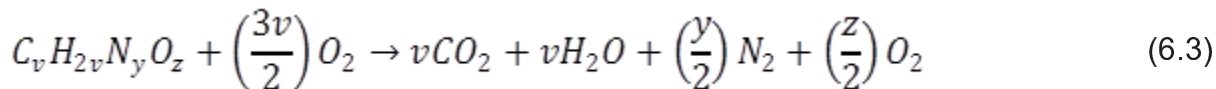
Due to the assumption of similarity of chemical species across the samples, it was decided that any assumption with regard to the calculation of the required quantity of oxidant could also be applied to all samples. Furthermore, due to the lack of knowledge of the form that the waste took other than that it was an organic waste that potentially consisted of nitrogen-containing species and relatively small quantities of heteroatoms, some assumptions were made for the task of calculating the exact quantity of oxidant required for each oxidation:

- Organic species took the form,  $C_vH_xN_yO_zCl_w$ . Other heteroatoms such as Br, F, P, S, etc were not considered.
- Inorganic compounds (salts) were not considered when calculating the quantity of oxidant required, as their presence was negligible.
- Every mole of carbon atoms requires two moles of oxygen atoms to undergo complete conversion to carbon dioxide.

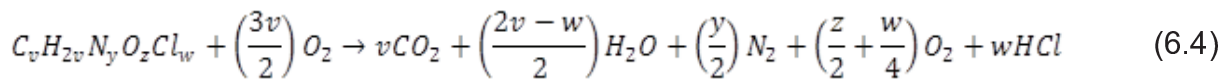
- Every two moles of hydrogen atoms require one mole of oxygen atoms to undergo complete conversion to water.
- There are a maximum of two moles of hydrogen atoms to every mole of carbon atoms when all organic species are taken into account. Aromatic compounds generally have an H/C quotient between 1 and 2 hydrogen atoms per carbon atom and non-substituted aliphatic compounds generally have an H/C quotient that approaches 2 as the size of the molecule increases due to the presence of - CH<sub>2</sub>- groups, i.e. x-->2v with increasing aliphatic chain length. For example, for non-substituted alkanes, hexane has an H/C quotient of 2.33 but decane would have a quotient of 2.2. However, when carboxyl groups (e.g. for ketones, aldehydes, carboxylic acids, etc) or multiple halogen-substituted groups (e.g. dichloroethane, dibromopropane, etc) are present this quotient is much closer to 2. Combinations of aromatic and aliphatic features also adhere to this scheme (e.g. ethylbenzene = 1.25, 2,4,5-trimethylbenzenemethanol = 1.4, etc). Thus an assumption of two moles of hydrogen atoms for every mole of carbon atoms was applied with the appropriate quantity of oxidant (tripled to ensure a large excess) delivered accordingly.
- All organic nitrogen was assumed to form diatomic nitrogen, i.e. it was assumed that nitrogenous anions ( $NO_2^-$  and  $NO_3^-$ ) and ammonium nitrogen ( $NH_4^+$  and  $NH_3$ ) did not form.
- Any chlorine combined with hydrogen to form HCl and thus its effect on the amount of oxygen required was limited to reducing the stoichiometric need, as less water would be formed

- Any on-board oxygen contributed to the oxygen excess of the reaction system, as enough oxygen to oxidise the carbon and hydrogen was delivered by means of the oxidant stream.

Given the above assumptions, each species was assumed to undergo the following reaction, which could, by extension, apply to a global ideal reaction, amended from equation 6.1:



and similarly, if the assumptions are incorporated into equation 6.2 to consider the fate of any organic chlorine:



In the schemes shown in equations 6.3 and 6.4, the number of moles of carbon atoms can be determined via TOC analysis. The quantity of oxidant required could then subsequently be estimated.

Thus, for each mole of carbon present in the feed samples, 1.5 moles of molecular oxygen (from hydrogen peroxide as the oxygen source) would be required for stoichiometric conversion of the organic waste to the ideal products if no chlorine were present. This delivered quantity becomes a slight excess as the number of heteroatoms increases provided that the final products in which any heteroatoms are contained don't contain oxygen. The amount of on-board oxygen (e.g. in carbonyl or hydroxyl groups, etc) was ignored because it couldn't be quantified prior to treatment, with the understanding being that any such source would contribute to any overall oxygen excess.

## 6.2 Treatment Protocol

The single-stage reactor configuration was used for the treatment of the waste samples as this is most similar to what would be used on an industrial scale. In general, the experimental protocol was similar to that employed in chapter 4, with the addition that due to the particulate content of the samples, particular attention was paid to the reactor pressure and effluent flowrates in order to be assured that fouling of the pumps' inlet and outlet line filters did not occur. If such an effect was observed, it was important that it was remedied quickly. Despite both this level of attention and the installation of ( $7\ \mu\text{m}$ ) filters, it was necessary to shut down the apparatus on two separate occasions to remove blockages caused by the agglomeration of very small particles. This effect was able to occur due to the relatively low flowrates that were a consequence of the residence times used, as described in §6.3.

It was required by SCFI as a condition of providing the samples that the waste samples undergo treatment under supercritical conditions at oxidant excess, a pressure of 250 bar and a temperature in excess of 450°C for as great a residence time as possible. Therefore, it was decided that the conditions at which the experimental runs should be performed would be as indicated in Table 6.2.

**Table 6.2** – General reaction conditions for the treatment of waste samples.

Temperature °C	Pressure (bar)	Oxidant Ratio	[TOC] <sub>Stock</sub> (ppm)	Residence Time (s)
500	250	3	See Table 6.1	Max feasible

The temperature was set to 500°C to ensure that the reaction took place sufficiently far from the critical point as to ensure that no density change effects were

experienced, and also in an attempt to increase the TOC removal experienced further to the conclusions from chapters 4 and 5, and the data in the literature which almost universally indicate that increasing the reaction temperature has the largest effect on the increasing the rate constant for the disappearance of TOC, and thus similarly increases its removal. The implementation of an oxidant ratio of 3 times that which was required by the assumed stoichiometry was due to a compromise between the need to have an obvious excess of oxygen and the need to have as great a residence time as possible without requiring an unfeasibly small delivery of the organic feed in order to achieve this (i.e. in order to increase the residence time, the global volumetric flowrate must be reduced and if the required oxidant flowrate is too high, the organic flowrate to be delivered becomes extremely small to compensate).

The sample dilution factor, which was selected in order to produce reliable TOC determinations, also affected this residence time by dictating the oxidant flowrate that needed to be delivered in order to oxidise the quantity of organic being delivered. It was decided that an oxidant ratio of 3 would be sufficient to allow an obvious oxygen excess but maintain sensible flow conditions within the reactor. The dilution factor was then coupled with the required oxidant flowrate to indicate the maximum possible residence time.

## 6.3 Experimental Runs

### 6.3.1 Initial Experiment and Reactor Adjustment

As well as an analysis of the first sample, the first experiment also served as a means of assessing whether or not the reactor configuration was suitable, bearing in

mind that to test to an industrial tolerance in terms of oxidative efficiency, a TOC removal approaching 99.99% was desired. The first experiment was conducted under the conditions shown in Table 6.3.

**Table 6.3** – Initial experimental conditions

Experiment	Sample	Feed TOC Concentration, ppm	Temperature, °C	Pressure bar	Oxidant Ratio	Residence Time, s
A1, A2	T105	674.0	500	250	3	0.68, 7.89

The results of the preliminary experiments in terms of the removal of TOC, which is the main method by which the efficacy of the SCWO process would be assessed, are shown in Table 6.4.

**Table 6.4** – Experiment A1/A2 results.

Residence Time (s)	Sample TOC (ppm)	TOC Removal
0 (Feed)	186.2	--
0.68	110.9	46.69%
7.89	60.4	68.69%

As with previous calculations, the TOC concentration in the feed sample was adjusted to incorporate the dilution effect caused by the water in the oxidant stream when calculating the quantity of TOC removed.

Due to the TOC removal at the maximum residence time of ~8 s being ~68.5%, it was decided that the reactor configuration used – specifically the reactor length – was not suitable to assess the treatment of this waste to an industrial specification. Consequently the reactor length was extended by 12 m to 24.35 m, resulting in a

maximum practical residence time of 17 s. All subsequent experiments were conducted using this lengthened reactor.

### 6.3.2 SCWO of Waste Samples

All of the waste samples were then treated at similar conditions as in §6.3.1 with the exception that the residence times investigated were ~2, 8 and 17 s as shown in Table 6.5.

**Table 6.5** – Amended experimental conditions.

Experiment	Sample	Feed TOC Concentration, ppm	Temp °C	Pressure bar	Oxidant Ratio	Target Residence Time, s
A3	T105	679.8	500	250	3	17
B2, B3	E72	1498	500	250	3	8, 17
C1, C2	E95	869.3	500	250	3	8, 17
D1, D2, D3	E134	4946	500	250	3	1.55, 8, 17
E1, E2, E3	E135	2178	500	250	3	1.78, 8, 17
F1, F2	NE	1741	500	250	3	8, 17

Samples of the gas and liquid effluent were analysed using TOC, GC-MS and GC-TCD techniques. First and foremost, the destructive efficiency of the process was assessed using the TOC data. The GC-MS and GC-TCD data was then used in an attempt to determine both the initial constituents of the waste samples and degree to which these compounds may have been consumed (or indeed generated) within the reactor, however the lack of component assay data for ‘intermediate’ residence times limited the ability to draw conclusions regarding the dynamics of specific components.

Finally, the parameters for a global kinetic model of the reaction were calculated and an assessment of the reaction conditions that would be necessary upon and industrial-scale treatment was made.

### 6.3.3 Assay Analysis of Feed Samples

Samples of the diluted feed were taken prior to the experiment being carried out and were analysed using GC-MS. The data from this analysis was not available before the experiments were conducted and as such could not be taken into account when calculating the reaction conditions, e.g. the quantity of oxidant delivered to the reactor. The resulting spectra enabled estimations of the make-up of the raw waste samples to be made. For these multi-component samples in which the constituent compounds can be complex organics, definitive identification of each chemical species was not always possible; however in the majority of these cases, it was possible to determine broadly what type of species (aromatic, carboxylic acid, amino-organic, etc) was present.

Initially, each sample was split into its constituent components using gas chromatography. Each component in turn upon leaving the chromatograph column was then fed into the mass spectrometer. Figure 6.1 indicates the retention data of sample E95 as an example. Mass spectra were provided for the most important peaks, which could then be analysed in a manner as shown in Figure 6.2 in order to evaluate the components in each sample, where the example is the fifth identified component in sample E95 eluted from the GC at a time of 3.18 minutes.

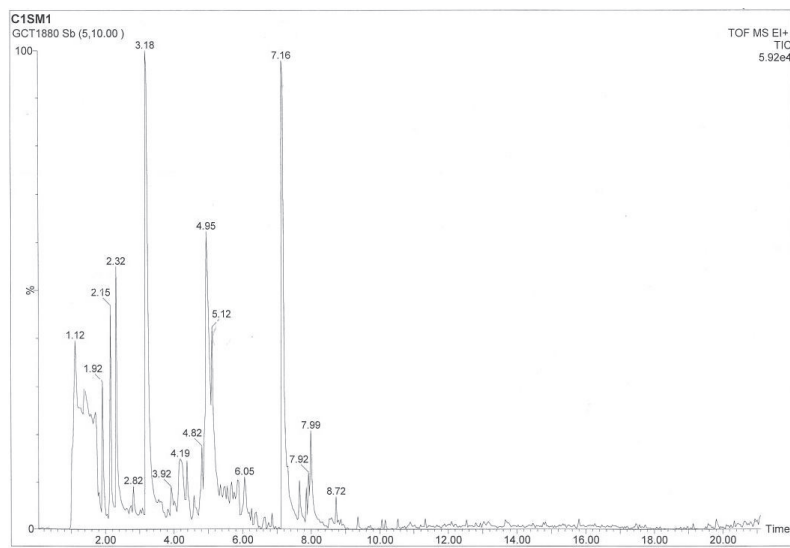


**Figure 6.1** – GC retention profile of sample E95.

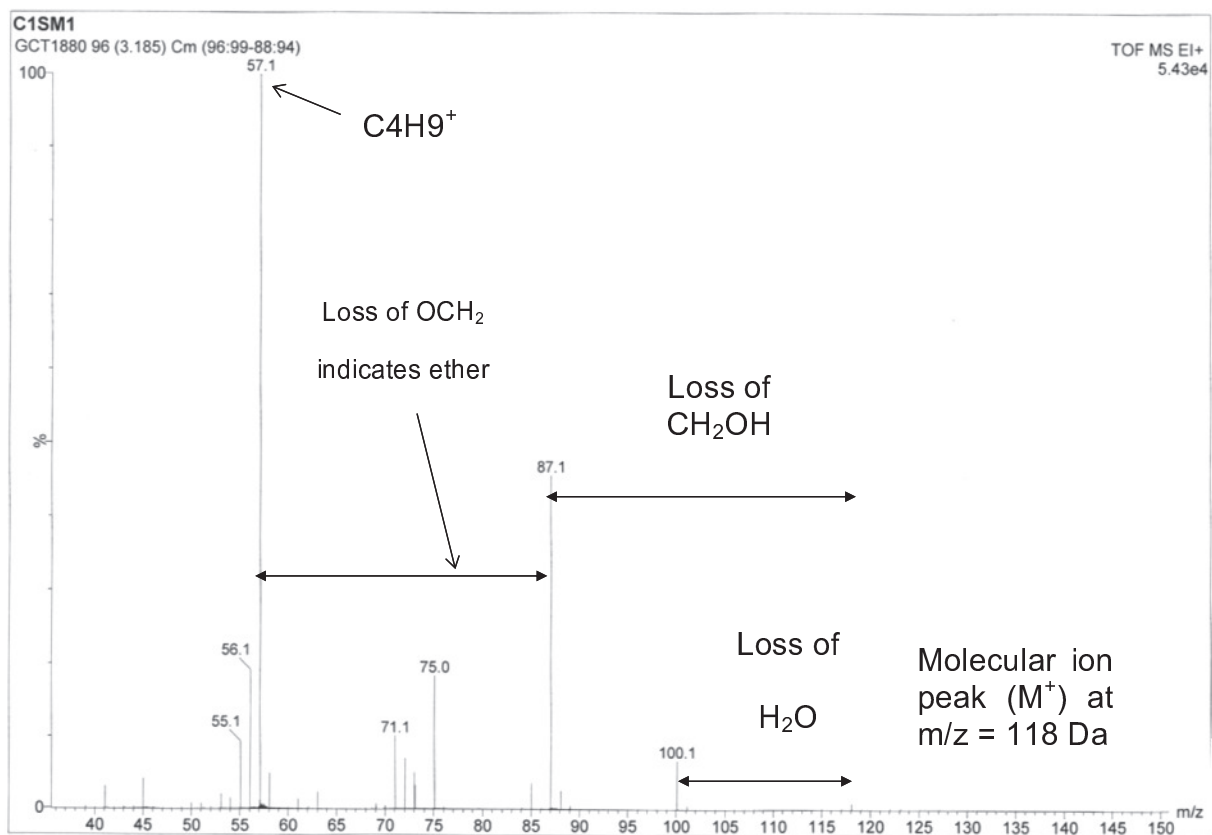


**Figure 6.2** – Mass spectrum of component eluted at 3.18 minutes in sample E95.

The peaks on this spectrum allow a good attempt at ascertaining what the detected compound is. The molecular ion appears at  $m/z = 118$ , which means that the component has a molecular mass of 118 and has had a single electron stripped away to yield the positively charged ion. The peak at  $m/z = 100$  indicates the loss of  $\text{H}_2\text{O}$  and because this corresponds to  $M^+-18$ , it is a good indicator that there is a hydroxyl group in the form of a primary alcohol. If the alcohol were secondary, a peak at  $M^+-15$  would be likely. The peak at  $m/z = 87$  (or  $M^+-31$ ) is an indicator of the loss of a  $\text{CH}_2\text{OH}\cdot$  radical and the loss of 30 between  $m/z = 87$  and 57 can either indicate the loss of a carbohydroxyl group [ $\text{CH}(\text{OH})$ ] or a  $-\text{CH}_2\text{O}-$  group. The  $\text{CH}_2\text{O}$  group is more likely, which implies that the compound is an ether. The very large peak at  $m/z = 57$  implies a stable butyl fragment meaning that the compound is likely to be 2-butoxyethanol. The peak at  $m/z = 45$ , which is likely to be a  $\text{CH}_2\text{CH}_2\text{OH}^+$  fragment corroborates this conclusion.

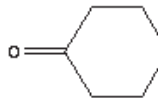
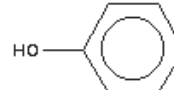
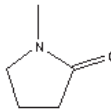
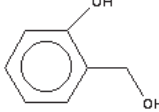
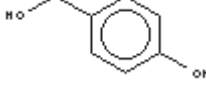
A similar analysis was performed on the components of all six feed samples. Descriptions of mass spectra for the analytes in sample T105, E72, E95, E134 and E135, and NE are given in appendices 3.1 – 3.5 respectively, with some assay data as far as could be determined in appendix 3.6.

Table 6.6 to Table 6.10 summarise the components that comprise each sample as far as can be determined.

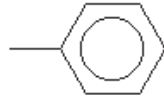
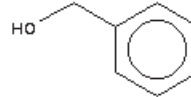
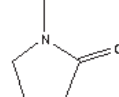
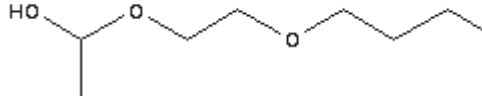
**Table 6.6** – Identified components in sample T105.

Component	Compound	Diagram
T105-1	Possibly a trihydroxy-substituted biphenyl methanone	
T105-2	1-methyl-1,4-cyclohexadiene	
T105-3	Likely an aliphatic-substituted benzyl compound	
T105-4	Likely a chloroalkenyl ester or alcohol	
T105-5	1-hepten-3-ol	
T105-6	Phenol	
T105-7	Amino-aliphatic ester, likely an aminopropyl ethanoate.	
T105-8	1-methyl-4-(1-methylethenyl)-benzene	
T105-9	Isoquinoline	
T105-10	Likely similar to T105-8 but with different locations for methyl/ethyl groups. Formula C <sub>10</sub> H <sub>12</sub>	
T105-11	Likely similar to T105-8 but with different locations for methyl/ethyl groups. Formula C <sub>10</sub> H <sub>12</sub>	
T105-12	2,4,5-trimethylbenzenemethanol	
T105-13	Ethyl 2-cyano-3-phenylacrylate	

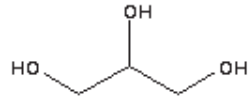
**Table 6.7** – Identified components in sample E72.

Component	Compound	Diagram
E72-1	3-isopropoxypropylamine (seems most plausible – certainly it is likely that the compound is represented by C <sub>6</sub> H <sub>15</sub> NO)	
E72-2	Possibly an amino-substituted ester	
E72-3	Likely an amino-substituted carboxylic acid	
E72-4	Likely to be a version of (m)-methyl-(n)-aminobutanoic acid where 'm' and 'n' are the location of the methyl and amine group respectively. Formula = C <sub>5</sub> H <sub>11</sub> NO <sub>2</sub>	
E72-5	Cyclohexanone	
E72-6	2-butoxyethanol	
E72-7	Phenol	
E72-8	3-ethoxypropan-1-ol	
E72-9	1-methyl-2-pyrrolidinone	
E72-10	2-hydroxybenzenemethanol	
E72-11	4-hydroxybenzenemethanol	

**Table 6.8** – Identified components in sample E95.

Component	Compound	Diagram
E95-1	Toluene	
E95-2	Likely an aminoester of some kind.	
E95-3	Likely an aminoester of some kind.	
E95-4	Possibly an aminobenzyl carboxylic acid	
E95-5	2-butoxyethanol	
E95-6	Phenylmethanol	
E95-7	1-methyl-2-pyrrolidinone	
E95-8	1-(2-butoxyethoxy)-ethanol	

**Table 6.9** – Identified component in samples E134 and E135.

Component	Compound	Diagram
E134-1 E135-1	propan-1,2,3,-triol (glycerol)	

**Table 6.10** – Identified compounds in sample NE.

Figure	Compound	Diagram
NE-1	Butanoic acid	
NE-2	2-butoxyethanamine	
NE-3	Likely a brominated form of hexanoic acid	
NE-4	Likely a (non-brominated) form of hexanoic acid (analogous to NE-3).	
NE-5	Piperidine	
NE-6	1-methyl-2-pyrrolidinone	

The majority of the components were aromatic compounds with various substitutions and functional groups (aldehydes, alcohols, amines), or ethers of varying aliphatic species.

There were similarities between samples. For example, the only major detectable compound in the samples E134 and E135 was glycerol [C<sub>3</sub>H<sub>5</sub>(OH)<sub>3</sub>]. The similar labelling of the two samples and the existence of only this one major compound indicated that the samples would come from roughly similar processes or similar locations in the plant. According to the GC data, glycerol comprised approximately 93% of the organic content in both samples. An analyte that could not be identified (Unknown 11 - U11) was present in the signal of the analysis of both E134 and E135 at a retention time of 2.30 – 2.36 minutes. No mass spectrum was

obtained for this sample but GC data suggests that it represented 4.5% and 3.3% of the organic content in each respective sample. Two further compounds common to both E134 and E135 were present with retention times of 6.94 – 7.02 minutes (unidentified but potentially identical to peak NE-5) and 21 minutes (U13). The former peak comprised approximately 0.5% of the samples and the latter peak represented a high molecular weight polycyclic aromatic compound and represented about 0.1% of the organic content in both samples. The polycyclic aromatic compound, U13 was also present in samples E72 and NE. The relative simplicity of these samples in terms of the relative lack of variety and complexity of the constituent components would indicate that these two samples might be more readily oxidised than the others.

Samples E72 and E95 were inherently more complex mixtures than E134 and E135. These had between eight (E95) and eleven (E72) MS-identified compounds with numerous other discrete unidentified peaks on the chromatograms. Again, there was some degree of similarity between these samples as with regards to their composition, they shared phenol, 2-butoxyethanol and 1-methyl-2-pyrrolidinone (also shared by sample NE) while their remaining constituents were also related in that for the most part, they were substituted benzene derivatives (benzaldehyde, toluene, phenylmethanol, hydroxyl-substituted phenylmethanols, etc) and ether compounds that incorporated hydroxyl functional groups. In addition, some peaks that had associated mass spectra on one sample's chromatogram were present on the other sample's chromatogram but without associated spectra. For example, sample E72's data indicated a compound (phenol) eluted at a retention time at 4.22 minutes and a corresponding peak appears on sample E95's chromatogram although at a much lower intensity. Compound U13 is also present in sample E72 and E95. Sample NE

also seemed to be of a similar complexity to these two samples, with 13 discernible peaks. Of these, mass spectra were obtained for 6, with it also appearing likely that toluene was also present after comparison with sample E95's spectra.

The complexity of their constituent compounds, coupled with their similarities in terms of their make-up indicate that these samples should exhibit more resistance to complete oxidation than samples E134 and E135 but also that they may show similar oxidative behaviour to each other.

The most complicated sample was sample T105, which had 13 MS-identified compounds along with several other unidentified, but obviously discrete peaks, on the GC chromatogram. The compounds for which mass spectra were provided invariably had a high molecular weight i.e. only two compounds had their molecular ion at  $m/z < 100$  and several were at  $m/z > 150$  which indicated multi-substituted aromatics and multi-aromatics rather than simpler aliphatic compounds. Indeed, the list of compounds in Table 6.6 is dominated by these more complex molecules. GC data suggests that the majority compound in this sample is 1-methyl-4-(1-methylethenyl)-benzene, constituting 58.5% of the organic content. The unknown polycyclic aromatic compound U13 was also present in this sample according to mass spectra profiles but was not quantified via GC. One would expect that it would be likely that these compounds in T105 would put up more resistance to complete oxidation than, for example, the glycerol-dominated samples E134 and E135 but may show similar oxidative behaviour to samples E72 and E95. The consistent complexity of the components may indicate that T105 may show more resistance than these two compounds.

### 6.3.4 Effect of Residence Time

For these experiments, in order to assess their potential treatability at an industrial scale, a high residence time was required and as described in §6.3.1, the maximum practically feasible residence was 17 s. Generally each sample was exposed to a residence time of ~16.6 s. All samples were also treated at a residence time of ~7.8 s and if possible, a third very short residence time that was determined by the maximum deliverable flow from the oxidant pump whilst still maintaining the required oxidant to organic flow ratios. This was only attempted if the rig had avoided the formation of particulate obstructions during previous runs. The third residence time was 0.68, 1.78 and 1.99 s for samples T105, E135 and E134 respectively. Such a short time was possible for sample T105 because this experiment was performed before the reactor was lengthened.

Each waste sample was treated as per the conditions stated in Table 6.5 and the TOC results were as indicated in Table 6.11. Figure 6.3 indicates the extent to which TOC was removed from each of these samples as a function of residence time.

From the data, it can be seen that at a residence time of 17 s, the TOC removal was either at or approaching the target of >99.99% for at least 3 of the samples. Certainly for all samples, at a residence time in excess of 17 s, the TOC removal was well in excess of 90%, with the trend indicating that TOC removal was still rising with increasing residence time.

**Table 6.11** – TOC removal for each sample treatment with the TOC determination from experiments E3 and F2 being below the analyser's lower limit of detection

Sample	Experiment	Residence Time, s	Sample TOC Concentration, ppm	TOC Removal
T105	A1	0.68	110.9	14.00%
	A2	7.89	57.5	68.69%
	A3	16.58	7.6	95.84%
E72	B2	7.85	51.0	74.62%
	B3	16.47	14.5	92.72%
E95	C1	8.00	24.6	86.67%
	C2	16.73	10.8	94.08%
E134	D1	1.99	176.7	59.02%
	D2	7.77	13.0	96.01%
	D3	16.37	0.6	99.82%
E135	E1	1.78	68.7	74.88%
	E2	7.80	6.4	97.10%
	E3	16.61	--	>99.99%
NE	F1	7.74	4.5	97.87%
	F2	16.80	--	>99.99%

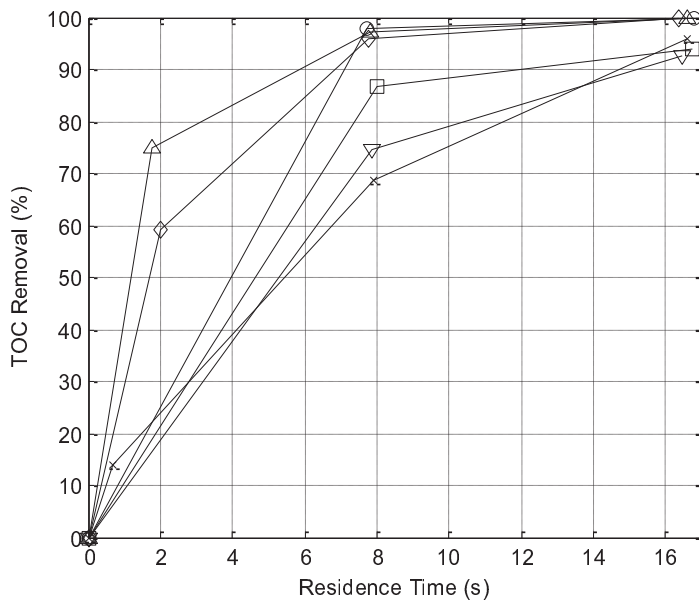


**Figure 6.3** – TOC removal as a function of residence time for samples: T105 (x), E72 (▽), E95 (□), E134 (◊), E135 (Δ) and NE (○)

These removals were lower than those of the single-stage oxidation of DMF at similar conditions and residence times. This was to be expected, as the real waste samples were much more complex mixtures, although the simpler of these (e.g. E134, and E135) exhibited removals that were more comparable to the single-component oxidation. E134 and E135 were comprised mainly of glycerol which has a similar molecular weight and identical carbon content (3 atoms) to DMF, indicating that its treatability could be broadly similar to that of DMF in terms of TOC removal. At 500°C, three times the stoichiometric oxidant and 8 s residence time all investigated concentrations of DMF exhibited complete TOC removal, while the glycerol samples had removals of 96% and 97%. Near-complete removals of TOC for these samples was achieved at a residence time of 17 s.

As shown in Figure 6.4, the initial samples appeared decidedly brown as a result of the fine suspended particulate matter that was present. A comparison between the colour of the feed samples and the treated samples are shown in Figure 6.5.

The diluted organic feed samples also invariably smelt unpleasant. A facemask had to be worn when using the pure samples to prepare the samples which were to be fed to the reactor. As such, an additional observation of the effectiveness of the SCWO treatment was the smell of the liquid reactor product samples. It was observed that at the shortest residence times (< 2 s), the smell was in no way as unpleasant as for the feed samples, but there was still a noticeable odour. This could imply that the foul-smelling components had been converted to other intermediates, that they had been completely destroyed and the odour of other components had come to the fore or that the unpleasant odour arose from a

relatively large concentration of certain components and that a reduction of this concentration resulted in a reduction of the unpleasantness of the smell. At residence times of 8 and 17 s, an odour was not detected for any reactor product sample indicating a high degree of removal of such compounds.



**Figure 6.4** – Undiluted sample of E95

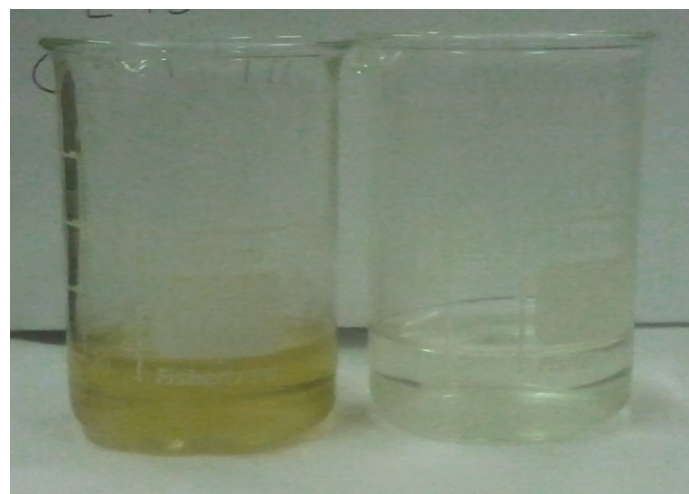


**Figure 6.5** – Comparison between diluted E95 feed sample and liquid product after 17 s of SCWO.

The major products from the SCWO process after ~16.5 s were CO<sub>2</sub> and IC, most likely in the form of carbonate salts in various distributions depending on the sample being oxidised. Carbon monoxide was detected as an intermediate product in all experiments apart from D3. Methane was detected in the gaseous product for the oxidation of sample E134, likely a result of this sample having the highest initial concentration and it being mostly comprised of glycerol. The radical attack of this molecule could quite conceivably yield C<sub>1</sub> fragments that could be converted to methane. A summary of the yields of TOC, IC, CO, CO<sub>2</sub> and CH<sub>4</sub> for each experiment is given in Table 6.12.

CO yields were highest at the low residence time oxidation of samples E134 and E135. This indicated that glycerol was readily broken down into smaller intermediates. The CO yields then subsequently decreased towards zero as further conversion to CO<sub>2</sub> occurred.

**Table 6.12** – Carbon fraction yields for SCWO of industrial waste samples.

Sample	Expt #	Residence Time, s	Component Yields, %				
			TOC	IC	CO	CO <sub>2</sub>	CH <sub>4</sub>
T105	A1	0.68	86.00	0.94	3.17	9.30	0.0
	A2	7.89	31.31	3.74	4.78	60.17	0.0
	A3	16.58	4.16	4.12	8.42	83.30	0.0
E72	B2	7.85	25.38	3.34	7.77	63.51	0.0
	B3	16.47	7.28	2.70	4.46	85.56	0.0
E95	C1	8.00	13.33	5.26	--	--	--
	C2	16.73	5.92	6.07	2.47	85.54	0.0
E134	D1	1.99	40.98	7.72	17.73	31.70	1.87
	D2	7.77	3.99	8.00	7.82	79.33	0.86
	D3	16.37	0.18	7.90	0.0	91.92	0.0
E135	E1	1.78	25.12	5.41	10.69	58.79	0.0
	E2	7.80	2.90	6.84	4.79	85.47	0.0
	E3	16.61	<0.01	6.16	0.80	93.04	0.0
NE	F1	7.74	2.13	8.52	1.64	87.70	0.0
	F2	16.80	<0.01	15.59	0.70	83.65	0.0

The IC yield generally increased and plateaued as the residence time increased, however the IC yields of sample E95 were near-identical to the initial yields indicating that the waste sample included carbonates (or similar) and that very little additional IC was formed during the SCWO process. The highest yield of IC (15.6%) was obtained for sample NE at 16.8 s residence time, whereas at a lower residence time this yield was 8.5% with the difference accounted for in the CO<sub>2</sub> yield. Carbon dioxide dissolves in water producing carbonic acid in equilibrium which could be contributing to the increased IC yield, although it's not clear from the assay of the sample why this yield should be 3-5 times higher than that of the SCWO of samples E72 and E95. Higher initial TOC concentrations for sample NE producing higher concentrations of CO<sub>2</sub> than for the other 2 samples could contribute to an increased production of carbonate.

The carbon fraction yields as a function of residence time for samples E134 and E135 are given in Figure 6.6 indicating similar profiles of each fraction which would be expected due to the similarity in their component makeup.

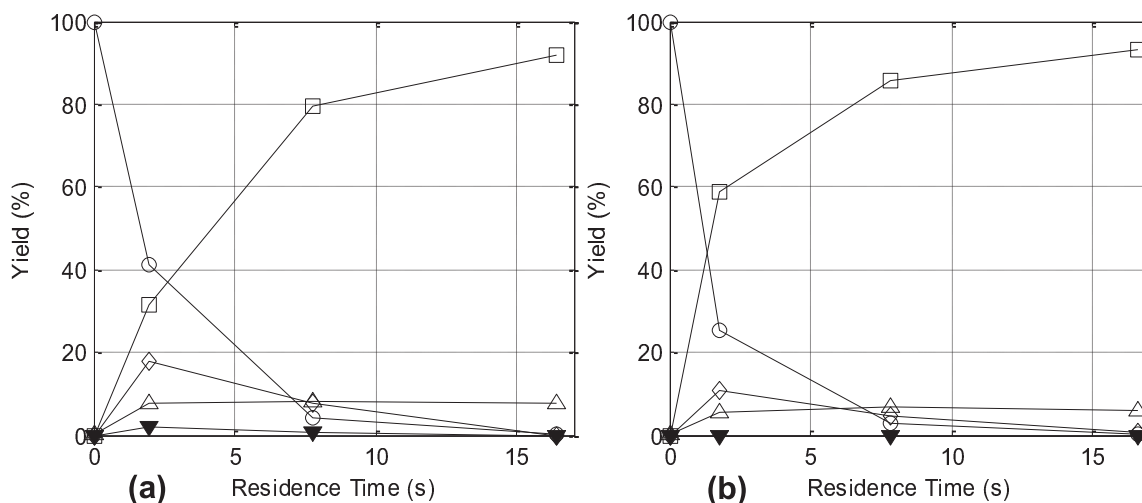


**Figure 6.6** – Carbon fraction yields of samples E134 (a) and E135 (b) as a function of residence time: TOC (O), IC ( $\Delta$ ), CO ( $\diamond$ ), CO<sub>2</sub> ( $\square$ ), CH<sub>4</sub> ( $\blacktriangledown$ ).

Nitrogen gas was detected in the gaseous effluents of all experiments, although the signal was drastically reduced for samples E134 and E135, consistent with their being mostly glycerol. The presence of nitrogen in the effluent indicated the presence of nitrogen in the other unnamed components (U11 and U13) as well as in component NE-5 which was speculated to be Piperidine, a heterocyclic amine. Nitrogen species analysis was conducted only for the destructions of sample T105 and the nitrogen fraction yields for these experiments are presented in Figure 6.7.

It was found that the major nitrogen fractions after 17 s were ammonia and non-specific nitrogen (likely in liquid) at 70% and 22% respectively. The initial proportion of ammonia in the feed was 15% of the total nitrogen. It was also possible that a reasonable proportion of the non-specific nitrogen could be as part of N<sub>2</sub>O due to the high excess of oxidant. It was seen first-hand in data from experiments by Fujii and Oshima at the University of Tokyo (2011) that increasing the oxidant ratio past that necessary for stoichiometry for the SCWO of multi-component feeds can increase the selectivity of N<sub>2</sub>O in comparison to N<sub>2</sub>.

Additional inorganic nitrogen in the form of nitrite and nitrate were detected. The nitrite yield was very insignificant, but the nitrate yield was in excess of 10% at 8 s residence time. Musin and Lin (1998) suggest that HNO<sub>3</sub> and NH<sub>3</sub> can react in the gas phase to form H<sub>2</sub>NONO and water, a process that could be applicable to single-phase SCWO reactions and may explain the decreased yield of nitrate at 17 s residence time whilst the increased progress of oxidant in general could still increase the ammonia yield. H<sub>2</sub>NONO can decompose to NH<sub>2</sub>• and NO<sub>2</sub> and can also terminate in the formation of N<sub>2</sub> and N<sub>2</sub>O (Ploeger *et al.*, 2008).

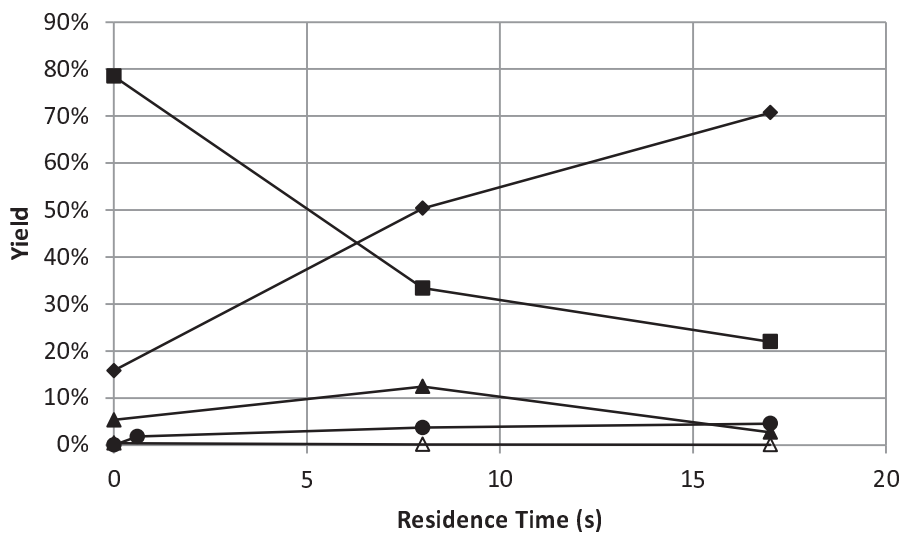


**Figure 6.7** – Nitrogen fraction yields for the oxidation of sample T105 as a function of residence time:  $\text{NH}_4^+$  (◆),  $\text{NO}_2^-$  (Δ),  $\text{NO}_3^-$  (▲),  $\text{N}_2$  (●), other N in liquid/gas product (■).

The yield of ammonia is very high and constitutes a large disadvantage to the employment of SCWO at industrial scales as something must ultimately be done to separate the ammonia from the output stream during downstream processing. As such, it is likely that for the oxidation of such wastes, higher temperatures than those employed herein would be necessary, which would contribute to higher operational costs. As such, the employment of hydrothermal flame regimes as well as energy integration for temperature control should be considered in the industrial treatment of such wastes in order to reduce this operating cost burden necessary to mitigate for the ammonia yield.

Additional nitrogen product determinations were not made due both to the high cost of the cell test kits and the anticipation that such data may be obtained from GC-MS analysis. It was discovered after the fact that such data had not specifically been obtained.

### 6.3.5 Effect of Feed TOC Concentration and Type

Although each sample had a different composition, complex waste samples in the literature are characterised primarily by their TOC concentration or their chemical or biological oxygen demand (COD/BOD) and each sample had a different TOC concentration both before and after they were diluted. As such, it was ultimately advantageous to investigate the effect of TOC concentration on removal. Indeed, due to the fact that the reactor temperature, reactor pressure and oxidant ratio were kept constant, the only other variable in the experimental run was the organic feed concentration.

The concentrations of the samples investigated were not originally going to be studied, however dilution of stock samples that were already of vastly different TOC concentrations allowed some basic investigation of the effect that the TOC concentration would have on treatability. The dilutions of each sample prior to experimentation was performed purely to ensure that the desired reaction residence times could be attained and to ensure that the TOC concentrations of any resulting samples would lie within the TOC analyser's accuracy range. It was particularly difficult to achieve this with sample E134 which had been provided with a raw TOC concentration of approximately  $128,000\text{ mg L}^{-1}$  TOC. As such, comparison between samples as to their TOC removals as a function of residence time is difficult due to the differing TOC concentrations both in the feed and in the reactions themselves. Neglecting the differences in sample composition, experiments were performed with stock concentrations of 680, 870, 1498, 1791, 2178 and  $4946\text{ mg litre}^{-1}$  TOC. An attempt to begin to visualise the effect of both feed concentration and residence time

is shown in Figure 6.8 and Figure 6.9. Figure 6.9 is included to clarify the position of the points on the z-axis on Figure 6.8.

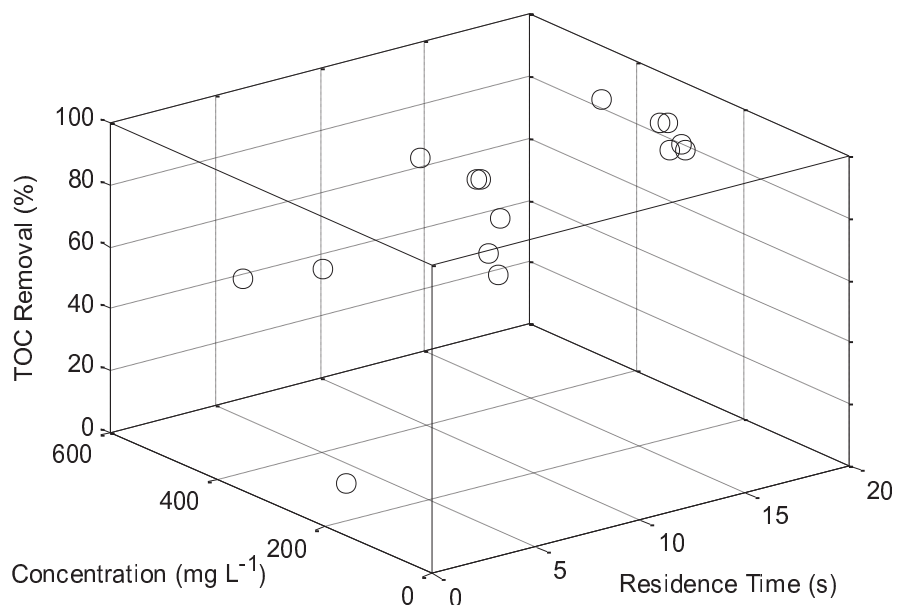


**Figure 6.8** – TOC removal as a function of the organic concentration and residence time.

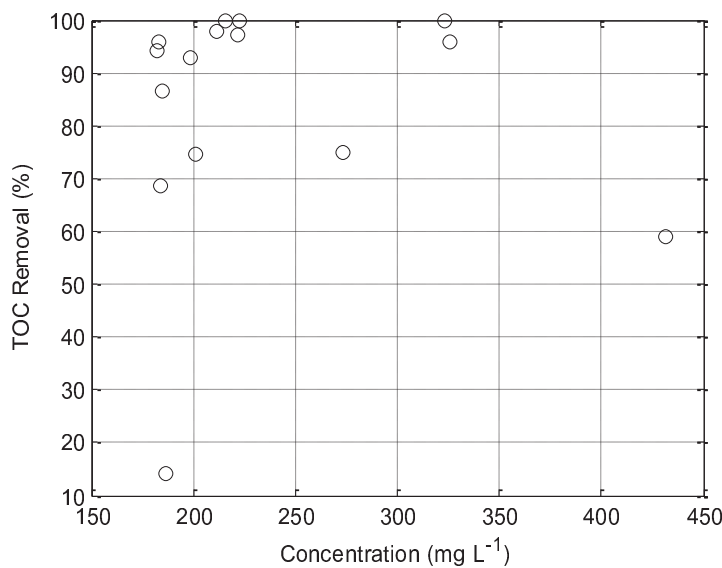


**Figure 6.9** – 2D projection of TOC removal as a function of initial organic concentration (various times).

The relationship between feed sample concentration and TOC removal was not a straightforward one. Indeed, there was a good deal of deviation from the effect that would be expected were all of the samples to have had the same composition relative to one another. Data presented in earlier chapters indicated that TOC removals show a positive dependence on the initial concentration of TOC in the reactor, whereas Figure 6.8 doesn't show such a distinction, e.g. the data point at  $180 \text{ mg litre}^{-1}$  only underwent 14% TOC conversion, whereas other points at a similar concentration exhibit higher removals. This lower data point represents sample T105, a very complex waste sample. This lack of distinction indicates that a characterisation of all of the waste samples purely by their TOC content will not necessarily be enough to predict the conditions by which the greatest degree of TOC removal may be achieved. In addition to the TOC quantification, an assessment of the complexity of the waste may also need to be included.

Defining samples E134, E135 and NE as 'less complex' than T105, E72 and E95 allows the generation of two further plots which indicate the TOC removal as a function of initial reaction concentration for residence times of  $\sim 7.8 \text{ s}$  and  $\sim 16.7 \text{ s}$  as shown in Figure 6.10. The 'complex' wastes, T105, E72 and E95 (20 or more detected components, although not all have been positively identified) are indicated by ( $\Delta$ ), with the 'simpler' compounds indicated by (O). In these figures, it is possible to see that there are differences in TOC removals between the 'simple' and 'complex' wastes, and that although globally higher removals are observed for higher initial concentrations, there is a demarcation between simple and complex wastes. Indeed, within each classification it seems that the higher concentrations don't necessarily

produce higher TOC removals indicating that even these classifications may be too generalised.

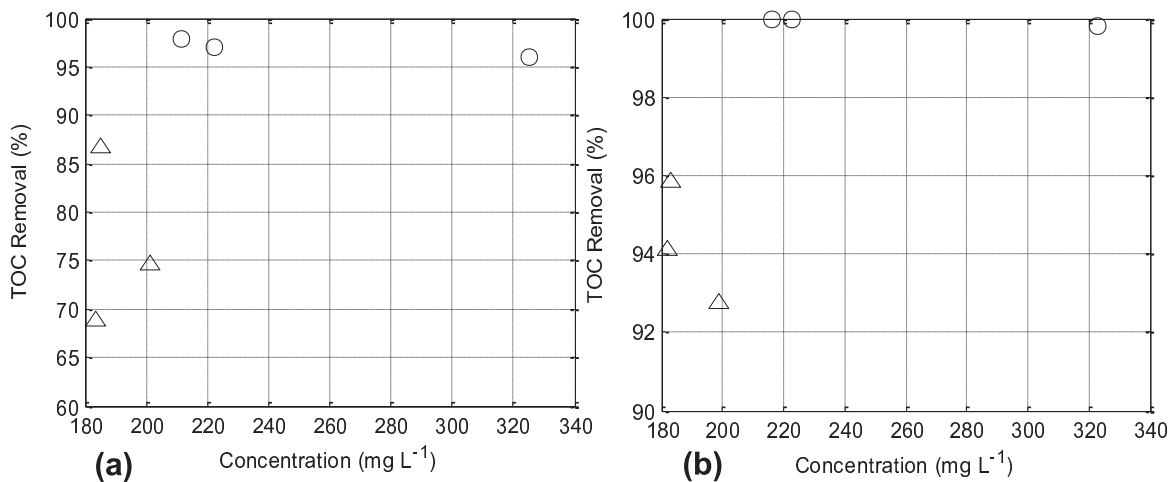


**Figure 6.10** – TOC removal as a function of concentration: 7.8 s (a) and 16.7 s (b).

Plotting Figure 6.3 in a similar manner to Figure 6.10 clarifies that the initial TOC concentration has the broad effect that would be expected, where in Figure 6.11 the lower initial concentrations result in lower removals of TOC with increasing residence time.

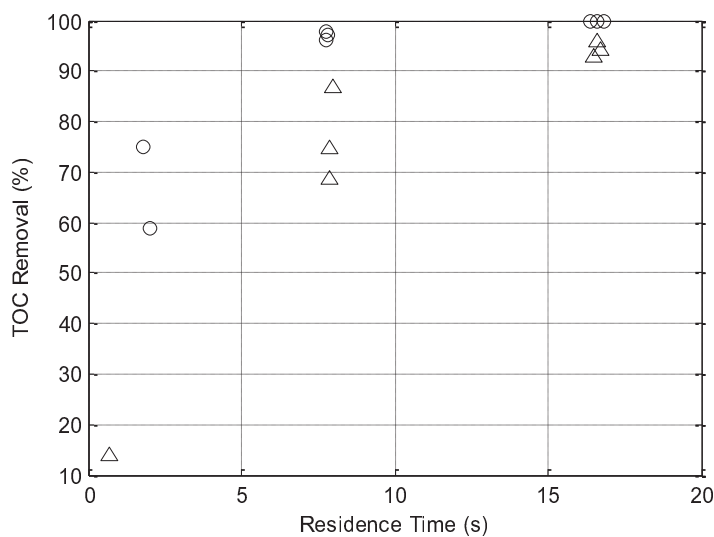


**Figure 6.11** – TOC Removal vs residence time for ‘simple’ (O) and ‘complex’ ( $\Delta$ ) wastes.

However, variations in this effect at a smaller scale as seen in Figure 6.10 are present. As such, further classification of the waste in terms of its number of specific compounds and the types of these compounds (aliphatic or aromatic) would be very advantageous, with a view to its prospective treatment via SCWO. It should be remembered that all wastes experienced high TOC removals at the relatively low residence time of 16.7 s for the concentrations studied, and as such, SCWO is clearly a viable treatment method in terms of chemical suitability. However, for a better understanding of the process of destroying complex waste mixtures, further investigation of the SCWO of complex wastes, with specific focus on the degree of complexity of the waste, rather than just the TOC content should be undertaken.

## 6.4 Global Kinetics

The qualitative analysis of the effect of the process variables was given in §6.3. Temperature, pressure and oxidant ratio were held constant but there was variation in the initial concentration of the organic feed and the residence time was varied in order to obtain an understanding of the dynamics of the reaction. The oxidant ratio's constancy was subject to uncertainty based upon the assumptions that were made in calculating a stoichiometric quantity of oxidation that would be required, however for the purposes of analysis, it was assumed that the oxidant ratio was constant and equal for all experiments.

A more complete understanding of this process would require a more quantitative analysis and as such, the reaction kinetics were analysed in order to be able to evaluate some of the parameters of the following generalised rate expression which is an adaptation of equation 4.2:

$$\frac{d[TOC]}{dt} = k[TOC]^a [O_2]^b [H_2O]^c \quad (6.5)$$

where  $k$  is the reaction rate constant governing this Arrhenius-type power law rate expression. The units of this constant would depend on  $a$ ,  $b$ , and  $c$  and can be expressed as  $k [M^{(1-a-b-c)} s^{-1}]$ . It should be noted that the temperature for all experiments was held constant at 500°C and as such, evaluation of the activation energy and the pre-exponential factor for this system could not be found by regression analyses of the available data.

Due to the excess of oxidant, the assumption was initially made that the oxidation obeyed either pseudo-first order kinetics or that the rate of disappearance of TOC was proportional to the TOC concentration raised to some power,  $a$ , the reaction order with respect to TOC; that is, that the reaction order with respect to the oxidant was zero. The oxidant ratio was maintained at three times that which would be required for a stoichiometric reaction meaning that the concentration of oxidant could be approximated as unchanging. In a similar vein, and as is almost ubiquitous in similar analyses, the order of reaction with respect to water is assumed to be zero, given that water constitutes approximately 99% of this system.

After these assumptions were taken into account, the reaction kinetics were evaluated by fitting experimentally-derived data would conform to different models and observing how good a fit was obtained for each comparison. Three different approaches were employed for this comparison.

- Approximation to a pseudo-first order system
- Consideration of non-unity TOC order
- A regression method that compares a power law model to experimental data and minimises the sum of squared differences (least squares)

#### 6.4.1 Approximation to Pseudo-first Order System

A pseudo-first order model was applied to the experimental data as an initial assessment of the dynamics of the treatment of the real waste samples. The derivation of this model is relatively simple and is analogous to equations 4.4 – 4.6, with the result being equation 6.6.

$$k = -\frac{1}{\tau} \ln(1 - X_{TOC}) \quad (6.6)$$

Table 6.13 displays the reaction rate constant calculated for each experiment as a function of the TOC concentration determined via experiment and residence time.

**Table 6.13 – Pseudo-first order reaction rate constants for each experiment.**

Sample	Experiment	Residence Time, s	Sample TOC Concentration, ppm	$k_{TOC}$ $s^{-1}$
T105	A1	0.68	110.9	0.222
	A2	7.89	57.4	0.147
	A3	16.58	7.6	0.192
E72	B2	7.85	51.0	0.175
	B3	16.47	14.5	0.159
E95	C1	8.00	24.6	0.252
	C2	16.73	10.8	0.169
E134	D1	1.99	176.7	0.448
	D2	7.77	13.0	0.415
	D3	16.37	0.6	0.388
E135	E1	1.78	68.7	0.776
	E2	7.80	6.4	0.454
	E3	16.61	--	>0.554
NE	F1	7.74	4.5	0.497
	F2	16.80	--	>0.548

The average reaction rate constant was found to be  $0.360\text{ s}^{-1}$  implying that each experimentally obtained value could be obtained from a rate constant described by the range  $k=0.360 \pm 0.19\text{ s}^{-1}$ . Employing this average rate constant over the residence times and initial feed concentrations used in the experiments allowed the calculation of TOC conversions. These calculated conversions were compared with the experimental data, and although the first order approximation seemed accurate for some points at high conversions, many other points had under- and over-predictions as implied by the relatively wide range of rate values.

A least squares fitting of the experimental data suggested a rate constant of  $0.410\text{ s}^{-1}$ . Using this value in a first order model yielded the data shown in Figure 6.12. This data shows less of an under-prediction in the middle data points, but also subsequently introduces a larger over-prediction for the points at the top of the plot.

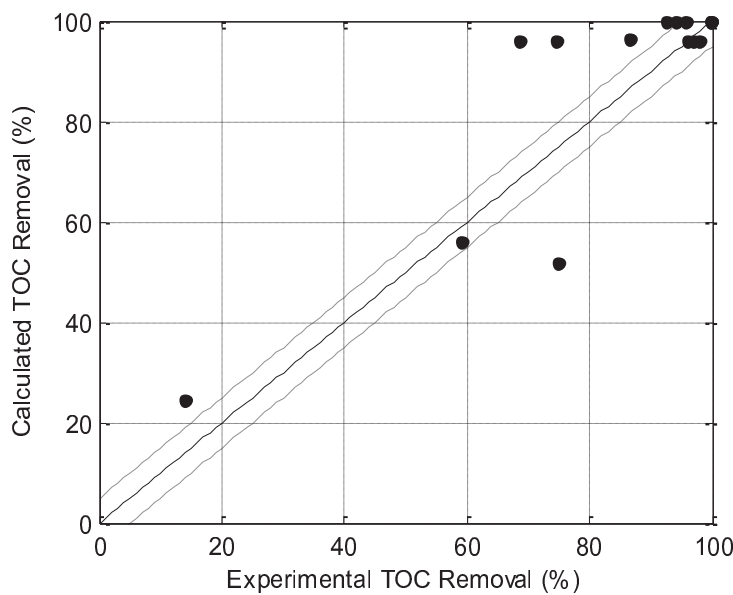


**Figure 6.12** – Parity plot of pseudo-first order model and experimental data for fitted rate constant.

Several studies of more complex wastes (Goto *et al.*, 1999; Sögüt and Akgün, 2010) show that first order approximations describe the systems reasonably well, and consequently it was additionally decided to consider the oxidation of each sample separately. Plotting  $\ln[1/(1 - X_{TOC})]$  against residence time yielded Figure 6.13. Each series can be approximated to a straight line with  $R^2$  values approaching 1 as indicated in Table 6.14. This suggests that although it might not be the case that global TOC concentrations can be described by a single first order rate constant, each individual system may submit to such an analysis.

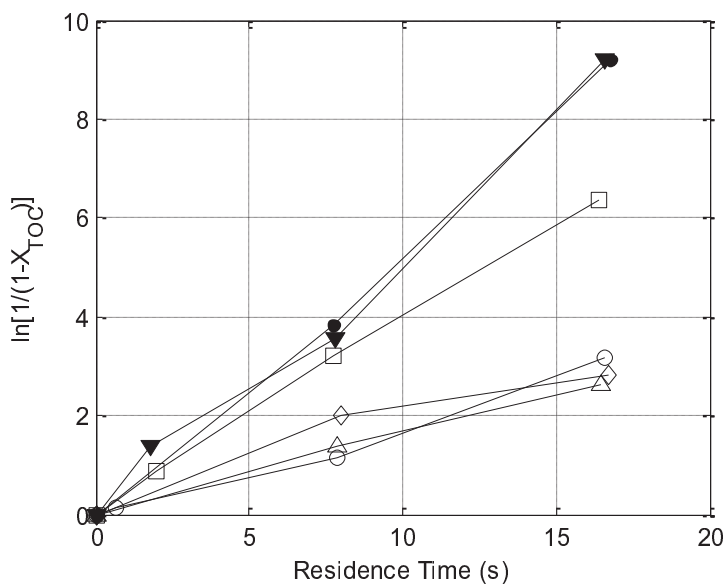


**Figure 6.13** – Normalised decay versus residence time for T105 (O), E72 ( $\Delta$ ), E95 ( $\diamond$ ), E134 ( $\square$ ), E135 ( $\blacktriangledown$ ) and NE ( $\bullet$ ) indicating demarcated groups of straight lines.

**Table 6.14** – Residual values for series in Figure 6.13.

Sample	R <sup>2</sup>
T105	0.979
E72	0.997
E95	0.915
E134	0.998
E135	0.986
NE	0.997

From these profiles it seemed likely that the oxidation of each sample could be approximated to a first order system, although a clear demarcation between two groups of series, can be seen which seemed to correspond to the ‘complex’ samples (T105, E72, E95) and the ‘simple’ samples (E134, E135, NE). As such, the Matlab routine shown in appendix 5 was used for each experimental series separately to find the rate constant that best fitted the experimental data, and the minimisation routine used in chapter 4 (appendix 4) was also applied as a comparison. Due to the low number of points to which to fit a curve, these constants were not assumed to be completely accurate; however both methods provided comparable values and the parity plot fit was relatively good. These fitted rate constants were as shown in Table 6.15, with the corresponding parity plot as indicated in Figure 6.14.

**Table 6.15** – Best-fit first order rate constants for each sample.

Sample	Fit k <sub>TOC</sub> [s <sup>-1</sup> ]	Matlab k <sub>TOC</sub> [s <sup>-1</sup> ]
T105	0.171	0.165
E72	0.172	0.167
E95	0.242	0.210
E134	0.337	0.417
E135	0.669	0.595
NE	0.503	0.523

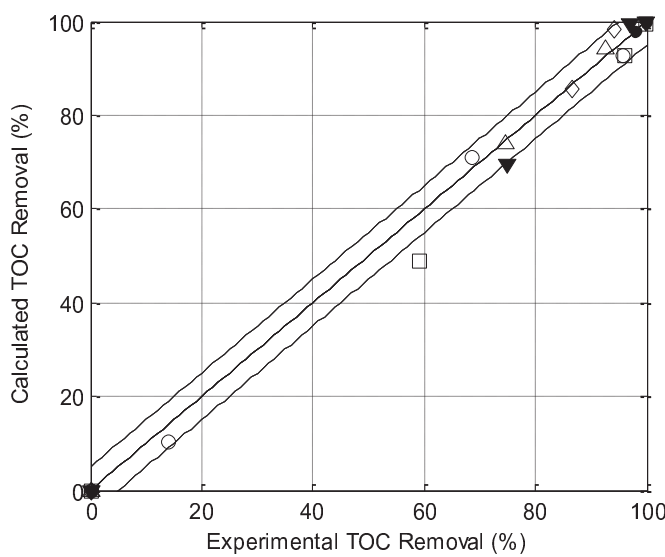


**Figure 6.14** – Parity plot of pseudo-first order model and samples T105 (O), E72 ( $\Delta$ ), E95 ( $\diamond$ ), E134 ( $\square$ ), E135 ( $\blacktriangledown$ ) and NE ( $\bullet$ ) for constants fitted to each sample.

These specifically-fitted rate constants showed a good adherence to a first order model. However, this data also shows that when considering the TOC content and removal as a global indicator of the progression of the oxidation of complex wastes, one single first-order model is not necessarily suitable as a predictive tool, especially if wide variation in the initial concentrations of the samples to be treated, or components therein can be expected. The ‘complex’ wastes had pseudo-first order rate constants  $0.16 - 0.25 \text{ s}^{-1}$  and the ‘simple’ wastes had pseudo-first order rate constants in the range  $0.33 - 0.67 \text{ s}^{-1}$ . It was therefore decided that fitting separate models to the SCWO of the ‘simple’ and ‘complex’ samples could allow better prediction of the destruction efficiencies. The fitted rate constants were  $0.501 \text{ s}^{-1}$  and  $0.192 \text{ s}^{-1}$  for the ‘simple’ and ‘complex’ wastes respectively. The results of these fits are depicted in Figure 6.15.

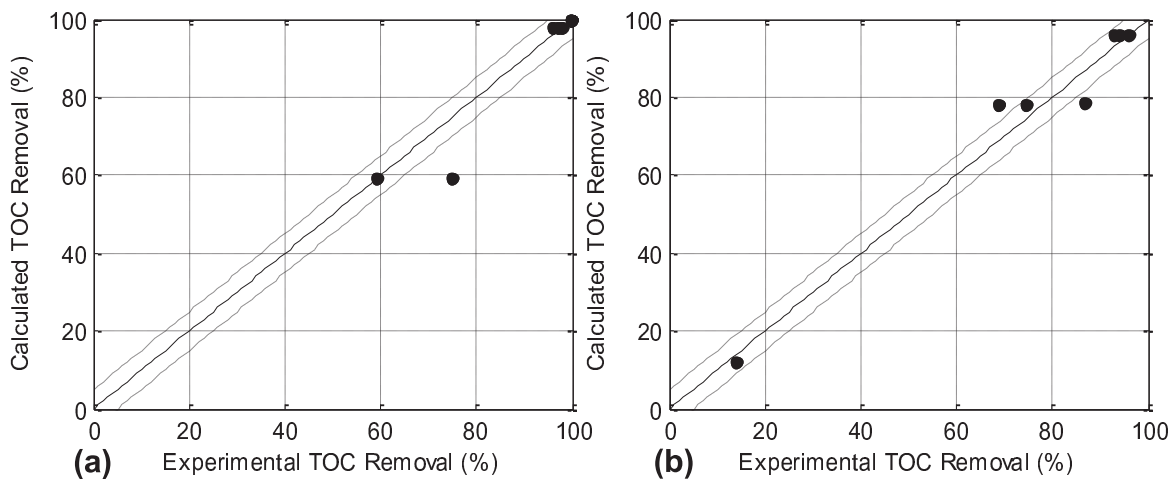


**Figure 6.15** – Parity plots of ‘simple’ (a) and ‘complex’ (b) component TOC removals using optimised first order rate constants.

Although it appears that various first order models can describe these oxidative systems reasonably well, some non-linearity in Figure 6.13 could suggest that a power law model may be appropriate. Consequently, analyses using a power law model were also conducted to see if this might better describe the global system.

#### 6.4.2 Non-unity TOC Order Model

For cases in which the oxidant is still in excess but the order of reaction with respect to TOC is not unity, i.e. where  $a \neq 1$  but  $b$  is still equal to zero,  $X_{TOC}$  can be evaluated by redefining the rate of reaction as:

$$-r_{TOC} = -\frac{d[TOC]}{dt} = k[TOC]^a \quad (6.7)$$

which can be incorporated into the PFR design equation yielding equation 6.8:

$$\int_0^{X_{TOC}} \frac{dX_{TOC}}{(1 - X_{TOC})^a} = k[TOC]_0^{a-1}\tau \quad (6.8)$$

which was solved to give the TOC analogue of equation 4.7:

$$X_{TOC} = 1 - (1 + (a - 1)k\tau[TOC]_0^{a-1})^{1/(1-a)} \quad (6.9)$$

Experimental data was fitted to this equation in order to be able to evaluate the reaction rate constant and the order with respect to TOC concentration. Each sample's value of  $a$  (for which the best straight-line fits were obtained) is given in Table 6.16.

**Table 6.16** – TOC reaction order fitted to  $a \neq 1$  model.

Sample	A	R <sup>2</sup>
T105	0.91	0.998
E72	1.140	1
E95	1.21	1
E134	1.040	1
E135	0.960	0.989
NE	0.960	1

From this data, the order of reaction was evaluated to  $1.08 \pm 0.17$  to 95% confidence. Using this order with a least-square regression suggested that the rate constant should be  $0.47 \text{ litre}^{0.08} \text{ mol}^{0.08} \text{ s}^{-1}$ . Using this data to produce a parity plot yielded Figure 6.16. This model still generally results in an over-prediction of the experimental data at higher residence times, with the overall profile not appearing to be much different to that in Figure 6.12 other than being a slightly lower over-estimate .

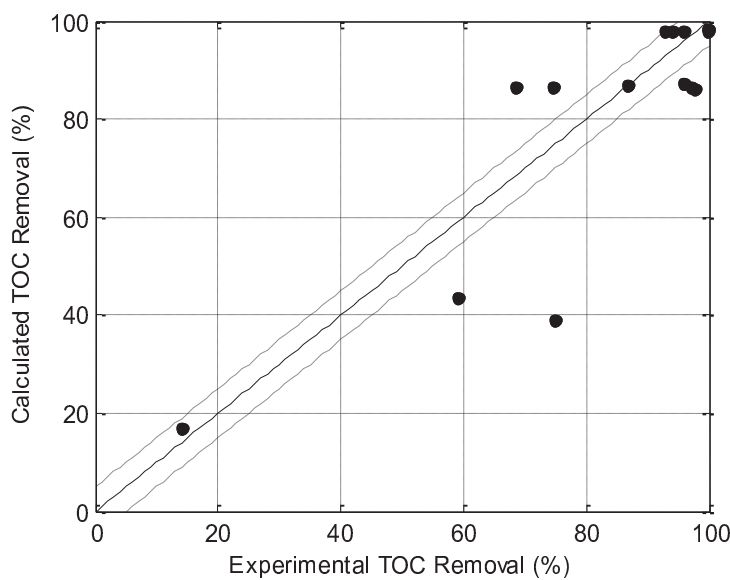


**Figure 6.16** – Parity plot for  $a = 1.08$  and  $k = 0.47 \text{ litre}^{0.08} \text{ mol}^{-0.08} \text{ s}^{-1}$ .

Again, differentiating between the more complex and simpler waste samples allowed the fitting of different models to each data set. Using the order of reaction of 1.08 each time, the data were fitted as shown in Figure 6.17 where the rate constants were  $0.823 \text{ litre}^{0.08} \text{ mol}^{-0.08} \text{ s}^{-1}$  and  $0.374 \text{ litre}^{0.08} \text{ mol}^{-0.08} \text{ s}^{-1}$  for the simple and complex samples respectively.

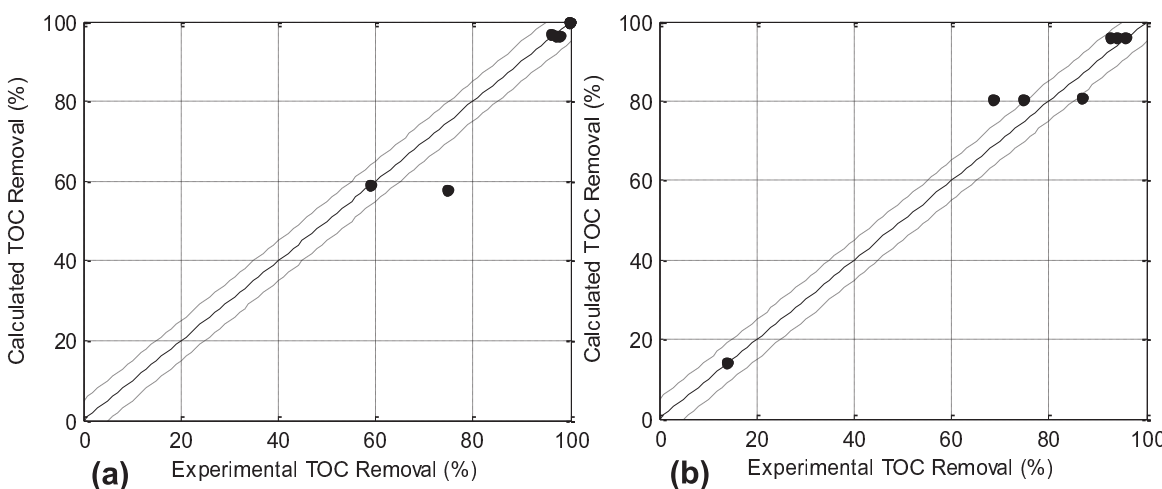


**Figure 6.17** – Parity plots of ‘simple’ (a) and ‘complex’ (b) component TOC removals using optimised power law rate constants.

Good fits for each set of samples were achieved from this demarcation indicating that the rate constant for the simple samples was roughly twice that of the complex samples, which, in conjunction with the differing initial concentrations contributed to the differing rates of TOC removal observed between the two sets of samples.

A brief investigation into the nature of the order of reaction with respect to the oxidant, i.e. whether or not it could reliably be assumed to be zero, was also undertaken.

#### 6.4.3 Non-zero Oxygen Reaction Order

A similar analysis as that in §4.4.3 was undertaken for these waste samples in which the global disappearance of TOC could be modelled by equation 6.10:

$$-r_{TOC} \frac{[TOC]}{dt} = k[TOC]^a [O_2]^b \quad (6.10)$$

A caveat is that although the concentration of the oxidant might affect the rate of reaction, the oxidant would be in such great excess that its concentration would not change appreciably during each experimental run. The solution of combining equation 6.10 with the equation 4.3 is therefore:

$$(1 - X_{TOC})^{1-a} = 1 + (a - 1)k\tau[TOC]^{a-1}[O_2]_0^b \quad (6.11)$$

Consequently, if one plots  $[(1 - X_{TOC})^{1-a} - 1]/((a - 1)[TOC]^{a-1})$  against the residence time for the samples where the initial TOC concentrations are similar,

the gradient of a fitted straight line through the origin will be equal to  $k[O_2]_0^b$  in each case. Plotting  $\ln(k[O_2]_0^b)$  against  $\ln([O_2]_0)$  as indicated by equation 4.15, allowed the evaluation of,  $b$ . It was found that there was a demarcation between the ‘simple’ and ‘complex’ wastes in a similar manner to that seen in the above analyses. For ‘simple’ wastes, the order of reaction was essentially zero. For ‘complex’ wastes, this order of reaction was very slightly above zero ( $b \sim 0.02$ ), but not enough to make a considerable difference to the reaction rate. As such, as long as the oxidant is in great enough excess, its concentration can be assumed to have a negligible effect on the rate of destruction of TOC.

#### 6.4.4 Time to Complete TOC Removal

The rate constants calculated by a least-squares first order analysis of each data set, and a the power law model used to extrapolate the data in order to predict the residence time that would have been sufficient in order to ensure a TOC removal approaching >99.99% for all samples in an attempt to compare these values to the industrial constraint. Table 6.17 displays the time needed to achieve this removal threshold for both model approaches.

**Table 6.17** – Rate constants and predicted residence times to 99.99% TOC removal.

Sample	Rate Constant / Order			Projected Time to 99.99% Removal, s	
	$k$ (1 <sup>st</sup> order)	K	a	First Order	Power Law
T105	0.171	0.123	0.91	53.8	35.3
E72	0.172	0.349	1.14	53.4	88.1
E95	0.242	0.453	1.12	38.0	61.1
E134	0.337	0.570	1.040	27.4	22.6
E135	0.669	0.590	0.96	13.9	10.9
NE	0.503	0.357	0.96	18.4	17.6

This initial extrapolation based on rate constants determined via a least squares pseudo-first order method indicates that all six samples would be subject to a TOC removal of upwards of 99.99% within a residence time of one minute, and that four of the six samples would achieve this in a residence time of less than 40 s.

Individual power law models suggested that 99.99% conversion would be achieved for the ‘simple’ samples in a residence time of ~30 s or less, however, the ‘complex’ samples would take significantly longer with sample E72 not exhibiting 99.99% TOC removal unless being exposed to SCWO for almost 90 s at such a temperature and initial concentration.

Using the rate constants fitted to the ‘simple’ and ‘complex’ waste mixtures implied that the ‘simple’ wastes could exhibit TOC removals of >99.99% within 22 s, where the ‘complex’ wastes could achieve the same levels at residence times of within 50 s.

The plant at which prospective treatment of larger quantities of these wastes would take place has the ability to offer a residence time of up to one minute at supercritical conditions and thus indicates that the oxidation of these waste samples could potentially adhere to the >99.99% TOC removal constraint in an existing treatment plant, were the kinetics to be invariant of geometry. In reality, further research is necessary due to the variability of induction times with reactor geometry, specifically, the increase in induction time found for increased diameter piping.

Further work should also be conducted into estimating the rate constants of waste mixtures from combinations of their TOC and GC-MS assay data. Cocero *et al.* (2002) indicated that heat of formation values could be estimated from the C, H and

O content of specific molecules which could subsequently be used to estimate the energy efficiency of an adiabatic reactor. A similar analysis regarding estimates of activation energies and pre-exponential factors, or a global estimate of the rate constant would be advantageous in assessing optimum reactor design (sizing, residence times, etc) and process conditions. Subsequently it would be hoped that for a given initial TOC concentration and assay of the complexity of the waste sample, and taking into account the operational limits of a reactor, predictions could be made as to how long the sample would need to be exposed to SCWO conditions in order to result in TOC removals above 99.99%.

## 6.5 Assay Analysis after the SCWO Treatment

In order to quantify the destruction of specific compounds from the initial feed samples and the evolution (and possible destruction) of reaction intermediates, the GC-MS data obtained from analysis of the feed samples was compared to GC-MS and, to a lesser extent, GC-TCD analysis of samples obtained during experimental runs at a residence time of 17 s. Due to the cost of analysis, GC-MS data was not obtained for intermediate residence times and thus conclusions about the destruction of evolved intermediates are difficult to draw. However, comparisons between GC-MS data for different feed samples at residence times of 17 s were attempted.

Samples for GC-MS analysis were taken after SCWO at the maximum residence time of 17 s. TOC removal analysis in §6.3.4 indicated that over 92% of TOC was removed at 17 s in all samples and for three of the samples this figure was well over 99%. Consequently, the GC chromatograms also exhibited a large reduction in both the number and magnitude of the peaks.

Table 6.18 shows the eluted peaks from each treated sample along with an indication of the proportion of peaks (and thus components in the feed) that had been removed by the SCWO process.

**Table 6.18** – Number of discrete components eluted from each GC-MS sample

analysis.

Sample	Components Eluted		% Components Completely Removed
	Feed Sample	Treated Sample	
T105	33	10	69.7%
E72	30	7	76.7%
E95	32	11	65.6%
E134	7	5	28.6%
E135	8	4	50.0%
NE	17	5	70.6%

One would expect there to potentially be additional peaks on the treated sample chromatograms representing any intermediate compounds evolved during the reaction, but such was the degree of TOC removal in the experiments for which GC-MS data was obtained (i.e. at maximum residence times), that the minor peaks were almost indistinguishable from the detector noise. The obviously discrete peaks on the treated sample chromatograms were matched to those for the feed samples for the majority of cases enabling an indication both of the components that were destroyed during the treatment runs and of the extent to which this may have occurred. Clearly, the primary indicator of the reaction extents would still be the TOC removal data.

### 6.5.1 Samples E134 and E135

For samples E134 and E135, GC data indicated that the signal for glycerol is not present in the analysis of samples subjected to SCWO. This implies that all glycerol was destroyed in the oxidation of both samples. The chromatograms for these samples indicate that approximately 97% and 91% of compound U11 was removed from sample E134 and E135 respectively after 17 s of SCWO and that piperidine destruction of approximately 88% from E134 with similar removal of this component from sample E135 was observed. Compound U13 was not present in the final sample analysis for either of the samples, indicating complete removal. Table 6.19 indicates the removal of compounds from these samples.

**Table 6.19** – Removal of E134 and E135 components

Compound	Name	E134 Removal %	E135 Removal %
E134-1, E135-1	Glycerol	> 99.99	> 99.99
NE-5	Piperidine	88	86
U11	Unknown	97	91
U13	Unknown	> 99.99	> 99.99

### 6.5.2 Sample E72

Mass spectra data indicates that the majority of the compounds present in the feed sample were destroyed. The compound likely to be 3-isopropoxypropylamine as well as three associated peaks remained after oxidation, along with only two other peaks that could be discerned from the baseline noise. One of these peaks corresponded with compound U13 and the other could be identified as benzaldehyde. GC data indicated that approximately 5% of 3-isopropoxypropylamine remained after oxidation which corresponded to about 16% of the remaining organic content, with

the bulk of the remainder being attributed to the unidentified peaks near to this retention time. Up to 95% of the hydroxybenzenemethanols were oxidised. Table 6.20 indicates the removals of components from this sample.

**Table 6.20** – Removal of E72 components

Compound	Name	Removal %
E72-1	3-isopropoxypropylamine	95
E72-2	Unknown	94
E72-3	Unknown	92
E72-4	Unknown	> 99.99
E72-5	Cyclohexanone	> 99.99
E72-6	2-butoxyethanol	> 99.99
E72-7	Phenol	> 99.99
E72-8	3-ethoxypropan-1-ol	> 99.99
E72-9	1-methyl-2-pyrrolidinone	> 99.99
E72-10	2-hydroxybenzenemethanol	~95
E72-11	4-hydroxybenzenemethanol	~95
U13	Unknown	~80
U14	Benzaldehyde	~67

### 6.5.3 Sample E95

Mass spectra data indicated that all of the compounds explicitly identified from the feed sample were removed apart from toluene of which a small proportion remained. Four other discernible peaks also appeared on the product chromatogram: benzaldehyde, phenol, acetophenone and compound U13. In this case, benzaldehyde, phenol and U13 could all be accounted for on the feed spectra indicating that the benzaldehyde seen in the product sample for sample E72 probably also entered the reactor with the feed. Acetophenone could not be specifically identified from the feed chromatograms, although there was a grouping of increased signals around the corresponding retention time. Table 6.21 indicates the removal of components from this sample.

**Table 6.21** – Removal of E95 components

Compound	Name	Removal %
E95-1	Toluene	50
E95-2	Unknown	> 99.99
E95-3	Unknown	> 99.99
E95-4	Unknown	> 99.99
E95-5	2-butoxyethanol	> 99.99
E95-6	Phenylmethanol	> 99.99
E95-7	1-methyl-2-pyrrolidinone	90
E95-8	1-(2-butoxyethoxy)-ethanol	98
U13	Unknown	25
--	Phenol	95

#### 6.5.4 Sample NE

GC-FID data indicated that of the 17 compounds present in the reaction mixture, 5 remained after SCWO at 16.8 s residence time, including toluene, compound piperidine and compound U13. Table 6.22 indicates the removals of compounds in this sample.

**Table 6.22** – Removal of NE components

Compound	Name	Removal %
E95-1	Toluene	95
NE-1	Butanoic Acid	> 99.99
NE-2	2-butoxyethanamine	> 99.99
NE-3	Unknown	> 99.99
NE-4	Unknown	> 99.99
NE-5	Piperidine	97
NE-6	1-methyl-2-pyrrolidinone	> 99.99
U13	Unknown	90

#### 6.5.5 Sample T105

Mass spectra data indicated that upon the treatment of sample T105, approximately 70% of the mixture's major components were completely destroyed

but of the remaining 8 obvious component peaks on the GC chromatogram, the analytes with the highest molecular weights (235 Da and 292 Da) experienced relatively low destructions. These components exhibited a higher resistance to oxidation than those of lower molecular weight. Table 6.23 indicates the removal of components from this sample.

**Table 6.23** – Removal of T105 components

Compound	Name	Removal %
T105-1	Unknown (complex)	80
T105-2	1-methyl-1,4-cyclohexadiene	> 99.99
T105-3	Unknown	95
T105-4	Unknown	> 99.99
T105-5	1-hepten-3-ol	> 99.99
T105-6	Phenol	> 99.99
T105-7	Unknown	> 99.99
T105-8	1-methyl-4-(1-methylethenyl)-benzene	> 99.99
T105-9	Isoquinoline	> 99.99
T105-10	Isomer of T105-8	> 99.99
T105-11	Isomer of T105-8	> 99.99
T105-12	2,4,5-trimethylbenzenemethanol	> 99.99
T105-13	Ethyl 2-cyano-3-phenylacrylate	> 99.99
U13	Unknown	~85

The first order and power-law rate expressions indicate that the TOC concentration can affect the TOC removal rate, with higher concentrations resulting in higher removal rates. Figure 6.8 and Figure 6.9 showed the relationship between initial TOC concentration and TOC removal percentage.

Countless papers and the data in chapters 4 and 5 indicate a strong proportional relationship between the feed TOC concentration and the subsequent rate of removal, however this is not definitively exhibited in Figure 6.8. It should be remembered that these differing concentrations were not dilutions of the same feed sample and thus the compositions of each sample were not identical. It seems that

this variance in composition has had an effect on the TOC removal efficiency. Samples T105, E72 and E95 were oxidised at feed concentrations roughly similar to those of samples E135 and NE, but exhibited markedly lower TOC removal efficiencies (compared to those that are common for SCWO processes) at a residence time of 17 s. The GC-MS analysis indicates that samples T105, E72 and E95 were much more complex mixtures than the others and their lower treatment efficiency would appear to be explained by this fact.

For treatment on an industrial scale, the differences of composition between samples should be taken into account when calculating the quantity of oxidant that should be delivered to the reactor and the general conditions at which the reaction should be conducted. It seemed that using just the TOC concentration with some generalised assumptions with regard to the H/C quotient of the components potentially resulted in the waste samples with more complex components, e.g. T105, either not receiving enough oxidant, or not being exposed to the supercritical conditions for a long enough time. The result was that the complex samples were not oxidised to the same extent as the simpler mixtures at identical reaction conditions. These variations in kinetics parameters would need to be taken into account when designing both the treatment protocols and the control systems governing the reaction.

## 6.6 Engineering Issues

Engineering feasibility is another facet that should be considered when assessing the treatability of a waste via SCWO.

### 6.6.1 Solids Plugging

The real waste samples were chemically complex, and this affected the ability of SCWO to destroy them, but coupled with this nature was the fact that they also contained solid, potentially tarry, particulates an example of which is shown in Figure 6.18. Unfortunately, the particle size distribution of the particulate matter in the waste samples were not evaluated at the time of conducting the experiments.

**Figure 6.18** – Particulate matter present in samples.



Evidently, the particle shown, which has a maximum length dimension of approximately 6 *mm*, is much too large to be able to make its way into the reactor system thanks both to the fact that the pipes have a diameter of just over 0.5 *mm* and

that the pump inlet and outlet filters had grades of  $10 \mu\text{m}$  and  $2 \mu\text{m}$  respectively. However, there were much smaller particles than these that were present, which were held in suspension in the waste. This suspended particulate matter was what gave the samples their turbidity and colour as shown in Figure 6.19.



**Figure 6.19** – Suspended particulate matter causing opacity of sample T105.

Solid particles that were smaller than the  $2 \mu\text{m}$  would have remained in suspension as the sample was pumped into the reactor system. Thus, these samples showed the potential to cause problems similar to both of the major issues that are associated with SCWO as described in §2.6:

- Corrosion – from the corrosive species that may form from any salts or heteroatom-containing organics present in the samples.

- Plugging – both from the precipitation of ionic salts that could form from heteroatoms present in the samples when the reactor conditions permit such precipitation and from the potential agglomeration of particulate matter.

During the treatment of sample E72, a number of operational issues became apparent. The reactor effluent flowrate started to fall, while the organic feed HPLC pump pressure display indicated a feed pressure that was much higher than desired with occasional spikes to pressures measured by the organic pump high enough to exceed the programmed safety value of 35 MPa. Despite this pressure excess, the indicated reactor pressure dropped sharply before slowly rising back to the correct pressure (due to the BPR setting and continued flow from the oxidant pump).

The increased pressure measured by the organic pump coupled with the initially decreased overall reactor pressure indicated that a blockage had formed between the organic pump and the reactant mixing point. It was possible to disconnect part of the organic preheater and test it in sections to ascertain where exactly the blockage was positioned. Once found, it was subsequently possible to remove the blockage by forcing zero grade water through the isolated preheater tube section. Figure 6.20 indicates the blockage material that was subsequently ejected from the preheater.

Note the size of the larger particles close to the surface of the water in the right hand image. These were much larger than the  $2 \mu\text{m}$  mesh size of the pump outlet line filter indicating that particles of the order  $<10^{-6} \text{ m}$  had been able to enter the reactor system and agglomerate inside the preheater tube. As the agglomerated mass formed and grew larger, so too did the resistance to the organic feed flow,

which resulted in an increased pressure. This process continued until the agglomeration grew to dimensions similar to the diameter of the preheater tube and stopped the flow entirely. The discrete particles visible in Figure 6.20b are of a similar size to the internal pipe diameters.

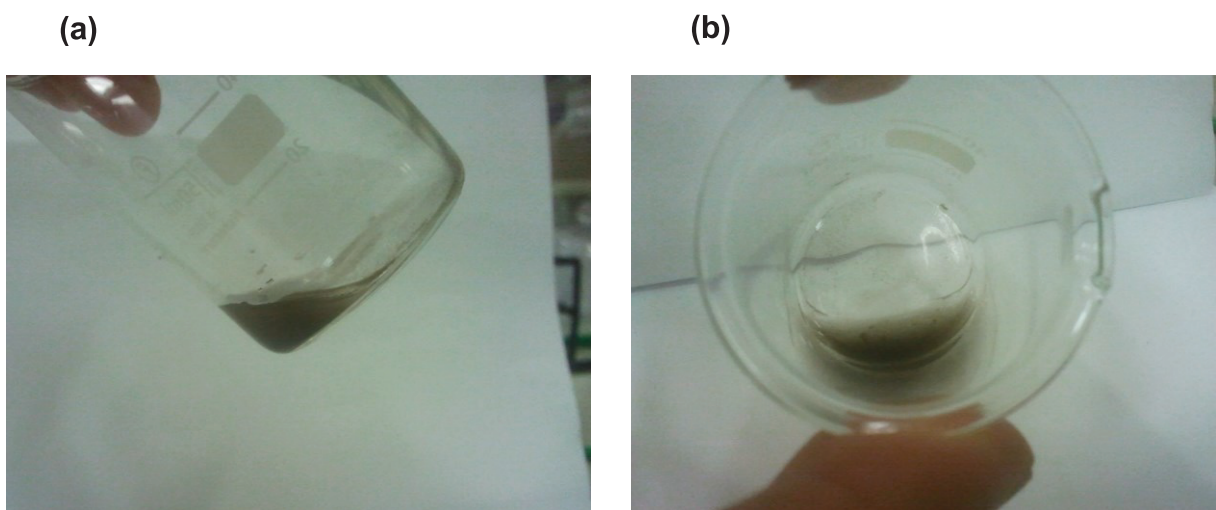


**Figure 6.20** – Particulate matter ejected from the organic sample preheater.

This blockage formation happened on other occasions while treating samples E95 and NE. The time lost due to having to stop an experiment, cool and depressurise the apparatus and dismantle and clear the preheater tube amounted to approximately eight hours on each occasion. These delays were largely unavoidable due to the inability to mitigate for this effect through changing the experimental conditions, however pumping zero grade water through the reactor rig for significant periods after each experimental run could reduce the frequency of such blockages.

Consequently, when considering using SCWO for the treatment of the wastewaters that produced these samples, it should be noted that the process would have the potential to be prone to blockages. On an industrial scale, larger pipes that

have diameters of the order of an inch would be employed and would thus be less prone to the agglomeration of small particles that was seen in the experiments detailed above, however the larger particulates would likely cause a similar effect were they not to be filtered out. The removal of such a blockage at industrial-scale would be much more difficult than the lab-scale removal that was frequently performed during these experiments and the resulting necessary downtime would only impact negatively on the economics of the treatment process.

As such, in the SCWO of these and similar samples, removal of particulates from the organic feed via microfiltration or similar technology could be carried out prior to preheating thus reducing the particulate size distribution to such a grade at which there should be a good deal of confidence that no agglomeration will be able to occur prior to reactant mixing. Alternatively, the process should be carefully monitored and optimised such that the solid particles are able to dissolve into the water as the temperature rises and the water transitions to the critical state before they are able to agglomerate to form a blockage.

One positive observation with respect to the transit of particulate matter into the reactor is that no particulates were present in the outlet samples at residence times in excess of 8 s. The existence of the agglomeration issues show that particulate matter was able to enter the reactor system, but the fact that no particulate matter was observed in the outlet samples or on the BPR filter mesh suggests that this was also degraded by the SCWO process.

### 6.6.2 Corrosion

The oxidation products from the SCWO of DMF were generally not corrosive. As such, corrosion effects were not considered during the investigations undertaken in chapters 4 and 5. Conversely, corrosion effects were observed after the oxidation of the waste samples studied in this chapter. The effects observed were attributed in totality to the action of the oxidation products of these waste samples.

Although the reactor coils and fittings were replaced periodically (generally after approximately 200 heating cycles), the other ancillary components (heat exchanger, preheaters, etc) were not. As such, each component had endured over 400 load cycles (ambient heating and cooling, exposure to hot fluid, exposure to oxidative environment, etc) prior to the investigations in this chapter, with no apparent decrease in performance or integrity.

However, during operation some weeks after the investigations in this chapter had been completed, the effluent piping inside the heat exchanger failed. Examination of this unit showed that the inner piping had been completely corroded approximately 20% of the way along its length from the high-temperature end. This is the approximate region at which the temperature of the reactor effluent would have been returned to subcritical conditions with oxidation products such as HCl and any trace concentration mineral salts becoming soluble in the high temperature medium. This resulted in a highly corrosive environment, which consequently damaged the heat exchanger, culminating in its failure at a later date.

This propensity towards corrosion would be a critical design issue for the treatment of similar wastes under SCWO, to which various solutions have been

proposed with each having varying windows of efficacy in terms of physical and chemical conditions as discussed in §2.6.2. Manufacturing the effluent tubing within the heat exchanger from titanium alloys may avoid the corrosion issues in this particular system; however the level of protection could decrease if sulphates turned out to be present. They are also very expensive, meaning that the benefits of their installation should be balanced against the use of less-resistant alloys with the knowledge that components may need to be replaced during turnaround. Nickel alloys have also been shown to confer resistance to corrosion, but there are operating windows in which the chemistry of the surface layers is suitable for this use. The large change in temperature that occurs within the heat exchanger could result in a high degree of difficulty in maintaining adequate protection, implying that some alloy that is resistant to the known acid components at a wide range of temperatures should be selected if available.

## 6.7 Summary

Six complex aqueous organic waste samples were oxidised after dilution at various residence times at 500°C, 250 bar and at an oxidant ratio of 3 in order to assess the effectiveness of SCWO as a treatment technology for these samples.

SCWO was an effective treatment technology for the complex multicomponent waste samples at residence times of at least 17 s under excess oxidant conditions. TOC removal efficiencies of over 99% were exhibited in three of the six samples under these conditions and taking the reaction rate constants into account allowed the prediction that at the dilutions studied, a minimum residence time of 90 s would allow 99.99% TOC removal in all samples if a first order model was suitable. This

predicted time would seem to be reduced to 50 s when considering ‘a’, the reaction order with regard to TOC, to be 1.08. Given that the reaction will progress via a free-radical route, the non-integer reaction order seems more likely in practice, although a pseudo-first order model didn’t seem to be a bad approximation. It was noted that considering ‘simple’ and ‘complex’ waste mixtures separately resulted in more accurate modelling of the TOC conversions indicating that TOC content alone may not be a good enough indicator of a waste’s treatability. The rate constant for a ‘simple’ waste may be as much as twice as high as a rate constant for a ‘complex’ waste. Assessment of the complexity of the waste in terms of the molecular weight of its constituents and the type (aliphatic, aromatic, etc) of components would be a key factor in both design and informing a control architecture to govern the SCWO process on a large scale.

The majority of components in the wastes were converted into gaseous products and H<sub>2</sub>O, or intermediates of much lower molecular mass. All wastes exhibited TOC removals in excess of 92% at 17 s residence time, and this was increased to >99.8% for samples E134, E135 and NE. A small number of components of large molecular mass (greater than 180 Da) exhibited a greater resistance to oxidation which accounted for the lower TOC removal efficiencies of samples T105, E72, E95 and consequently, higher residence times would be required to ensure removal rates of these compounds increase to the levels demanded of SCWO treatment technologies to compete economically and environmentally with other treatment protocols such as incineration. In the oxidation of sample T105, the majority nitrogen fraction in the product was ammonia at 70%.

The engineering issue of plugging was experienced during the experiments. This effect was likely mostly caused by small particulate matter agglomerating prior to preheating but chloride and sulphate salts were also present in the samples and this could have resulted in precipitation blockages at supercritical conditions in the reactor. Because of the non-specialist nature of the reactor (the reactor was not designed to withstand this phenomenon), it was not possible to mitigate for this effect. As such, if SCWO were to be used to treat this grade of waste it would be necessary to ensure that as little particulate matter as possible enters the reactor system which would involve the use of suitably sized filters, the possible employment of upstream processing, and a well optimised control system.

Assay data suggested that heteroatoms that could potentially result in the formation of ionic salts that could precipitate were present. However, no evidence of obstruction from precipitated salt was observed. When the effect of solids agglomeration can be removed, further investigation should be carried out to see if salt plugging or particulate aggregation is likely to be a major problem in treating this grade of waste. If this were to be the case, it would be necessary to consider reactor solutions targeted to the mitigation of obstruction phenomena.

Corrosion effects were noticed in the heat exchanger, but these became apparent weeks after the experimental runs had ceased. Hydrobromic and hydrochloric acids were likely reactor products from the oxidation of different samples. These products likely contributed to the corrosion damage on the heat exchanger.

# CHAPTER 7 – CONCLUSIONS AND RECOMMENDATIONS FOR FURTHER WORK

## 7.1 Conclusions

The work presented herein focuses on an under-investigated area of SCWO, namely the development of flexible reactor designs with regards to the injection of oxidant streams. Multi-stage SCWO of DMF was undertaken and its performance was compared with the performance of the single-stage SCWO of the same compound under similar conditions in terms of physical parameters. A single-stage configuration reactor was also employed in the destruction of hazardous industrial wastewater samples as part of a treatability study that would contribute to the relatively sparse body of knowledge pertaining to the application of SCWO to the destruction of more complex wastes.

### 7.1.1 Rig Apparatus

A continuous plug flow reactor was designed and constructed such that there would be the flexibility necessary to inject a secondary oxidant stream at any one of three additional ports if required. The ancillary components for the rig such as pumps, preheaters, the cooler and gas-liquid separation units were all sourced, designed and assembled from scratch as necessary. A counter-current heat exchanger was also designed and built to ensure that the reactions could be properly quenched and that the experimental work was carried out in a safe manner.

### 7.1.2 Study of the Single-stage Oxidation of DMF

The SCWO of DMF in a single-stage PFR was investigated. The rate of reaction was found to obey an Arrhenius-type rate law that was essentially first order with respect to the concentration of DMF (and TOC) and fractional order ( $b \sim 0.36$ ) with respect to oxygen. As expected, DMF, TOC and TC conversions displayed positive dependences on the reactor temperature, organic concentration and residence time, with the oxidant ratio still positively affecting the conversions even at large excess. Near-complete conversions of DMF and TOC were observed at temperatures in excess of 500°C. Kinetic parameters were as shown in Table 7.1.

**Table 7.1** – Kinetic parameters of single-stage SCWO of DMF

Parameter	First Order	Integral Regression	Matlab Model
$E_A [kJ mol^{-1}]$	-131	-140	-176
$A [M^{(1-a-b)} s^{-1}]$	$1.71 \times 10^9$	$4.8 \times 10^{10}$	$2.6 \times 10^{13}$
a	1	1	1.03
b	0	0.36	0.36

$\text{CO}_2$ , IC and  $\text{N}_2$  were the major products of oxidation, with the yield of ammonia varying depending on the reaction conditions. Ammonia yield was observed to be suppressed slightly by increasing the DMF feed concentration.

### 7.1.3 Study of the Multi-stage Oxidation of DMF

The multi-stage SCWO of DMF was a novel investigation into the optimisation of the injection of oxidant into a SCWO system. It was found that there are several configurations that provide superior performance to a single-stage oxidation in terms of TOC removal and nitrogen speciation. However, any optimisation must be carried out carefully as there were several configurations in which multi-stage oxidation were

slightly inferior to the single-stage oxidation. These phenomena occurred due to the complex radical species dynamics introduced with the secondary injector.

#### 7.1.4 Destruction of Real Waste

A hazardous waste was treated in a single-stage SCWO reactor configuration. This work will add to the body of knowledge that is slowly growing pertaining to the treatability of complex industrial waste. It was found that at temperatures of 500°C and at residence times approaching 17 s, near complete removal of TOC occurred and that the majority of the complex components were either degraded completely or decomposed into smaller intermediates.

In conducting kinetic analyses it was assumed that the activation energy of TOC was similar to that observed in literature and previous work ( $\sim 175 \text{ kJ mol}^{-1}$ ). It was found that models that were first order with respect to the TOC concentration could describe the oxidation of these waste samples quite well, although one single model for all samples was not found to be able to predict accurately. Splitting the samples into ‘simple’ and ‘complex’ classifications (less than 20 components and 20 or more, respectively) allowed refinement of models that could better predict for TOC conversion. As such, it was found that kinetic models of the SCWO of industrial waste samples should not solely take into account the TOC content, but also the type of molecules present in the sample. Kinetic parameters are shown in Table 7.2.

**Table 7.2** – Kinetic parameters for SCWO of wastewater samples.

Parameter	Simple Samples			Complex Samples		
	1 <sup>st</sup> Order	Power Law	Matlab	1 <sup>st</sup> Order	Power Law	Matlab
k [M <sup>(1-a-b)</sup> s <sup>-1</sup> ]	0.501	0.823	0.823	0.192	0.347	0.347
a	1	1.08	1.08	1	1.08	1.08
b	0	0	0	0	0	0.02

It was found that although the rate constants between each type of waste differed, the oxidation generally followed kinetics that was zero order with respect to the oxidant concentration and slightly in excess of first order with respect to the organic concentration.

Reactor plugging and corrosion effects were also observed in the reactor. These effects were caused by salts present in the waste feed precipitating under supercritical conditions to block the reactor, and heteroatoms forming inorganic salts in the products which dissolved under subcritical conditions to form a corrosive environment.

## 7.2 Recommendations for Further Work

What follows are recommendations for investigations that would be of benefit to this area of research that have arisen from issues in this work that it was not possible to investigate further.

### 7.2.1 Adiabatic Operation of a Multi-stage SCWO Rig

The ultimate goal of this kind of research is to assess SCWO's suitability as a waste-treatment protocol. Pilot-plant studies of SCWO of wastes in single-stage reactors have been carried out, but in order to assess the feasibility of multi-stage

reactors, they must be operated under adiabatic conditions, more similar to those that would be used on an industrial scale.

The temperature control of such a reactor and its preheaters would be a critical variable because the injection of multiple oxidant sources has the potential to cause hotspots in the reactor. It would be advantageous to calculate the temperature at which the secondary preheater(s) should operate in order to control the reactor temperature. In a similar manner to reactors operating under a hydrothermal flame condition, it may not be necessary to heat the secondary oxidant stream(s) to supercritical temperatures in order to maintain a stable reaction. Both experimental and simulation investigations would be very useful in assessing the operating conditions of such an adiabatic setup.

More detailed monitoring of the reactor temperature would also allow more accurate modelling of the dynamics of several chemical species as a function of the reactor length or reactor residence time, an approach that was not possible in this work given that there was no temperature measurement at the secondary injector.

Models to describe the dynamics of DMF, the oxidant and the major products as a function of the reactor length will also be derived as the next logical computational step towards describing both the progress of the reaction and the distribution of the temperature. These models will incorporate partial differential equations to describe both the time and length independent variables.

### 7.2.2 Co-oxidation of DMF and an Auxiliary Fuel

Ammonia was observed in the effluent in all experimental runs. It has been shown in a growing number of studies that when combined with an auxiliary fuel like

ethanol or isopropyl alcohol (IPA), ammonia conversions can be very high at temperatures below 650°C. It would therefore beneficial to see if the addition of an auxiliary fuel could reduce the ammonia yields in the SCWO of nitrogenated organics.

### 7.2.3 Destruction of More Complex Wastes

The treatment of complex wastes is chemically, logically and economically challenging. It was shown that a multi-stage reactor can enhance the removal of organic compounds. A logical next step from chapters 5 and 6 of this thesis would be to assess the treatability of the complex waste samples in the multi-stage reactor in order to see if these enhanced removals translate to wastewaters that may be more complicated or harmful in nature.

### 7.2.4 Simulation of DMF Reaction Kinetics

Detailed simulations of the SCWO of simple molecules like methanol are possible with computer programs like ChemKin®. It would be extremely useful to be able to use such computer software to simulate the SCWO of more complex (and/or nitrogen-containing) molecules. Such a model would require hundreds of sets of kinetic parameters to be calculated/estimated. If such a model could be found to be sufficiently accurate, the effect of various oxidant inputs, co-oxidant fuels, etc, on the treatability of DMF could be investigated for feasibility without needing to build expensive experimental rigs. If such a model could be generalised to accept assay data in terms of TOC/COD and total nitrogen as inputs, and to predict the subsequent yields of N<sub>2</sub>, CO<sub>2</sub>, CO, etc, then the preparation of such a model would be of even greater benefit.

## APPENDICES

### Appendix 1 Reaction Mechanism for C<sub>1</sub> Compounds

Below are four tables taken from Brock and Savage (1995) detailing reactions that occur in the oxidation of organic compounds, specifically those in the oxidation of C<sub>1</sub> compounds forming C-, O- and H-based products and radicals. Data was taken from SCWO reaction kinetics, and atmospheric and combustion chemistry. For each reaction, a pre-exponential factor, temperature exponent and activation energy are provided. Notes on specific reactions can be found in Brock and Savages paper where shown.

**Table A.1 – List of elementary reactions of C<sub>1</sub>, hydrogen and oxidant compounds**

	Reactions <sup>a</sup>	A <sup>b</sup>	n	E <sub>a</sub> <sup>c</sup>
1	CH <sub>4</sub> + H → CH <sub>3</sub> + H <sub>2</sub>	1.33E + 04	3.00	8,038 <sup>d</sup>
2	CH <sub>4</sub> + O <sub>2</sub> = CH <sub>3</sub> + HO <sub>2</sub>	3.97E + 13	0.00	56,894 <sup>d</sup>
3	CH <sub>4</sub> + O → CH <sub>3</sub> + OH	6.92E + 08	1.56	8,485 <sup>d</sup>
4	CH <sub>4</sub> + OH = CH <sub>3</sub> + H <sub>2</sub> O	1.57E + 07	1.83	2,782 <sup>d</sup>
5	CH <sub>4</sub> + HO <sub>2</sub> = H <sub>2</sub> O <sub>2</sub> + CH <sub>3</sub>	9.04E + 12	0.00	24,641 <sup>d</sup>
6	CH <sub>4</sub> + CH <sub>3</sub> O = CH <sub>3</sub> OH + CH <sub>3</sub>	1.57E + 11	0.00	8,843 <sup>e</sup>
7	CH <sub>4</sub> + CH <sub>2</sub> = CH <sub>3</sub> + CH <sub>3</sub>	4.30E + 12	0.00	10,039 <sup>f</sup>
8	CH <sub>4</sub> + CH <sub>2</sub> OH = CH <sub>3</sub> OH + CH <sub>3</sub>	2.16E + 01	3.10	16,227 <sup>g</sup>
9	CH <sub>4</sub> + HCO = CH <sub>3</sub> O + CH <sub>3</sub>	7.27E + 03	2.85	22,515 <sup>e</sup>
10	CH <sub>4</sub> + CH <sub>3</sub> O <sub>2</sub> = CH <sub>3</sub> O <sub>2</sub> H + CH <sub>3</sub>	1.81E + 11	0.00	18,481 <sup>e</sup>
11	CH <sub>4</sub> (+ M) ⇌ CH <sub>3</sub> + H(+ M)	3.71E + 17	-0.558	104,888 <sup>hh</sup>
		LOW/1.29E + 33	-3.732	106,506 <sup>hh</sup>
		SRI/0.45	797	7,791 <sup>hh</sup>
		K <sub>c</sub> 14.6	0.26	104,572 <sup>hh,ii</sup>
12	CH <sub>3</sub> + H → CH <sub>2</sub> + H <sub>2</sub>	6.03E + 13	0.00	15,103 <sup>d</sup>
13	CH <sub>3</sub> + O <sub>2</sub> = CH <sub>3</sub> O + O	1.32E + 14	0.00	31,398 <sup>d</sup>
14	CH <sub>3</sub> + O <sub>2</sub> (+ M) = CH <sub>3</sub> O <sub>2</sub> (+ M)	7.83E + 08	1.20	0 <sup>d</sup>
		LOW/5.81E + 25	-3.30	0 <sup>d</sup>
		TROE/F <sub>c</sub> = 0.466 - 1.30 × 10 <sup>-4</sup> T <sub>j</sub> <sup>d</sup>		
15	CH <sub>3</sub> + O <sub>2</sub> = CH <sub>2</sub> O + OH	3.31E + 11	0.00	8,942 <sup>d</sup>
16	CH <sub>3</sub> + O = CH <sub>3</sub> O	7.95E + 15	-2.12	624 <sup>h</sup>
17	CH <sub>3</sub> + O = H + CH <sub>2</sub> O	8.43E + 13	0.00	0 <sup>d</sup>
18	CH <sub>3</sub> + O = CH <sub>2</sub> + OH	5.00E + 13	0.00	1,200 <sup>i</sup>
19	CH <sub>3</sub> + OH = CH <sub>3</sub> O + H	5.74E + 12	-0.23	13,930 <sup>g</sup>
20	CH <sub>3</sub> + OH = CH <sub>2</sub> O + H <sub>2</sub>	3.19E + 12	-0.53	10,810 <sup>h</sup>
21	CH <sub>3</sub> + HO <sub>2</sub> = CH <sub>3</sub> O + OH	1.81E + 13	0.00	0 <sup>d</sup>
22	CH <sub>3</sub> + CH <sub>3</sub> O = CH <sub>4</sub> + CH <sub>2</sub> O	2.41E + 13	0.00	0 <sup>g</sup>
23	CH <sub>3</sub> + CH <sub>2</sub> OH = CH <sub>4</sub> + CH <sub>2</sub> O	2.41E + 12	0.00	0 <sup>g</sup>
24	CH <sub>3</sub> + HCO = CH <sub>4</sub> + CO	1.21E + 14	0.00	0 <sup>g</sup>
25	CH <sub>3</sub> + CH <sub>3</sub> O <sub>2</sub> = CH <sub>3</sub> O + CH <sub>3</sub> O	2.41E + 13	0.00	0 <sup>g</sup>
26	CH <sub>3</sub> (+ M) ⇌ CH <sub>2</sub> + H(+ M)	3.16E + 15	0.00	109,720 <sup>bb</sup>
		LOW/1.02E + 16	0.00	90,616 <sup>d</sup>
27	CH <sub>3</sub> O + H → CH <sub>2</sub> O + H <sub>2</sub>	1.81E + 13	0.00	0 <sup>d</sup>
28	CH <sub>3</sub> O + O <sub>2</sub> = CH <sub>2</sub> O + HO <sub>2</sub>	3.61E + 10	0.00	2,126 <sup>d</sup>
29	CH <sub>3</sub> O + O = CH <sub>2</sub> O + OH	6.03E + 12	0.00	0 <sup>e</sup>
30	CH <sub>3</sub> O + OH = CH <sub>2</sub> O + H <sub>2</sub> O	1.81E + 13	0.00	0 <sup>e</sup>
31	CH <sub>3</sub> O + HO <sub>2</sub> = CH <sub>2</sub> O + H <sub>2</sub> O <sub>2</sub>	3.01E + 11	0.00	0 <sup>e</sup>
32	CH <sub>3</sub> O + CH <sub>3</sub> O = CH <sub>2</sub> O + CH <sub>3</sub> OH	6.03E + 13	0.00	0 <sup>e</sup>
33	CH <sub>3</sub> O + CH <sub>2</sub> OH = CH <sub>3</sub> OH + CH <sub>2</sub> OH	3.01E + 11	0.00	4,074 <sup>g</sup>
34	CH <sub>3</sub> O + CH <sub>2</sub> = CH <sub>3</sub> + CH <sub>2</sub> O	1.81E + 13	0.00	0 <sup>e</sup>
35	CH <sub>3</sub> O + CH <sub>2</sub> O = CH <sub>3</sub> OH + HCO	1.02E + 11	0.00	2,981 <sup>e</sup>
36	CH <sub>3</sub> O + CH <sub>2</sub> OH = CH <sub>3</sub> OH + CH <sub>2</sub> O	2.41E + 13	0.00	0 <sup>g</sup>
37	CH <sub>3</sub> O + HCO = CH <sub>3</sub> OH + CO	9.04E + 13	0.00	0 <sup>g</sup>
38	CH <sub>3</sub> O + CO = CH <sub>3</sub> + CO <sub>2</sub>	1.57E + 13	0.00	11,804 <sup>e</sup>
39	CH <sub>3</sub> O + CH <sub>3</sub> O <sub>2</sub> = CH <sub>2</sub> O + CH <sub>3</sub> O <sub>2</sub> H	3.01E + 11	0.00	0 <sup>e</sup>
40	CH <sub>3</sub> O(+ M) ⇌ CH <sub>2</sub> O + H(+ M)	1.60E + 14	0.00	25,096 <sup>k</sup>
		LOW/1.90E + 26	-2.70	30,603 <sup>/d</sup>

**Table A.2** – Reaction mechanism, continued.

	Reactions <sup>a</sup>	$A^b$	$n$	$E_{\text{a}}^c$
41	$\text{CH}_3\text{OH} + \text{H} = \text{CH}_3\text{O} + \text{H}_2$	4.00E+13	0.00	6,095 <sup>k</sup>
42	$\text{CH}_3\text{OH} + \text{H} = \text{H}_2 + \text{CH}_2\text{OH}$	8.18E+13	0.00	7,592 <sup>j</sup>
43	$\text{CH}_3\text{OH} + \text{H} = \text{CH}_3 + \text{H}_2\text{O}$	1.00E+13	0.00	5,300 <sup>j</sup>
44	$\text{CH}_3\text{OH} + \text{O}_2 = \text{CH}_2\text{OH} + \text{HO}_2$	2.05E+13	0.00	44,911 <sup>g</sup>
45	$\text{CH}_3\text{OH} + \text{O} = \text{OH} + \text{CH}_2\text{OH}$	1.72E+13	0.00	4,914 <sup>m</sup>
46	$\text{CH}_3\text{OH} + \text{O} = \text{OH} + \text{CH}_3\text{O}$	1.00E+13	0.00	4,684 <sup>k</sup>
47	$\text{CH}_3\text{OH} + \text{OH} = \text{H}_2\text{O} + \text{CH}_2\text{OH}$	1.35E+13	0.00	1,881 <sup>j</sup>
48	$\text{CH}_3\text{OH} + \text{OH} = \text{H}_2\text{O} + \text{CH}_3\text{O}$	1.00E+13	0.00	1,697 <sup>k</sup>
49	$\text{CH}_3\text{OH} + \text{HO}_2 = \text{H}_2\text{O}_2 + \text{CH}_2\text{OH}$	9.64E+10	0.00	12,579 <sup>g</sup>
50	$\text{CH}_3\text{OH} + \text{CH}_2 = \text{CH}_3 + \text{CH}_2\text{OH}$	3.19E+01	3.20	7,172 <sup>g</sup>
51	$\text{CH}_3\text{OH} + \text{CH}_2 = \text{CH}_3 + \text{CH}_2\text{O}$	1.44E+01	3.10	6,935 <sup>g</sup>
52	$\text{CH}_3\text{OH} + \text{HCO} = \text{CH}_2\text{O} + \text{CH}_2\text{OH}$	9.66E+03	2.90	13,108 <sup>g</sup>
53	$\text{CH}_3\text{OH} + \text{CH}_3\text{O}_2 = \text{CH}_3\text{O}_2\text{H} + \text{CH}_2\text{OH}$	1.81E+12	0.00	13,712 <sup>g</sup>
54	$\text{CH}_3\text{OH}(+\text{M}) = \text{CH}_2\text{OH} + \text{H}(\text{+M})$	3.16E+15	0.00	96,010 <sup>bb</sup>
		LOW/2.00E+17	0.00	75,502 <sup>g</sup>
55	$\text{CH}_3\text{OH}(\text{+M}) = \text{CH}_3 + \text{OH}(\text{+M})$	1.90E+16	0.00	91,793 <sup>g</sup>
		LOW/2.00E+17	0.00	68,358 <sup>g/k</sup>
56	$\text{CH}_2 + \text{H} = \text{H}_2 + \text{CH}$	6.03E+12	0.00	-1,788 <sup>d</sup>
57	$\text{CH}_2 + \text{O}_2 = \text{CO} + \text{H}_2\text{O}$	2.41E+11	0.00	0 <sup>c</sup>
58	$\text{CH}_2 + \text{O}_2 = \text{CH}_2\text{O} + \text{O}$	3.29E+21	-3.30	2,868 <sup>g</sup>
59	$\text{CH}_2 + \text{O}_2 = \text{HCO} + \text{OH}$	4.30E+10	0.00	-500 <sup>j</sup>
60	$\text{CH}_2 + \text{O}_2 = \text{CO} + \text{OH} + \text{H}$	8.60E+10	0.00	-500 <sup>j</sup>
61	$\text{CH}_2 + \text{O}_2 = \text{CO}_2 + \text{H}_2$	2.63E+21	-3.30	2,868 <sup>g</sup>
62	$\text{CH}_2 + \text{O}_2 = \text{CO}_2 + \text{H} + \text{H}$	3.29E+22	-3.30	2,868 <sup>g</sup>
63	$\text{CH}_2 + \text{O} = \text{CO} + \text{H}_2$	6.00E+13	0.00	0 <sup>c</sup>
64	$\text{CH}_2 + \text{O} = \text{CH} + \text{OH}$	3.00E+14	0.00	11,923 <sup>g</sup>
65	$\text{CH}_2 + \text{O} = \text{HCO} + \text{H}$	3.02E+13	0.00	0 <sup>c</sup>
66	$\text{CH}_2 + \text{O} = \text{CO} + \text{H} + \text{H}$	7.26E+13	0.00	0 <sup>d</sup>
67	$\text{CH}_2 + \text{OH} = \text{CH}_3\text{O} + \text{H}$	1.81E+13	0.00	0 <sup>e</sup>
68	$\text{CH}_2 + \text{OH} = \text{CH} + \text{H}_2\text{O}$	4.50E+13	0.00	3,000 <sup>i</sup>
69	$\text{CH}_2 + \text{H}_2\text{O}_2 = \text{CH}_3 + \text{HO}_2$	6.03E+09	0.00	0 <sup>c</sup>
70	$\text{CH}_2 + \text{H}_2\text{O} = \text{CH}_3 + \text{OH}$	9.64E+07	0.00	0 <sup>c</sup>
71	$\text{CH}_2 + \text{CH}_2 = \text{CH}_3 + \text{CH}$	2.40E+14	0.00	9,936 <sup>g</sup>
72	$\text{CH}_2 + \text{CH}_2\text{O} = \text{CH}_3 + \text{HCO}$	6.03E+09	0.00	0 <sup>c</sup>
73	$\text{CH}_2 + \text{CH}_2\text{OH} = \text{CH}_3 + \text{CH}_2\text{O}$	1.21E+12	0.00	0 <sup>g</sup>
74	$\text{CH}_2 + \text{HCO} = \text{CH}_3 + \text{CO}$	1.81E+13	0.00	0 <sup>c</sup>
75	$\text{CH}_2 + \text{CO}_2 = \text{CH}_2\text{O} + \text{CO}$	2.35E+10	0.00	0 <sup>c</sup>
76	$\text{CH}_2 + \text{CH}_3\text{O}_2 = \text{CH}_2\text{O} + \text{CH}_3\text{O}$	1.81E+13	0.00	0 <sup>c</sup>
77	$\text{CH}_2(+\text{M}) = \text{CH} + \text{H}(\text{+M})$	3.16E+15	0.00	101,560 <sup>bb</sup>
		LOW/4.00E+15	0.00	83,065 <sup>g</sup>
78	$\text{CH}_2\text{O}(\text{+M}) = \text{H} + \text{HCO}(\text{+M})$	3.59E+14	0.00	89,680 <sup>j</sup>
		LOW/1.26E+16	0.00	77,898 <sup>g/d</sup>
79	$\text{CH}_2\text{O} + \text{H} = \text{H}_2 + \text{HCO}$	2.29E+10	1.05	3,279 <sup>d</sup>
80	$\text{CH}_2\text{O} + \text{O}_2 = \text{HCO} + \text{HO}_2$	6.03E+13	0.00	40,658 <sup>d</sup>
81	$\text{CH}_2\text{O} + \text{O} = \text{HCO} + \text{OH}$	4.16E+11	0.57	2,762 <sup>d</sup>
82	$\text{CH}_2\text{O} + \text{O} = \text{H} + \text{CO} + \text{OH}$	6.03E+13	0.00	0 <sup>r</sup>
83	$\text{CH}_2\text{O} + \text{OH} = \text{HCO} + \text{H}_2\text{O}$	3.43E+09	1.18	-447 <sup>d</sup>
84	$\text{CH}_2\text{O} + \text{HO}_2 = \text{CH}_2\text{OH} + \text{O}_2$	3.39E+12	0.00	19,121 <sup>g</sup>
85	$\text{CH}_2\text{O} + \text{HO}_2 = \text{H}_2\text{O}_2 + \text{HCO}$	3.01E+12	0.00	13,076 <sup>d</sup>
86	$\text{CH}_2\text{O} + \text{CH}_3\text{O}_2 = \text{CH}_3\text{O}_2\text{H} + \text{HCO}$	1.99E+12	0.00	11,665 <sup>g</sup>
87	$\text{CH}_2\text{O}(\text{+M}) = \text{H}_2 + \text{CO}(\text{+M})$	3.16E+13	0.00	1,280 <sup>bb</sup>
		LOW/4.52E+15	0.00	35,300 <sup>g/d</sup>

**Table A.3 – Reaction mechanism, continued.**

	Reactions <sup>a</sup>	$A^b$	$n$	$E_g^c$
88	$\text{CH}_3\text{OH} + \text{H} = \text{CH}_3 + \text{OH}$	9.64E+13	0.00	0 <sup>g</sup>
89	$\text{CH}_3\text{OH} + \text{H} = \text{CH}_2\text{O} + \text{H}_2$	6.03E+12	0.00	0 <sup>g</sup>
90	$\text{CH}_3\text{OH} + \text{O} = \text{CH}_2\text{O} + \text{OH}$	4.22E+13	0.00	0 <sup>g</sup>
91	$\text{CH}_3\text{OH} + \text{HO}_2 = \text{H}_2\text{O}_2 + \text{CH}_2\text{O}$	1.21E+13	0.00	0 <sup>g</sup>
92	$\text{CH}_3\text{OH} + \text{CH}_2\text{OH} = \text{CH}_3\text{OH} + \text{CH}_2\text{O}$	4.82E+12	0.00	0 <sup>g</sup>
93	$\text{CH}_3\text{OH} + \text{HCO} = \text{CH}_3\text{OH} + \text{CO}$	1.21E+14	0.00	0 <sup>g</sup>
94	$\text{CH}_3\text{OH} + \text{HCO} = \text{CH}_2\text{O} + \text{CH}_2\text{O}$	1.81E+14	0.00	0 <sup>g</sup>
95	$\text{CH}_3\text{OH} (+ \text{M}) - \text{CH}_2\text{O} + \text{H} (+ \text{M})$	7.00E+14	0.00	29,637 <sup>f</sup>
		LOW/4.51E+25	-2.50	34,190 <sup>g</sup>
96	$\text{CH} + \text{H}_2 = \text{CH}_3$	3.61E+10	0.00	-1,463 <sup>ii,jj</sup>
97	$\text{CH} + \text{OH} = \text{HCO} + \text{H}$	3.00E+13	0.00	0 <sup>j</sup>
98	$\text{CH} + \text{O} = \text{CO} + \text{H}$	3.97E+13	0.00	0 <sup>d</sup>
99	$\text{CH} + \text{O}_2 = \text{HCO} + \text{O}$	3.30E+13	0.00	0 <sup>j</sup>
100	$\text{CH} + \text{O}_2 = \text{CO} + \text{OH}$	5.00E+13	0.00	0 <sup>u</sup>
101	$\text{CH} + \text{CO}_2 = \text{HCO} + \text{CO}$	3.40E+12	0.00	690 <sup>j</sup>
102	$\text{CH} + \text{H}_2\text{O} = \text{CH}_2\text{OH}$	5.71E+12	0.00	-755 <sup>w</sup>
103	$\text{HCO} + \text{H} = \text{H}_2 + \text{CO}$	9.04E+13	0.00	0 <sup>d</sup>
104	$\text{HCO} + \text{O}_2 = \text{CO} + \text{HO}_2$	5.12E+13	0.00	1,689 <sup>e</sup>
105	$\text{HCO} + \text{O} = \text{CO} + \text{OH}$	3.01E+13	0.00	0 <sup>d</sup>
106	$\text{HCO} + \text{O} = \text{CO}_2 + \text{H}$	3.01E+13	0.00	0 <sup>d</sup>
107	$\text{HCO} + \text{OH} = \text{H}_2\text{O} + \text{CO}$	1.02E+14	0.00	0 <sup>g</sup>
108	$\text{HCO} + \text{HCO} = \text{CH}_2\text{O} + \text{CO}$	3.01E+13	0.00	0 <sup>d</sup>
109	$\text{HCO} (+ \text{M}) - \text{CO} + \text{H} (+ \text{M})$	3.16E+15	0.00	15,270 <sup>bb</sup>
		LOW/5.11E+21	-2.14	20,424 <sup>e</sup>
110	$\text{CO} + \text{O}_2 = \text{CO}_2 + \text{O}$	2.53E+12	0.00	47,693 <sup>c</sup>
111	$\text{CO} + \text{O} (+ \text{M}) = \text{CO}_2 (+ \text{M})$	2.21E+14	0.00	10,470 <sup>f</sup>
		LOW/6.17E+14	0.00	3,001 <sup>/e</sup>
112	$\text{CO} + \text{OH} \Rightarrow \text{H} + \text{CO}_2$	1.17E+7	1.354	-725 <sup>dd</sup>
		HIGH/2.45E-3	3.864	-1,234 <sup>/dd,kk</sup>
		SRI/1.391	2,365	2,020 <sup>/d</sup>
113	$\text{HOCO} (+ \text{M}) = \text{H} + \text{CO}_2 (+ \text{M})$	1.74E+12	0.307	32,928 <sup>dd</sup>
		LOW/2.29E+26	-3.024	35,074 <sup>/d</sup>
		SRI/2.490	5,755	1,601 <sup>/dd</sup>
		$K_c$ 1.23E-1	-0.01	8,700 <sup>/dd,ii</sup>
114	$\text{HOCO} (+ \text{M}) = \text{OH} + \text{CO} (+ \text{M})$	5.89E+12	0.53	33,981 <sup>dd</sup>
		LOW/2.19E+23	-1.89	35,273 <sup>/d</sup>
		SRI/1.37	4,110	2,676 <sup>/dd</sup>
		$K_c$ 7.41E+5	-1.32	34,617 <sup>/dd,ii</sup>
115	$\text{HOCO} + \text{O}_2 = \text{CO}_2 + \text{HO}_2$	1.00E+12	0.00	0 <sup>x</sup>
116	$\text{HOCO} + \text{HO}_2 = \text{CO}_2 + \text{H}_2\text{O}_2$	1.00E+12	0.00	0 <sup>x</sup>
117	$\text{HOCO} + \text{CH}_3\text{O}_2 = \text{CO}_2 + \text{CH}_3\text{O}_2\text{H}$	1.00E+12	0.00	0 <sup>x</sup>
118	$\text{CO} + \text{HO}_2 = \text{OH} + \text{CO}_2$	1.51E+14	0.00	23,648 <sup>r</sup>
119	$\text{CO} + \text{CH}_3\text{O}_2 = \text{CH}_3\text{O} + \text{CO}_2$	4.22E+06	0.00	0 <sup>y</sup>
120	$\text{CH}_3\text{O}_2 + \text{H}_2 = \text{CH}_3\text{O}_2\text{H} + \text{H}$	3.01E+13	0.00	26,032 <sup>c</sup>
121	$\text{CH}_3\text{O}_2 + \text{H} = \text{CH}_3\text{O} + \text{OH}$	9.64E+13	0.00	0 <sup>e</sup>
122	$\text{CH}_3\text{O}_2 + \text{O} = \text{CH}_3\text{O} + \text{O}_2$	3.61E+13	0.00	0 <sup>e</sup>
123	$\text{CH}_3\text{O}_2 + \text{OH} = \text{CH}_3\text{OH} + \text{O}_2$	6.03E+13	0.00	0 <sup>e</sup>
124	$\text{CH}_3\text{O}_2 + \text{HO}_2 = \text{CH}_3\text{O}_2\text{H} + \text{O}_2$	4.63E+10	0.00	-2,583 <sup>r</sup>
125	$\text{CH}_3\text{O}_2 + \text{H}_2\text{O}_2 = \text{CH}_3\text{O}_2\text{H} + \text{HO}_2$	2.41E+12	0.00	9,936 <sup>r</sup>
126	$\text{CH}_3\text{O}_2 + \text{CH}_3\text{O}_2 = \text{CH}_3\text{O} + \text{CH}_3\text{O}_2 + \text{O}_2$	6.88E+10	0.00	-219 <sup>r</sup>

**Table A.4** – Reaction mechanism, continued.

	Reactions <sup>a</sup>	$A^b$	$n$	$E_c^c$
127	$\text{CH}_3\text{O}_2\text{H} + \text{H} = \text{CH}_3\text{O} + \text{H}_2\text{O}$	7.27E+10	0.00	3,720 <sup>aa</sup>
128	$\text{CH}_3\text{O}_2\text{H} + \text{OH} = \text{CH}_3\text{O}_2 + \text{H}_2\text{O}$	7.23E+11	0.00	-258 <sup>d</sup>
129	$\text{H} + \text{H}(\text{+M}) = \text{H}_2(\text{+M})$	1.40E+12 LOW/9.78E+16	0.50 -0.60	$\text{O}^j$ $0^{\text{j}}{}^d$
130	$\text{H} + \text{O}_2(\text{+M}) = \text{HO}_2(\text{+M})$	1.63E+13 LOW/1.56E+18	0.00 -0.80	76 <sup>cc</sup> $0^{\text{j}}{}^d$
131	$\text{H} + \text{O}_2 = \text{OH} + \text{O}$	1.99E+14	0.00	16,812 <sup>d</sup>
132	$\text{H} + \text{OH} = \text{O} + \text{H}_2$	4.88E+03	2.80	3,875 <sup>e</sup>
133	$\text{H} + \text{OH}(\text{+M}) = \text{H}_2\text{O}(\text{+M})$	1.62E+14 LOW/1.41E+23	0.00 -2.00	149 <sup>cc</sup> $0^{\text{j}}{}^d$
134	$\text{H} + \text{HO}_2 = \text{OH} + \text{OH}$	1.69E+14	0.00	874 <sup>d</sup>
135	$\text{H} + \text{HO}_2 = \text{H}_2 + \text{O}_2$	4.28E+13	0.00	1,411 <sup>d</sup>
136	$\text{H} + \text{HO}_2 = \text{O} + \text{H}_2\text{O}$	3.01E+13	0.00	1,721 <sup>d</sup>
137	$\text{H} + \text{H}_2\text{O}_2 = \text{H}_2 + \text{HO}_2$	1.69E+12	0.00	3,756 <sup>d</sup>
138	$\text{H} + \text{H}_2\text{O}_2 = \text{OH} + \text{H}_2\text{O}$	1.02E+13	0.00	3,577 <sup>d</sup>
139	$\text{H} + \text{H}_2\text{O} = \text{H}_2 + \text{OH}$	4.52E+08	1.60	18,421 <sup>d</sup>
140	$\text{O} + \text{H}(\text{+M}) = \text{OH}(\text{+M})$	1.03E+13 LOW/4.71E+18	0.50 -1.00	$\text{O}^j$ $0^{\text{j}}{}^c$
141	$\text{O} + \text{O}(\text{+M}) = \text{O}_2(\text{+M})$	7.64E+12 LOW/1.89E+13	0.50 0.00	$\text{O}^j$ -1,788 <sup>ef</sup>
142	$\text{O} + \text{HO}_2 = \text{OH} + \text{O}_2$	3.25E+13	0.00	0 <sup>d</sup>
143	$\text{O} + \text{H}_2\text{O}_2 = \text{OH} + \text{HO}_2$	9.63E+06	2.00	3,974 <sup>e</sup>
144	$\text{O} + \text{H}_2\text{O} = \text{OH} + \text{OH}$	4.58E+09	1.30	17,100 <sup>e</sup>
145	$\text{HO}_2 + \text{HO}_2 = \text{O}_2 + \text{H}_2\text{O}_2$ second exponential	4.20E+14 1.30E+11	0.00 0.00	6,030 <sup>ee</sup> 820 <sup>ee</sup>
146	$\text{H}_2\text{O}_2(\text{+M}) = \text{OH} + \text{OH}(\text{+M})$	3.00E+14 LOW/1.21E+17 TROE/ $F_c = 0.5$ / <sup>d</sup>	0.00 0.00	48,488 <sup>d</sup> 45,507 <sup>d</sup>
147	$\text{OH} + \text{HO}_2 = \text{H}_2\text{O} + \text{O}_2$	2.89E+13	0.00	-497 <sup>d</sup>
148	$\text{OH} + \text{H}_2\text{O}_2 = \text{HO}_2 + \text{H}_2\text{O}$	7.83E+12	0.00	1,331 <sup>d</sup>

## Appendix 2 Risk Assessments

Appendices

### Appendix 2.1 Chemical Hazard and Risk Assessment for DMF

School/Dept	CHEMICAL ENGINEERING	Assessment Number	
Assessor	IAIN KINGS	Date of Assessment	19/10/2010

1	LOCATION OF THE WORK ACTIVITY	CHEMICAL ENGINEERING G36
---	-------------------------------	--------------------------

2	PERSONS WHO MAY BE AT RISK	List names where possible IAIN KINGS, DR. BUSHRA AL-DURI, OTHER USERS OF G36
---	----------------------------	---

3	ACTIVITY ASSESSED	Oxidation of dimethylformamide in supercritical water medium
---	-------------------	--

4	MATERIALS INVOLVED	Attach copies of data sheet(s)
---	--------------------	--------------------------------

NAME and CAS NUMBER	AMOUNT and FORM	HAZARD	RISK PHRASES	REPORTABLE?
Dimethylformamide CAS: 68-12-2	150mM max Aqueous	Harmful	R20, R21, R36, R61	No
Hydrogen Peroxide CAS: 7722-84-1	30% Aqueous	Harmful Corrosive	R8, R22, R34, R41	No

If substance is reportable, have you reported it to the Health and Safety Unit? YES/NO (see Note 4)

5	INTENDED USE and JUSTIFICATION (where appropriate)
Give brief details and attach protocol/instructions. Justification is needed for exceptionally hazardous substances(see Note 5) DMF will be oxidised by hydrogen peroxide (after decomposition to water and oxygen) in a low-volume, High temperature, high pressure tubular reactor (1/16 inch tube diameter).	

6	RISKS to HEALTH and SAFETY from INTENDED USE
From personal exposure or hazardous reactions. Refer to WELs, flash points, etc., as appropriate. Are pregnant women, breast-feeding mothers especially at risk? - R61 indicates that unborn babies would be at risk from DMF were the pregnant mother to ingest or inhale it. - If hydrogen peroxide and DMF are kept completely separate before meeting as desired, then unwanted hazardous reactions can be avoided. However, during the intended use, oxidation will occur. This reaction is exothermic and as such precautions taking into account the temperature and pressure control of the rig are in place.	

7	CONCLUSIONS ABOUT RISKS
Is level of risk acceptable? Can risk be prevented or reduced by change of substance/procedure? Are control measures necessary? Acceptable Risk Avoid physical contact with chemicals without PPE	

**8 CONTROL MEASURES**

Additional to *Good Chemical Practice*, e.g., fume cupboard, etc. Any special requirements, e.g., glove type, etc.

Use acid-resistant gloves when handling hydrogen peroxide if possible as well as other PPE (lab coat, and mask for DMF).

Both should be stored in the hazardous chemicals store

Take care when opening hydrogen peroxide containers as pressure can build up due to decomposition to water and oxygen.

**9 INSTRUCTION/TRAINING**

Specify course(s) and/or special arrangements.

Standard compulsory university health and safety course.

**10 MONITORING**

Performance of control measures,

N/A

Personal exposure	Health Surveillance, specify measures agreed with Health and Safety Unit
N/A	N/A

**11 WASTE DISPOSAL PROCEDURE**

Include name, 6-digit code and H numbers if to be sent away for disposal

DMF – Send to solvent store and dispose as per UoB procedure.

Hydrogen Peroxide – Solution is already very dilute, but dilute further with 10x water volume and drain.

**12 REVIEW**

Enter the date or circumstances for review of assessment (maximum review interval 5 years)

Yearly – 10/05/12

**13 EMERGENCY ACTION**

**TO CONTROL HAZARDS** To stabilize situation eg spread absorbent on liquid spill; eliminate sources of ignition, etc.

Eliminate sources of ignition, mop with soapy water if spilt.

**TO PROTECT PERSONNEL** Evacuation, protection for personnel involved in clean-up, Special First Aid

If either chemical is spilt, ventilate area and wear gloves, lab coat and facemask when mopping up. If ingested or inhaled, seek immediate medical advice and show all bottle labels.

**TO RENDER SITE OF EMERGENCY SAFE** Clean-up/decontamination

Clean thoroughly with soapy water

**14 EMERGENCY CONTACT**

NAME DR IAN TIDMARSH

PHONE 45259

## Appendix 2.2 Chemical Hazard and Risk Assessment for Complex Samples

School/Dept	CHEMICAL ENGINEERING	Assessment Number	
Assessor	IAIN KINGS	Date of Assessment	11/05/2011

<b>1</b>	<b>LOCATION OF THE WORK ACTIVITY</b>	CHEMICAL ENGINEERING G36
----------	--------------------------------------	--------------------------

<b>2</b>	<b>PERSONS WHO MAY BE AT RISK</b>	List names where possible IAIN KINGS, DR. BUSHRA AL-DURI, OTHER USERS OF G36
----------	-----------------------------------	---

<b>3</b>	<b>ACTIVITY ASSESSED</b>	Oxidation of industrial wastewater samples in supercritical water medium
----------	--------------------------	--

<b>4</b> MATERIALS INVOLVED		Attach copies of data sheet(s)		
NAME and CAS NUMBER	AMOUNT and FORM	HAZARD	RISK PHRASES	REPORTABLE?
6 waste samples of similar Composition. No known CAS numbers.	150mM max Aqueous	Harmful	R20/21/22, R25 R36, R61	No
Hydrogen Peroxide CAS: 7722-84-1	30% Aqueous	Harmful Corrosive	R8, R22, R34, R41	No

If substance is reportable, have you reported it to the Health and Safety Unit? YES/NO (see Note 4)

<b>5</b>	<b>INTENDED USE and JUSTIFICATION (where appropriate)</b>
Give brief details and attach protocol/instructions. Justification is needed for exceptionally hazardous substances(see Note 5)	
Waste samples will be oxidised by hydrogen peroxide (after decomposition to water and oxygen) in a low-volume, high temperature, high pressure tubular reactor (1/16 inch tube diameter).	

<b>6</b>	<b>RISKS to HEALTH and SAFETY from INTENDED USE</b>
From personal exposure or hazardous reactions. Refer to WELs, flash points, etc., as appropriate. Are pregnant women, breast-feeding mothers especially at risk?	
<ul style="list-style-type: none"> <li>- During the intended use, oxidation will occur. This reaction is exothermic and as such precautions taking into account the temperature and pressure control of the rig are in place.</li> </ul>	

<b>7</b>	<b>CONCLUSIONS ABOUT RISKS</b>
Is level of risk acceptable? Can risk be prevented or reduced by change of substance/procedure? Are control measures necessary?	
Acceptable Risk	
Avoid physical contact with chemicals without PPE	

**8 CONTROL MEASURES**

Additional to Good Chemical Practice, e.g., fume cupboard, etc. Any special requirements, e.g., glove type, etc.

Use acid-resistant gloves when handling hydrogen peroxide if possible as well as other PPE (lab coat, and mask for organic samples).

Both should be stored in the hazardous chemicals store

Take care when opening hydrogen peroxide containers as pressure can build up due to decomposition to water and oxygen.

**9 INSTRUCTION/TRAINING**

Specify course(s) and/or special arrangements.

Standard compulsory university health and safety course.

**10 MONITORING**

Performance of control measures,

N/A

Personal exposure

N/A

Health Surveillance, specify measures agreed with Health and Safety Unit

N/A

**11 WASTE DISPOSAL PROCEDURE**

Include name, 6-digit code and H numbers if to be sent away for disposal

Waste samples - return to source

Hydrogen Peroxide – Solution is already very dilute, but dilute further with 10x water volume and drain.

**12 REVIEW**

Enter the date or circumstances for review of assessment (maximum review interval 5 years)

Yearly – 10/05/12

**13 EMERGENCY ACTION**

**TO CONTROL HAZARDS** To stabilize situation eg spread absorbent on liquid spill; eliminate sources of ignition, etc.

Eliminate sources of ignition, mop with soapy water if spilt.

**TO PROTECT PERSONNEL** Evacuation, protection for personnel involved in clean-up, Special First Aid

If either chemical is spilt, ventilate area and wear gloves, lab coat and facemask when mopping up. If ingested or inhaled, seek immediate medical advice and show all bottle labels.

**TO RENDER SITE OF EMERGENCY SAFE** Clean-up/decontamination

Clean thoroughly with soapy water

**14 EMERGENCY CONTACT**

NAME

DR IAN TIDMARSH

PHONE

45259

## Appendix 3      Mass Spectra Analysis of Complex Waste Feed Samples

### Appendix 3.1      Sample T105

Sample T105 component 1 indicates a complex spectrum with multiple groups of prominent peaks. The monoisotopic parent ion was taken to be at  $m/z = 229.9$  although small signals were visible all the way up to  $m/z = 300$  which indicated either that a much more complicated molecule could be being represented, or numerous interaction between created radicals and ions could be occurring. The large peak at  $m/z = 77$ , the small peaks at  $m/z = 74$  and  $75$  and the gap between  $m/z = 105$  and  $182$  suggested the potential presence of two aromatic groups: possibly a non-substituted phenyl group and a multi-substituted benzene ring. However, there are peaks of almost identical height at  $m/z = 184$  and  $186$  which, coupled with the peak at  $m/z = 105$  could indicate the presence of a bromine atom. The groups of peaks between  $m/z = 180$  and  $240$  have gaps of  $16$  or  $17$  which implies that two amino groups and a hydroxyl group could be lost from this substituted benzene segment. Another explanation of the peak at  $m/z = 182$  would be the formation of a bibenzyl group from two benzyl radicals. The peak at  $m/z = 105$  could potentially be  $[C_6H_5C=O]^+$  or  $[C_6H_5(CH_2)_2]^+$ . This compound could be tentatively identified as either a trihydroxy-substituted biphenyl methanone or a bromo-substituted dihydroxybenzoic acid, but the large quantity of fragment peaks coupled with non-zero signal above  $m/z = 240$  indicates that the compound could be much larger and thus more complex.

Sample T105 component 2 has a spectrum that is very sparse. The base peak is at m/z = 79 (which is unusual in itself) and two other major peaks at m/z = 56 and 94 (the molecular ion). The 79, 94 series can indicate a retro Diels-Alder fragmentation and the m/z = 56 ion can sometimes indicate a butenyl group, but when combined with the retro Diels-Alder fragmentation, could be a C<sub>4</sub>H<sub>8</sub> group from the opening of a ring. The molecular ion indicates that the likely formula is C<sub>7</sub>H<sub>10</sub>, with the likely structure corresponding to 1-methyl-1,4-cyclohexadiene.

Sample T105 component 3 couldn't be definitively identified due to a difficulty in identifying the molecular ion, but a very distinctive peak at m/z = 77 amongst others separated by fragments of 15 and 14 indicated that it was potentially some form of aliphatic phenyl compound.

Sample T105 component 4 has a complex fragmentation pattern and could not be definitively identified save that two molecular ion peaks at m/z = 182 and 184 with the latter peak at 33% of the intensity of the former clearly indicated the presence of chlorine. The base peak at m/z = 57.1 strongly indicates the presence of a butyl ion and a strong signal at m/z = 87.1 could suggest a [C<sub>4</sub>H<sub>9</sub>-CH(OH)-]<sup>+</sup> ion or a butyl ester. Peaks separated by 13 at m/z = 87.1, 100.1 and 113.1 could indicate an alkenyl group (-CH=CH-). There is also a peak with 25% relative intensity at m/z = 75 which could possibly represent a triple substituted benzene ring, but this was unlikely, due to the less stable molecular ion. On balance, this compound is likely to be a chlorinated alkenyl-aliphatic ester or alcohol.

Sample T105 component 5 shows a relatively low molecular ion at m/z = 114.1 and large peaks at m/z = 57.1 and 87.1 indicating a secondary pentyl alcohol

ion. The fragment difference between  $m/z = 114.1$  and  $87.1$  indicates the loss of a  $C_2H_3$  fragment, indicating an alkenyl group in the chain and making this compound likely to be 1-hepten-3-ol.

Sample T105 component 6 has a characteristic stable molecular ion peak at  $m/z = 94$  and intermediate peaks at  $m/z = 65$  and  $66$ . This most likely indicates that the compound is phenol, however, an increased signal at  $m/z = 61$  over what would be expected could indicate an ester undergoing McLafferty rearrangement.

Sample T105 component 7 has an unusual base peak at  $m/z = 61$ . An ion with this mass to charge ratio can be formed from McLafferty rearrangement of an ester of the form  $R-O-CO_2H$ , where  $R$  is an aliphatic chain of at least  $C_2$  in length. It seemed most likely that the molecular ion was at  $m/z = 117$  meaning that the alkyl part of the ester needed to have a molecular weight of 58. A small peak at  $m/z = 73$  corroborates the classification of ester and corresponds to the loss of a  $CH_3CO$  fragment. In addition, the weight of the molecular ion being an odd number meant that the compound contained a nitrogen atom, most likely in the form of an amine group. The compound is most likely 2-aminopropyl acetate, but the amino group could be substituted to other locations.

Sample T105 component 8 indicates an aromatic compound with aliphatic substitutions with the molecular ion likely lying at  $m/z = 132$ . Peaks at  $m/z = 91$  and  $117$  imply the loss of a methylethenyl group and a methyl group respectively. It therefore seems probable that the compound is 1-methyl-4-(1-methylethenyl)-benzene.

Sample T105 component 9 is a relatively sparse spectrum with a grouping around m/z = 74-77 implying aromatics. The molecular ion is at m/z = 129 and the difference of 27 implies the loss of either a -CH(=CH<sub>2</sub>) radical or a CH-N section from an aromatic. The peaks at m/z = 94 and 77 make the latter more likely. This compound is likely to be isoquinilone.

Sample T105 components 10 and 11 have very similar major peaks to sample T105 component 8, but there are slightly different ion profiles around the major peaks. This implies that these components are differently-substituted isomers of 1-methyl-4-(1-methylethenyl)-benzene with the formula of C<sub>10</sub>H<sub>12</sub>.

In sample T105 component 12, the large peaks at m/z = 77 and 91 indicate a Ph-CH<sub>2</sub> group. Peaks down from the molecular ion (m/z = 150) in steps of 15 and from [M<sup>+</sup>-18] in steps of 15 indicate the presence of three methyl groups and a hydroxyl group. Finally, the peak at m/z = 119 (M<sup>+</sup>-31) implies the loss of a -CH<sub>2</sub>OH radical. From these indicators, the compound is 2,4,5-trimethyl benzenemethanol.

Sample T105 component 13 includes gaps between peaks of 25 and 26, which are both indicators of unusual bonding. These imply a -CH=C group where R<sub>1</sub> and R<sub>2</sub> branch from the second C, and a C≡N triple bond respectively. The peak at m/z = 77 indicates an aromatic. The molecular ion is at m/z = 201. The removals from the molecular ion indicate an ethyl ester (with associated carbonyl group), and a cyanide group. This compound is ethyl 2-cyano-3-acrylate (C<sub>12</sub>H<sub>11</sub>NO<sub>2</sub>).

## Appendix 3.2      Sample E72

Sample E72 component 1 has prominent peaks at m/z = 58 and m/z = 59 with a molecular ion at m/z = 117. This compound can be tentatively identified as 3-isopropoxypropylamine.

Sample E72 component 2 has an unusual spectrum. The base peak is at m/z = 62 which is an unusual fragment that could represent the McLafferty rearrangement of an aliphatic ester with an amine group on the carboxylate. It was not possible to discern the identity of this component further than this.

Sample E72 component 3 has peaks that imply a carboxylic acid functional group undergoing McLafferty rearrangement. The molecular ion is at m/z = 87 which indicates that there is an amino group.

Sample E72 component 4 has a molecular ion at m/z = 117 indicating a nitrogenous compound. Mass fragment losses of 14, 15, 17, 29 and 45 indicate NH<sub>2</sub>, CH<sub>3</sub>, OH, C<sub>2</sub>H<sub>5</sub> and C(=O)OH radical losses respectively. This suggests a methylaminobutanoic acid with the methyl- and amino-groups on the 2<sup>nd</sup> or 3<sup>rd</sup> carbon as the most likely identity.

Sample E72 component 5 shows a very high molecular ion peak at m/z = 98 with peaks at m/z = 55, 69, 70 and 83. The loss of 28 from the molecular ion implies a carbonyl bond with various CH<sub>3</sub> and CH<sub>2</sub> losses visible in terms of losses of fragments with mass 14 and 15. These losses coupled with the stable molecular ion as the base peak imply that the compound is likely to be cyclohexanone, although various aliphatic versions of C<sub>6</sub>H<sub>10</sub>O also have similar spectra making it difficult to settle on one compound with any certainty.

The high peak at  $m/z = 57$  in sample E72 component 6 indicates an aliphatic butyl group and  $M^+-17$  and  $M^+-31$  indicate losses of OH and  $\text{CH}_2\text{OH}$  radicals respectively. It's very likely that this compound is 2-butoxyethanol.

Sample E72 component 7 has the molecular ion at  $m/z = 94$  as the base peak with a peak at  $M^+-18$  indicating the loss of  $\text{H}_2\text{O}$  from the molecule. This implies an aromatic alcohol, with only phenol fitting this profile.

Sample E72 component 8 has a molecular ion at  $m/z = 104$  and a dominant base peak at  $m/z = 59$ . This peak can commonly represent a carboxylic acid or an ether group, however the peak at 87 [ $M^+-17$ ] indicates the loss of an OH radical. This peak is not high enough to indicate that there are 2 OH groups, suggesting that the ether is more likely. The losses of 14 between 87, 73 and 59 suggest losses of progressive  $\text{CH}_2$  groups, resulting in a probable identification as 3-ethoxypropan-1-ol.

Sample E72 component 9 was more difficult to characterise. The molecular ion at  $m/z = 99$  is an odd number which indicates a nitrogenous compound, but this value is unusual. Peaks at  $m/z = 71$ , 70 and 56 would be represented by  $\text{C}=\text{O}$ ,  $\text{NCH}_3$  and  $\text{CH}_2\text{NCH}_3$  fragment losses respectively. The compound is tentatively identified as 1-methyl-2-pyrrolidinone, a common, polar industrial solvent with a high boiling point, and a precursor for some pharmaceutical drugs.

Sample E72 components 10 and 11 show similar spectra, indicating roughly the same compound. The molecular ion is at  $m/z = 124$  and the reduction of 17 and 18 from this to  $m/z = 107$  and 106 (the base peak) implies OH groups (plural) are present. The peak at  $m/z = 95$  implies the loss of C-OH from the benzene ring implied by peaks at  $m/z = 77$  and 78. Cross referencing the mass spectra with those

stored on the NIST database indicates that the compounds are 2-hydroxybenzenemethanol and 4-hydroxybenzenemethanol respectively.

### Appendix 3.3      Sample E95

Sample E95 component 1 was relatively simple to identify. The molecular ion at  $m/z = 92$  coupled with a loss of 26 from  $m/z = 91$  (formed via hydrogen removal) to  $m/z = 65$  indicates the loss of the  $\text{CH}_3\text{CH}$  radical. The peaks at  $m/z = 65$  and 51 thus represent  $[\text{C}_5\text{H}_5]^+$  and  $[\text{C}_4\text{H}_3]^+$  respectively. This implies fragmentation of a benzene ring, suggesting that this compound is toluene.

Sample E95 components 2 and 3 had near-identical spectra. They had very unusual peaks at  $m/z = 62$ . This didn't match any common ion, but would match a McLafferty rearrangement of an ester with an amino group instead of a methyl group on the carboxylate portion. Peaks at  $m/z = 58$  and 61 correspond to McLafferty rearrangements of an ester or carboxylic acid, but the peak at  $m/z = 77$ , although not large, usually implies a benzyl group. The molecular ion is at  $m/z = 122$  indicating the presence of an even number of nitrogen atoms (potentially zero, but given that some intermediate ions have even mass numbers, likely two amino groups of which one is associated with the carboxylate).

Sample E95 component 4 had an unusual spectrum and was very difficult to discern. McLafferty rearrangement peaks at  $m/z = 58$  and 61 coupled with a peak at  $m/z = 45$  indicates the presence of a carboxylic acid functional group. However, the molecular ion peak could not be discerned. Very low intensity peaks at  $m/z = 76$ , 122 and 137 suggested that the molecule could be a bi-substituted benzyl structure with an amino group and a carboxylic acid, however the molecular ion for this structure

would be at  $m/z = 137$  and the intensity signal was much lower than would be expected for this stable compound.

The profile of sample E95 component 5 was almost identical to that of sample E72 component 6 indicating that this compound is very likely to be 2-butoxyethanol.

Sample E95 component 6 was also simple to identify. A peak at  $m/z = 77$  indicates an aromatic, with removals of 17 and 31 from the molecular ion ( $m/z = 108$ ) indicating the loss of OH and  $\text{CH}_2\text{OH}$  radicals respectively. The base peak at  $m/z = 79$  is the loss of a  $\text{CH}_3\text{CH}_2$  radical. This compound is likely to be phenylmethanol.

Sample E95 component 7 is similar to sample E72 component 9 indicating that this compound could be 1-methyl-2-pyrrolidinone.

Sample E95 component 8 is similar to that expected for aliphatic chains with the base peak indicating a butyl-group. The molecular ion, which was not visible on the spectrum is actually at  $m/z = 162$  so a tiny signal at  $m/z = 144$  is the loss of  $\text{H}_2\text{O}$ . Repeated gaps of 16 imply the losses of more than one O radical, indicating that the compound has multiple ether functionality. Cross referencing with the NIST database produced a good match with the spectrum of 1-(2-butoxyethoxy)-ethanol.

#### **Appendix 3.4      Samples E134 and E135**

Only one component spectrum was found for sample E134. It had a base peak at  $m/z = 61$  and a further peak at  $m/z = 43$ . This profile is a strong indicator of the compound being glycerol (molecular ion at  $m/z = 92$ ). The large peak at  $m/z = 61$  is the removal of  $\text{CH}_2\text{OH}$  radicals from either end of the molecule, with the peak at  $m/z = 43$  being the removal of  $\text{H}_2\text{O}$  from after this. The spectrum of the only

compound from sample E135 is near-identical to that of sample E134 indicating that this compound is also glycerol.

### Appendix 3.5      Sample NE

Sample NE component 1's spectrum is rather sparsely populated. The molecular ion is the small peak at  $m/z = 88$ . The peak at  $m/z = 73$  is the removal of the  $\text{CH}_3$  radical, the peak at  $m/z = 45$  is a carboxylic acid ion  $[\text{C}(=\text{O})\text{OH}]^+$  and the base peak at  $m/z = 60$  is likely to imply the removal of a carboxyl group or the  $\text{CH}_3\text{CH}$  radical. This compound is very likely to be butanoic acid.

Sample NE component 2 displays 2 prominent peaks at  $m/z = 57$  and  $60$  and a molecular ion at  $m/z = 117$ . The peaks at  $m/z = 57$  and  $60$  are almost equal in intensity indicating that the bonds are roughly symmetrical. A peak at  $m/z = 73$  indicates that a butyl ether group is likely. The compound would appear to be 2-butoxyethanamine.

Sample NE component 3 has very prominent peaks at  $m/z = 45, 60, 73$  and  $87$  indicating that a carboxylic acid group is present. There are also peaks of identical intensity at  $m/z = 78.9$  and  $80.9$ , and  $m/z = 79.9$  and  $81.9$  which is strongly indicative of the presence of Br and HBr ions, implying that the compound is brominated. The exact form of the aliphatic portion was very difficult to deduce but the intermediate peaks indicate that a butyl group could be present indicating that some form of brominated hexanoic acid is likely. The molecular ion was not on the spectrum indicating that the compound had very little in the way of branching. This compound is notable because it's likely to be a source of HBr under oxidation, which will dissociate in subcritical water to form strong hydrobromic acid.

Sample NE component 4 had a very similar spectrum to sample NE component 3, except there was no signal indicating the presence of bromine. As such, it is likely that this is a non-brominated form of some type of hexanoic acid.

Sample NE component 5 is a sparse spectrum with a stable molecular ion peak at  $m/z = 85$  indicating a cyclic molecule incorporating a nitrogen atom. There is no peak at  $m/z = 77$  implying the absence of an aromatic group. A peak at  $m/z = 56$  indicates a  $C_4H_8$  group from the fragmentation of a saturated ring. This compound could be piperidine (the saturated form of pyridine).

Sample NE component 6's spectrum is very similar to those of sample E72 component 9 and sample E95 component 9 implying that this compound too is likely to be 1-methyl-2-pyrrolidinone.

## Appendix 3.6 Assay Overviews

The following tables display GC-derived assays of the likely compounds:

**Table A.5 – T105 Assay**

Compound	Name	Mass %
T105-1	A trihydroxy-substituted biphenylmethanone?	20.8
T105-2	1-methyl-1,4-cyclohexadiene	8.3
T105-3	Unknown	2.4
T105-4	Unknown	5.8
T105-5	1-hepten-3-ol	5.3
T105-6	Phenol	4.0
T105-7	2-aminopropyl ethanoate or similar	4.1
T105-8	1-methyl-4-(1-methylethenyl)-benzene	14.1
T105-9	Isoquinoline	3.8
T105-10	Alternately-substituted isomer of T105-8	3.4
T105-11	Alternately-substituted isomer of T105-8	4.1
T105-12	2,4,5-trimethylbenzenemethanol	15.6
T105-13	Ethyl 2-cyano-3-phenylacrylate	2.3
U13	Unknown	0.8
Others	--	5.2

**Table A.6 – E72 Assay**

Compound	Name	Mass %
E72-1	3-isopropoxypropylamine	7.4
E72-2	Unknown	6.1
E72-3	Unknown	6.3
E72-4	Unknown	4.2
E72-5	Cyclohexanone	6.3
E72-6	2-butoxyethanol	4.2
E72-7	Phenol	17.0
E72-8	3-ethoxypropan-1-ol	2.4
E72-9	1-methyl-2-pyrrolidinone	4.9
E72-10	2-hydroxybenzenemethanol	8.6
E72-11	4-hydroxybenzenemethanol	17.1
U13	Unknown	1.2
U14	Benzaldehyde (unquantified)	--
Others	--	14.3

**Table A.7 – E95 Assay**

<b>Compound</b>	<b>Name</b>	<b>Mass %</b>
E95-1	Toluene	11.3
E95-2	Unknown	3.9
E95-3	Unknown	15.6
E95-4	Unknown	7.2
E95-5	2-butoxyethanol	15.6
E95-6	Phenylmethanol	3.9
E95-7	1-methyl-2-pyrrolidinone	6.7
E95-8	1-(2-butoxyethoxy)-ethanol	25.8
U13	Unknown	< 0.1
Others	Includes phenol	9.9

**Table A.8 – E134 Assay**

<b>Compound</b>	<b>Name</b>	<b>Mass %</b>
E134-1	Glycerol	93.7
U11	Unknown	4.5
NE-5	Piperidine	0.5
U13	Unknown	0.1
Others	--	1.2

**Table A.9 – E135 Assay**

<b>Compound</b>	<b>Name</b>	<b>Mass %</b>
E135-1	Glycerol	93.3
U11	Unknown	4.2
NE-5	Piperidine	0.1
U13	Unknown	< 0.1
Others	--	2.3

**Table A.10 – NE Assay**

Compound	Name	Mass %
NE-1	Butanoic acid	24.2
NE-2	2-butoxyethanamine	5.0
NE-3	Unknown	1.8
NE-4	Unknown	1.5
NE-5	Piperidine	20.7
NE-6	1-methyl-2-pyrrolidinone	12.4
E95-1	Toluene	18.9
U13	Unknown	4.1
Others	--	11.4

## Appendix 4 Matlab Regression Regime for Kinetic Parameters

### Appendix 4.1 Calling and Calculation Script

```

clear all; clc; close all; format short g
global oa ob Caol Cbol R Tcal Texp n k AD AAD xcal
t_ind=0.573;
t_s=0;
oa=1;
ob=0.36;
RmmC=12.0107;
chk=0:0.01:1;
chkUB=chk+0.1;
chkLB=chk-0.1;
Tplot=650:1:850;
TUB=Tplot+0.05*(Tplot);
TLB=Tplot-0.05*(Tplot);

%% EXPERIMENTAL DATA

n=?; %number of experiments
Cao=?; %DMF Concentration (M)
Cbo=?; % O2 Concentration (M)
tau=?; % Residence Time (s)
Texp=?; % Temperature (K)
x=?; %DMF Conversion

%% MODEL

xcal_i=zeros(length(x));
R=8.314;
int=zeros(n, 1); y=zeros(n, 1);
for j=1:n
    Caol=Cao(j);
    Cbol=Cbo(j);
    tau1=tau(j);
    Texpl=Texp(j);
    x1=x(j);
    int1=quad(@integral, 0, x1);
    y1=integral(x1);
    int(j)=int1;
    y(j)=y1;
end
int=int';
display(int)
k=int./(tau.* (Cao).^(oa+ob-1));
display(k)

```

```
% Minimisation
d=[100000;1000000000000];
options=optimset('MaxFunEvals',100000,'MaxIter',10000,'TolX',1e-4,'TolFun',1e-4);
[D,FVAL,EXITFLAG,OUTPUT]=fminsearch(@minimise,d,options);
display(D(1)); display(D(2))
figure(1)
plot(Texp,Tcal,'k.',Tplot,Tplot,'k',Tplot,TUB,'k:',Tplot,TLB,'k:')
xlabel('Experimental Temperature (K)')
ylabel('Calculated Temperature (K)')
axis([650 850 650 850])

if oa~=1
    h=(oa-1)*D(2).*exp((-1*D(1))./(R*Texp)).*(Cao).^(oa-1).*Cbo^ob.*tau;
    xcal=1-((h+1).^(1/(1-oa)));
else
    h=exp(-1*D(2).*exp((-1*D(1))./(R*Texp)).*tau.*((Cbo)^ob));
    xcal=1-h;
end

if oa~=1
    h=(oa-1)*D(2).*exp((-1*D(1))./(R.*Texp)).*(Cao)^(oa-1).*Cbo^ob.*tau_t_ind;
    xcal_i=1-((h+1)^(1/(1-oa)));
else
    h=exp(-1*D(2).*exp((-1*D(1))./(R.*Texp)).*(tau_t_ind).*((Cbo)^ob));
    xcal_i=1-h;
end

ADD=abs(100.* (xcal-x)./x); AADD=sum(ADD)./n; b=xcal./x;
display(mean(b))

figure(2)
plot(x,xcal,'k.',chk,chk,'k',chk,chkLB,'k:',chk,chkUB,'k:')
xlabel('Experimental Conversion')
ylabel('Calculated Conversion')
axis([0 1 0 1])

if t_ind>0
    figure(3)

plot(x,xcal_i,'k.',chk,chk,'k',chk,chkLB,'k:',chk,chkUB,'k:')
    xlabel('Experimental Conversion')
    ylabel('Calculated Conversion')
    axis([0 1 0 1])
end
```

## Appendix 4.2 Integral Function

Sample T105 component 1 indicates a complex spectrum with multiple groups of prominent peaks.

```
function y=integral(x)
global oa ob Caol Cbo1

y=1./(((1-x)^oa).*((Cbo1./Caol)-4.25.*x)^ob));
```

## Appendix 4.3 Minimisation Function

Sample T105 component 1 indicates a complex spectrum with multiple groups of prominent peaks.

```
function AAD = minimise(d)
global R Texp n k AD Tcal

Tcal=d(1)./(R*log(d(2)./k));
AD=abs(100.* (Tcal-Texp)./Texp);
AAD=sum(AD)/n;
```

## Appendix 5 Matlab Model for Parameter Evaluation

```

t1=?; % Residence times at which TOC data has been found (inc. 0 s)
C1=?; % TOC concentrations at each residence time (in order)
Ci=C1(1); % Set initial concentration

a=linspace(0.95,2,200); % For TOC order sweep
k=linspace(0.001,20,200); % For rate constant sweep

Lk=length(k); Ln=length(a); % Used for memory assignment
C2=zeros(Lk,1,Ln); % Assign memory
diff=C2;sqDiff=diff; % Assign memory
sumSqDiff=zeros(Lk,Ln); % Assign memory
for m=1:Ln
    for l=1:Lk
        if a(m) ~=1
            h=(a(m)-1)*k(l)*Ci^(a(m)-1)*t1;
            xcal=1-((h+1).^(1/(1-a(m)))); % Calculation of xcal
            C2(l,:,m)=Ci*(1-xcal);
        else
            C2(l,:,m)=Ci*exp(-k(l)*t1);
        end
        diff(l,:,m)=C2(l,:,m)-C1;
        sqDiff(l,:,m)=diff(l,:,m).^2;
        sumSqDiff(l,m)=sum(sqDiff(l,:,m));
    end
end
[mk, pos]=min(sumSqDiff);
[mk1, pos1]=min(mk); % Check positions of optimum a and k

k_res=k(pos1);
a_res=a(pos1);
result=[k_res a_res mk1] % Output optimum k and a

% Use found parameters to plot TOC destruction profile and compare
% to experimental data

t=linspace(0,17,200);
h2=(a_res-1)*k_res*Ci^(a_res-1)*t;
xcal2=1-((h2+1).^(1/(1-a_res)));
C3=Ci*(1-xcal2);
C5=(Ci^(1-a_res)-k_res*t1*(1-a_res)).^(1/(1-a_res));
figure(2)
plot(t1,C1,'ks',t,C3)
xlabel('Residence Time (s)')
xlabel('TOC Concentration (ppm)')

```

## LIST OF REFERENCES

- Abeln, J., Kluth, M., Petrich, G., Schmieder, H., Supercritical Water Oxidation (SCWO): A process for the treatment of industrial waste effluents, *Journal of High Pressure Research* 20 (2001)
- Anderko, A., Pitzer, K. S., Equation-of-state representation of phase equilibria and volumetric properties of the system NaCl-H<sub>2</sub>O above 573K, *Geochimica et Cosmochimica Acta* 57 (1993)
- Anikeev, V. I., Yermakova, A., Goto, M., Decomposition and Oxidation of Aliphatic Nitrocompounds in Supercritical Water, *Industrial and Engineering Chemistry Research* 43 (2004)
- Anikeev, V. I., Yermakova, A., Semikolenov, V. A., Goto, M., Effect of supercritical water density on the rate constant of aliphatic nitro-compounds decomposition, *Journal of Supercritical Fluids* 33 (2005)
- Application of ion exchange processes for the treatment of radioactive waste and management of spent ion exchangers, *International Atomic Energy Agency (IAEA), Vienna* (2002)
- Atkins, P. W., The Elements of Physical Chemistry 2<sup>nd</sup> Ed., Oxford University Press, Oxford (1996)
- Augustine, C., Tester, J. W., Hydrothermal flames: From phenomenological experimental demonstrations to quantitative understanding, *Journal of Supercritical Fluids* 47 (2009)

- Aymonier, C., Beslin, P., Jolivalt, C., Cansell, F., Hydrothermal oxidation of a nitrogen-containing compound: the fenuron, *Journal of Supercritical Fluids* 17 (2000)
- Aymonier, C., Gratias, A., Mercadier, J., Cansell, F., Global reaction heat of acetic acid oxidation in supercritical water, *Journal of Supercritical Fluids* 21 (2001)
- Baulch, D.L., Cobos, C.J., Cox, R.A., Esser, C., Frank, P., Just, T., Kerr, J.A., Pilling, M.J., Troe, J., Walker, R.W., Warnatz, J., Evaluated kinetic data for combustion modelling, *Journal of Physical Chemistry Reference Data* 21 (1992)
- Benjamin, K. M., Savage, P. E., Hydrothermal reactions of methylamine, *Journal of Supercritical Fluids* 31 (2004)
- Benjamin, K. M., Savage, P. E., Supercritical Water Oxidation of Methylamine, *Industrial and Engineering Chemistry Research* 44 (2005a)
- Benjamin, K. M., Savage, P. E., Detailed Chemical Kinetic Modelling of Methylamine in Supercritical Water, *Industrial and Engineering Chemistry Research* 44 (2005b)
- Bermejo, M. D., Cocero, M. J., Supercritical water oxidation: A technical review, *AIChE Journal* 52 (11) (2006)
- Bermejo, M. D., Martín, A., Cocero, M. J., Application of the Anderko-Pitzer EoS to the calculation of thermodynamic properties of systems involved in the supercritical water oxidation process, *Journal of Supercritical Fluids* 42 (2007)
- Bermejo, M. D., Cantero, F., Cocero, M. J., Supercritical water oxidation of feeds with high ammonia concentrations: Pilot plant experimental results and modelling, *Chemical Engineering Journal* 137 (2008)

- Bermejo, M. D., Cabeza, P., Queiroz, J. P. S., Jiménez, C., Cocero, M. J., Analysis of the scale up of a transpiring wall reactor with a hydrothermal flame as a heat source for the supercritical water oxidation, *Journal of Supercritical Fluids* 56 (2011)
- Boukis, N., Freidrich, C., Dinjus, E., Titanium as reactor material for SCWO applications. First experimental results, Corrosion'98 National Association of Corrosion Engineers, Houston, TX, Paper No. 417 (1998)
- Bozzelli, J. W., Dean, A. M., Energised complex quantum Rice-Ramsperger-Kessel analysis on reactions of NH<sub>2</sub> with HO<sub>2</sub>, O<sub>2</sub>, and O atoms, *Journal of Physical Chemistry* 93 (1989)
- Bozzelli, J. W., Dean, A. M., Hydrocarbon radical reactions with O<sub>2</sub>: comparison of allyl, formyll, and vinyl to ethyl, *Journal of Physical Chemistry* 97 (1993)
- Bozzelli, J. W., Chang, A., Dean, A. M., Analysis of the reactions H + N<sub>2</sub>O and NH + NO: pathways and rate constants over a wide range of temperature and pressure, *Symposium (International) on Combustion Proceedings* 25 (1994)
- Bozzelli, J. W., Dean, A. M., O-NNH: a possible new route for NO<sub>x</sub> formation in flames, *International Journal of Chemical Kinetics* 27 (1995)
- Brock, E. E., Savage, P. E., Detailed chemical kinetics model for supercritical water oxidation of C<sub>1</sub> compounds and H<sub>2</sub>, *AIChE Journal* 41 (8) (1995)
- Brock, E. E., Oshima, Y., Savage, P. E., Barker, J. R., Kinetics and mechanism of methanol oxidation in supercritical water, *Journal of Physical Chemistry* 100 (1996)

Bröll, D., Kaul, C., Krämer, A., Krammer, P., Richter, T., Jung, M., Vogel, H., Zehner, P., Chemistry in supercritical water, *Angewandte Chemie International Edition* 38 (1999)

Brunner, G., Near and supercritical water. Part I: Hydrolytic and hydrothermal processes, *Journal of Supercritical Fluids* 47 (2009)

Brunner, J., Near and supercritical water. Part II: Oxidative processes, *Journal of Supercritical Fluids* 47 (2009)

Burrows, J. P., Cliff, D. I., Harris, G. W., Thrush, B. A., Wilkinson, J. P. T., Atmospheric reactions of the HO<sub>2</sub> radical studied by laser magnetic resonance spectroscopy, *Proceedings of the Royal Society A* 368 (1980)

Calzavara, Y., Joussot-Dubien, C., Turc, H. –A., Fauvel, E., Sarrade, S., A new reactor concept for hydrothermal oxidation, *Journal of Supercritical Fluids* 31 (2004)

Campomanes, P., Menendez, I., Sordo, T. L., A Theoretical Study of the <sup>2</sup>NCO + <sup>2</sup>OH Reaction, *Journal of Physical Chemistry A.* 105 (2001)

Cocero, M. J., Alonso, E., Toro, R., Valletado, D., Fdz-Polanco, F., Supercritical Water Oxidation in a Pilot Plant of Nitrogenous Compounds: 2-Propanol Mixtures in the Temperature Range 500 - 750°C, *Industrial and Engineering Chemistry Research.* 39 (2000)

Cocero, M. J., Alonso, E., Sanz, M. T., Fdz-Polanco, F., Supercritical water oxidation process under energetically self-sufficient operation, *Journal of Supercritical Fluids* 24 (2002)

- Cohen, N., Westberg, K. R., Chemical kinetic data sheets for high-temperature reactions. Part II, *Journal of Physical Chemistry Reference Data* 20 (1991)
- Coulson, J. M., Richardson, J. F., Backhurst, J. R., Harker, J. H., Coulson and Richardson's Chemical Engineering, Volume 1: Fluid Flow, Heat Transfer and Mass Transfer 6<sup>th</sup> Ed., Butterworth-Heinemann, Oxford (1999, reprinted 2005)
- Chakraborty, D., Park, J., Lin, M. C., Theoretical study of the OH + NO<sub>2</sub> reaction: formation of nitric acid and the hydroperoxyl radical, *Chemical Physics* 231 (1998)
- Dagaut, P., Cathonnet, M., Bettner, J-C., Chemical Kinetic Modelling of the Supercritical-Water Oxidation of Methanol, *Journal of Supercritical Fluids* 9 (1) (1996)
- Darwent, B. de B., Bond Dissociation Energies in Simple Molecules, *US National Bureau of Standards* 31 (1970)
- Decision Makers' Guide to Municipal Solid Waste Incineration, The International Bank for Reconstruction and Development / The World Bank, Washington DC, USA (1999)
- Department for Environment, Food, and Rural Affairs (DEFRA), Waste and Recycling: Household waste recycling, by material – England, URL: <http://www.defra.gov.uk/statistics/environment/waste/wrfg15-hhmaterial/>, Retrieved 21/11/12
- Dickinson, E., Hydrocolloids as emulsifiers and emulsion stabilisers, *Food Hydrocolloids* 23 (2009)

- Dutournié, P., Mercadier, J., Matéos, D., Cansell, F., Hydrothermal oxidation treatment reactor: Experimental and simulated study of a non-anticipated phenomenon at the reactor inlet, *Journal of Supercritical Fluids* 42 (2007)
- Economic and Social Commission for Western Asia (ESCWA), Waste-water treatment technologies: A general review, *United Nations* (2003)
- Environmental Protection Agency, N,N-Dimethylformamide, United States Environmental Protection Agency Technology Transfer Network (1992; Updated 2007), URL: <http://www.epa.gov/ttnatw01/hlthef/di-forma.html>, Retrieved 12/06/12
- Fourcault, A., García-Jarana, B., Sánchez-Oneto, J., Marias, F., Portela, J. R., Supercritical water oxidation of phenol with air. Experimental results and modelling, *Chemical Engineering Journal* 152 (2009)
- Fujii, T., Hayashi, R., Kawasaki, S., Suzuki, A., Oshima, Y., Water density effects on methanol oxidation in supercritical water at high pressure up to 100 MPa, *Journal of Supercritical Fluids* 58 (2011)
- Fukuda, T., Katsume, Y., Watabe, N., Kurosu, S., Whitby, R. L. D., Maekawa, T., Deposition of C<sub>60</sub>, C<sub>70</sub> and C<sub>84</sub> fullerene molecules, in benzene via a change of the fluid state, from a gas-liquid two phase region to the critical point, *Journal of Supercritical Fluids* 58 (3) (2011)
- Goto, M., Shiramizu, D., Kodama, A., Hirose, T., Kinetic Analysis for Ammonia Decomposition in Supercritical Water Oxidation of Sewage Sludge, *Industrial and Engineering Chemistry Research*. 38 (1999)

- Grotheer, H., Riekart, G., Walter, D., Just, T., Non-Arrhenius behaviour of the reaction of hydroxymethyl radicals with molecular oxygen, *Journal of Physical Chemistry* 92 (1988)
- Hatakeda, K., Ikushima, Y., Sato, O., Aizawa, T., Saito, N., Supercritical water oxidation of polychlorinated biphenyls using hydrogen peroxide, *Chemical Engineering Science* 54 (1999)
- Hayashi, R., Onishi, M., Sugiyama, M., Koda, S., Oshima, Y., Kinetic analysis on alcohol concentration and mixture effect in supercritical water oxidation of methanol and ethanol by elementary reaction model, *Journal of Supercritical Fluids* 40 (2007)
- Hodes, M., Marrone, P. A., Hong, G. T., Smith, K. A., Tester, J. W., Salt precipitation and scale control in supercritical water oxidation – Part A: fundamentals and research, *Journal of Supercritical Fluids* 29 (2004)
- Institution of Civil Engineers: Building information modelling, Innovation in water and waste water treatment plants, URL: <http://www.ice.org.uk/topics/BIM/Case-studies/Innovation-in-water-and-waste-water-treatment-plan>, Retrieved 01/11/12
- International Programme on Chemical Safety (IPCS), Health and Safety Guide No. 43: Dimethylformamide (DMF), World Health Organisation (1990)
- Iyer, S. D., Klein, M. T., Effect of pressure on the rate of butyronitrile hydrolysis in high-temperature water, *Journal of Supercritical Fluids* 10 (1997)
- Izsaki, Z., Kalman, J., Varga, A. T., Kovacs, L., Disposal of PCBs by Wet Air Oxidation, *Organohalogen Comp.* 3 (1990)

- Jin, F., Cao, J., Kishita, A., Enomoto, H., Moriya, T., Oxidation reaction of high molecular weight dicarboxylic acids in sub- and supercritical water, *Journal of Supercritical Fluids* 44 (2008)
- Kantak, M. V., De Manrique, K. S., Aglave, R. H., Hesketh, R. P., Methylamine Oxidation in a Flow Reactor: Mechanism and Modelling, *Combustion and Flame* 108 (1997)
- Killilea, W. R., Swallow, K. C., Hong, G. T., The Fate of Nitrogen in Supercritical-Water Oxidation, *Journal of Supercritical Fluids* 5 (1992)
- Koo, M., Lee, W. K., Lee, C. H., New reactor system for supercritical water oxidation and its application on phenol destruction, *Chemical Engineering Science* 52 (7) (1997)
- Kritzer, P., Dinjus, E., An assessment of supercritical water oxidation (SCWO): Existing problems, possible solutions and new reactor concepts, *Chemical Engineering Journal* 83 (2001)
- Kruse, A., Dinjus, E., Hot compressed water as a reaction medium and reactant: Properties and synthesis reactions, *Journal of Supercritical Fluids* 39 (2007)
- Kruse, A., Dinjus, E., Hot compressed water as a reaction medium and reactant: 2. Degradation reactions, *Journal of Supercritical Fluids* 41 (2007)
- Kutney, M. C., Dodd, V. S., Smith, K. A., Herzog, H. J., Tester, J. W., A hard-sphere volume-translated van der Waals equation of state for supercritical process modelling: 1. Pure components, *Fluid Phase Equilibria* 128 (1997)

- Lachance, R., Paschkewitz, J. DiNaro, J., Tester, J. W., Thiodiglycol hydrolysis and oxidation in sub- and supercritical water, *Journal of Supercritical Fluids* 16 (1999)
- Lee, D-S., Gloya, E. F., Efficiency of H<sub>2</sub>O<sub>2</sub> and O<sub>2</sub> in Supercritical Water Oxidation of 2,4-Dichlorophenol and Acetic Acid, *Journal of Supercritical Fluids* 3 (1990)
- Lemmon, E. W., McLinden, M. O., Friend, D. G., Thermophysical Properties of Fluid Systems, *NIST Chemistry WebBook, NIST Standard Reference Database Number 69 (most recent version)*, National Institute of Standards and Technology, Gaithersburg MD, 20899; URL: <http://webbook.nist.gov>, Retrieved on numerous occasions: January 2009 – December 2012
- Levenspiel, O., Chemical Reaction Engineering 2<sup>nd</sup> Ed., Wiley, New York (1972)
- Leybros, A., Roubaud, A., Guichardon, P., Boutin, O., Supercritical water oxidation of Ion Exchange Resins: Degradation mechanisms, *Process Safety and Environmental Protection* 88 (3) (2010)
- Li, L., Chen, P., Gloya, E. F., Generalised Kinetic Model for Wet Oxidation of Organic Compounds, *AIChE Journal* 37 (11) (1991)
- Li, S. C., Williams, F. A., Experimental and numerical studies of two-stage methanol flames, *Symposium (International) on Combustion Proceedings* 26 (1996)
- Lin, K-S., Wang, H. P., Catalytic oxidation of 2-chlorophenol in confined channels of ZSM-48, *Journal of Physical Chemistry B* 105 (21) 2001

- Lin, M. C., He, Y., Melius, C. F., Theoretical interpretation of the kinetics and mechanisms of the HNO + HNO and HNO + 2NO reactions with a unified model, *Int. Journal of Chemical Kinetics* 24 (1992)
- Lin, M. C., He, Y., Melius, C. F., Theoretical aspects of product formation from the NCO + NO reaction, *Journal of Physical Chemistry* 97 (1993)
- Linder, D. P., Duan, X., Page, M., Thermal rate constants for  $R + N_2H_2 \rightarrow RH + N_2H$  ( $R = H, OH, NH_2$ ) determined from multireference configuration interaction and variational transition state theory calculations, *Journal of Chemical Physics* 104 (1996)
- Long, G., Meek, M. E., Lewis, M., *N,N-Dimethylformamide: Concise International Chemical Assessment Document* 31, World Health Organisation, Geneva (2001)
- Manion, J. A., Huie, R. E., Levin, R. D., Burgess Jr, D. R., Orkin, V. L., Tsang, W., McGivern, W. S., Hudgens, J. W., Knyazev, V. D., Atkinson, D. B., Chai, E., Tereza, A. M., Lin, C.-Y., Allison, T. C., Mallard, W. G., Westley, F., Herron, J. T., Hampson, R. F., and Frizzell, D. H., NIST Chemical Kinetics Database, NIST Standard Reference Database 17, Version 7.0 (Web Version), Release 1.4.3, Data version 2008.12, National Institute of Standards and Technology, Gaithersburg, Maryland, 20899-8320, URL: <http://kinetics.nist.gov/>
- Marias, F., Vielcazals, S., Cezac, P., Mercadier, J., Cansell, F., Theoretical study of the expansion of supercritical water in a capillary device at the output of a hydrothermal oxidation process, *Journal of Supercritical Fluids* 40 (2007)

- Marrone, P. A., Supercritical Water Oxidation – Current Status of Full-scale Commercial Activity for Waste Destruction, *Proceedings of 10<sup>th</sup> International Symposium on Supercritical Fluids (ISSF)*, San Francisco (2012)
- Marrone, P. A., Hodes, M., Smith, K. A., Tester, J. W., Salt precipitation and scale control in supercritical water oxidation – part B: commercial/full-scale operations, *Journal of Supercritical Fluids* 29 (2004)
- Marrone, P. A., Hong, G. T., Corrosion control methods in supercritical water oxidation and gasification processes, *Journal of Supercritical Fluids* 51 (2009)
- Martin, A., Armbruster, U., Müller, P., Deuschle, E., Oxidative conversion of alkyl naphthalenes to carboxylic acids in hot pressurised water, *Journal of Supercritical Fluids* 45 (2008)
- Merck Millipore, Spectroquant® Nova 60 General Information, Merck KGaA, Damstadt, Germany (2012)
- Merck Millipore, Ammonium, Nitrate, Nitrite, and Total Nitrogen Cell Test Manuals, Merck KGaA, Damstadt, Germany (2009-2012)
- Meyer, J. C., Marrone, P. A., Tester, J. W., Acetic Acid Hydrolysis and Oxidation in Supercritical Water, *AIChE Journal* 41 (9) (1995)
- Mishra, V. S., Joshi, J. B., Mahajani, V. V., Kinetics of Wet Air Oxidation of Diethanolamine and Morpholine, *Water Research* 28 (7) (1993)
- Mishra, V. S., Mahajani, V. V., Joshi, J. B., Wet Air Oxidation, *Industrial and Engineering Chemistry Research*. 34 (1995)

- Moussiere, S., Joussot-Dubien, C., Guichardon, P., Boutin, O., Turc, H. -A., Roubaud, A., Fournel, B., Modelling of heat transfer and hydrodynamics with two kinetics approaches during supercritical water oxidation process, *Journal of Supercritical Fluids* 43 (2007)
- Munro, N. B., Talmage, S. S., Griffin, G. D., Waters, L. C., Watson, A. P., King, J. F., Hauschild, V., The Sources, Fate and Toxicity of Chemical Warfare Agent Degradation Products, *Environmental Health Perspectives* 107 (12) (1999)
- Musin, R. N., Lin, M. C., Novel bimolecular reactions between NH<sub>3</sub> and HNO<sub>3</sub> in the gas phase, *Journal of Physical Chemistry A* 102 (1998)
- Needham, D. P., Ziebland, H., The thermal conductivity of liquid and gaseous ammonia, and its anomalous behaviour in the vicinity of the critical point, *International Journal of Heat and Mass Transfer* 8 (11) (1965)
- Oe, T., Suzugaki, H., Naruse, I., Quitain, A. T., Daimon, H., Fujie, K., Role of Methanol in Supercritical Water Oxidation of Ammonia, *Industrial and Engineering Chemistry Research*. 46 (2007)
- Onwudili, J. A., Williams, P. T., Reaction mechanisms for the hydrothermal oxidation of petroleum derived aromatic and aliphatic hydrocarbons, *Journal of Supercritical Fluids* 43 (2007)
- Osada, M., Watanabe, M., Sue, K., Adschariri, T., Arai, K., Water density dependence of formaldehyde reaction in supercritical water, *Journal of Supercritical Fluids* 28 (2004)

- Oshima, Y., Hori, K., Toda, M., Chommanad, T., Koda, S., Phenol oxidation kinetics in supercritical water, *Journal of Supercritical Fluids* 13 (1998)
- Pagsberg, P. B., Eriksen, J., Christiensen, H. C., Pulse Radiolysis of Gaseous Ammonia-Oxygen Mixtures, *Journal of Physical Chemistry* 83 (1979)
- Park, J., Lin, M. C., A mass spectrometric study of the NH<sub>2</sub> + NO<sub>2</sub> reaction, *Journal of Physical Chemistry A.* 101 (1997)
- Park, J., Lin, M. C., Product Branching Ratios in the NH<sub>2</sub> + NO Reaction: A Re-Evaluation, *Journal of Physical Chemistry A.* 103 (1999)
- Pérez, I. V., Rogak, S., Brанию, R., Supercritical water oxidation of phenol and 2,4-dinitrophenol, *Journal of Supercritical Fluids* 30 (2004)
- Perry, R. H., Green, D. W., Perry's Chemical Engineers' Handbook 7<sup>th</sup> Ed., McGraw-Hill, New York (1997)
- Petts, J., "Incineration as a Waste Management Option" in *Waste Incineration and the Environment*, Eds. Hester, R. E., Harrison, R. M., Royal Society of Chemistry (1994)
- Philips, R. J. and associates, Wastewater Reduction and Recycling in Food Processing operations, Food Manufacturing Coalition for Innovation and Technology Transfer, URL: <http://www.ciprocess.co.uk/pdfs/article-wastewater.pdf>, Retrieved 16/12/12

- Pinto, L. D. S., Supercritical water oxidation of nitrogen-containing organic compounds: Process operating conditions and reaction kinetics, University of Birmingham, PhD Thesis (2004)
- Ploeger, J. M., Mock, M. A., Tester, J. W., Cooxidation of Ammonia and Ethanol in Supercritical Water, Part 1: Experimental Results, *AIChE Journal* 53 (4) (2007)
- Ploeger, J. M., Green, W. H., Tester, J. W., Co-oxidation of Ammonia and Ethanol in Supercritical Water, Part 2: Modelling Demonstrates the Importance of  $H_2NNO_x$ , *International Journal of Chemical Kinetics* 40 (2008)
- Plugatyr, A., Hayward, T. M., Svishchev, I. M., Thermal decomposition of hydrazine in sub- and supercritical water at 25 MPa, *Journal of Supercritical Fluids* 55 (2011)
- Polikhronidi, N. G., Abdulagatov, I. M., Stepanov, G. V., Batyrova, R. G., Isochoric heat capacity measurements for pure ethanol in the near-critical and supercritical regions, *Journal of Supercritical Fluids* 43 (1) (2007)
- Portella, J., Mateos, D., Mancini, F., Marraud, C., Cansell, F., Hydrothermal oxidation with multi-injection of oxygen: Simulation and experimental data, *Journal of Supercritical Fluids* 40 (2007)
- Richardson, J. F., Harker, J. H., Coulson and Richardson's Chemical Engineering, Volume 2: Particle Technology and Separation Processes 5<sup>th</sup> Ed., Butterworth-Heinemann, Oxford (2002, reprinted 2006)
- Romming, H. J., Wagner, H. G., A kinetic study of the reactions of  $NH(X^3\Sigma^-)$  with  $O_2$  and NO in the temperature range from 1200 to 2200 K, *Symposium (International) on Combustion Proceedings* 26 (1996)

Royal Pharmaceutical Society, The British National Formulary (BNF) 64, BMJ Group and Pharmaceutical Press, London (2012)

Sánchez-Oneto, J., Portela, J. R., Nebot, E., de la Ossa, E. M., Hydrothermal oxidation: Application to the treatment of different cutting fluid wastes, *Journal of Hazardous Materials* 144 (2007)

Sandler, S. I., Chemical and Engineering Thermodynamics 3<sup>rd</sup> Ed., Wiley, New York (1999)

Savage, P. E., Yu, J., Stylski, N., Brock, E.E., Kinetics and mechanism of methane oxidation in supercritical water, *Journal of Supercritical Fluids* 12 (1998)

Savage, P. E., Rovira, J., Stylski, N., Martino, C. J., Oxidation kinetics for methane/methanol mixtures in supercritical water, *Journal of Supercritical Fluids* 17 (2000)

Savage, P. E., A perspective on catalysis in sub- and supercritical water, *Journal of Supercritical Fluids* 47 (2009)

Sato, T., Watanabe, M., Smith, R. L., Adschariri, T., Arai, K., Analysis of the density effect on partial oxidation of methane in supercritical water, *Journal of Supercritical Fluids* 28 (2004)

Segond, N., Matsumura, Y., Yamamoto, K., Determination of Ammonia Oxidation Rate in Sub- and Supercritical Water, *Industrial and Engineering Chemistry Research* 41 (24) (2002)

- Schanzenbächer, J., Taylor, J. D., Tester, J. W., Ethanol oxidation and hydrolysis rates in supercritical water, *Journal of Supercritical Fluids* 22 (2002)
- Shimadzu Corporation, Total Organic Carbon Analyser Model TOC-5050A Instruction Manual, Shimadzu Europe, Duisburg, Germany (1996)
- Shin, Y. H., Shin, N. C., Veriansyah, B., Kim, J., Lee, Y-W., Supercritical water oxidation of wastewater from acrylonitrile manufacturing plant, *Journal of Hazardous Materials* 163 (2009)
- Sögüt, O. O., Akgün, M., Treatment of dyehouse waste-water by supercritical water oxidation: a case study, *Journal of Chemical Technology and Biotechnology* 85 (5) (2010)
- Sonntag, R. E., Borgnakke, C., van Wylen, G. J., Fundamentals of Thermodynamics 6<sup>th</sup> Ed., Wiley, New York (2003)
- Sudhir, N. V., Aki, K., Abraham, M. A., An Economic Evaluation of Catalytic Supercritical Water Oxidation: Comparison with Alternative Waste Treatment Technologies, *Environmental Progress* 17 (4) (1998)
- Sudhir, N. V., Aki, K., Abraham, M. A., Catalytic supercritical water oxidation of pyridine: kinetics and mass transfer, *Chemical Engineering Science* 54 (1999)
- Sumathi, R., Peyerimhoff, S. D., A quantum statistical analysis of the rate constant for the HO<sub>2</sub> + NH<sub>2</sub> reaction, *Chemical Physics Letters* 263 (1996)

- Sun, Z., Takahashi, F., Odaka, Y., Fukushi, K., Oshima, Y., Yamamoto, K., Effects of potassium alkalis and sodium alkalis on the dechlorination of o-chlorophenol in supercritical water, *Chemosphere* 66 (2007)
- Sun, M., Wu, X., Zhang, Z., Han, E-H., Oxidation of 316 stainless steel in supercritical water, *Corrosion Science* (2009)
- Svishchev, I. M., Plugatyr, A., Supercritical water oxidation of o-dichlorobenzene: degradation studies and simulation insights, *Journal of Supercritical Fluids* 37 (2006)
- Thornton, T. D., Savage, P. E., Phenol Oxidation in Supercritical Water, *Journal of Supercritical Fluids* 3 (4) (1990)
- Tsang, W., Hampson, R. F., Chemical kinetic data base [sic] for combustion chemistry. Part I. Methane and related compounds, *Journal of Physical Chemistry Reference Data* 15 (1986)
- Tsang, W., Chemical kinetic data base [sic] for combustion chemistry. Part 2. Methanol, *Journal of Physical Chemistry Reference Data* 16 (1987)
- Tsang, W., Herron, J. T., Chemical kinetic data base [sic] for propellant combustion. I. Reactions involving NO, NO<sub>2</sub>, HNO, HNO<sub>2</sub>, HCN and N<sub>2</sub>O, *Journal of Physical Chemistry Reference Data* 20 (1991)
- Tsao, C. C., Zhou, Y., Liu, X., Houser, T. J., Reactions of Supercritical Water with Benzaldehyde, Benzylidenebenzylamine, Benzyl Alcohol, and Benzoic Acid, *Journal of Supercritical Fluids* 5 (1992)

United Kingdom Environment Agency, *Waste Incineration in 2006*, URL: <http://www.environment-agency.gov.uk/research/library/data/34181.aspx>, Retrieved 21/11/12

Vandooren, J., Oldenhove de Gueretechin, L., van Tiggelen, P. J., Kinetics in a lean formaldehyde flame, *Combustion and Flame* 64 (1986)

Veolia Environmental Services Birmingham Limited, Tyseley, Energy Recovery, URL: <http://www.veoliaenvironmentalservices.co.uk/Birmingham/Facilities/Energy-recovery>, Retrieved 02/12/12

Veriansyah, B., Kim, J-D., Lee, J-C., Supercritical Water Oxidation of Thiodiglycol, *Industrial and Engineering Chemistry Research* 44 (2005)

Veriansyah, B., Kim, J-D., Supercritical water oxidation for the destruction of toxic organic wastewaters: A review, *Journal of Environmental Sciences* 19 (2007)

Vielcazals, S., Mercadier, J., Marias, F., Matéos, D., Bottreau, M., Cansell, F., Marraud, C., Modelling and Simulation of Hydrothermal Oxidation of Organic Compounds, *AIChE Journal* 52 (2) (2006)

Vogel, F., DiNaro Blanchard, J. L., Marrone, P. A., Rice, S. F., Webley, P. A., Peters, W. A., Smith, K. A., Tester, J. W., Critical review of kinetic data for the oxidation of methanol in supercritical water, *Journal of Supercritical Fluids* 34 (2005)

Wang, X., Gron, L. U., Klein, M. T., Brill, T. B., The Influence of High-Temperature Water on the Reaction Pathways of Nitroanilines, *Journal of Supercritical Fluids* 8 (1995)

Weber, M., Wellig, B., von Rohr, P. R., "SCWO apparatus design – towards industrial availability" in *Proceedings of the Corrosion/NACE 1999, 54<sup>th</sup> Annual Conference and Exposition*, Paper No, 258, San Antonia, TX, USA, (April 25-30 1999)

Webley, P. A., Tester, J. W., Holgate, H. R., Oxidation Kinetics of Ammonia and Ammonia-Methanol Mixtures in Supercritical Water in the Temperature Range 530-700°C at 246 bar, *Industrial and Engineering Chemistry Research*. 30 (1991)

Wellig, B., Lieball, K., von Rohr, P. R., Operating characteristics of a transpiring-wall SCWO reactor with a hydrothermal flame as internal heat source, *Journal of Supercritical Fluids* 34 (2005)

Whiting, P., Metha, A. H., Supercritical water oxidation of organics using a mobile surface, *US Patent 5,543,057* (1996)

Zhou, H., Smith, D. W., Advanced technology in water and wastewater treatment, *Journal of Environmental Engineering Science* 1 (2002)

## LIST OF PUBLICATIONS

Al-Duri, B., Kings, I., Garcia-Jarana, B., Portela, J. R., SCWO of Hydrocarbon-Contaminated Waters: Continuous Systems with Split-Entry Oxidant, *Proceedings of 10<sup>th</sup> International Symposium on Supercritical Fluids (ISSF)*, San Francisco (2012)

García-Jarana, M. B., Kings. I., Sánchez-Oneto, J., Portela, J. R., Al-Duri, B., Supercritical water oxidation of nitrogen compounds with multi-injection of oxygen, *Journal of Supercritical Fluids* (2013)

Alsoqyani, F., Kawase, F., Kings, I., Al-Duri, B., Supercritical Water Oxidation (SCWO) for Hazardous Waste Destruction: Enhanced Removal of N-Containing Hydrocarbons by Using Isopropyl Alcohol (IPA), *Proceedings of 10<sup>th</sup> EU Conference on Supercritical Fluids, Naples* (2013)